Development of Novel Biochar-Molecularly Imprinted Polymer Composites for Targeted Adsorption of Per- and Polyfluoroalkyl Substances in Water Treatment Applications

Jessica Marie Steigerwald

A Dissertation

submitted in partial fulfillment of the

requirements for the degree of

Doctor of Philosophy

University of Washington

2023

Reading Committee:

Jessica Ray, Chair

Gregory Korshin

Michael C Dodd

Program Authorized to Offer Degree:

Civil and Environmental Engineering

University of Washington

Abstract

Development of Novel Biochar-Molecularly Imprinted Polymer Composites for Targeted Adsorption of Per- and Polyfluoroalkyl Substances in Water Treatment Applications

Jessica Marie Steigerwald

Chair of the Supervisory Committee
Jessica Ray
Civil and Environmental Engineering

Per- and polyfluoroalkyl substances (PFAS) are a class of emerging contaminants which have received considerable research and regulatory attention in the last decade because of their toxicity, persistence, and prevalence in environmental and human reservoirs. Adsorption by activated carbon is the industry standard for PFAS removal from water; however, biochar produced from agricultural food waste has recently been explored as a sustainable, cost-effective alternative for PFAS treatment. For example, a novel spent coffee grounds biochar ("SCGKOH") produced and tested herein possessed perfluorooctanesulfonate (PFOS) removal capabilities (43.4 mg/g maximum adsorption capacity) comparable to a commercially available Filtrasorb® F300 activated carbon (55.7 mg/g) and a wood-based fly ash char (79.5 mg/g). PFOS adsorption increased in the presence of divalent cations but decreased when simulated effluent organic matter was added. This phenomenon has been observed in a number of studies which have shown that PFAS removal by biochar and activated carbon decreases significantly in matrices with high concentrations of organic matter or competing organic and inorganic species. Thus, there is a need for a more selective PFAS removal method for water treatment. Molecularly imprinted polymers (MIPs) possess high selectivity for a template compound used to create adsorption binding sites with tailored size, shape, and affinity; however, MIP morphology hinders deployment in water

treatment. In this study, the aforementioned SCGKOH was modified with a MIP coating to facilitate targeted PFAS adsorption in (waste)water. Waste derived biochar presents a low cost, widely available, easily tunable, and high surface area substrate ideal for MIP functionalization. Amine groups (either native or functionalized on the biochar) served as attachment points for MIP during thermally activated radical initiated polymerization. A quaternary nitrogen-containing monomer was chosen to confer positive surface charge over a wide pH range—an important characteristic for effective PFAS adsorption. Initial synthesis of a PFOS-templated biochar-MIP (BC@MIP) composite demonstrated adsorption of perfluoroalkyl acids (PFAAs) comparable to unmodified biochar in ultrapure water (0.043 and 0.039 mg PFAA/g*g/m^2, respectively), and increased adsorptive removal (by 0.012 mg PFAA/g*g/m^2) in synthetic wastewater due to reduced MIP swelling and non-specific binding. However, the high selectivity of the BC@MIP ($K_{selectivity}$ of 4.52 for perfluorobutanesulfonate [PFBS] and 3.76 for perfluorooctanoic acid [PFOA]) resulted in lower removal of non-template PFAS which is not ideal for water treatment. In particular, good removal of short chain PFAS compounds—which are replacing longer chain PFAS in manufacturing applications and have shown similar toxic end points to their longer chain counterparts—is a requirement for high performing PFAS adsorbents. To overcome this challenge, a multi-template BC@mMIP was synthesized via simultaneous templating with 6:2-fluorotelomer sulfonate (6:2-FTS), perfluorobutanesulfonate (PFBS), and perfluoropentanoate (PFPeA). The BC@mMIP adsorbent was capable of treating PFOA, PFBS, and perfluorohexanesulfonate (PFHxS) to below their proposed US EPA MCL in ultrapure water containing nine PFAS at (waste)water-relevant concentrations. Column testing in real wastewater effluent revealed competition between total dissolved solids (TDS) species and PFAS; thus, this material is recommended for use in water treatment with low TDS or used in series with a pre-treatment like

ion exchange for optimal performance These BC@MIP materials present a novel, cost-effective option for targeted removal of PFAS from (waste)waters.

Acknowledgements

I would like to take this opportunity to thank my advisor, Jessica Ray, for providing me with the opportunity to conduct this research and for being an incredible mentor and role model. I also want to acknowledge the members of my research group, in particular Fanny Okaikue-Woodi, Yuemei Ye, Nicole Redden, Jennifer Hooper, Alanna Hildebrant, Amy Quintanilla, Reagan Beers, Daniela Soilis, Shawnie Peng, Anusha Srivastava, Reyna Morales Lumagui, Sophia Jessum, and Joshua Chong this work would not have been possible without their help and friendship. Thank you as well to my committee members, Michael Dodd, Gregory Korshin, Christopher Higgins, and Christine Luscombe. Thank you to Martin Sadilek at the University of Washington Department of Chemistry Mass Spectrometry Facility for assistance and expertise with LC-MS/MS quantification and Samantha Young at the University of Washington Molecular Analysis Facility for assistance with X-Ray Photoelectron Spectroscopy data collection and analysis. Finally, I would like to thank my family and friends, in particular my parents Sheila and Joe Steigerwald, whose support allowed me to complete my graduate school journey.

Part of this work was conducted at the Molecular Analysis Facility, which is supported in part by funds from the Molecular Engineering & Sciences Institute, the Clean Energy Institute, the National Science Foundation and the National Institutes of Health. Part of this work was conducted at the Washington Clean Energy Testbeds, a facility operated by the University of Washington Clean Energy Institute. This material is based upon work supported by the National Science Foundation Graduate Research Fellowship Program under Grant No. DGE-1762114. Any opinions, findings, and conclusions or recommendations expressed in this material are those of the authors and do not necessarily reflect the views of the National Science Foundation.

Contents

List of Figures

adsorption in the synthetic wastewater matrix. Percent regeneration was calculated as the percent recovery of mass adsorbed during the 4-day equilibrium adsorption test. Error bars represent the standard deviation from triplicate samples.

Figure 4.1 Scanning electron microscope image of BC substrate (A) and transmission electron microscope image of multi-template MIP-BC composite (B) showing adsorbent morphology.

Figure 4.2 (A) Adsorption of nine PFAS by 100 mg/L of unmodified and polymer modified biochar materials over a 4-day equilibration time. Error bars represent standard deviation from triplicate samples. Initial concentrations were 58 ± 3.7 μg/L PFOS, 50 ± 5.5 μg/L PFHxS, 49 ± 5.1 μg/L PFBS, 48 ± 3.2 μg/L 6:2-FTS, 50 ± 4.9 μg/L PFOA, 58 ± 4.8 μg/L PFHxA, 52 ± 5.4 μg/L PFPeA, 53 ± 5.5 μg/L PFBA, and 41 ± 7.8 μg/L TFA. Figures (B) through (D) show a comparison of selectivity coefficients for single- and multi-template BC@MIP materials calculated from adsorption of nine PFAS shown in (A) with 6:2-FTS, PFBS, and PFPeA used as templates in calculations for (B), (C), and (D), respectively. Non-imprinted polymer (BC@NP) was used as a reference material for these calculations.

Figure 4.3 Adsorption of approximately 5 – 5000 μg/L of individual templates (6:2-FTS, PFBS, PFPeA) onto BC@mMIP. Error bars represent standard deviation of triplicate samples. Data is modeled with the Langmuir and Freundlich isotherms. Calculated model parameters are shown in the **Figure 4.3 table**.

Figure 4.4 Adsorption of nine PFAS by 100 mg/L of BC@mMIP over four in ultrapure water with an initial pH of 7.0 are shown as solid bars. Subsequent PFAS recovery over 7 days in a 70% methanol, 1% sodium chloride, and 2.8 mM sodium hydroxide solution at a solids concentration of 1 g/L are shown as hashed bars. Error bars represent standard deviation of triplicate samples. Data labels give equilibrium solution concentration in ng/L following the adsorption phase. Initial PFAS concentrations were: 217 ± 93 ng/L PFOS, 114 ± 28 ng/L PFHxS, 109 ± 29 ng/L PFBS, 112 ± 10 ng/L 6:2-FTS, 93 ± 10 ng/L PFOA, 87 ± 19 ng/L PFHxA, 96 ± 19 ng/L PFPeA, 98 ± 6 ng/L PFBA, and 197 ± 50 ng/L TFA.

Figure 4.5 Time series normalized column effluent concentrations for representative PFAS and organic compounds with initial concentration of approximately 20 μg/L each in a wastewater effluent matrix delivered at 1 mL/min. Error bars represent standard deviation from triplicate columns for each media type.

Figure 4.6 Mass adsorbed and desorbed over from column media over four sequential cycles for representative PFAS and organic compounds. Initial concentrations for each compound during adsorption was approximately 20 μg/L in a wastewater effluent matrix delivered at 1 mL/min. Desorption was achieved by flushing with 70% methanol and 1% sodium chloride at 0.5 mL/min. Error bars represent standard deviation from triplicate columns for each media type.

Figure A1. Chemical structures of PFOS (A) and caffeine (B).

Figure A2. Kinetics modeling of PFOS adsorption rates onto (a) SCGKOH, (b) F300, and (c) MCG with the Langmuir-derived non-linear pseudo first order, linear pseudo first order, and linear pseudo second order models.

Figure B1 Thermogravimetric analysis of nitrogen modified biochar materials.

Figure B2 DRIFTS spectra of nitrogen modified and unmodified spent coffee grounds biochar.

Figure B3 Carbon (C1s) XPS data for SCGKOH (A), BC-N (B), BC-M (C), and BC-A (D).

Figure B4 Oxygen (O1s) XPS data for SCGKOH (A), BC-N (B), BC-M (C), and BC-A (D).

Figure B5 Percent removal of 4490 ± 478 μg/L PFOS by 100 mg/L of nitrogen modified and unmodified SCGKOH biochar in an ultrapure water matrix following a 4-day equilibration period. Error bars represent standard deviation from triplicate samples.

Figure B6 Percent removal of 4174 ± 302 μg/L PFOS by 100 mg/L of MIP coated and unmodified SCGKOH biochar in an ultrapure water matrix following a 4-day equilibration period. Error bars represent standard deviation from triplicate samples.

Figure B7 Percent removal of 1478 ± 185 μg/L PFOS, 1152 ± 135 μg/L PFBS, and 1380 ± 515 μg/L PFOA by 100 mg/L of MIP coated and unmodified SCGKOH biochar in an ultrapure water matrix following a 4-day equilibration period. Error bars represent standard deviation from triplicate samples.

Figure B8 Percent removal of 1659 ± 99 μg/L PFOS, 1400 ± 11 μg/L PFBS, 2313 ± 71 μg/L PFOA, 1916 ± 76 μg/L caffeine, 1520 ± 63 μg/L fipronil, and 3385 ± 217 μg/L pentachlorophenol by sEfOM, biochar, and biochar MIP composite materials in a synthetic wastewater matrix with pH controlled to 7.0 ± 0.2 using a 5 mM HEPES buffer following a 4-day equilibration period. Error bars represent standard deviation from triplicate samples.

Figure B9 Equilibrium adsorption of 4275 ± 342 μg/L PFOS by 100 mg/L MIP modified and unmodified biochar materials in an ultrapure water only matrix following a 4-day equilibration period. Error bars represent the standard deviation from triplicate samples.

Figure B10 Equilibrium adsorption of 1476 ± 207 μg/L PFOS, 1166 ± 153 μg/L PFBS, and 1453 ± 582 μg/L PFOA by 100 mg/L MIP modified and unmodified biochar materials in an ultrapure water only matrix following a 4-day equilibration period. Error bars represent the standard deviation from triplicate samples.

Figure B11 Equilibrium adsorption of 1659 ± 99 μg/L PFOS, 1400 ± 11 μg/L PFBS, 2313 ± 71 μg/L PFOA, 1916 ± 76 μg/L caffeine, 1520 ± 63 μg/L fipronil, and 3385 ± 217 μg/L pentachlorophenol by 100 mg/L MIP modified and unmodified biochar materials in synthetic wastewater following a 4-day equilibration period. Error bars represent the standard deviation from triplicate samples.

Figure B12 Chemical structures of PFOS (A), PFBS (B), PFOA (C), caffeine (D), fipronil (E), and pentachlorophenol (F).

Figure C1 PFAS adsorption 100 mg/L of BC@mMIP synthesized with and without the macromolecular crowding approach. Equilibrium adsorption was evaluated after 4 days. Error bars represent standard deviation from triplicate samples. Initial concentrations were 58 ± 3.7 μg/L PFOS, 50 ± 5.5 μg/L PFHxS, 49 ± 5.1 μg/L PFBS, 48 ± 3.2 μg/L 6:2-FTS, 50 ± 4.9 μg/L PFOA, 58 ± 4.8 μg/L PFHxA, 52 ± 5.4 μg/L PFPeA, 53 ± 5.5 μg/L PFBA, and 41 ± 7.8 μg/L TFA.

Figure C2 PFAS desorption kinetics from BC@mMIP following a 4-day adsorption of (waste)water relevant concentrations in ultrapure water. PFAS recovery was achieved in a 70% methanol, 1% sodium chloride, 2.8 mM sodium hydroxide solution with a solids concentration of 1 g/L. Graph (A) displays the full dataset while (B) displays a closer look at the PFAS with recovered mass from 0 – 60 ng.

Figure C3 Column test set-up. Test columns contain 1 wt.% of adsorbate in sand.

Figure C4 Column tracer test graphical results.

Figure C5 Time series adsorption of for PFAS and organic compounds not shown in **Figure 4.5**. Initial concentrations for each compound during adsorption was approximately 20 μg/L in a wastewater effluent matrix delivered at 1 mL/min. Error bars represent standard deviation from triplicate columns for each media type.

Figure C6 Mass adsorbed and desorbed from column media over four sequential cycles for PFAS and organic compounds not shown in **Figure 4.6**. Initial concentrations for each compound during adsorption was approximately 20 μg/L in a wastewater effluent matrix delivered at 1 mL/min. Desorption was achieved by flushing with 70% methanol and 1% sodium chloride at 0.5 mL/min. Error bars represent standard deviation from triplicate columns for each media type.

Figure C7 Chemical structures of PFOS (A), PFHxS (B), PFBS (C), 6:2-FTS (D), PFOA (E), PFHxA (F), PFPeA (G), PFBA (H), TFA (I), and Fipronil (J).

List of Tables

Chapter 1: Background and Motivation

Perfluoroalkyl acids (PFAAs) are a subclass of the per- and polyfluoroalkyl substances (PFAS) which have received considerable research and regulatory attention in recent decades due to their persistence, prevalence, and toxicity. Wastewater has recently been recognized as an important, low level source of PFAAs to environmental and drinking waters. Unfortunately, commonly used filtration media such as activated carbon and ion exchange resin do not perform well in the presence of competing organics and ions found in wastewater. Biochar has been explored as a more environmentally friendly, cost-effective alternative to activated carbon for water treatment applications; however it shares many of the same limitations as activated carbon for PFAA treatment. Thus, there is a need for a more selective adsorbent for treatment of PFAAs in (waste)water. A PFAA-imprinted polymer functionalized on a biochar substrate is proposed to meet this need. Molecularly imprinted polymers (MIPs) have recently been explored as a more selective adsorbent for a range of organic compounds, including PFAAs. The low cost, high surface area, and easily modifiable nature of biochar makes it an ideal substrate for immobilization of a PFAS MIP adsorbent to produce a highly selective composite adsorbent that is easily deployable in existing water treatment infrastructure.

1.1 WASTEWATER EFFLUENT IS A SOURCE OF PFAAs TO ENVIRONMENTAL AND DRINKING WATERS

Population increase, urbanization, climate change impacts on precipitation patterns, and anthropogenic contamination of some freshwater sources has resulted in water scarcity around the globe.[2-4] One option for water scarce communities is to implement water reuse to alleviate some of the demand for new water resources through either direct or indirect potable reuse or non-potable reuse.[5, 6] However, emerging contaminants that remain following advanced water treatment present a challenge for water reuse.[7-9] In the case of potable reuse, there may be drinking water regulations that mandate specific treatments for or maximum concentration levels of emerging contaminants.[5] Similarly, where wastewater effluent is diverted to non-potable reuse or environmental water bodies, the effluent may become a source of these contaminants to the environment. The diversion of secondary wastewater effluent could negatively impact aquatic life and increase concentrations of emerging contaminants in downstream drinking water sources, and thus may be regulated under other frameworks like the National Pollutant Discharge Elimination System (NPDES) permit.[5, 9]

PFAS are a particular class of emerging contaminants that have received considerable attention in recent decades because of their prevalence,[10-12] persistence,[12, 13] treatment challenges,[8] and toxicity at low nanogram or microgram per liter concentrations.[14-16] Originally created in the 1930s,[17] PFAS have since been used in the United States and around the world for the manufacture of a range of products including non-stick and stain resistant coatings (e.g., Scotchgard®),[18] electronics manufacturing,[19] food packaging,[18] and firefighting foams.[18, 20] The U.S. Environmental Protection Agency (US EPA) has identified a list of 9,252 distinct PFAS compounds,[21] all of which contain a carbon chain that is either partially (poly) or fully (per) fluorinated. Many PFAS also contain a charged head group that is often anionic but may be

Table 1.1 Per- and polyfluoroalkyl acids of interest to this study.

compound name	abbreviation	chemical structure
perfluorooctanesulfonate	PFOS	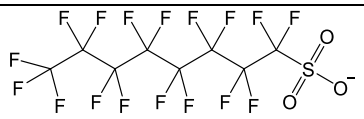
perfluorohexanesulfonate	PFHxS	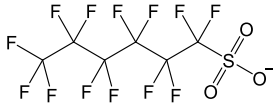
perfluorobutanesulfonate	PFBS	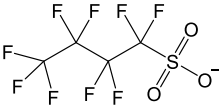
6:2-fluorotelomer sulfonate	6:2-FTS	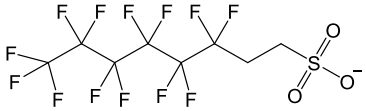
perfluorooctanoate	PFOA	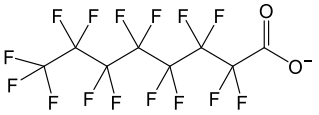
perfluorohexanoate	PFHxA	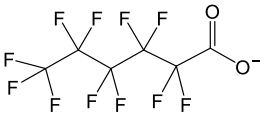
perfluoropentanoate	PFPeA	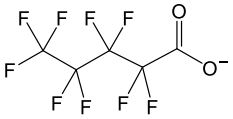
perfluorobutanoate	PFBA	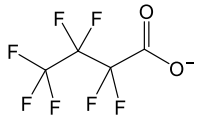
trifluoroacetate	TFA	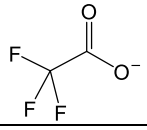

cationic or zwitterionic.[18, 21] A particularly persistent and toxic subclass of PFAS are PFAAs[18] which can be further divided into perfluoroalkyl carboxylic acids (PFCAs) or perfluoroalkyl sulfonic acids (PFSAs). PFCAs and PFSAs characteristically have a fully fluorinated, hydrophobic carbon backbone that can vary in length from one to more than ten carbons, and a carboxylic or sulfonic head group which confers a negative charge at most environmental pH (**table 1.1**).[18, 21] This structure gives PFAAs surfactant-like properties which facilitate their transport over long distances in the environment.[22] The strength of the fluorocarbon bond (one of the strongest bonds

possible) also makes these compounds resistant to passive environmental, chemical or biological degradation.[18, 22] More recently, perfluoroalkyl compounds containing an ether linkage within the fluorocarbon tail have been developed for manufacturing use with the goal that the ether would provide a degradation route for these chemicals which would decrease their longevity in the environment.[12] Unfortunately, recent studies have shown these compounds often transform within the environment to shorter chain PFCAs,[13, 18] and share many of the same toxic end points with their long chain and non-ether containing counterparts.[14, 15, 23]

A number of negative health impacts have been linked to human exposure to PFAAs including immunosuppression and induction of tumors in liver, thyroid, and mammary glands.[24] Two of the more commonly identified PFAAs in environmental systems, perfluorooctanoate (PFOA) and perfluorooctanesulfonate (PFOS), have received considerable research attention because of their prevalence and toxicity.[14, 25, 26] PFOA has been classified as possibly carcinogenic to humans and evidence has been found for the carcinogenicity of PFOS in humans as well.[24, 25, 27] Three main routes of human exposure to PFAAs are inhalation of PFAA-containing dust, and consumption of contaminated food or drinking water.[24] Studies in rats have shown oral routes of exposure result in a high fraction of absorption of over 95% and account for the greatest portion of chronic exposures.[24] Once it enters the body, PFAAs can bind to albumin proteins allowing them to become widely distributed through the body with highest concentrations found in the liver, kidneys, and blood serum.[24] PFAAs may also be transferred from mother to fetus during pregnancy or to infants via breast milk.[27] Many of the toxic outcomes of PFAA exposure identified to date result from activation of PPARα, a peroxisome proliferator-activated receptor that is important for energy homeostasis and helps regulate gene expression for fatty acid oxidation.[24, 28] The structure

of PFAA molecules allow them to mimic the fatty acid molecules that typically activate the PPARα nuclear receptors.[27]

In the early 2000s, PFOS and PFOA began to be phased out of production and manufacturing processes (and replaced with shorter homologous compounds) in the U.S. and elsewhere around the world in response to findings concerning their toxicity.[24] By 2015, their use in manufacturing in the U.S. had been almost completely eliminated.[19] In 2009, the US EPA released guidance on a human health advisory limit (HAL) for PFOS and PFOA in drinking water.[29] This HAL was updated in 2016 when the recommended drinking water limits for PFOS and PFOA either separately or combined were reduced to 70 nanograms per liter (ng/L).[29] It was further updated in 2022 with much lower HAL for PFOS (0.02 ng/L) and PFOA (0.004 ng/L) as well as new HALs for hexafluoropropylene oxide-dimer acid (HFPO-DA, or GenX; 10 ng/L) and perfluorobutanesulfonate (PFBS; 2000 ng/L).[30]

An important source of PFAAs to environmental systems and drinking water sources is wastewater treatment plant (WWTP) effluent. Recent research has focused on quantifying the presence, types, and fate of PFAAs in WWTP.[31-36] An EPA memorandum released in April 2021 recognized wastewater as a potentially important source of PFAAs as well.[37] Studies have identified a range of long and short-chain PFAAs as well as various precursor compounds in WWTP influent and effluent streams with concentrations ranging from the low nanogram per liter to high microgram per liter.[31, 32]A recent study by Thompson et al. noted a national trend of decreasing concentrations of long-chain PFAAs and a potential increase in concentrations of short chain PFAAs in WWTP.[31] During wastewater treatment, a fraction of the PFAAs partition to the suspended solids and end up in the biosolids stream while the rest remain in the aqueous phase and exit the plant in the wastewater effluent stream.[31, 32] Precursor compounds are often transformed

to their PFAA counterparts through biological or abiotic processes, increasing the total PFAA load through the plant.[31, 32] Thus, there is a need for research into best practices for management of PFAAs in wastewater, including treatment options for separation of PFAAs from wastewater effluent.

1.2 EMERGING THEMES IN PFAA DETECTION AND SEPARATION TECHNIQUES

With increased regulation of PFAAs and reductions in the acceptable levels of PFAAs in drinking water, there is an increasing need for cost-effective separation of low concentrations of PFAAs in aquatic systems. AC and ion exchange resins are the industry standard for removal of PFAAs from drinking water. However, these materials do not perform well in complex matrices – like wastewater effluent – containing competing organic compounds and ions that are often present in higher concentrations.[8, 38-40] Furthermore, they have been observed to remove shorter chain PFAAs poorly as a result of the higher water solubility of short-chain PFAAs, greater reliance of short-chain PFAA removal on electrostatic interactions, and replacement of short-chain PFAAs at adsorption sites by longer chain PFAAs and co-occurring organics.[8, 38, 41] Membrane filtration (i.e., nanofiltration and reverse osmosis) is another well-studied water treatment technology which has been applied for separation of PFAAs from aqueous systems.[42] However, this is a relatively cost and energy intensive option which often requires pre-treatment to remove high concentrations of organics which may foul the membranes, increasing operational costs. Ozofractionation is another alternative for PFAA separation which involves bubbling ozone gas through columns containing PFAA-impacted water to concentrate PFAAs in a foam layer at the top of the column which can then be removed for further treatment or disposal.[43] This technology has been shown to be viable for removal of short- and long-chain PFAAs as well as PFAS precursors in a full scale wastewater treatment plant, and has the advantage of simultaneous oxidation of other organics.[43]

However, there is some concern that this technology would not be capable of achieving low ng/L concentrations required by more recent regulatory standards.[43] Thus, more selective, low cost detection and treatment options are needed to effectively quantify and remove PFAAs from wastewater and other aquatic systems containing high concentrations of organics.

Many of the more selective separation techniques that have been explored can be used for either treatment or detection of PFAAs. For example, hydrogels,[44-49] metal organic frameworks,[50-52] and molecularly imprinted polymers[53-56] have all been explored as options for both detection and separation of PFAAs in aqueous systems. Although preliminary research on these technologies has shown promise, all require significant additional research before they could be ready for deployment in full scale water treatment applications.

1.3 MOLECULARLY IMPRINTED POLYMERS

Molecularly imprinted polymers (MIPs) are a class of materials characterized by their ability to selectively adsorb a target compound at tunable binding sites tailored to have high affinity for the target. One of the most common methods for production of MIP materials is via non-covalent imprinting.[57] First, the target compound(s) and functional monomer(s) are mixed for a period of time (from 30 min to > 10 h) during the pre-polymerization step. This step promotes coordination between the target and functional monomers via weak van der Waals forces (e.g., hydrogen bonding, hydrophobic attraction, or electrostatic attraction) and the creation of self-assembled ligands. Functional monomers are typically chosen to have specific moieties (e.g., quaternary nitrogen moieties for electrostatic attraction with negatively charged compounds) or properties (e.g., hydrophilicity or hydrophobicity) that promote coordination with the target compound.[53-55, 57] Following pre-polymerization, the crosslinker is added which combines the functional monomers and provides structure and morphology to the final product. The crosslinker typically comprises the majority of the final MIP (molar ratios of crosslinker to monomer are often around

10:1), giving it a large impact on the physicochemical properties of the MIP.[53, 57] Crosslinkers are usually selected to be highly soluble in the intended solvent (e.g., water or organic solvent), and to have a large number of polymerizable vinyl groups.[57] Polymerization is initiated via introduction of an initiator compound or specific initiation conditions and can be either allowed to continue to completion or terminated after a set amount of time. Thermally activated radical-initiated polymerization is a common option in which a thermally activated initiator compound is added to the mixture to promote formation of radicals from –NH moieties on the crosslinker or functional monomer. The radicals then react with vinyl groups on the crosslinker or functional monomers, starting a chain polymerization reaction. Once polymerization is completed, the target compound template is then extracted from the MIP to leave behind the empty binding sites. Extraction can be completed through sequential wash steps or via Soxhlet extraction with a wash solution in which the template is highly soluble.[53, 56-58]

MIP materials were originally developed for targeted sensing and detection of compounds, particularly as a mimic for the biological antigen-antibody receptor systems.[59] More recently, however, MIPs have been explored as an option for targeted adsorption of compounds or classes of compounds from aquatic systems.[58, 60] For example, Dai et al. developed a multi-template MIP using 2-vinylpyridine as the functional monomer for selective removal of several acidic pharmaceuticals from environmental waters.[58] Several recent studies have also explored the use of MIP materials for PFAS removal in water treatment applications. For example, Deng et al. achieved over 60% removal of 200 mg/L PFOS using a PFOA-templated MIP with 4-vinylpyridine as the functional monomer.[61]

Pure MIP material is often a powder which swells to a gelatinous substance when hydrated, making it difficult to deploy for water treatment. To overcome this challenge, several studies have

explored the functionalization of MIP materials onto a substrate material. This option has several advantages including easier deployment of the final adsorbent and creation of a thinner MIP layer that avoids diffusion limitations to adsorption kinetics that are associated with adsorption into hydrogels or other permeable adsorption materials.[53, 60] For example, Guo et al. successfully functionalized a PFOS-templated MIP onto carbon microspheres creating a MIP layer with a thickness of around 30 nm capable of adsorbing 75.99 mg/g of PFOS. Similarly, Cao et al. functionalized a PFOA-templated MIP onto multi-walled carbon nanotubes which produced a MIP layer with thickness in the tens of nanometers capable of adsorbing 12.4 mg/g of PFOA.[56] Glasscott et al. functionalized a HFPO-DA templated MIP sensor onto a gold microelectrode for targeted sensing of picomolar concentrations of HFPO-DA in environmental waters.[54] However, to facilitate deployment of PFAA selective composite materials, it is desirable to use lower-cost substrates.

1.4 BIOCHAR

Biochar presents a potential cost-effective substrate option that has morphologies amenable to existing water treatment infrastructure (i.e., as a substitute for AC) for easy deployment. Biochar is a solid material with characteristic high aromatic carbon content and specific surface area.[62, 63] It is produced via the thermochemical carbonization of biomass in an oxygen poor environment, often from biomass feedstocks derived from waste products in the agriculture or timber industries.[62, 63] Biochar has been used for a number of applications including agricultural soil amendments, animal feed additives, carbon sequestration, and as a byproduct of energy production.[64] More recently, it has been explored as an alternative to AC for water treatment applications.[39] The high surface area and high aromatic carbon content of biochar give it many of the same adsorption capabilities as AC, while the waste-derived feedstocks reduce costs and environmental burden from producing the adsorbent material.

The biochar production process has been broken down into four distinct steps by Fuchs et al., using a campfire as a model to describe each step.[64] The first step takes place between 0 – 200 °C and involves the evaporation of any water in the biochar material. The second step occurs between 200 – 300 °C, when acidic components of the biomass burn off producing the irritating smoke associated with campfires. From around 300 – 650 °C the oils and tars contained in the biomass are burned off, producing a thicker black smoke and the bio-oil often associated with energy production from biochar. Above 650 °C, the remaining biomass becomes oxidized, resulting in a loss of surface functional groups on the final material.[63, 64] Two of the most common biochar production methods are gasification and pyrolysis, both of which rely on thermal conversion of biomass.[64] Gasification is more commonly employed as an energy production process in which biomass is burned at high temperatures (i.e., 700 – 1400 °C) in a low oxygen environment and either heat or bio-oil are recovered for energy conversion.[64] The fly ash from this process can be captured and used as biochar.[39, 64] Production of biochar via pyrolysis involves heating the biomass to high temperatures while maintaining flow of an inert gas through the pyrolysis chamber to remove carbon dioxide that is produced during pyrolysis before it can deposit on the material.[64] Pyrolysis processes are easily scalable, making this a good option for production of biochar in a lab setting.

Increased use of biochar materials for a variety of processes has prompted a focus on production of biochar materials with physicochemical properties optimized for a particular end use (e.g., removal of organic contaminants in water treatment applications). One option is activation of biochar materials through physical[65, 66] (e.g., steam activation) or chemical (e.g., alkaline hydroxide[67] or acid activation[66, 68]) methods. Activation processes can be used to increase material surface area[63] or add certain surface functional groups.[66, 68, 69] Research has also focused on

addition of specific surface functional groups through other methods. For example, several studies have focused on addition of nitrogen containing functional groups for improved atmospheric adsorption of carbon dioxide[70, 71] or aqueous adsorption of copper.[72] This highly tunable nature of biochar materials makes them an ideal option for a variety of end uses, including as a substrate for MIP functionalization.

Chapter 2: Adsorption Behavior of Perfluorooctanesulfonate (PFOS) onto Activated Spent Coffee Grounds Biochar in Synthetic Wastewater Effluent[1]

Biochar materials produced from agricultural food waste have recently been explored as alternatives to granular activated carbon for PFAS removal in water. A so-called SCGKOH biochar (produced from a 1:1 mass ratio of pyrolyzed spent coffee grounds (SCG) and potassium hydroxide (KOH)) was evaluated for PFOS adsorption and shown to have a maximum adsorption capacity of 43.4 mg/g compared to Filtrasorb® F300 activated carbon (55.7 mg/g) and a wood-based fly ash char (79.5 mg/g). PFOS removal by all adsorbents decreased in the presence of simulated effluent organic matter. SCGKOH presents an exciting alternative to existing commercial char adsorbents used in water treatment applications. The widely available feedstock and low-input production process could make this material a viable water treatment option for resource-constrained communities.

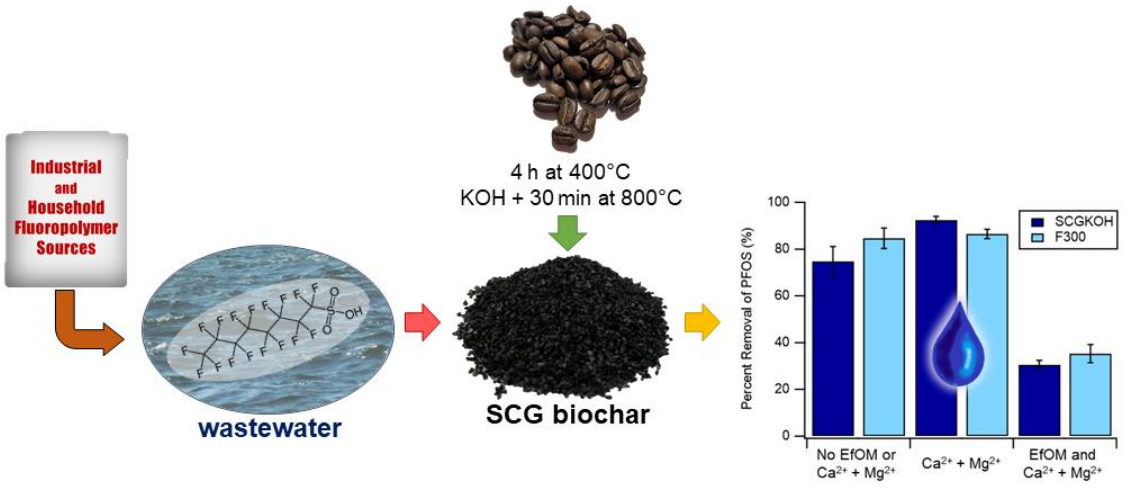

2.1 INTRODUCTION

Per- and polyfluoroalkyl substances (PFAS) are a class of surfactants with high thermal and structural stability used in aqueous film-forming foams for extinguishing hydrocarbon fires[20, 29, 73] and in the manufacture of many fluoropolymer end products.[29, 73-76] PFAS chemical properties also promote their transport in air,[11] water,[10, 11, 13, 22, 35, 36, 77] sediments,[78] and biota[78] allowing these compounds to: (i) disperse in the environment,[22, 35] (ii) resist degradation,[10, 13, 22, 35, 36, 77] and (iii) present multiple exposure pathways to humans.[11, 22, 77]

Perfluorooctanesulfonate (PFOS) is a commonly detected PFAS in the environment.[34] Wastewater effluent is an important source of low-level environmental PFOS concentrations which is particularly concerning where direct or indirect potable water reuse is being considered.[32, 33, 79, 80] Exposure to PFOS has been linked to potential for negative human developmental and reproductive effects (i.e., the basis for the Environmental Protection Agency (EPA) 70 ng/L health advisory limit and imminent regulatory limit), and has been shown to cause kidney, liver, and hematologic defects in rodents.[25, 29, 77] Recent guidance from regulatory agencies across the United States suggests even lower levels of PFOS (e.g., 10–15 ng/L) may present human health risks.[81-83]

PFAS adsorption using activated carbon is the most common approach to separate PFAS from water.[73, 77] Commercial activated carbons are traditionally produced from coal-based or coconut shell feedstocks via energy intensive pyrolysis, and activation with alkaline hydroxide or other more toxic chemicals.[77] Recently, biochar and activated biochar produced from carbonaceous agricultural food waste via less energy intensive methods have gained popularity as potentially more cost-effective and resource-efficient adsorbent alternatives for water treatment applications (e.g., in resource-constrained regions).[7, 84] Char materials produced from spent coffee grounds (SCG), an abundant food waste in many locales, is one such option. Potassium hydroxide (KOH) activation can be employed to oxidize the pyrolyzed char material, producing an activated char

with low ash content, relatively uniform pore size distribution, and high contaminant removal capabilities.[63] For example, Deng et al. (2015) achieved 75% removal of 100 mg/L PFOS in 24 h with a KOH-activated bamboo biochar.[85] Activated SCG biochar has been employed for adsorption of several (in)organic contaminants (including phenol and dysprosium);[71, 86-88] however, adsorption of PFAS with this material has not, to our knowledge, been investigated.

The focus of this study was to produce and characterize SCG biochar for PFOS adsorption.[63, 66, 86, 87] Due to its environmental prevalence and ease of adsorption by activated char materials,[34] PFOS was an ideal PFAS adsorbate candidate to evaluate the competitiveness of our material with commercial options. The SCG biochar physicochemical properties and performance were compared to those of commercial activated carbon (Filtrasorb® 300) and a mixed softwood gasification biochar with demonstrated high PFAS adsorption.[20, 39, 89] The objectives of this study were threefold: (1) to identify optimal SCG biochar production and activation conditions, (2) to relate char physicochemical properties to PFOS adsorption, and (3) to investigate adsorption capacities and mechanisms as a function of PFOS concentration, equilibrium time, and solution composition.

2.2 MATERIALS AND METHODS

2.2.1 Chemicals and Materials

Calgon Carbon™ Filtrasorb® 300 (F300) was obtained from the Calgon Carbon Corporation (Pittsburg, PA). Mountain Crest Gardens (MCG) biochar was obtained from Cal Forest Nurseries, a subsidiary of GrowPro Inc. located in Etna, CA. MCG is a waste byproduct of mixed softwood (high Ponderosa pine content) combustion energy generation at 1400 °C in a downdraft gasifier. Spent coffee grounds (SCG) were obtained from the University of Washington Bay Laurel Catering Services (Seattle, WA) from their industrial drip coffee makers which use Starbucks® Pike Place® grounds, a medium roast, arabica coffee sourced from Latin America.

All chemicals used were certified ACS reagent grade or equivalent unless otherwise noted. High purity nitrogen gas (99.998%) purchased from Praxair (Danbury, CT) was used for char material production. SCG biochar was activated with sodium hydroxide pellets (NaOH, food grade NF/EP/BP/FCC certification) or potassium hydroxide pellets (KOH) both purchased from Fisher Scientific (Waltham, MA). Activated SCG biochar was washed with hydrochloric acid (HCl, 36.5-38%) purchased from Macron Fine Chemicals™ (VWR International, Radnor, PA). FTIR grade potassium bromide (KBr) for diffuse reflectance infrared Fourier transform spectroscopy (DRIFTS) was obtained from Alfa Aesar (Haverhill, MA), and sodium chloride (NaCl) and nitric acid (HNO_3, 69%) for electrophoretic mobility (EPM) analysis were obtained from VWR Chemical. Samples prepared for EPM analysis were filtered with 0.45 µm, 25 mm diameter nylon syringe filters obtained from VWR. Stock solutions for adsorption experiments were prepared with perfluorooctanesulfonate potassium salt (98% purity) purchased from Sigma Aldrich (St. Louis, MO) in Optima™ LC/MS grade Methanol purchased from Thermo Fisher Scientific. Powdered 4-(2-hydroxyethyl)piperazine-1-ethanesulfonic acid (HEPES, 99.5% purity by titration) purchased from Sigma Aldrich was used to buffer the batch adsorption test solutions and the pH was adjusted with 0.05 M NaOH (food grade NF/EP/BP/FCC certification). Divalent cation stock solution was prepared with calcium chloride ($CaCl_2$) purchased from Sigma Aldrich and magnesium chloride hexahydrate ($MgCl_2$) purchased from VWR Chemical. The simulated wastewater treatment plant effluent organic matter (EfOM) was prepared with bovine serum albumin lyophilized powder (96% purity), alginic acid sodium salt from brown algae (sodium alginate, low viscosity), technical grade humic acid, and octanoic acid (98% purity), all purchased from Sigma Aldrich. Adsorption samples were filtered with 0.2 µm, 25 mm diameter cellulose acetate (CA) syringe filters purchased from Sigma Aldrich or 0.2 µm, 25 mm diameter glass fiber (GF) syringe filters obtained

from Foxx Life Sciences (Salem, NH). Analytical and internal PFAS standards were obtained from Wellington Laboratories (Ontario, CA). Reagent Plus® grade powdered caffeine and Pestanal® grade Diuron-d_6 purchased from Sigma Aldrich were used as the analytical and internal standards for caffeine quantification in SCGKOH.

2.2.2 Biochar Production

Upon receipt, Calgon Carbon™ Filtrasorb® 300 (F300) and Mountain Crest Gardens (MCG) biochar were ground and sieved to a No. 30 (595 µm) to 50 (297 µm) mesh fractions, rinsed with deionized water until the rinse water was clear, and dried at 90 °C overnight in a VWR 1500E incubator (VWR International, Radnor, PA). The SCG were obtained directly after use, and immediately dried at 90 °C for 42 hours and stored in an air-tight container to prevent molding.

Carbonization of the SCG was achieved using a Hogentogler Protégé Split Tube Furnace (Hogentogler, Colombia, MD). The material was heated to 200 °C at 10 °C/min and held there for 1 h to facilitate complete evaporation of trapped pore water. The material was then heated to 400 °C, 600 °C, or 800 °C at the same ramp rate and held at those temperatures for 4 h before cooling to produce the SCG400, SCG600, and SCG800 biochar, respectively. Nitrogen gas at 500 mL/min[71, 87] flowed through the furnace during heating and cooling to maintain oxygen poor environments.

2.2.3 SCG Biochar Activation with Alkaline Hydroxide

Chemical activation of the SCG400 biochar was performed with sodium hydroxide (NaOH) and potassium hydroxide (KOH) to increase surface area and improve adsorption capabilities. SCG400 was selected as a precursor material because of its high yield of particles larger than 297 µm (24%), and relatively lower energy input compared to SCG600 and SCG800 biochar (23% and 21% yield). Briefly, SCG400 was thoroughly mixed with alkaline hydroxide pellets in a quartz

crucible boat with SCG400:hydroxide mass ratios of 0.5, 1.0, 1.5, and 2.0. The boat was loaded in the tube furnace, and nitrogen gas flow (500 mL/min) was started and allowed to equilibrate prior to heating. The SCG400 was heated to 200 °C at 10 °C/min and held there for 1 h to evaporate residual water. The temperature was then increased to 800 °C at 10 °C/min and held there for 30 min to facilitate oxidation by the alkaline hydroxide.

Following activation, the media was first rinsed with a hydrochloric acid solution (0.002 – 0.01%) and then with deionized water until a 30-min equilibrium solution pH of 7.0 ± 0.5 was achieved. The activated SCG biochar was then dried at 90 °C overnight, sieved to obtain the 297 – 595 µm size fraction, and stored in air-tight containers until further use.

2.2.4 Char Elemental Composition

Proximate carbon analysis[90, 91] of F300, MCG, SCG chars and feedstock, and CHN elemental analysis of the char media were conducted to provide a better understanding of their chemical composition differences. Proximate carbon analysis was completed following the method detailed in ASTM D1762-84 (reapproved 2007).[90, 91] Briefly, triplicate samples of 0.3 g of char media were weighed and placed in ceramic crucibles. Samples were dried overnight at 100 °C with the crucible lids off and allowed to cool for at least one hour before weighing again to obtain the dry sample weight. Next, samples were heated at 900 °C for six minutes in a muffle furnace to remove the volatile matter. After 6 h, the SCG biochar samples in the ceramic crucible were allowed to cool for one hour before re-weighing. Finally, the SCG biochar samples were heated at 750 °C for 6 h to remove the fixed carbon, and then allowed to cool for at least one hour before collecting a final weight.

Elemental analysis was conducted via a two-step method. First, carbon, hydrogen, and nitrogen percentages were obtained with a Perkin Elmer (Waltham, MA) 2400 Series elemental

analyzer. Second, oxygen percentage was calculated as the remainder out of 100% after contributions from carbon, hydrogen, nitrogen, and inorganic components (ash from proximate carbon analysis) were accounted for. Both proximate carbon and elemental analyses were performed using the 297 – 595 µm size fraction of the adsorbent material.

2.2.5 Char Physicochemical Characterization

Caffeine release from the SCG char was evaluated to determine whether trapped caffeine in the SCG biochar could contaminate water sources during implementation. Caffeine release from SCGKOH was measured via three sequential 24-h equilibration steps followed by liquid chromatography tandem mass spectrometry (LC-MS/MS) quantification of caffeine content in the equilibrium solution. Leaching tests were conducted using the approach described by Belay et al.[92] Preliminary evaluations of caffeine concentrations in water and dichloromethane (as outlined by the Belay et al. colorimetric method) indicated negligible matrix effects in caffeine quantification. Thus, ultrapure water (Milli-Q systems, 18.2 MΩ-cm; Millipore Sigma, Burlington, MA) was used for all further analyses. Briefly, 10 mg of SCG char material (297 – 595 µm size fraction) and 5 mL of ultrapure water were combined in a 15 mL polypropylene tube and rotated at 40 rpm for 24 h. After 24 h, samples were allowed to settle for a few minutes. The supernatant was then decanted, filtered with a 0.2 µm nylon syringe filter, and placed in the refrigerator until analysis. An additional 5 mL of ultrapure water was added to the char material and the process was repeated to obtain caffeine release from a second and third wash.

LC-MS/MS analysis was done with a Waters Corporation (Milford, MA) Quatro Micro quadrupole tandem mass spectrometer preceded by a Phenomenex (Torrence, CA) Gemini 3 µm NX-C18 110A liquid chromatography column as detailed in **Appendix A** (**App. A**). Results are shown in **table 2.1**. The first, second, and third values given represent results from analysis of the

first, second, and third equilibrium solutions. Results show no caffeine in the equilibrium wash solutions from SCGKOH indicating low likelihood of caffeine leaching during water treatment applications.

Table 2.1 Caffeine content determined by LC-MS/MS, the 1, 2, and 3 designations correspond to the first, second and third washes.

sample ID	caffeine concentration (mg/L)
SCGKOH-1	0.00
SCGKOH-2	0.00
SCGKOH-3	0.00

Specific surface area was estimated from nitrogen adsorption data collected at 77 K with a Micromeritics (Norcross, GA) 3Flex instrument using the Brunner-Emmett-Teller (BET) surface area method. Pore size was estimated from the same data using the Barrett, Joyner, and Halenda (BJH) method while pore volume and micropore volume were estimated using the t-method. Approximately 0.1 g of sample was degassed at 300 °C for 12 h prior to data collection. Free space analysis was evaluated with helium gas following nitrogen adsorption.

Surface zeta potential was measured with a Zetasizer Nano ZS (Malvern Instruments, Malvern, UK). Briefly, 22.9 mg of char material fines (i.e., particles less than 297 μm) were suspended in 22.9 mL of 5 mM NaCl solution and allowed to equilibrate for 24 h. For the MCG biochar surface zeta potential measurement at pH 7.69, the pH of the solution was then brought to 7.7 ± 0.05 through addition of 1% HNO_3. Prior to analysis the sample was resuspended via sonication for 10 minutes and then filtered with a 0.45 μm nylon filter. Approximately 10 mL of sample volume was wasted through the filter prior to collection of 5 mL of sample for analysis to minimize particle loss across the filter. The solution pH was measured following particle size and zeta potential analysis with a Thermo Scientific (Waltham, MA) Orion™ Star A111 pH meter equipped with an Orion™ PerpHecT™ Ross™ combination pH micro electrode

Scanning electron microscopy (SEM) imaging of the biochar and activated carbon material morphology was measured with a ThermoFisher Scientific (Waltham, MA) Apreo VP SEM instrument following platinum sputtering of the media where necessary to increase electrical conductivity. Images are shown in **figure 2.1** and **figure 2.6** insets.

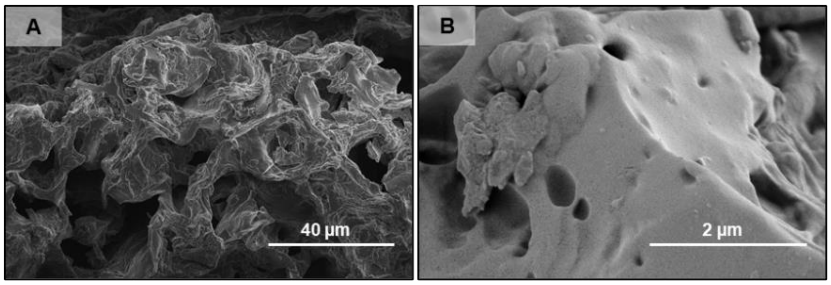

Figure 2.1 Scanning electron microscopy (SEM) images of the SCG400 precursor at lower (A) and higher (B) magnification.

Fourier transform infrared spectra were collected for the three SCG biochar pyrolysis temperatures, SCGKOH, and MCG with the DRIFTS of the Thermo Scientific™ (Waltham, MA) Nicolet™ iSTM10 FT-IR Spectrometer. DRIFTS spectra were not collected for the F300 material as this information has been well characterized elsewhere.[93] Samples were ground with a mortar and pestle and mixed at a 10:1 mass ratio of KBr to char material (except for MCG which used a 13:1 ratio) to optimize the signal to noise ratio.

2.2.6 Batch Testing

All batch testing was done with the 297 – 595 µm char size fraction in 50-mL polypropylene centrifuge tubes with samples equilibrated via rotation at 40 rpm using a Fisherbrand™ Multi-Purpose Tube Rotator (Fisher Scientific, Waltham, MA). Preliminary evaluation of PFOS adsorption was performed with the three pyrolyzed SCG biochar (SCG400, SCG600 and SCG800) to evaluate their PFOS removal capability and to determine optimal solid:liquid ratios for future adsorption studies. A PFOS stock solution in methanol was used to prepare 50 mL of 46 ± 4 µg/L PFOS in ultrapure water with variable biochar masses to achieve solid:liquid ratios of 50, 100, and

200 mg/L in 50-mL polypropylene centrifuge tubes. Methanol concentrations of no more than 0.2% were maintained in this and subsequent batch tests. This residual methanol is not expected to significantly impact the adsorption processes. Triplicate samples were prepared for each material and rotated at 40 rpm on a Fisherbrand™ (Waltham, MA) multipurpose tube rotator for 24 h. Equilibrated batch test samples were filtered with a 0.20 µm cellulose acetate syringe filter with 20 mL of sample wasted through the filter prior to collection of 5 mL for analysis. Results are displayed in **figure 2.2**.

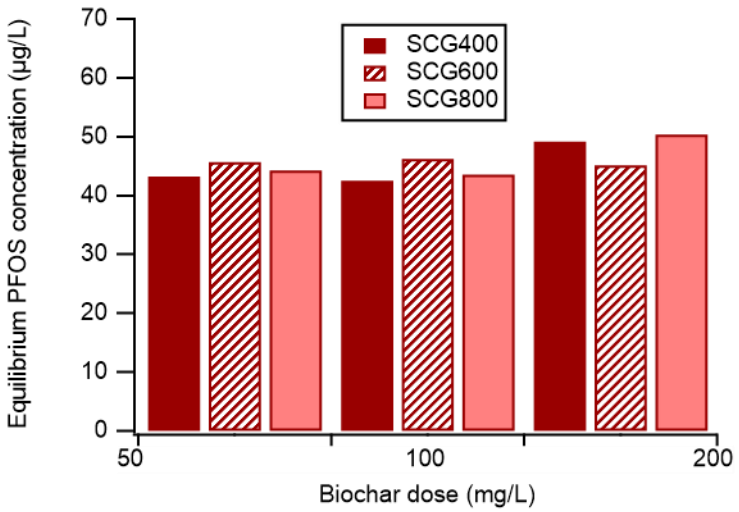

Figure 2.2 Equilibrium PFOS concentration from an initial concentration 46 ± 4 µg/L PFOS over a 24-h equilibrium batch adsorption test by SCG400, SCG600, and SCG800 at solid (mg biochar) to liquid (L of PFOS solution) ratios of 50, 100, and 200.

After SCG400 activation with various mass ratios of NaOH or KOH, 24-h batch adsorption tests were conducted with 100 mg/L char dose to evaluate their removal capabilities (**figure 2.3**). Briefly, 5.0 mg of adsorbent was added to 50 mL of ultrapure water in 50-mL polypropylene centrifuge tubes and spiked with PFOS stock

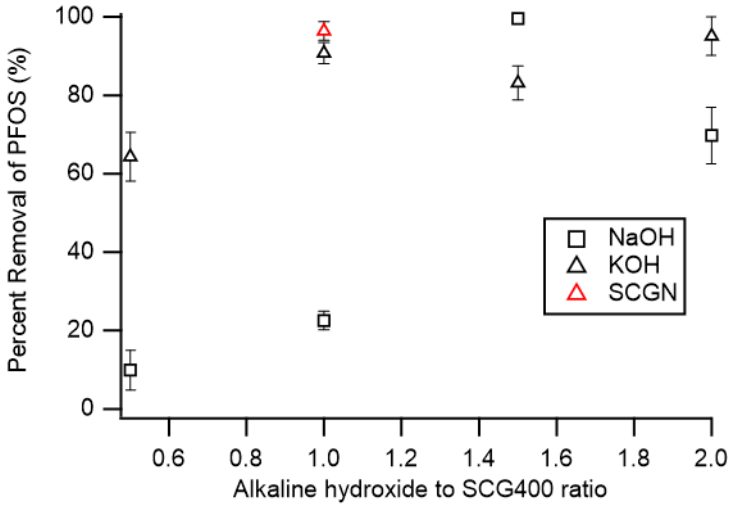

Figure 2.3 Percent removal of 44 ± 13 µg/L PFOS by 100 mg/L activated SCG biochar as a function of the ratio of alkaline hydroxide activating agent to SCG400 precursor used in production. SCGN was produced with the second batch of spent coffee grounds.

solution in methanol to obtain an initial PFOS concentration of 44 ± 13 µg/L. Samples were equilibrated for 24 h and filtered as described in **App. A**. The activated SCG400 biochar produced with 50 wt% KOH was selected for additional batch testing because of its good PFOS removal capabilities and comparatively low chemical input requirements. The activated SCG400 is henceforth identified as SCGKOH. Production and PFOS adsorption evaluation were repeated with a second SCGKOH material produced with a different batch of spent coffee grounds (SCGN; collected approximately 8 months after the first batch). Results show little difference in PFOS removal between SCGKOH batches, confirming the reproducibility of the pyrolysis and activation processes.

PFOS batch adsorption kinetics onto SCGKOH, F300, and MCG were evaluated over 5 days using triplicate, sacrificial samples for each time step. Approximately 5 mg of activated carbon was added to 50 mL of ultrapure water (Milli-Q systems, 18.2 MΩ-cm) and spiked with PFOS to obtain an initial PFOS concentration of 245 ± 20 µg/L. To control the solution pH and eliminate the effect of varying pH on PFOS adsorption,[94-96] a 4-(2-hydroxyethyl)piperazine-1-ethanesulfonic acid (HEPES) buffer was added at 5 mM, and the initial pH was adjusted to 7.0 ± 0.1 with 0.05 M NaOH. Samples were collected at various time points, filtered, and analyzed for PFOS adsorption as described in **App. A**. Kinetics data was fit to linear and non-linear pseudo first order, and linear pseudo second order kinetics models (calculations in **App. A**).

Batch adsorption isotherm tests were conducted with SCGKOH, F300, and MCG and fitted to the Langmuir and Freundlich isotherm models (calculations in **App. A**). Approximately 5 mg of activated carbon was added to 50 mL of ultrapure water and spiked with PFOS stock to obtain triplicate samples with initial PFOS concentrations between 2 and 8900 µg/L. HEPES buffer

addition and pH adjustment were conducted as described above. Samples were equilibrated for 5 days before filtration and PFOS quantification.

Effects of representative divalent cations (i.e., 26 mg/L calcium as $CaCl_2$ and 12 mg/L magnesium as $MgCl_2$) in the presence and absence of simulated wastewater effluent organic matter (sEfOM) on PFOS removal by SCGKOH, F300, and MCG were evaluated with 24-h batch testing at an initial PFOS concentration of 340 ± 23 µg/L to inform evaluation of material performance for water treatment applications. sEfOM was synthesized as discussed by Motsa et al.[97] Briefly, four representative compounds, bovine serum albumin (2.5 mg/L), sodium alginate (2 mg/L), octanoic acid (0.5 mg/L), and humic acid (5 mg/L) were chosen to mimic the protein, carbohydrate, fat, and humic composition of typical EfOM.[97-100]

2.2.6.1 Simulated Effluent Organic Matter, Divalent Cations, and HEPES Buffer

Stock solutions of BSA, sodium alginate, and humic acid were prepared by mixing 20 mg of powdered compound in 20 mL of ultrapure water, covering with parafilm, and mixing for 24-hours. Total organic carbon (TOC) concentrations of each stock solution were measured with a Shimadzu (Kyoto, Japan) TOC-L analyzer. The divalent cations, Ca^{2+} and Mg^{2+}, were added at concentrations of 26 mg/L (0.65 mM) and 12 mg/L (0.5 mM), respectively to mimic concentrations typically present in wastewater treatment plant effluent.[101]

The effect of HEPES buffer on PFOS adsorption was evaluated for the SCGKOH in the presence of divalent cations to confirm minimal interference by the buffer. HEPES was chosen as a buffer compound for: (1) its circumneutral pKa (7.0)[96] which is typical of the mid-range pH values associated with wastewater treatment plant effluent (i.e., the focus of this study);[102] (2) its lack of reaction with other species in the batch test aquatic matrices as predicted by Visual MINTEQ;[103] and, (3) its use in similar prior studies as an appropriate buffer for complex aqueous

systems containing divalent cations.[94-96] Briefly, 5 mg of SCGKOH was added to 50 mL of ultrapure water in a 50-mL polypropylene tube. An initial PFOS concentration of 91 ± 8 µg/L was achieved by spiking with a concentrated PFOS stock in methanol. Where applicable, HEPES was added at 5 mM and divalent cations were added at 26 mg/L of Ca^{2+} (0.65 mM) and 12 mg/L of Mg^{2+} (0.5 mM). Triplicate samples were rotated at 40 rpm for 24 h before filtration and LC-MS sample preparation as described previously. Results are shown in **figure 2.4** and indicate improved adsorption of PFOS in the presence of divalent cations and minimal effect of the HEPES buffer on PFOS adsorption.

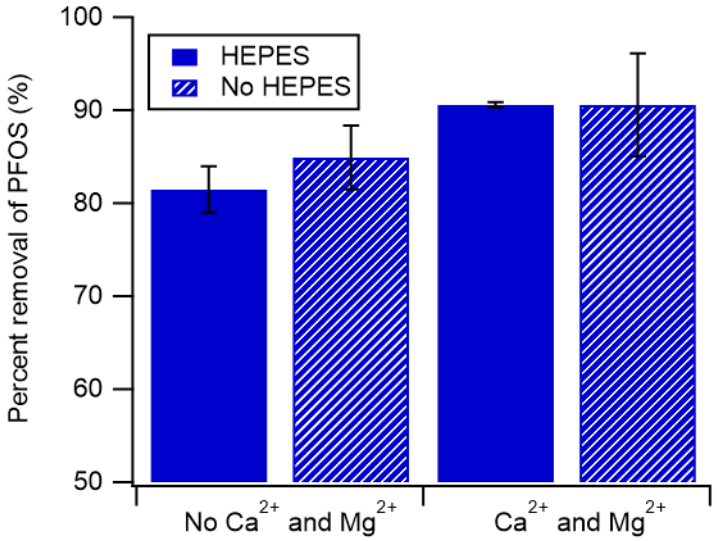

Figure 2.4 Percent removal of 91 ± 8 µg/L PFOS by 100 mg/L SCGKOH with and without calcium (26 mg/L) and magnesium (12 mg/L) ions in the presence and absence of 5 mM HEPES buffer.

2.3 RESULTS AND DISCUSSION

2.3.1 Increased Surface Area Through Alkaline Activation

Physicochemical characterization of the SCG materials indicate carbonization (i.e., increased fixed carbon content via elimination of volatile carbon) predominantly occurred in the initial pyrolysis step while a dramatic increase in surface area occurred in the second activation step. The SCG feedstock had a low fixed carbon content (17.0%) and a high volatile carbon content (81.9%, t**able 2.2**). After pyrolysis, the relative composition reversed with a fixed carbon content of 71.1%

(SCG400) to 87.1% (SCG800) and a volatile carbon content of 25.2% (SCG400) to 7.9% (SCG800). The pyrolyzed SCG had low surface areas with the SCG400 having a surface area of 3 m^2/g prior to activation and 858 m^2/g after activation.

Table 2.2 Elemental composition and proximate carbon analysis of all SCG chars, F300 and MCG materials.

sample ID[1]	elemental analysis[3,4]				proximate carbon analysis[4]		
	C %	H %	N %	O %[5]	VC %	FC %	Ash%
SCG	NA	NA	NA	NA	81.9 ± 0.3	17.0 ± 0.3	1.1 ± 0.0
SCG400	75.11 ± 0.55	4.24 ± 0.14	4.16 ± 0.05	12.76	25.2 ± 0.4	71.1 ± 0.4	3.7 ± 0.0
SCG600	79.56 ± 0.37	1.84 ± 0.08	3.86 ± 0.03	10.62	12.0 ± 0.5	83.7 ± 0.3	4.3 ± 0.2
SCG800	79.12 ± 0.79	1.15 ± 0.06	3.73 ± 0.22	11.35	7.9 ± 0.2	87.1 ± 0.1	5.0 ± 0.2
SCGKOH	81.42 ± 2.26	0.76 ± 0.02	2.17 ± 0.06	12.23	11.4 ± 0.7	84.8 ± 0.6	3.9 ± 0.2
F300[2]	87.37[2]	0.17[2]	0.72[2]	4.59[2]	5.0	83.0	6.8
MCG	81.33 ± 0.31	1.21 ± 0.05	ND	12.82	11.5 ± 0.2	83.5 ± 0.3	5.0 ± 0.5

1. Samples were 297 – 595 µm size fraction.

2. F300 elemental analysis data from the Ulrich et al. (2015).

3. Elemental analysis conducted on a wet-mass basis.

4. Values are the average of triplicate samples plus or minus the 95% confidence interval (with the exception of F300).

5. Oxygen composition calculated as 100% minus C, H, N, ash contributions.

SA – surface area; NA – not analyzed; ND – not detected, detection limit was 0.005%; VC – volatile carbon; FC – fixed carbon

The char materials used for PFOS adsorption experiments displayed comparable elemental composition characterized by high fixed carbon content. For example, the SCGKOH fixed carbon (84.8%) and ash content (3.9%) were comparable to that of F300 (83.0% and 6.8%) and MCG (83.5% and 5.0%, **table 2.2**). As expected, the proximate carbon results for F300 were similar to previously reported values[39] indicating minimal compositional change following grinding and washing processes. The SCGKOH displayed noticeably

higher nitrogen content (2.17%) than either F300 (0.72%, reported elsewhere[39]) or MCG (< 0.005%), potentially indicating the presence of nitrogen-containing functional groups (e.g., $–NH_2$ moieties) which have been shown to contribute to contaminant adsorption.[72, 104]

Table 2.3 BET surface area and pore surface area, volume, and diameter for the precursor and activated SCG biochar, F300, and MCG materials.

sample ID[1]	pore SA[2] (m^2/g)		pore size[3] (nm)	
	Adsorption	desorption	adsorption	desorption
SCG400 SCG600	No points within BJH pore size interval			
SCG800	0.61	1.25	45.55	22.50
SCGKOH	59.40	52.65	1.42	1.28
MCG	175.05	186.16	2.33	2.17
F300	112.92	121.71	2.21	2.10

1. All samples analyzed were #30 - #50 mesh particle size.
2. BJH cumulative surface area of pores between 0.8500 nm and 150.0000 nm radius
3. BJH average pore radius (2* volume/area)
SA – surface area

SCGKOH, F300 and MCG chars were characterized by high specific surface area and small average pore size (**table 2.3**), indicative of high adsorption capacity. Additionally, the char materials had a negative surface charge (**table 2.4**). DRIFTS results (**figure 2.5**) and indicate decreasing peak size and occurrence with increasing pyrolysis temperature and with activation for the SCG char materials. The peaks observed in these spectra are characteristic of highly aromatic

Table 2.4 Particle size, poly dispersity index (PDI), zeta potential, and pH measurements for the precursor and activated SCG biochar, F300, and MCG materials

	particle size (d.nm)	PDI	zeta potential (mV)	pH
SCG400	125.8	0.202	-37.8	7.46
SCG600	127.1	0.216	-47.0	7.45
SCG800	116.4	0.205	-46.2	7.64
SCGKOH	127.0	0.231	-52.0	7.66
F300	193.4	0.455	-21.5	7.68
MCG	372.8	0.377	-26.4	9.29
	232.4	0.339	-26.2	7.69

d.nm = particle diameter in nanometers
PDI = poly dispersity index

carbon materials. In particular, the broad peak observed centered around 1250 cm^{-1} for the SCG400 and SCG600 biochar can be attributed to a C–O stretching vibration,[105] the peaks near 1460 cm^{-1} and 1600 cm^{-1} are both attributed to aromatic C=C stretching vibrations,[106] the peaks centered around 2900 cm^{-1} (2800 to 3000 cm^{-1}) and the peak at 3050 cm^{-1} are attributed to aromatic C – H stretching vibration.[106] All of these physicochemical properties are characteristic of materials with a high aromatic carbon content, which is suitable for hydrophobic interactions with the hydrophobic C–F PFOS backbone (chemical structure in **figure A1, A**).[20, 107]

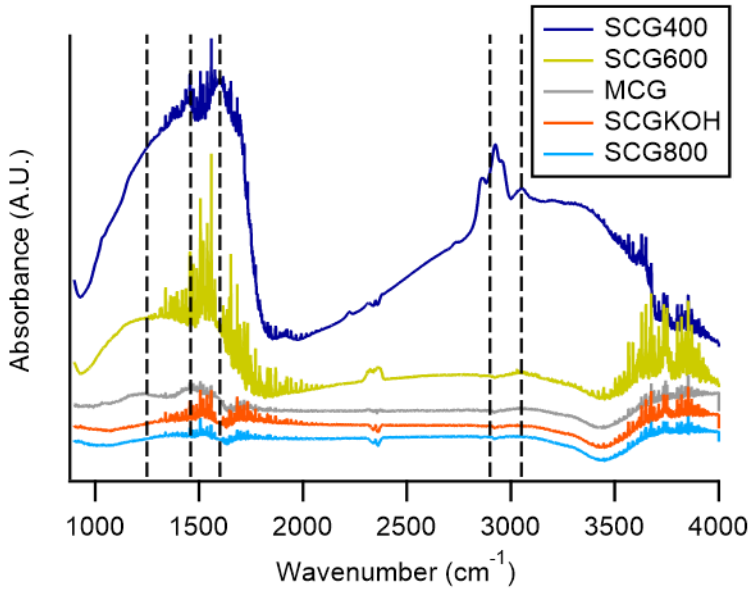

Figure 2.5 DRIFTS FTIR spectra of activated and precursor SCG biochar, and the MCG biochar. The ratio of KBr to biochar was 10:1 for all SCG char materials and 13:1 for the MCG.

2.3.2 Adsorption Kinetics Suggest Linear Driving Force

PFOS adsorption kinetics data were fit to pseudo first order (PFO) and pseudo second order (PSO) models (frequently used to describe liquid-to-solid adsorption) to obtain information about the PFOS uptake rates and dynamic adsorption behavior.[108] The non-linear PFO model derived from the Langmuir kinetic model described by Liu and Shen (calculations in **App. A**)[109] provided a better fit for all three char materials than the linear PFO and linear PSO models (**figure A2**). Results suggest PFOS adsorption is best described by a linear driving force as described by the non-linearized form of the PFO model. This corroborates previous findings that the log

transformation required for linear PFO decreases the model's ability to accurately predict adsorption processes.[110, 111] The SCGKOH, F300, and MCG chars showed fast initial PFOS uptake rates with over 70% PFOS removal within 24 h (**figure 2.6, A1-C1**). The MCG in particular exhibited rapid adsorption kinetics ($k_{1,\,MCG}$ = 0.414 h^{-1}) with the majority of adsorption occurring within the first 6 h and equilibrium attained within 24 h. Narrow pores extending throughout the MCG (**figure 2.6, C1**) may contribute to this by providing shorter diffusion distances for PFOS molecules to inner micropore spaces. The SCGKOH and F300 possessed slower initial adsorption rates ($k_{1,\,SCGKOH}$ = 0.062 h^{-1} and $k_{1,\,F300}$ = 0.090 h^{-1}), both reaching equilibrium around 48 hours and having a more uniform uptake rate throughout the initial 48 hours. This similarity in PFOS removal rates suggests SCGKOH is a promising candidate to replace commercial activated carbon during water treatment where adsorption time is often constrained by operational parameters.

2.3.3 Monolayer and Heterogeneous Binding of PFOS on Chars

Langmuir and Freundlich isotherm models fit to SCGKOH, F300, and MCG PFOS adsorption data suggest adsorption was characterized by both monolayer adsorption to homogeneous binding sites[112] (i.e., more dominant mechanism) and multilayer adsorption to heterogeneous binding sites (**figure 2.6, A2-C2**; model description in App. A). SCGKOH, F300, and MCG exhibited correlation coefficients (R^2) greater than 0.9 for both isotherm models (**figure 2.6 table**). Visual inspection of the data indicates adsorption on SCGKOH and F300 more closely follow a monolayer (Langmuir) scheme—particularly for data points at higher equilibrium PFOS concentrations—while the MCG adsorption data is equally well described by the Langmuir and Freundlich model, which denotes multilayer adsorption to sites with heterogeneous affinities for PFOS.[112] The heterogeneity of MCG adsorption sites could account for its more rapid PFOS uptake compared to SCGKOH and F300.

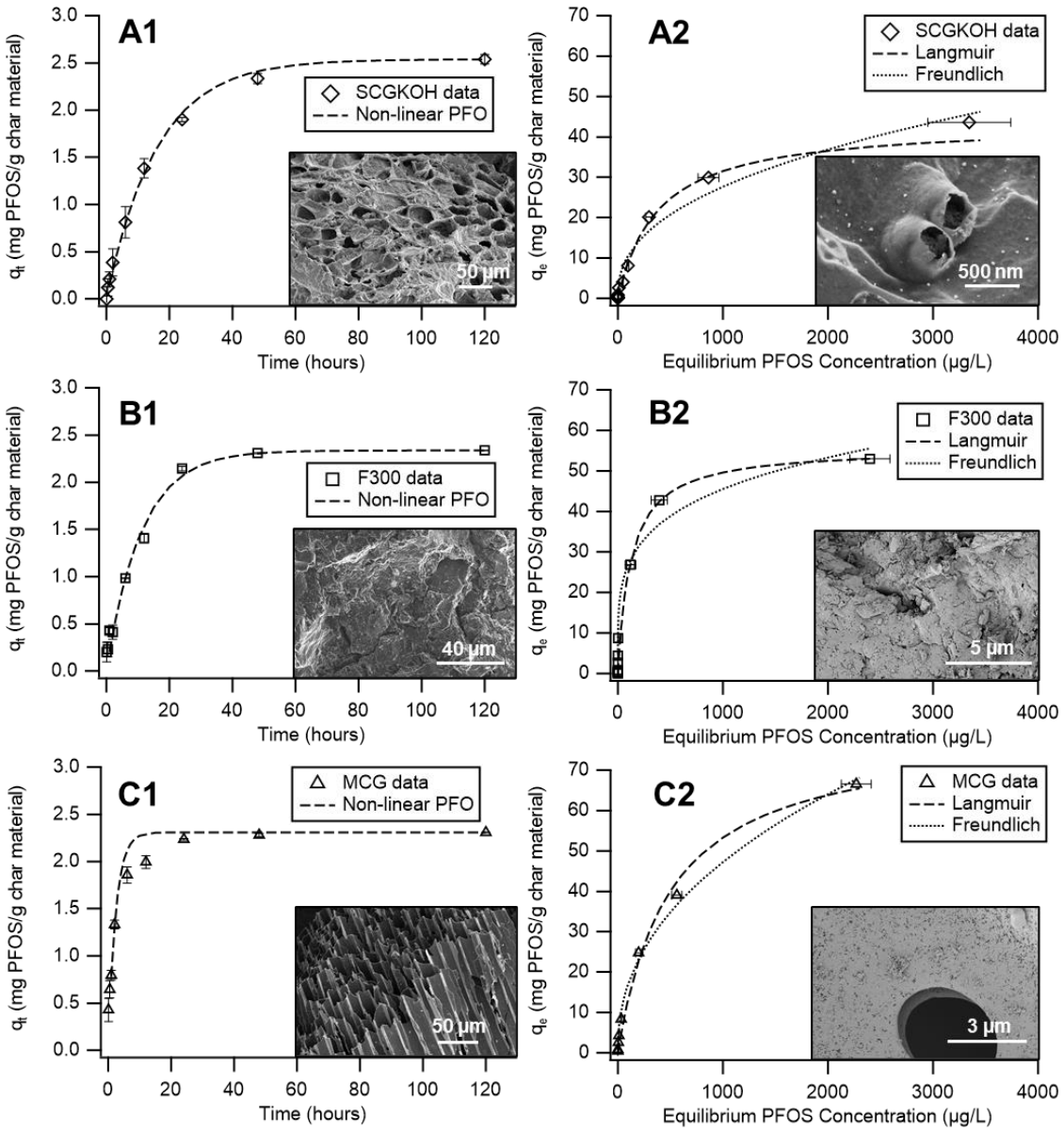

char material	non-linear pseudo first order		Langmuir			Freundlich		
	k_1 [h^{-1}]	σ^2	q_{max}	K_L	R^2	K_F	1/n	R^2
SCGKOH	0.069	0.003	43.4	0.003	0.996	1.581	0.414	0.988
F300	0.090	0.016	55.7	0.008	0.993	9.434	0.228	0.992
MCG	0.414	0.040	79.5	0.002	0.997	2.272	0.439	0.998

Figure 2.6 (1) Batch kinetics results of 245 ± 20 µg/L PFOS adsorption onto 100 mg/L (A) SCGKOH, (B) F300 and (C) MCG fit to the Langmuir kinetics-derived non-linear pseudo first order model with low magnification SEM image insets. (2) Isotherm PFOS adsorption data after a 5-d equilibrium fit to Langmuir and Freundlich models with high magnification SEM image insets. Error bars represent standard deviation of triplicate samples. Non-linear pseudo first order rate constant (k_1) and square error (σ^2), Langmuir maximum adsorption capacity (q_{max}) and adsorption rate constant (K_L), and Freundlich adsorption rate constant (K_F) and coefficient of non-linearity ($1/n$) are provided in the adjoining table.

The Freundlich n^{-1} coefficient also indicate a degree of adsorption site non-linearity (n^{-1} = 0.414, 0.228, 0.439 for the SCGKOH, F300, and MCG, respectively; **figure 2.6 table**) which may be due to multilayer adsorption or variability in adsorption site binding affinity. Some multilayer adsorption is likely due to PFOS-PFOS hydrophobic interactions[85, 113] and hemimicelle formation either in solution or on the adsorbent surface,[114] particularly at high PFOS concentrations. Additionally, differences in binding affinity may be due to decreased time required for PFOS diffusion within the larger pores and surface features (**figure 2.6, C1**).[110]

Interestingly, surface area alone was not a good predictor of adsorption capability for the three high surface area, high PFOS-adsorbing char materials. For example, MCG exhibited the lowest surface area but the greatest PFOS adsorption. Langmuir isotherm model parameter fitting for all three chars indicate MCG had the greatest PFOS adsorption capacity (79.5 mg PFOS/g char material) followed by F300 (55.7 mg/g) and then SCGKOH (43.4 mg/g). It is important to note that the unactivated SCG biochar (e.g., SCG400) possessing very low surface area also exhibit negligible PFOS adsorption (App. A), which suggests low surface area (i.e., 3–13 m^2/g) will decrease adsorption efficacy for chars. Zhi and Liu noted similar findings for PFOS adsorption onto various carbonaceous sorbents.[110] Furthermore, they suggested that point of zero charge (PZC) and adsorbent basicity (evaluated with Boehm titration) were better indicators of adsorption capability, and materials with high PZC and basicity will exhibit greater PFOS adsorption. Zeta potential results (**table 2.4**) indicate a similar hypothesis may apply to the chars examined in this study as the SCGKOH possesses the most negative zeta potential (-52.0 mV) followed by MCG (-26.2 mV) and F300 (-21.5 mV) under similar conditions. Evaluation of the PZC, surface acidity and basicity of these materials could provide a better understanding of the observed differences in PFOS adsorption capabilities.

2.3.4 Divalent Cations Improve and Hydrophobic EfOM Inhibits PFOS Adsorption

Batch adsorption tests with divalent cations common in wastewater (26 mg/L Ca^{2+}, and 12 mg/L Mg^{2+}) showed an increase in PFOS removal capability for all three chars (**figure 2.7**). In the presence of divalent cations alone, SCGKOH exhibited a 24% increase in PFOS adsorption from that exhibited in the calcium and magnesium free matrix (i.e., from 87.8% to 92.4%) while F300 and MCG each exhibited a 2% increase in PFOS removal (i.e., F300 from 84.7% to 86.5%; MCG from 93.3% to 95.3%). The presence of Ca^{2+} and Mg^{2+} has been observed elsewhere [115] to increase PFOS adsorption via ion bridging between the negatively charged char surface and the PFOS anionic headgroup. This mechanism is assumed to be principally responsible for the improved PFOS adsorption by SCGKOH as this adsorbent has the highest negative surface charge: -52.0 mV (SCGKOH) compared to -26.2 mV (MCG) and -21.5 mV (F300) under similar conditions (**table 2.4**).

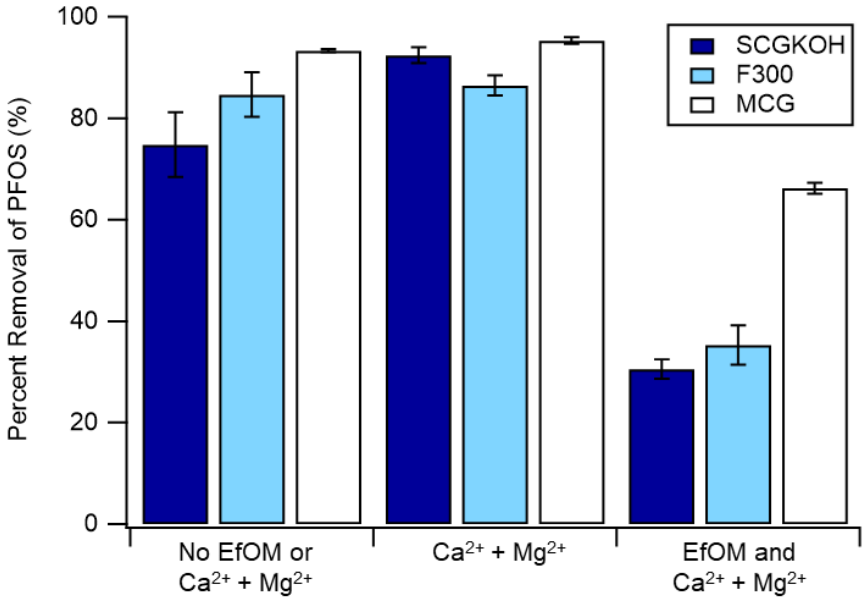

Figure 2.3 The effect of 10 mg/L simulated wastewater treatment plant EfOM, 26 mg/L Ca^{2+}, and 12 mg/L Mg^{2+} ions on 340 ± 23 µg/L PFOS removal by 100 mg/L SCGKOH, F300, and MCG.

By contrast, batch adsorption tests where representative wastewater effluent organic matter (10 mg/L simulated EfOM) was included in addition to divalent cations showed a significant reduction in PFOS removal for all media (**figure 2.7**). The SCGKOH and F300 both experienced a 60% reduction in PFOS adsorption compared to the removal in the absence of EfOM and divalent cations (i.e., SCGKOH from 74.8% to 33.6%; F300 from 84.7% to 35.3%). MCG was least

impacted with only 29% decrease in PFOS removal (i.e., from 93.3% to 66.2%). The greater MCG PFOS removal can be partially attributed to its faster uptake kinetics which allowed for the equilibrium adsorption capacity to be achieved at a faster rate. Even given this difference in uptake rates, it appears MCG is the most effective char in complex water matrices. The decrease in PFOS removal in the presence of EfOM was assumed to be largely due to competition between hydrophobic EfOM and PFOS for binding sites on the char materials, and surface passivation by EfOM.[40] Importantly, the positive effect of ion bridging by divalent cations is masked in the combined studies by the competitive adsorption of co-occurring EfOM. Further evaluation of adsorption behavior in matrices with increasing complexity could help elucidate these mechanisms.

2.4 CONCLUSIONS

Spent coffee grounds (SCG) are a widely available waste product and an ideal carbonaceous feedstock for low-cost biochar adsorbents. Initial pyrolysis of SCG produced a biochar with high carbon content, low surface area, and poor PFOS removal capabilities. Activation of this material with 50 wt% KOH resulted in more than 300-fold increase in surface area, yielding a char with PFOS removal capabilities comparable to Calgon F300 activated carbon and a wood-based biochar material with demonstrated efficacy in PFAS adsorption. Our isotherm results indicate that low µg/L PFOS concentrations found in wastewater effluent would be treated to below the EPA PFOS HAL (i.e., 70 ng/L) using the SCGKOH. Introduction of simulated wastewater EfOM decreased PFOS removal on all three char materials. However, dissolved organic matter concentrations in drinking water are expected to be much lower; therefore, drinking water treatment using SCGKOH could be a viable application. Furthermore, the high PFOS removal exhibited by SCGKOH in the presence of divalent cations indicate this material will perform well in applications with moderate to high hardness but low organic content, such as drinking water treatment. The promising PFOS

removal capabilities, abundant and low-cost waste-derived feedstock, and relatively low-resource production process make this material an advantageous option for water treatment in rural or resource-constrained areas. Future evaluation of short chain PFAS removal capability and options for spent adsorbent regeneration will improve our understanding of its capabilities for water treatment in varied systems. The size, structural integrity, and increased surface functional group heterogeneity of the SCGKOH can also facilitate further modification to improve adsorption capabilities for PFOS or other contaminants during water treatment.

Chapter 3: Novel Perfluorooctanesulfonate-Imprinted Polymer Immobilized on Spent Coffee Grounds Biochar for Selective Removal of Perfluoroalkyl Acids in Synthetic Wastewater[116]

A more selective adsorbent material is needed to efficiently treat PFAS in aqueous systems containing high concentrations of co-occurring organics and ions. Molecularly imprinted polymers (MIPs) are a class of materials designed with high selectivity for a template molecule used in production to create a binding site with size, shape, and affinity tailored to the template. In this chapter, a spent coffee grounds biochar was functionalized with a PFOS imprinted polymer layer for selective removal of PFAAs. The biochar MIP composite was shown to have higher selectivity for PFAAs than the unmodified biochar in a synthetic wastewater matrix. Regeneration of spent adsorbent was successfully achieved with a 70% methanol, 1% sodium chloride solution. This material presents a novel, low-cost option for targeted removal of PFAAs from wastewaters.

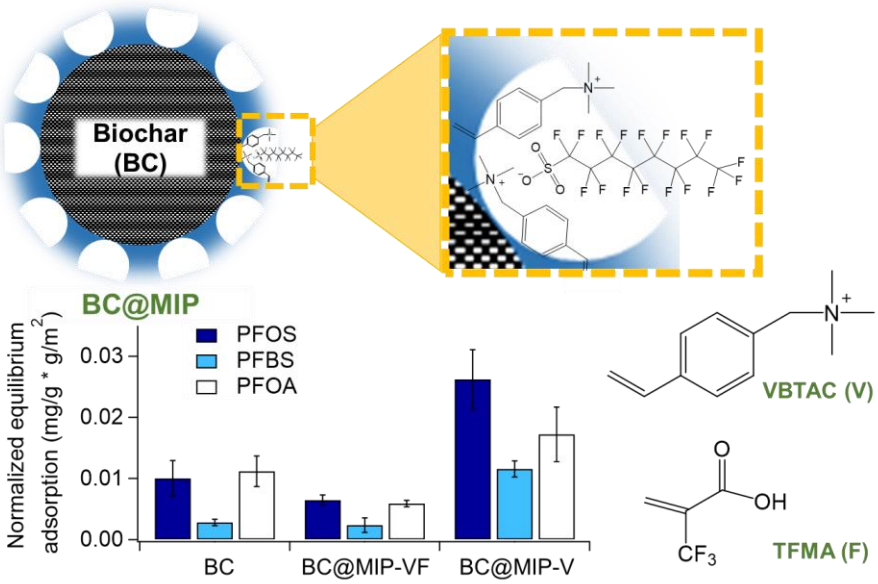

3.1 INTRODUCTION

Per- and polyfluoroalkyl substances (PFAS) are a class of chemicals which have drawn increasing attention in recent decades due to their prevalence,[10-12] persistence,[12, 13] and negative human health impacts.[14-16] In 2022 the EPA released new drinking water health advisory limits (HAL; a non-enforceable standard indicating the maximum concentration of a contaminant for which negative human health impacts are not expected to occur) for perfluoroalkyl acids (PFAAs), a particularly persistent and toxic subclass of PFAS. This HAL included exceptionally low interim levels for perfluorooctanesulfonate (PFOS, 0.02 ng/L) and perfluorooctanoate (PFOA, 0.004 ng/L), and final HALs for hexafluoropropylene oxide-dimer acid (10 ng/L) and perfluorobutanesulfonate (PFBS; 2,000 ng/L).[30] A maximum contaminant level (MCL) is currently being developed which is expected to be consistent with the 2022 HAL.[30, 117] Regulation of PFAAs has prompted a shift in manufacturing toward use of shorter-chain and polyfluorinated PFAAs which were initially thought to be less toxic and less persistent in the environment.[12] However, recent research has shown that many polyfluorinated compounds transform in water treatment systems to shorter-chain perfluorocarboxylic acids (PFCAs),[31, 118-122] and that these short-chain PFCAs share many of the same negative health outcomes with their longer-chain counterparts.[14, 15, 23] Consumption of PFAA-impacted drinking water has been identified as one of the dominant PFAA exposure routes for humans.[123] Thus, there is a critical need for identification of efficient strategies for water treatment and control of routes for PFAA contamination of water sources.

One important source of PFAAs to environmental waters and drinking water sources is wastewater treatment plant (WWTP) effluent.[11, 31-33, 117] PFAAs may enter sewage through household sources, industrial discharges,[117] or landfill leachate,[124, 125] and are then removed poorly (if at all) by conventional wastewater treatment processes.[31] Wastewater effluent and biosolids

containing PFAAs will be introduced to the environment (e.g., land application of PFAA-contaminated biosolids followed by leaching into stormwater runoff and to surface waters) where they may disperse or become PFAA point sources for downstream drinking water supply. This is a particularly important consideration for areas where water reuse is being implemented or considered, such as in water-constrained areas of the American (South)West.[80]

One challenge associated with PFAA removal from WWTP effluent is the lack of targeted separation approaches. The industry standard for PFAA separation in water is adsorption onto activated carbon (AC)[8, 85, 126]—a highly porous, pyrolyzed carbonaceous media with high specific surface area capable of adsorbing a wide variety of organic and inorganic pollutants. In WWTP effluent containing high dissolved organics or salt concentrations, competition for AC active sites arises leading to modest PFAA removal rates[40]—particularly for shorter-chain PFAA compounds.[12] For example, wastewater effluent typically contains around 10 mg/L of total organic carbon (TOC),[98, 100] 200–1000 mg/L of total dissolved solids (TDS; i.e., salts),[127] and much lower concentrations of PFAA (0.01 ng/L–50 μg/L)[31, 32] and other trace organics (0.0–20 μg/L).[98, 128] Effective removal of PFAAs from these complex wastewater matrices presents a unique challenge for activated carbons. This challenge was highlighted in our prior study that described the development of a sustainably sourced and cost-effective activated biochar which exhibited high PFAA removal comparable to a commercially available AC. In the absence of other organics, our biochar—sourced from spent coffee grounds—achieved 92.4% removal of 340 ± 23 μg/L PFOS but experienced a significant decrease in PFOS removal (i.e., 33.6% PFOS removed) when synthetic effluent organic matter (sEfOM) was included in the reaction matrix.[1] Pretreatment to remove dissolved organics and salts could increase PFAA separation efficacy by activated carbons and biochar; however, this is an expensive option and likely impractical for the majority of

WWTPs. In addition to reduced PFAA adsorption in complex aquatic systems, a safe and reliable disposal method for spent, PFAA-loaded AC has yet to be identified. Typically, spent AC is landfilled or incinerated,[19] both of which present environmental hazards.[125, 129] Thus, there is a need for more selective, regenerable adsorbent materials capable of achieving targeted removal of PFAAs over multiple adsorption and regeneration cycles.

Molecularly imprinted polymers (MIPs), a class of polymers traditionally used for sensing compounds,[54, 55] may offer an exciting opportunity for selective PFAA adsorption. During synthesis, a target organic molecule (e.g., the PFAA adsorbate) is used as a template to create an active site with size, shape, and affinity specifically tailored to the target molecule.[53-55] A three step approach is commonly employed for synthesis of molecularly imprinted polymer adsorbents: pre-polymerization mixing to form a template-monomer complex followed by polymerization and then washing to remove imprinted template.[53, 56, 60, 130-132] First, a functional monomer is typically mixed with the template compound for a defined pre-polymerization assembly time. During this step, weak attractive forces (i.e., van der Waals forces) promote binding of the template and monomer to form self-assembled ligands. Functional monomers are often selected with specific moieties (e.g., quaternary nitrogen or fluorocarbon) or properties (e.g., hydrophobicity, hydrophilicity, or charge) that will enhance the affinity for the template and increase imprinting success in this self-assembly step.[53-55, 57] Next, a crosslinker is introduced which links the functional monomers and provides structural stability for the final polymer product. Typically, a high crosslinker to monomer ratio is used, making crosslinker selection a key determining factor in the final morphology and physicochemical properties of the MIP.[55, 57] Finally, polymerization is initiated through chemical, thermal, or physical means and allowed to proceed for a set amount of time or until self-termination. A common polymerization technique—thermally activated

radical initiated polymerization—involves addition of an initiator compound (e.g., 2,2'-azobis(2-methylpropionitrile), AIBN) which, when heated, promotes formation of radical groups from –NH moieties and initiates the formation of a vinyl polymer from monomer and crosslinker compounds containing one or more R=R moieties.[55, 57] The final step is to rinse the MIP with an extraction solution to remove the target molecule. The same template extraction process can be leveraged to regenerate spent MIP media to create a concentrated PFAA solution from which PFAAs could be extracted either for reuse in manufacturing processes or for subsequent disposal.

The MIP synthesis approach enables high selectivity for the template compound—even in the presence of compounds with similar structure or charge—and makes MIPs an ideal candidate for use as a sensor or adsorbent for classes of compounds present at low concentrations in complex matrices (e.g., PFAA removal in wastewater effluent). For example, in a study by Krupadam et al., 82% of a 0.12 mg/L polycyclic aromatic hydrocarbon (PAH) mixture spike was removed and recovered by a six PAH-templated MIP in diluted groundwater containing 430 mg/L chemical oxygen demand (COD) and 690 mg/L TDS.[132] Prior research has demonstrated the effectiveness of MIP materials containing positively charged nitrogen and fluorocarbon moieties as PFAA sensors with detection limits in the low nanograms per liter range[54, 133, 134] and as adsorbent media with adsorption capacities as high as 76 mg/g.[53] For example, Deng et al. achieved around 60% removal of 200 mg/L PFOS at pH 4 with a PFOA-templated MIP using 4-vinylpyridine (a functional monomer containing a charged nitrogen moiety).[61] Takayose et al. demonstrated use of a fluorocarbon-containing functional monomer (2-(trifluoromethyl)acrylic acid, TFMA) and crosslinker (2,2,3,3,4,4-hexafluoropentan-1,5-diyl dimethacrylate, HFPDMA) that increased the PFOA retention factor of their MIP sensor 5–10 times when compared to a similar MIP sensor produced with non-fluorocarbon containing monomer and crosslinker.[55] However, while these and

other MIPs have been demonstrated to possess high selectivity and high affinity for templated PFAAs, polymerization results in a fine powder media which limits MIP use during traditional water filtration applications.

To overcome this obstacle to deployment, several studies have fixed MIPs onto structural frameworks such as silica particles, carbon and titanium oxide nano tube arrays, and carbonaceous media.[53, 56, 135-137] Biochar materials have several key advantages that make them an ideal substrate for MIP functionalization. First, the waste feedstock (e.g., spent coffee grounds) from which they are often produced have the advantage of being relatively low cost and widely available compared to many other substrate options.[138, 139] Second, the high specific surface area and density of micropores characteristic of activated carbons and biochar—which has been shown to be a significant contributor to the success of these materials as adsorbents[140]—is expected to be retained during the MIP functionalization and aid in their water treatment capabilities. Third, biochar materials contain a high density of surface functional groups and are easily modifiable to add or alter functional groups via well-established processes. In MIP functionalization applications, these functional groups can act as potential receptor sites where crosslinking of the substrate to the MIP may occur.[53] In particular, surface functional groups containing –NH moieties are expected to participate in radical-initiated polymerization since these bonds have been shown to form radicals upon interaction with radical initiator compounds like AIBN.[57, 61] One example of this method is the PFOS-templated MIP-functionalized carbon microsphere developed by Guo et al. using [2-(Methacryloyloxy)ethyl] trimethylammonium chloride and TFMA as functional monomers which removed 29.7% of 50 μM PFOS at pH 3 in the presence of other PFAAs and competing organics.[53] However, there is still a need for additional research into MIP-substrate composite adsorbents capable of removing both long- and short-chain PFAAs at environmentally relevant pH ranges.

In this study, a MIP material assembled with PFOS template was functionalized onto a previously developed spent coffee grounds activated biochar[1] to produce a novel adsorbent composite with high PFAA selectivity. PFOS was chosen as a template compound because: (1) it can participate in relatively strong electrostatic and hydrophobic interactions compared to other PFAAs which will increase the likelihood of successful imprinting;[20, 110] (2) the 8-carbon backbone length should result in MIP binding sites capable of adsorbing a number of equal-length and shorter PFAAs;[141, 142] and, (3) it is one of the most widely detected PFAAs in the environment.[79] The objectives of this study are to: (1) modify the spent coffee grounds biochar with nitrogen containing functional groups via low-impact methods that do not significantly alter the biochar structure or PFAA removal capability; (2) functionalize the nitrogen-modified biochar with a PFAA selective MIP layer; and, (3) evaluate the ability of the MIP-functionalized biochar (BC@MIP) to selectively remove and recover PFAAs in ultrapure water and synthetic wastewater matrices. Prior works have established MIP materials as strong candidates for selective removal of PFAAs from aqueous systems.[53, 54, 56, 143, 144] To our knowledge, however, functionalization of a MIP onto a biochar substrate and evaluation of PFAS imprinted polymer performance in synthetic wastewater have yet to be explored. Development and characterization of a BC@MIP adsorbent for targeted PFAA adsorption and recovery described herein can provide more environmentally sustainable and advantageous alternatives to activated carbon for PFAA separation during water treatment.

3.2 MATERIALS AND METHODS

3.2.1 Chemicals and materials

Spent coffee grounds (SCG) for biochar production were donated by Bay Laurel Catering Services at the University of Washington (Seattle, WA) from Starbucks® Pike Place® grounds,

medium roast, arabica coffee sourced from Latin America after use in an industrial drip coffee maker.

All chemicals used for this study were ACS reagent grade or equivalent unless otherwise noted. Potassium hydroxide pellets and high purity nitrogen gas (99.998%) used for biochar production were purchased from Fisher Scientific (Waltham, MA) and Praxair (Danbury, CT), respectively. Nitrogen modification of the SCG biochar was accomplished with sulfuric acid (H_2SO_4, 95 – 98%), nitric acid (HNO_3, 69%), glacial acetic acid (EMSURE®, 99.8%), ammonium chloride (99.5%) purchased from VWR Chemical (Radnor, PA); sodium dithionate (technical grade) and ammonium hydroxide solution (28 – 30%) purchased from Sigma Aldrich (St. Louis, MO); and isopropyl alcohol (IPA) and melamine (99% assay) purchased from Thermo Fisher Scientific (Hampton, NH).

Molecularly imprinted polymers were synthesized using perfluorooctanesulfonate potassium salt (PFOS, 98.0%) purchased from Sigma Aldrich as the template; vinylbenzyl trimethylammonium chloride (VBTAC, 96.0%) purchased from Thermo Fisher Scientific, and 2-(trifluoromethyl)acrylic acid (TFMA, 98%) and [2-(Methacryloyloxy)ethyl] trimethylammonium chloride solution (DMC, 75% in H_2O) purchased from Sigma Aldrich as functional monomers; N,N'-methylenebisacrylamide (MBA, 96.0%) purchased from Thermo Fisher Scientific as the crosslinker; 2,2'-azobis(2-methylpropionitrile) (AIBN, 98%) purchased from Sigma Aldrich as the initiator. Methanol purchased from Fisher Scientific and sodium chloride (NaCl) purchased from VWR Chemical were used for template washing and regeneration of spent adsorbent.

Optima™ LC/MS grade methanol purchased from Thermo Fisher Scientific was used for preparation of stock solutions and LC-MS/MS samples for all batch tests. Perfluorooctanesulfonate potassium salt (PFOS, 98.0%), perfluorooctanoate potassium salt

(PFOA, 95%), perfluorobutanesulfonic acid (PFBS, 97%), Reagent Plus® grade caffeine, pentachlorophenol (PCP, 97%), bovine serum albumin lyophilized powder (96%), alginic acid sodium salt from brown algae, technical grade humic acid, octanoic acid (98%), calcium chloride (99%), 4-(2-hydroxyethyl)piperazine-1-ethanesulfonic acid (HEPES, 99.5% purity by titration), and 0.2 micron, 25 mm diameter cellulose acetate (CA) syringe filters for sample filtration were purchased from Sigma Aldrich. HPLC grade fipronil (97%) was purchased from Chem-Impex International (Wood Dale, IL). Magnesium chloride (99%) was purchased from VWR Chemical and sodium hydroxide was purchased from Fisher Scientific. Analytical and mass-labeled PFAS standards were purchased from Wellington Laboratories (Ontario, Canada). Mass labeled diuron-d_6 purchased from Sigma Aldrich was used as the internal standard for caffeine quantification since both compounds elute at similar retention times and are measured via positive electrospray ionization in the mass spectrometer.

3.2.2 Spent Coffee Grounds Biochar Surface Nitrogen Functionalization

The spent coffee grounds biochar (so called "BC") was produced from locally sourced waste material via a two-step process: pyrolysis followed by chemical activation with potassium hydroxide. This process and the physicochemical characterization of the BC is described in detail in our previous publication.[1]

Two primary methods were explored for addition of nitrogen-containing surface functional groups to the BC substrate to facilitate subsequent polymer functionalization via radical initiated polymerization: (1) electrophilic aromatic substitution followed by reduction (adapted from Yang et al., 2014),[72] and (2) addition of melamine or ammonium chloride via heating in a muffle furnace (adapted from Kasera et al., 2021).[69] In the first method, nitro ($–NO_2$) groups were functionalized on the biochar surface by mixing the SCGKOH with equal volumes of concentrated nitric (69%)

and sulfuric (98%) acids at a 1:17 mass:volume ratio (i.e., for every 1 g of SCGKOH, 17 mL of each acid was added). This mixture was placed in an ice bath inside a fume hood and stirred for 3 h. At the end of the reaction period, the reaction solution was diluted five times with ultrapure water (Milli-Q; 18.2 MΩ-cm; Millipore Sigma) and filtered using a vacuum pump filter and Whatman GF/A 42.5 mm filter paper (Whatman, United Kingdom) to collect the biochar. The collected biochar was then added to 50 mL of ultrapure water in a polypropylene tube and rotated at 40 rpm for 30 minutes to wash off residual acid. The wash process was repeated with isopropyl alcohol, and the final product was dried at 90 °C overnight and stored in an airtight container prior to further modification or characterization. To reduce nitro groups to amine ($–NH_2$) groups, 2.2 g of the dried nitro-modified SCGKOH was added to 22 mL of ultrapure and 8.8 mL of ammonium hydroxide and stirred for 15 min. Then, 12.1 g of sodium dithionite was added, and the mixture was stirred for 20 h at 200 rpm. Next, 52.8 mL of acetic acid was added, and the mixture was heated at 98 °C under reflux for 5 h. After the 5-h reaction, the solution was filtered with Whatman GF 100 filter paper and washed to remove residual reaction solution. Washing steps were as follows: ultrapure water for 1 h, isopropyl alcohol for 1 h, ultrapure water for 30 min. All washes were conducted with 50 mL of wash solution in a polypropylene tube and rotated at 40 rpm. The final product was designated biochar-N (BC-N). A BC-N2 material was also prepared via the same general method (with a 6 h mixing time during the first nitration step) and functionalized with the MIP; however, initial evaluation of this substrate material showed poor PFOS removal. Thus, further discussion of this material and its modifications are confined to ***sections B1***, ***B2***, ***B4***, and ***B5***.

In the second method, either melamine or ammonium chloride was measured such that 1 g N was added per 1 g of SCGKOH. The melamine or ammonium chloride was mixed with ultrapure

water (15 mL water per g SCGKOH), and then added with the SCGKOH to a ceramic crucible (VWR, Radnor, PA). The crucible lid was added, then the vessel was heated in a muffle furnace (Seattle Pottery Supply, Inc., Seattle, WA) at 400 °C for 1 h before the crucible was allowed to cool to room temperature. The final material was rinsed with ultrapure water to remove unreacted melamine or ammonium chloride and dried at 90 °C for 24 hr. Modified biochar were designated BC-M (melamine) and BC-A (ammonium chloride).

Two alternative methods for nitrogen modification of biochar were also evaluated but found to perform poorly compared to the BC-N, BC-M, and BC-A materials, thus the experimental details and results for these materials are confined to the Supplemental Information (**Appendix B**).

3.2.3 Physicochemical Characterization of Nitrogen Functionalized Biochar

Several types of nitrogen-containing functional groups are commonly found in highly aromatic carbon materials (like biochar) and were expected here based on results of previous studies, including: pyrrolic-N, pyridinic-N, amine-N, graphitic-N, and pyridinic-N^+ oxides (**figure 3.1**).[69, 70, 72, 145] Pyrrolic, amine, and some quaternary nitrogen groups all contain an $–NH_x$ moiety that can participate in radical initiated polymerization, and were thus the desired types of nitrogen groups for this study.[57, 61] Nitrogen modification was performed to increase the naturally occurring percentage of -NHx groups on the biochar substrate. The BC-N, BC-M, and BC-A were characterized using several techniques described below to confirm modification success, characterize the types of nitrogen-containing functional groups, and quantify the coverage and extent of each type.

Thermogravimetric analysis (TGA) was performed to quantify the mass of nitrogen-containing functional groups added to the modified BC. The mass added was calculated as the

absolute value of the difference between the mass lost from the modified and unmodified BC. TGA was performed from room temperature to 800°C at a ramp rate of 10 °C/min on a TA Instruments (New Castle, DE) TGA Q50 with a nitrogen purge throughout.

Proximate carbon analysis paired with elemental analysis was performed to quantify the mass percentages of nitrogen and oxygen added to the biochar materials during nitrogen modification. Proximate carbon analysis was completed using the ASTM D1762-84 method (reapproved 2007),[90] and details are given in our previous study.[1] Carbon, hydrogen, nitrogen (CHN) elemental analysis was completed on a Perkin Elmer (Waltham, MA) 2400 Series elemental analyzer. The oxygen content was calculated as the remainder out of 100% after carbon, hydrogen, nitrogen, and ash.

Two spectroscopic analyses were performed to identify and quantify the nitrogen surface functional groups. X-ray photoelectron spectroscopy (XPS) was conducted on a Kratos (Manchester, UK) Axis Ultra DLD X-ray Photoelectron Spectrometer. XPS data was referenced to an adventitious carbon peak with binding energy of 285.0 eV. Additional peak fitting details are included in ***section B3***. Diffuse Reflectance Fourier Transform Infrared Spectroscopy (DRIFTS) measurements were collected on a Thermo Scientific™ (Waltham, MA) Nicolet™ iSTM10 FT-IR Spectrometer using a KBr to biochar mass ratio of 10:1. Collected spectra were corrected with the atmospheric suppression and auto background corrections available in the OMNIC processing software from Thermo Fisher.

3.2.4 Molecularly Imprinted Polymer Coating of Biochar

A layer of MIP was functionalized on the surface of the nitrogen-modified biochar via thermally activated radical initiated polymerization to increase selectivity of the adsorbent for PFAAs. Three functional monomers were chosen for polymerization: two containing a quaternary

nitrogen moiety (vinylbenzyl trimethylammonium chloride, VBTAC and [2-(Methacryloyloxy)ethyl] trimethylammonium chloride, DMC) and one containing a fluorocarbon moiety (TFMA). The monomers were used individually or in combination as described in **table 3.1**. Quaternary nitrogen moieties have been shown to retain a positive charge over a wide pH range and have been hypothesized to electrostatically attract the negatively charged headgroups of

Table 3.1 MIP composite composition, BET specific surface area and pore size.

				functional monomers	
adsorbent name[1]	biochar substrate	BET surface area (m^2/g)	pore size[2] (nm)	VBTAC 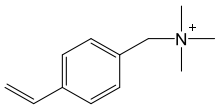	TFMA 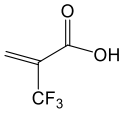
spent coffee grounds biochar	BC	858	1.42	-	-
BC-N@MIP-V	BC-N	741	1.53	Y	-
BC-A@MIP-VF	BC-A	1054	1.47	Y	Y
BC-M@MIP-VF	BC-M	806	1.56	Y	Y
BC-M@MIP-V	BC-M	155	8.88	Y	-

1. All samples analyzed were #30-#50 mesh particle size

2. BJH average pore radius (2V/A)

VBTAC: (vinylbenzyl) trimethylammonium chloride; TFMA: (2-(trifluoromethyl)acrylic acid

most PFAA compounds across environmentally-relevant pH ranges—an important feature for selective PFAA adsorption.[46, 53, 55, 146] Therefore, VBTAC and DMC were chosen for their similar molecular length to PFOS, a property which has been shown to increase interactions in aqueous systems.[141, 142] Fluorocarbon-containing functional monomers were demonstrated to improve adsorption of long-chain PFAAs during MIP synthesis.[53] N,N'-methylenebisacrylamide (MBA) was used as a crosslinker because it is highly water soluble and thus a common option for synthesis of hydrophilic MIP materials intended for use in aqueous systems;[53, 57] and 2,2'-azobis(2-

methylpropionitrile) (AIBN) was used as the radical initiator commonly used for MIP synthesis.[56, 61, 147]

MIP production was accomplished in three steps: pre-polymerization mixing, thermally activated radical initiated polymerization, and template washing. Briefly, approximately 0.43 mmol of PFOS and 0.86 mmol of each functional monomer were added to 170 mL of ultrapure water and stirred at 150 rpm at room temperature for 10 h to allow the template and functional monomers to align. At the same time, 0.5 g of N-modified biochar was added to approximately 40 mL of ultrapure water in a separate container and allowed to sit for 10 h to pre-wet the biochar. At the end of the pre-polymerization time, 8.59 mmol MBA and the wetted biochar were added to the polymerization mixture and mixed for 30 min. Next, 1.00 mmol AIBN was added to the reaction vessel to initiate polymerization and the reaction solution was mixed at 150 rpm and 60 °C in a water bath for 15 hr. Following polymerization, the functionalized biochar was separated from solution and rinsed with methanol to remove unattached polymer. Finally, the functionalized biochar was placed in 100 mL of a 70% methanol/1% NaCl solution and shaken at 200 rpm and 33 °C for 24 h to extract the template. This process was repeated until the PFOS concentration in the wash solution dropped below 2000 μg/L (a significant decrease from PFOS concentrations in the first wash which are typically around 100 – 200 mg/L), at which point the biochar was washed for 24 h in ultrapure water and then dried at 60 °C overnight. The final product was then stored in a sealed container for further use.

3.2.5 Characterization of Molecularly Imprinted Polymer Layer

Several characterization methods were undertaken to evaluate the extent and thickness of the polymer layer. A JOEL JSM-6010PLUS/LA Analytical Scanning Electron Microscope (SEM; JOEL, Peabody, MA) was used to image the samples and measure coating thickness. Transmission

Electron Microscopy (TEM) samples were embedded in a Mollenhauer epoxy resin which was polymerized at 60 °C overnight, then microtomed to 80 nm using a Leica EM UC6 and a hard diamond knife, dried on a carbon mesh, and stored in a desiccator until imaging. An FEI Tecnai G2 F20 Twin or Tecnai G2 F20 SuperTwin Transmission Electron Microscope (FEI, Hillsboro, OR) was used to visualize the thickness of the polymer layer and provide insight into the extent of the MIP functionalization. Specific surface area was measured with nitrogen adsorption at 77K and Brunner-Emmet-Teller (BET) fitting on a Micromeritics 3Flex Analyzer (Micromeritics, Norcross, GA) to quantify changes in the specific surface area (SSA) resulting from the nitrogen modification and polymer functionalization processes.

3.2.6 Batch Adsorption Tests for PFOS Selectivity

Three batch adsorption tests were performed to evaluate PFAA removal capabilities and selectivity of the MIP-biochar materials. For all batch tests, 50 mL of the reaction matrix and 5 mg of MIP-functionalized biochar were first added to a 50 mL polypropylene tube followed by sufficient volume of methanol-based PFAA (or organic contaminant) stock solution to achieve the desired initial concentration while maintaining a methanol concentration of not more than 1% v/v. Samples were prepared in triplicate, rotated for 4 days to achieve equilibrium adsorption, then filtered and prepared for analysis (***section B8***). First, adsorption of 4275 ± 342 μg/L PFOS was evaluated for all MIP materials in ultrapure water to provide information on the relative adsorption capacity for the template compound. The importance of functional monomer selection was particularly evident for this test because no competing contaminants were evaluated. Second, adsorption of 1476 ± 207 μg/L PFOS, 1166 ± 153 μg/L PFBS, and 1453 ± 582 μg/L PFOA in ultrapure water was performed to evaluate adsorption capabilities for PFAAs of different chain length (PFBS, 4-chain) and head group (PFOA, carboxylic acid) from the template (8-chain,

sulfonic acid). A PFAA shorter than PFOA and PFOS (i.e., PFBS) was included due to the greater production and environmental detection of short-chain PFAAs compared to longer PFAAs.[12] Sample pH was not adjusted or controlled during these two screening batch tests; however, final pH was measured and found to be 6.5 ± 0.5. Results from these tests were used to screen the MIP-functionalized biochar composites, and the BC-N@MIP-V, BC-M@MIP-VF, and BC-M@MIP-V composites were chosen for further evaluation (**table 3.1**). Finally, PFAA adsorption was evaluated in a synthetic wastewater matrix containing compounds representative of key components found in WWTP effluent: divalent cations and synthetic effluent organic matter (sEfOM; details provided in ***section B6*** and in a prior publication),[1] PFAAs (i.e., 1659 ± 99 µg/L PFOS, 1400 ± 11 µg/L PFBS and 2313 ± 71 µg/L PFOA), and co-occurring organic contaminants (i.e., 1916 ± 76 µg/L caffeine, 1520 ± 63 µg/L fipronil, and 3385 ± 217 µg/L pentachlorophenol (PCP)). Concentrations of PFAAs and co-occurring organics were set to be approximately equal to each other to assess the ability of the MIP-biochar composites to selectively adsorb PFAAs in a complex matrix representative of secondary wastewater effluent conditions[32, 33, 148-150] Concentrations were much higher than would typically be found in wastewater effluent to better differentiate the adsorption capabilities of each adsorbent material. The pH was adjusted at the start of the test to 7.0 ± 0.1 with sodium hydroxide (NaOH) and buffered with 5 mM HEPES to maintain a constant pH throughout the test. Final concentrations of PFAAs and organic contaminants were analyzed via tandem liquid chromatography-mass spectrometry (LC-MS/MS, ***section B8***).

Normalized equilibrium adsorption ($q_{e,SSA}$) and the liquid-solid distribution coefficient (K_d) were calculated from the results of each batch test using the following equations:

$$q_{e,SSA} = (C_0 - C_e) * \frac{V}{m_{ads}} * \frac{1}{BET\ SA} \qquad \text{Eqn. (3.1)}$$

$$K_d = \frac{C_0 - C_e}{C_e} * \frac{V}{m_{ads}}$$ Eqn. (3.2)

Where C_0 and C_e were the initial and equilibrium adsorbent concentrations (mg/L), V was the sample volume (L), m_{ads} was the adsorbate mass (g), and the BET surface area (*BET SA*) was taken from **table 3.1** (g/m^2). The selectivity coefficient ($K_{selectivity}$) was calculated from the results of the PFAS competition test in ultrapure water and the synthetic wastewater batch tests using equations 3–5, as described by Fan et al. and de Escobar et al.[131, 151] The PFOS template was used as the reference adsorbate and the unmodified BC was used as the reference adsorbent.

$$K_{imprinted} = \frac{q_{e,BC@MIP,PFOS}}{q_{e,BC@MIP,PFOA/PFBS/organics}}$$ Eqn. (3.3)

$$K_{comparison} = \frac{q_{e,SCGKOH,PFOS}}{q_{e,SCGKOH,PFOA/PFBS/organics}}$$ Eqn. (3.4)

$$K_{selectivity} = \frac{K_{imprinted}}{K_{comparision}}$$ Eqn. (3.5)

3.2.7 Regeneration of Spent Adsorbent

Single cycle regeneration of spent adsorbent was performed following adsorption of PFOS in ultrapure water and following adsorption of PFAAs and co-occurring organics in the synthetic wastewater matrix to assess opportunities for reuse. The template extraction wash solution described in ***section 3.2.4*** was used for composite imprinting site regeneration. Briefly, after collection of LC-MS/MS samples for each adsorption test, the remainder of the adsorption solution was decanted and 50 mL of 70% MeOH/1% NaCl was added to each test tube of spent adsorbent. Samples were capped, wrapped in parafilm to minimize evaporation of MeOH, and rotated at 40 rpm for 24 h to facilitated desorption prior to analyte concentration quantification (***section B8***).

3.3 RESULTS AND DISCUSSION

3.3.1 Comparable total nitrogen obtained from biochar modification

Elemental and proximate carbon analyses reveal an increase in both nitrogen and oxygen composition for the BC-N, BC-M, and BC-A that was corroborated by an increase in total surface functional group mass identified with TGA. Elemental analysis revealed a wide range of nitrogen compositions: 13.0% for BC-M, 3.0% for BC-A, and 1.8% for BC-N (**table B1**). It is important to note that a significant portion of the nitrogen from the melamine modified materials is expected to be unavailable for MIP polymer attachment because it is not bonded to one or more hydrogen atoms (i.e., pyrrolic-N, amine-N, or quaternary-N). Percent mass change in oxygen composition, obtained through elemental and proximate carbon analysis, was not directly correlated with percent change in nitrogen composition. BC-A had the highest oxygen content (29.4%) followed by BC-N (23.7%) while BC-M had the lowest oxygen (19.5%). Increased oxygen content is often correlated with a greater negative surface charge since many of the common oxygen-containing surface functional groups are deprotonated at environmental pH ranges. Thus, high oxygen content may be an indicator of poor PFAA removal if the negative surface charge is of sufficient magnitude to repel the negatively charged PFAAs (particularly PFBS) and interfere with other adsorption processes.

TGA, in contrast, provided information on the total mass of nitrogen- and oxygen-containing surface functional groups and the strength of their attachment (**figure B1**). TGA results revealed that the BC-N material experienced a larger increase in mass lost (23.1%) than either the BC-M (9.1%) or BC-A (3.4%) materials when compared to the unmodified BC. The mass loss during TGA can represent the mass of surface functional groups present on a substrate surface.[152, 153] The larger mass loss from the BC-N compared to BC-M is somewhat contradictory since the melamine modified biochar exhibited the greatest increase in nitrogen composition and indicate a higher

temperature is needed for complete volatilization of functional groups required for effective analysis of these materials using the TGA method. Even so, both elemental analysis and TGA results suggest the BC-M material will have the greatest success for MIP attachment. Melamine addition appeared to present the most stable reaction of a nitrogen source with the bulk biochar substrate which likely accounts for the high nitrogen yield from this method. Nitrogen addition with ammonium chloride (i.e., BC-A) instead of melamine as the nitrogen source was likely less successful because a large percentage of the ammonium chloride volatilized before reacting with the biochar (as evidenced by the formation of ammonium chloride crystals in the interior of the muffle furnace following production).[154] Similarly, nitrogen addition via nitration with concentrated acids (i.e., BC-N approach) may have been ineffective because exposure to the acids may have eroded aromatic moieties from the biochar surface to form nitroaromatic compounds (observed as a yellow color in the diluted final reaction solution).

XPS results confirmed the BC-M material was likely to undergo the most successful MIP functionalization owing to the high density of –NH moieties on the surface. Interestingly, the number of –NH moieties were noticeably higher for the BC-M substrate than for either the BC-A or BC-N substrates despite the large percentage of nitrogen on the BC-M only bonded to carbon or oxygen. Four main types of nitrogen containing surface functional groups were identified via XPS (**figure 3.1A - D**): pyridinic-N (398.9 ± 0.1eV), pyrrolic-N (400.4 ± 0.2eV), quaternary-N (401.5 ± 0.3eV), and pyridinic-N^+ oxides (403.4 ± 0.8eV).[69, 70, 145] Amine-N (near 399.5eV) was not identified on any of the materials.[69] Both the total nitrogen and density of $–NH_x$ groups hypothesized to be available for MIP attachment followed the trend BC-M > BC-A > BC-N > unmodified BC, as detailed in the **figure 3.1 table**.

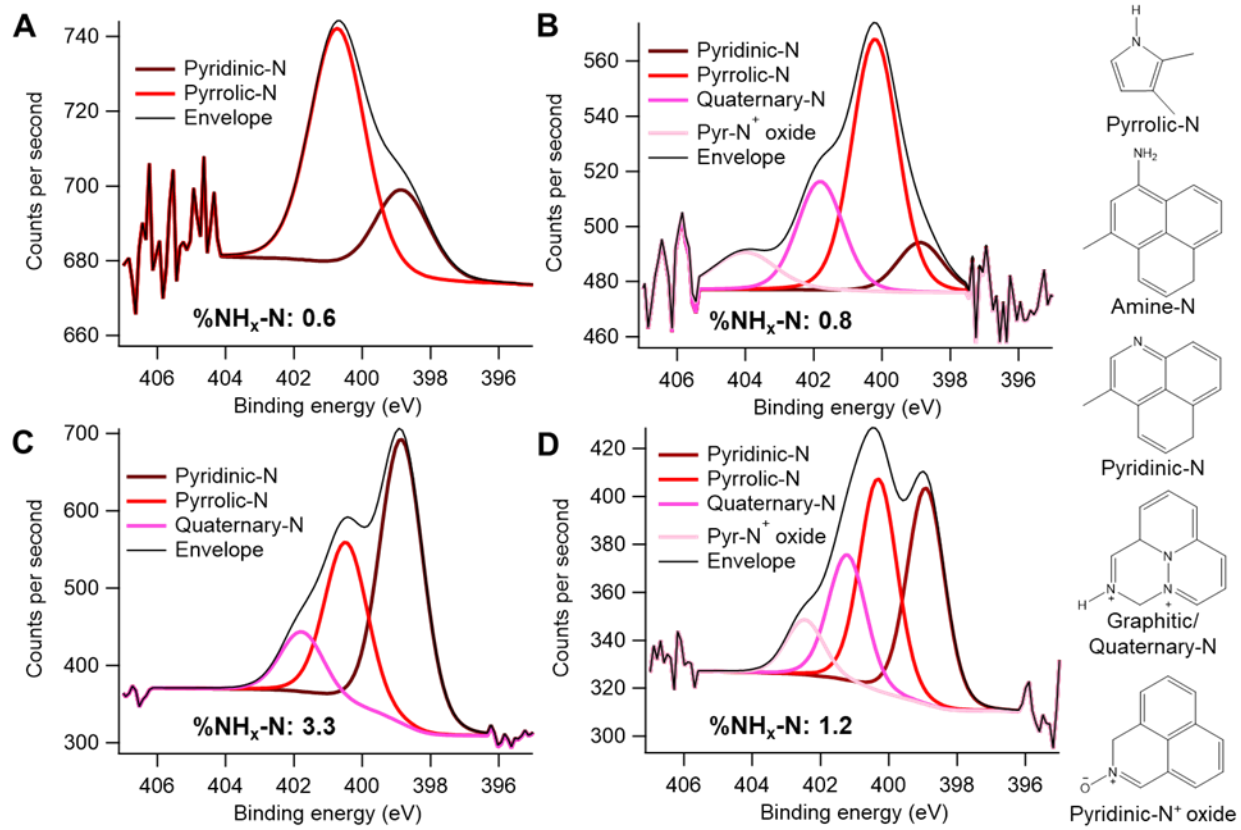

		SCGKOH	BC-N	BC-M	BC-A
survey scan					
atomic percentage	C	87.1	86.1	81.2	88.5
	O	11.7	10.9	5.3	8.0
	Cl	0.3	0.0	0.0	0.0
	N	0.9	1.8	13.5	3.5
high resolution scan					
%N as:	pyridinic-N	27.6	54.8	61.8	37.0
	pyrrolic-N	66.2	23.6	24.5	35.9
	quaternary-N	0.0	10.9	13.7	20.2
	pyridinic-N oxide	6.2	10.8	0.0	6.8
summary					
total %N from elemental analysis		2.2	1.8	13.0	3.0
total $\%NH_x$-N		0.6	0.8	3.3	1.2

Figure 3.1 Nitrogen (N 1s) XPS spectra for (**A**) BC, (**B**) BC-N, (**C**) BC-M, and (**D**) BC-A. Structures of each type of nitrogen-containing functional group identied by XPS are shown on the far right. Table summarizes the composition of unmodified and nitrogen modified biochar materials determined by XPS and elemental analysis.

DRIFTS spectra (**figure B2**) of the BC-N, BC-M, and BC-A substrates agreed with results from XPS analysis, demonstrating a lower nitrogen density on the BC-N in particular (***section***

B2). Therefore, the complementary surface characterization results for the BC-M indicate this substrate may exhibit a faster and more uniform MIP attachment, while the BC-N and BC-A are expected to experience similar and poorer MIP attachment.

3.3.2 Thicker MIP Layer Significantly Decreases Composite Specific Surface Area

Successful and relatively uniform MIP functionalization on the biochar substrates was verified with TEM (**figure 3.2A - D**). Imaging revealed MIP layer thickness ranging from 10s to 100s of nm across much of the surface for all four materials of interest. Notably, the MIP layer on the BC-M@MIP-V material was significantly thicker, with a thickness of approximately 200 nm observed across much of the material surface. MIP modified and unmodified biochar were also imaged via SEM to further characterize the MIP layer (**figure 3.2A - D insets**); however, the MIP was indistinguishable from the biochar surface, which is likely a result of the thin MIP layer, highly irregular biochar surface, and SEM contrasting.

The MIP functionalization generally reduced the SSA of the biochar composites, with significant variability in the final SSA observed based on the nitrogen modification method and slightly from the unmodified BC (858 m^2/g) to 741 m^2/g and 806 m^2/g (**table 3.1**). By contrast, the BC-M@MIP-V material synthesis resulted in a significant decrease in the inherent SSA to 155 m^2/g, which was accompanied by a corresponding increase in average pore size from 1.42 nm for BC to 8.88 nm, indicating the MIP layer has covered some or all of the smallest micropores in the biochar substrate. Interestingly, the BC-A@MIP-VF SSA increased significantly to 1035 m^2/g, functional monomer selection. The SSA of BC-N@MIP-V and BC-M@MIP-VF decreased only which is possibly due to an increase in ammonium chloride modified biochar SSA. BET analysis of the BC-A was not performed to confirm this finding due to the relatively lower PFAA removal observed for BC-A@MIP-VF (discussed in the following sections). The SSA data also suggests

that more attachment points (i.e., greater percentage of –NH moieties) for MIP functionalization may not be beneficial unless other factors like polymerization time or monomer concentration are adjusted. Interestingly, the thicker polymer layer and corresponding reduction in composite BET SSA was not observed when the TFMA monomer was included during MIP synthesis. Further work is needed to better understand this relationship.

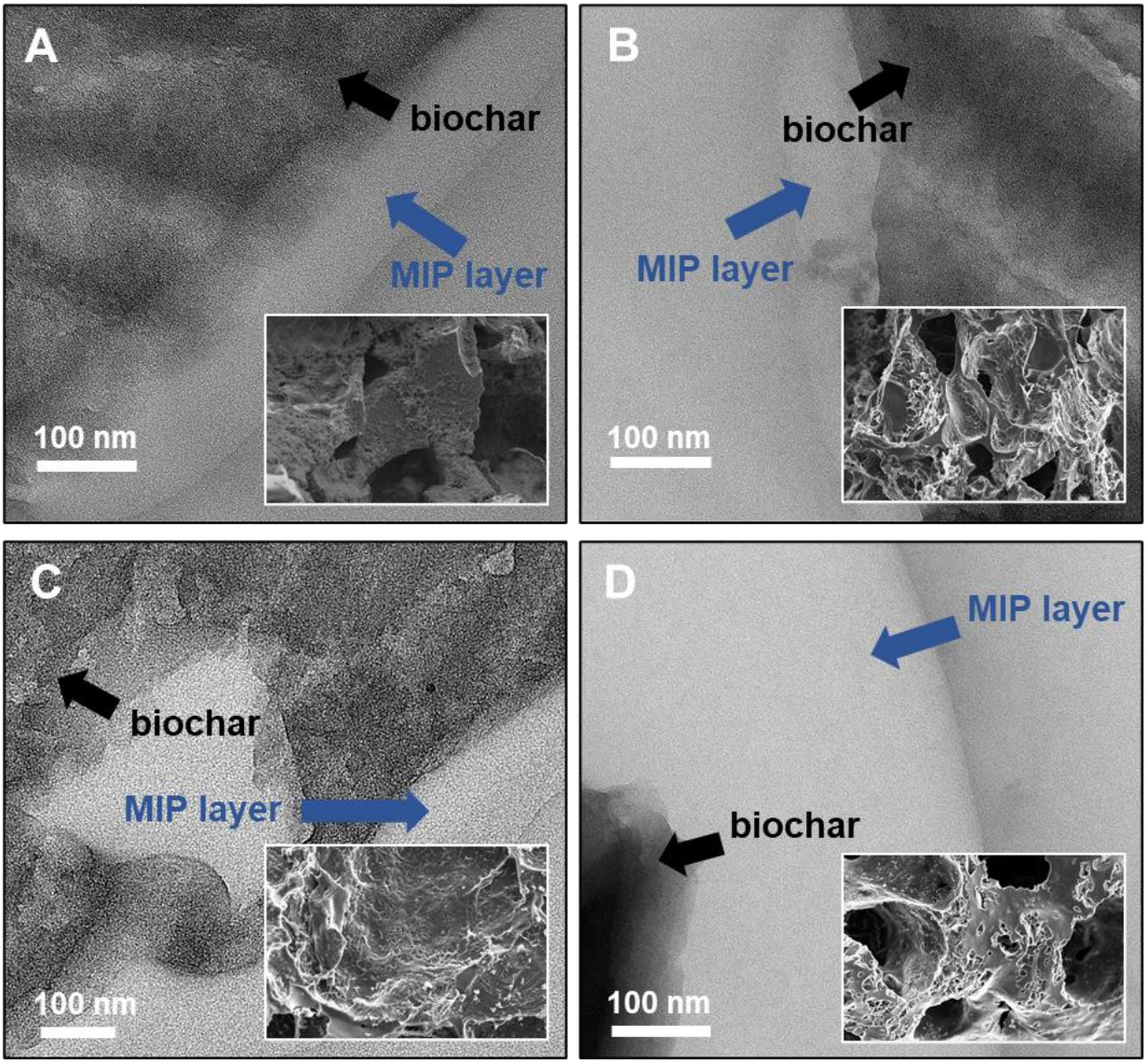

Figure 3.2 TEM images with SEM image insets of MIP modified biochar materials: (**A**) BC-N@MIP-V, (**B**) BC-A@MIP-VF, (**C**) BC-M@MIP-VF, and (**D**) BC-M@MIP-V.

3.3.3 PFAA Batch Adsorption Tests

3.3.3.1 Functional Monomer Choice Directs PFOS Adsorption

BET SSA had a significant impact on the PFOS adsorption capabilities of each material as evidenced by a comparison of their distribution coefficients (K_d, **figure 3.3A**). The BC and BC-N@MIP-V exhibited high K_d values (1410 and 882 L/g), corresponding to their high BET SSA (858 and 741 m^2/g). BC and BC-N@MIP-V also had low equilibrium PFOS concentrations, which suggests that PFOS adsorption was the highest compared to the other adsorbents. Similarly, the BC-M@MIP-V possessed the lowest SSA at 155 m^2/g and a low K_d (1.89 L/g) and a large equilibrium aqueous PFOS concentration. The poor PFOS removal by the BC-M@MIP-V adsorbent was expected since a number of previous studies have demonstrated the importance of SSA on adsorption capabilities of a material.[1, 20, 63, 140] Interestingly, the BC-A@MIP-VF and BC-M@MIP-VF materials also exhibited low K_d values despite their high SSA. The presence of the TFMA monomer in these materials is hypothesized to be responsible for the decreased adsorption, as discussed in further detail below. In order to better evaluate the effects of functional monomer selection and nitrogen modification method on BC@MIP capabilities, further comparison of adsorbent performance was evaluated using normalized equilibrium adsorption ($q_{e,SSA}$; **figure 3.3A inset**).

Normalized equilibrium adsorption results indicate the VBTAC monomer alone produced a BC@MIP material with high PFOS adsorption capabilities regardless of nitrogen modification approach while inclusion of the TFMA monomer reduced PFOS adsorption capabilities. The BC-M@MIP-V and BC-N@MIP-V demonstrated PFOS removal capabilities comparable to or greater than the unmodified BC, with normalized equilibrium PFOS adsorption of 0.055, 0.049, and 0.052 $mg/g*g/m^2$, respectively. The addition of the fluorinated TFMA functional monomer in the BC-M@MIP-VF reduced PFOS equilibrium adsorption to 0.037 $mg/g*g/m^2$. Similarly, the BC-

A@MIP-VF material exhibited PFOS equilibrium adsorption of only 0.029 mg/g*g/m^2. The low PFOS adsorption by BC-A@MIP-VF is particularly interesting given the high SSA of the material (1035 m^2/g). This may be due in part to the density and speciation of oxygen and nitrogen containing surface functional groups (see **figure 3.1D** and **figure B3D**) resulting from the ammonium chloride modification method used for the BC-A substrate. Specifically: (1) if portions of the biochar surface do not have MIP attached, the high oxygen content of the exposed BC-A (28.9% oxygen) will be negatively charged at the solution pH and repel negatively charged PFAAs like PFOS; and (2) the nitrogen functional group speciation (i.e., high pyridinic-N and low pyrrolic-N and quaternary-N) may have affected the morphology and function of the MIP layer. Thus, it appears functional monomer selection had a

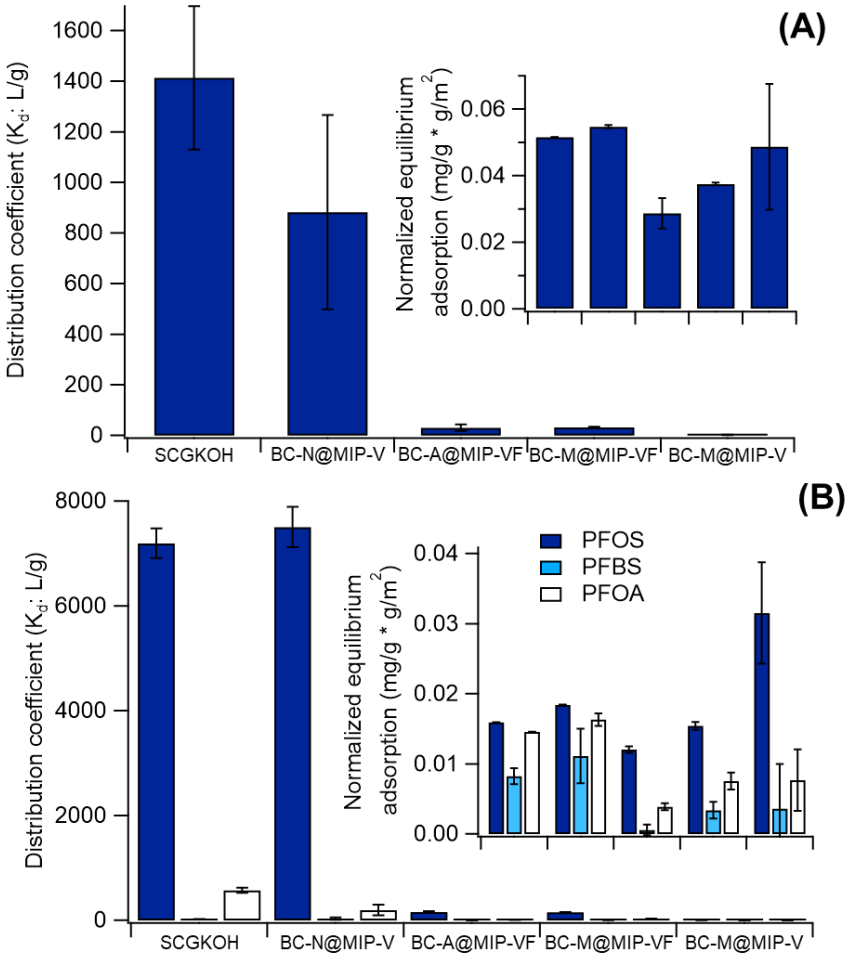

Figure 3.3 Equilibrium adsorption of (A) 4275 ± 342 µg/L PFOS and (B) 1476 ± 207 µg/L PFOS, 1166 ± 153 µg/L PFBS, and 1453 ± 582 µg/L PFOA by 100 mg/L MIP modified and unmodified biochar materials in an ultrapure water only matrix following a 4-day equilibration period. Main graphs display the distribution coefficient while insets display the normalized equilibrium adsorption. Error bars represent the standard deviation from triplicate samples.

significant impact on PFOS adsorption while the nitrogen modification method had a lower impact.

3.3.3.2 Preferential adsorption of longer-chain PFAAs over short-chain PFAAs

Competition studies revealed high selectivity for the template by the PFOS-imprinted MIP composites and preferential adsorption of long-chain PFAAs. The preferential adsorption of PFOS is not surprising as high selectivity for the template compound is characteristic for MIP materials; however, it is important to note the adsorption of PFOA and PFBS was also observed. The normalized equilibrium adsorption of PFOS was only slightly greater than PFOA for the BC and BC-N@MIP-V materials with equilibrium adsorption of 0.016 mg PFOS/m^2 and 0.015 mg PFOA/m^2, and 0.018 mg PFOS/m^2 and 0.016 mg PFOA/m^2, respectively (**figure 3.3B inset**). Selectivity coefficient ($K_{selectivity}$) calculations (**table B4**) similarly indicated only a minor improvement in PFOS selectivity for the BC-N@MIP-V compared to the unmodified BC while the other three adsorbents showed much greater increases in PFOS selectivity. For the other three BC@MIPs, however, higher PFOS selectivity was observed. For example, the PFOA adsorption was approximately half that for PFOS for the BC-M@MIP-VF, and even lower for the BC-A@MIP-VF and BC-M@MIP-V. The BC-M@MIP-V in particular exhibited much higher PFOS selectivity, which is possibly due to the thick MIP layer and the corresponding decrease in non-specific adsorption from exposed biochar surfaces. By contrast, PFBS adsorption was significantly lower than that of PFOS and PFOA for all three BC@MIP composites. The lower PFBS affinity may indicate greater template imprinting success on the BC-A@MIP-VF, BC-M@MIP-VF, and BC-M@MIP-V materials and higher rates of non-specific binding on the BC-N@MIP-V. We hypothesize that orientation of the functional monomer with the quaternary nitrogen located farther into the binding site may also be negatively impacting adsorption of short-chain PFAAs (i.e.,

PFBS) that rely more strongly on electrostatic attraction rather than hydrophobic interactions.[155] Thus, the shorter-chain PFBS that primarily rely on electrostatic attraction for adsorption are poorly removed while the longer-chain PFOS and PFOA that rely primarily on hydrophobic attraction are removed well. Our observations from the PFAA competition studies confirm the hypothesis that the PFOS template would create a binding site capable of removing other perfluoroalkyl sulfonic acids (PFSAs) and perfluoroalkyl carboxylic acids (PFCAs) in addition to the PFOS template.

Generally, the total mass of PFAAs adsorbed decreased for all MIP composite materials in the presence of competing PFAAs. For example, the BC-N@MIP-V composite had a normalized PFAA equilibrium adsorption of 0.055 mg PFOS/m^2 that decreased to 0.046 mg PFAA/m^2 for the PFAA competition test. The BC-A@MIP-VF composite in particular experienced a significant decrease in normalized equilibrium adsorption (from 0.029 mg PFOS/m^2 to 0.016 mg PFAA/m^2). Therefore, no additional tests were performed using this particular MIP composite material. The diminished PFAA adsorption performance by all composites compared to PFOS-only reaction systems is likely due to adsorption competition, and the lower initial concentration of each individual PFAA (1476 ± 207 μg/L PFOS, 1166 ± 153 μg/L PFBS, and 1453 ± 582 μg/L PFOA) compared to the PFOS only test (4275 ± 342 μg/L PFOS). It should be noted, however, that total PFAA load was similar between tests (4637 μg/L PFOS compared to 4314 μg/L PFAAs). The exception to this general observation was the BC-M@MIP-V composite which demonstrated comparable PFAA adsorption between the single and multi-PFAA tests (0.049 mg PFOS/m^2 and 0.043 mg PFAA/m^2). The contrasting results of reduced PFAA adsorption by BC-N@MIP-V and sustained PFAA adsorption by BC-M@MIP-V composites prepared using the VBTAC functional monomer imply that the biochar substrate can impact PFAA selectivity directly via non-specific

binding to exposed biochar or indirectly via the corresponding MIP layer morphology. For example, low imprinting success on the BC-N@MIP-V may have led to lower adsorption in the presence of competing PFAAs.[131, 151] This conclusion is supported by the high $K_{selectivity}$ values calculated for the BC-M@MIP-V (4.52 and 3.76 for PFBS and PFOA; **table B4**) compared to BC-N@MIP-V (0.86 and 1.03 for PFBS and PFOA) revealing a higher selectivity for the template compound by the BC-M@MIP-V.

Interestingly, the fluorinated TFMA monomer did not appear to improve PFAA adsorption in this study, which is contrary to findings from other PFAA-MIP studies.[53, 55] For example, the BC-M@MIP-VF material exhibited significantly lower total PFAA adsorption (0.026 mg/g*g/m^2) compared to the BC-M@MIP-V material (0.043 mg/g*g/m^2) despite having a SSA nearly five times greater (806 m^2/g compared to 155 m^2/g). This observation was particularly surprising for the more hydrophobic PFAAs (i.e., PFOA and PFOS) which possess a strong affinity for fluorocarbon-containing structures.[44, 45, 55] The observed reduced PFAA adsorption may be a result of the highly acidic, anionic nature of the TFMA monomer at near-neutral pH ranges that would repel the negatively charged PFAAs.[56, 130] However, additional work outside the scope of this study would be necessary to further elucidate the mechanism behind this finding. For example, surface charge analysis would provide valuable information about the physicochemical characteristics of this sample, however the particle size (297 – 595 microns) was too large to measure with conventional approaches like zeta potential analysis.

3.3.3.3 Increased Complexity in Reaction Matrix Increased PFAA Adsorption by BC-M@MIP-V

Interestingly, the BC-M@MIP-V material displayed an increase in total PFAA adsorbed in the synthetic wastewater (0.055 mg PFAAs/m^2) compared to the ultrapure water matrix (0.043 mg PFAAs/m^2 or 0.049 mg PFOS/m^2). We hypothesize that the elevated ionic strength from the

synthetic wastewater decreased swelling of the MIP layer and exposed more of the binding sites within the inner pores.[54, 156] The effect was likely expressed to a greater extent in the BC-M@MIP-V material compared to the other adsorbents because of the greater thickness of the MIP layer.

PFOS selectivity in the synthetic wastewater remained high for all of the BC@MIP composites, particularly when compared with adsorption of other PFAAs, caffeine, and fipronil. The BC-N@MIP-V and BC-M@MIP-V composites demonstrated much higher affinity for all PFAAs than the unmodified BC substrate, while the BC-M@MIP-VF composite demonstrated lower adsorption of all three PFAAs. However, the hierarchy of PFAA adsorption remained the same (**figure 3.4**). The lower PFAA adsorption by the BC-M@MIP-VF material compared to the other composites follows the trend observed in previous sections. PFOS removal remained higher than that of other PFAAs with equilibrium adsorption of 0.010 mg/g*g/m^2, 0.021 mg/g*g/m^2, 0.006 mg/g*g/m^2, and 0.026 mg/g*g/m^2 for the BC, BC-N@MIP-V, BC-M@MIP-VF, and BC-M@MIP-V, respectively. PFOA adsorption was generally more comparable to PFOS adsorption

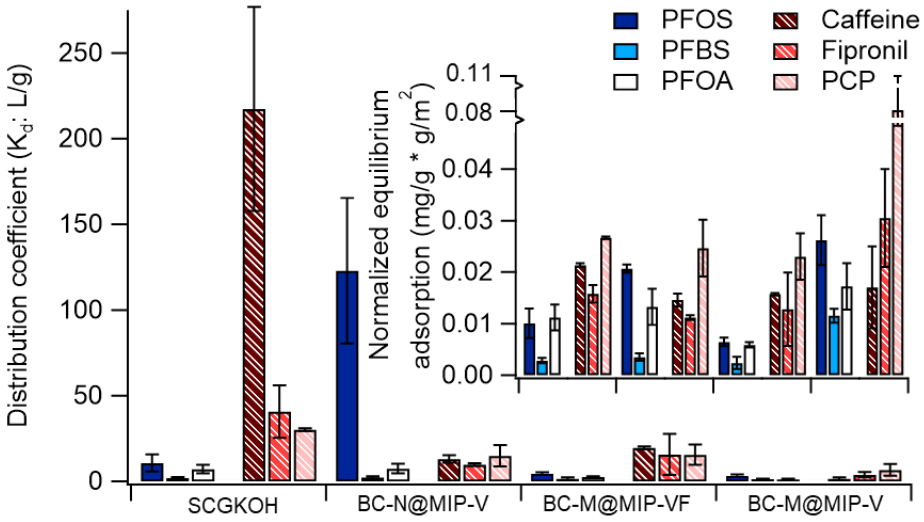

Figure 3.4 Equilibrium adsorption of 1659 ± 99 µg/L PFOS, 1400 ± 11 µg/L PFBS, 2313 ± 71 µg/L PFOA, 1916 ± 76 µg/L caffeine, 1520 ± 63 µg/L fipronil, and 3385 ± 217 µg/L pentachlorophenol by 100 mg/L MIP modified and unmodified biochar materials in synthetic wastewater following a 4-day equilibration period. The main graph displays the distribution coefficient while the inset displays the normalized equilibrium adsorption. Error bars represent the standard deviation from triplicate samples.

in the synthetic wastewater matrix test (equilibrium PFOA adsorption of 0.013 mg/g*g/m^2, 0.006 mg/g*g/m^2, 0.017 mg/g*g/m^2 for the BC-N@MIP-V, BC-M@MIP-VF, and BC-M@MIP-V, respectively) than it was in the PFAA competition test in the ultrapure water matrix. Therefore, the presence of salts and sEfOM reduced selectivity for the template compound due to competition at binding sites and potential fouling of the composite surface. PFBS removal was lower than the other PFAAs with adsorbed quantities of 0.003 mg/g*g/m^2, 0.004 mg/g*g/m^2, 0.002 mg/g*g/m^2, and 0.012 mg/g*g/m^2 for the BC, BC-N@MIP-V, BC-M@MIP-VF, and BC-M@MIP-V materials, respectively. Notably, the mass of PFBS adsorbed on the BC-M@MIP-V material is more than three times the PFBS mass adsorbed on any other composite, which is potentially a result of the reduced MIP swelling and greater availability of binding sites on the thick MIP layer.[54, 156] Poor PFBS removal compared to other PFAAs may be partially due to interference of Cl^- 40 mg/L) at the quaternary nitrogen binding site which may interrupt electrostatic attraction and adsorption of short-chain PFAAs.[46, 157] Additionally, complexation of PFAAs with divalent Ca^{2+} and Mg^{2+} may be hindering electrostatic attraction to the BC@MIP composite surface, a phenomenon which likely impacts PFBS adsorption to a greater degree due to its reliance on electrostatic attraction.[158]

The BC adsorbed the lowest amount of PFAAs in the synthetic wastewater mixture compared to the more selective BC-N@MIP-V and BC-M@MIP-V composites. The BC and BC-M@MIP-V demonstrated higher K_d values and higher normalized equilibrium adsorption for all three competing organics than for any of the PFAAs. For example, K_d values for caffeine ranged from 217 L/g for BC to 1.59 L/g for BC-M@MIP-V. Normalized equilibrium adsorption of competing organics ranged from 0.016 to 0.027 mg/g*g/m^2 for BC and 0.008 to 0.022 mg/g*g/m^2 for BC-M@MIP-VF. For the BC-N@MIP-V and BC-M@MIP-V composites, normalized equilibrium

adsorption of co-occurring organics (i.e., caffeine, fipronil, and pentachlorophenol) was generally comparable to that of PFAAs. The normalized equilibrium adsorption of PFAAs ranged from 0.003 to 0.011 mg/g*g/m^2 for BC and from 0.003 to 0.007 mg/g*g/m^2 for BC-M@MIP-VF. For the BC-N@MIP-V and BC-M@MIP-V composites, the caffeine and fipronil removal were lower than or comparable to removal of PFOS and PFOA, but higher than the PFBS removal. Normalized equilibrium adsorption for caffeine and fipronil were 0.015 and 0.011 mg/g*g/m^2 for BC-N@MIP-V and 0.016 and 0.025 mg/g*g/m^2 for BC-M@MIP-V. Equilibrium adsorption results appear to indicate removal of PCP was greater than for any other contaminant for all adsorbents; however, PCP quantification via LC-MS/MS was compromised due to issues with carry-over of PCP during analysis, potentially resulting in higher calculated equilibrium adsorption values than are representative of what occurred. Comparison of the distribution coefficients (K_d) reveals PCP removal on the same order of magnitude as the other co-occurring contaminants, which is assumed to be a more accurate interpretation of what occurred in this system. Very little adsorption of PFAAs onto sEfOM was observed in control samples (**figure B8**), confirming removal of PFAAs was primarily facilitated by the adsorbents. Therefore, the data suggest that while selective removal of PFAAs on the composites was high, some non-selective adsorption of competing organic compounds still occurred, likely due to binding to non-imprinted VBTAC and TFMA or adsorption onto exposed biochar substrate. The BC-M@MIP-V material in particular showed high removal of all PFAAs in the synthetic wastewater matrix, making this material a promising option for use in water treatment systems and may improve PFAS adsorption capabilities—especially where salts and co-contaminants are likely to be present.

Overall, imprinting success and selectivity for the PFOS template appears higher for the BC@MIP materials containing only the VBTAC functional monomer as evidenced by comparison

of the calculated selectivity coefficient ($K_{selectivity}$) values (**figure 3.5** and **table B4**). A $K_{selectivity}$ of greater than one indicates the BC@MIP material has a greater selectivity for the PFOS template over another adsorbate compared to the unmodified BC. The BC-N@MIP-V and BC-M@MIP-V materials had particularly high $K_{selectivity}$ values for the co-occurring organics reflecting a decrease in adsorption of these compounds where only the VBTAC functional monomer was used. By contrast, $K_{selectivity}$ values for the BC-M@MIP-VF were less than one for all adsorbates except PFOA (for which $K_{selectivity}$ was 1.22), indicating poor imprinting success and low selectivity for the template. These results corroborate observations (**figures 3.3** and 3.**4**) indicating the VBTAC monomer alone produces a more selective BC@MIP adsorbent material capable of effective PFAA removal in a complex synthetic wastewater matrix.

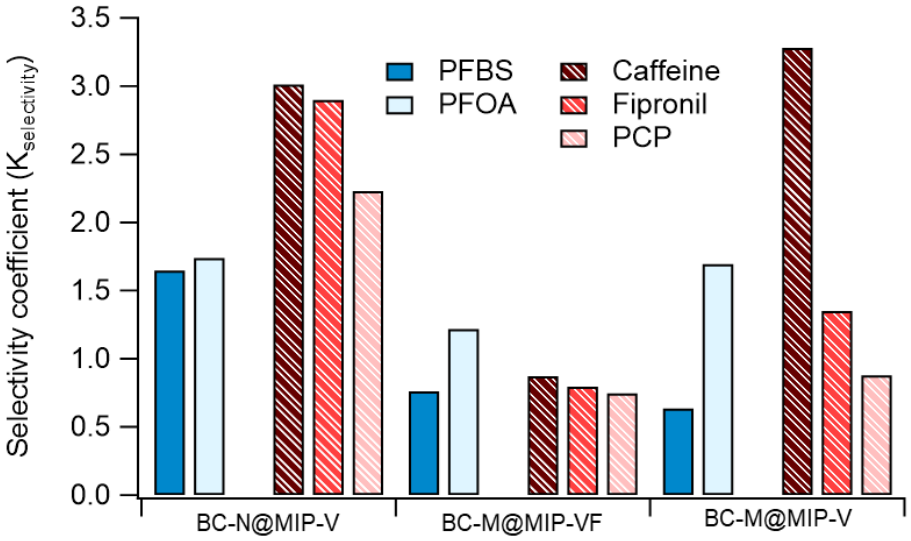

Figure 3.5 Selectivity coefficient from synthetic wastewater test calculated using equations 3 – 5 with PFOS as the reference adsorbate and unmodified BC as the reference adsorbent**.**

3.3.4 Regeneration of Spent Composites Indicates High Potential for Material Reuse

Results from a single use regeneration of spent adsorbents signify high potential for successful material reuse which would increase the functional lifetime of the adsorbent and reduce capital costs for water treatment. Following PFOS adsorption in the ultrapure water system, nearly complete regeneration of spent adsorbent was observed for both MIP functionalized and

unmodified BC materials with percent regeneration ranging from 99% for BC-M@MIP-V to 118% for BC-N@MIP-V (**figure 3.6A**). Adsorbent regeneration following PFAA adsorption in the synthetic wastewater was more varied with recovery of PFOS > PFOA ≥ PFBS (**figure 3.6B**). PFOS recovery generally decreased compared to that observed in the ultrapure water matrix. The exception to this observation was the BC-N@MIP-V material for which PFOS recovery remained high at 102%. PFOA recovery ranged between 72% from BC-N@MIP-V to 31% from BC-M@MIP-V, and PFBS recover ranged between 31% from BC-M@MIP-VF to 10% from BC-M@MIP-V. The low recovery of PFOA and PFBS from BC-M@MIP-V composites is likely a result of the thicker MIP

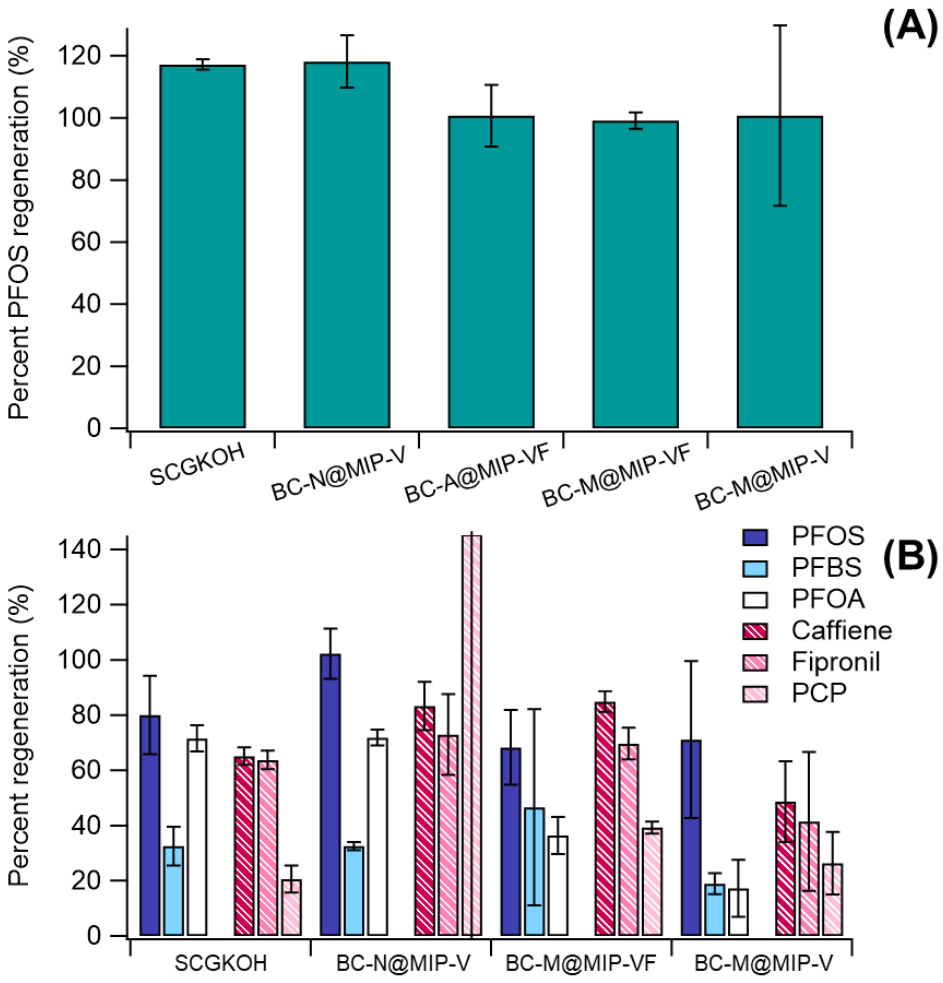

Figure 3.6 Percent recovery of adsorbate from spent adsorbent following batch adsorption tests with (**A**) 4275 ± 342 µg/L PFOS only in a water matrix, and (B) 1659 ± 99 µg/L PFOS, 1400 ± 11 µg/L PFBS, 2313 ± 71 µg/L PFOA, 1916 ± 76 µg/L caffeine, 1520 ± 63 µg/L fipronil, and 3385 ± 217 µg/L pentachlorophenol adsorption in the synthetic wastewater matrix. Percent regeneration was calculated as the percent recovery of mass adsorbed during the 4-day equilibrium adsorption test. Error bars represent the standard deviation from triplicate samples.

layer (~200 nm) and additional time required to desorb PFAAs from interior portions of that MIP layer when compared to the thinner MIP layers (~100 nm) on the other composite materials.[159] A comparable material with a thinner MIP layer (e.g., produced using a shorter polymerization time) is expected to experience improved regeneration capabilities more similar to that seen for the BC-N@MIP-V. Recovery of caffeine and fipronil was comparable to that of PFOS and PFOA on both the modified and unmodified biochar materials. Percent recovery of caffeine ranged between 46% from BC-M@MIP-V to 85% from BC-M@MIP-VF while percent recovery of fipronil ranged between 29% from BC-M@MIP-V to 66% from BC-M@MIP-VF (**figure 3.6B**). Adsorption and regeneration over multiple cycles is needed to obtain a better understanding of the full material lifetime capabilities; however, these preliminary results indicate promising reuse potential in water treatment applications.

3.4 CONCLUSIONS

Novel nitrogen modification and MIP functionalization of a spent coffee grounds biochar was successfully performed resulting in an adsorbent material with high potential for selective PFAA removal from water. Of three biochar nitrogen modification methods explored, the melamine modification resulted in the highest fixation of nitrogen containing surface functional groups. The higher density of nitrogen containing surface functional groups (i.e., on the BC-M substrate) resulted in a thicker MIP layer but decreased the composite specific surface area and increased average pore size. Functional monomer selection had a large impact on the BC@MIP composite performance. In particular, the fluorocarbon containing TFMA monomer appeared to decrease PFAA adsorption capabilities, potentially due to electrostatic repulsion. This finding is contrary to findings from previous studies reporting enhanced affinity for PFAAs using a fluorinated functional monomer. A hierarchy of PFAA removal capabilities was observed for all modified and unmodified biochar materials with mass adsorbed of PFOS > PFOA > PFBS. A similar trend was

observed during regeneration with mass desorbed of PFOS > PFOA > PFBS. Although total PFAA adsorption capability did not increase significantly as a result of the MIP modification, the modified material exhibited a significant increase in selectivity for PFAAs when compared to the unmodified spent coffee grounds biochar in a synthetic wastewater matrix. In fact, total mass of PFAAs adsorbed increased for the BC-M@MIP-V material in the synthetic wastewater compared to the ultrapure water matrix. The higher salt concentration in the synthetic wastewater test is expected to reduced swelling of the thicker MIP layer for the BC-M@MIP-V composite, thereby increasing the specific surface area and subsequently the PFAA removal capabilities. Selective PFAA adsorbent materials are needed to fill a technology gap for treatment of PFAAs in complex waters containing a range of PFAAs, co-occurring organic contaminants, and dissolved organic matter for which more traditional adsorbents like activated carbon and ion exchange resins. The data presented herein indicates these biochar-MIP adsorbents are capable of selective PFAA adsorption the presence of competing organics, although additional work is required to refine the synthesis process and fully evaluate the removal capabilities of these materials. The nitrogen modification and MIP functionalization method detailed here is expected to be easily adaptable for any amorphous carbon substrate (e.g., carbon nanotubes, other activated carbons, or carbon membranes) to produce a highly selective PFAA adsorbates with a range of functionalities depending on the physical characteristics of the substrate.

In future work, a shorter polymerization time and use of the unmodified biochar as a substrate for immobilization of the VBTAC MIP will be explored in an effort to consistently obtain a composite adsorbent with a thin MIP layer, and to reduce time and cost associated with the synthesis process. This modified synthesis process is expected to increase the specific surface area without sacrificing the superior PFAA adsorption performance of the VBTAC MIP coating.

Further investigation of the impacts of the TFMA monomer on MIP structure and performance could also help elucidate the impacts of the fluorocarbon moiety on PFAA adsorption. Additionally, a multi-template MIP using short- and long-chain PFAAs during polymerization could improve adsorption of shorter-chain PFAAs by reducing competition between short- and long-chain PFAAs. Finally, evaluation of adsorption performance over multiple adsorption and regeneration cycles with PFAA concentrations more representative of those commonly found in WWTP effluent and environmental systems would provide a better understanding of the effectiveness of these adsorbents for water treatment applications.

Chapter 4: Immobilization of a Multi-Template Imprinted Polymer on Biochar for Improved Adsorption of Short- and Long-Chain Per- and Polyfluoroalkyl Substances

Increased detection frequency of short-chain PFAAs in wastewater and environmental samples has revealed a need for adsorbents capable of selective removal of short- and long-chain PFAAs simultaneously from complex matrices. Our previous studies suggest that imprinted polymers prepared using a single PFOS template can result in preferential adsorption of PFOS over short-chain PFAS. To address this need, a multi-PFAS imprinted polymer composite (mMIP) was synthesized. A synergistic effect was observed when using multiple PFAS templates that resulted in an increased imprinting factor compared to the single-template MIPs. The BC@mMIP composite was capable of treating approximately 100 ng/L each of PFOA, PFBS, and PFHxS to below their proposed US EPA MCL in ultrapure water containing a mix of nine PFAS at (waste)water-relevant concentrations. Column testing in real wastewater effluent revealed competition between TDS species and PFAS for adsorption sites on BC@mMIP, non-imprinted BC@NP, and a commercial activated carbon (F400). This mMIP composite material is recommended for use in water treatment with low TDS or used in seriAes with a pre-treatment like ion exchange for optimal performance.

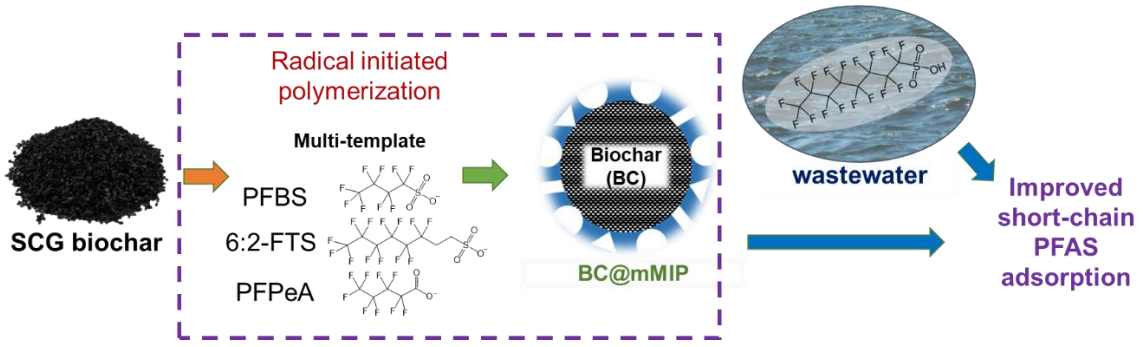

4.1 INTRODUCTION

PFAS are a widespread contaminant of concern which have been identified globally in both human, animal, and environmental reservoirs including drinking[11, 160, 161] and wastewater,[31, 32, 120, 162, 163] rain, human[164-166] and animal[167-169] blood serum, and freshwater fish.[170-172] Recent regulatory action limiting the use of such long-chain PFAS as perfluorooctanesulfonate (PFOS) and perfluorooctanoate (PFOA)[173] and their presence in drinking water[174] and environmental waters[175, 176] has caused them to be phased out of production in the US and European Union. With this shift, researchers have noted a corresponding increase in the prevalence and concentrations of short-chain PFAS in the environment and (waste)water treatment.[12, 31] Adsorption with activated carbon (AC) or ion exchange resins has long been the standard for PFAS separation in water;[8, 20, 38] however, removal efficiency by these materials has been shown to be poor for short-chain and perfluorocarboxylic acids.[160, 177] The presence of organics[40] and counterions[38] in some matrices (e.g., wastewater) have also been demonstrated to reduce the efficacy of these adsorbents for PFAS removal.[38, 46, 178] These limitations are of particular concern when considering technology needs to meet the recently proposed US Environmental Protection Agency (EPA) maximum contaminant level (MCL) for PFAS in drinking water.[174] This rule proposes limits of 4 ng/L for PFOS and PFOA separately, and a combined hazard index for perfluorononanoate (PFNA), perfluorohexanesulfonate (PFHxS), perfluorobutanesulfonate (PFBS), and hexafluoropropylene dimer acid (HFPO-DA) which references their respective health based reference concentrations of 10 ng/L PFNA, 9 ng/L PFHxS, 2000 ng/L PFBS, and 10 ng/L HFPO-DA.[174] Thus, there is a need for a more selective PFAS treatment method with greater affinity for short-chain PFAS to overcome existing limitations with conventional PFAS separation media.

Molecularly imprinted polymers (MIPs) are a class of customizable adsorbents with high specificity for one or more target compounds which are used in synthesis as a template.[53, 57, 116]

Functional monomer(s) (the building blocks of the MIP) are chosen to have specific affinity for the template (e.g., charged moieties that electrostatically attract or aromatic groups that hydrophobically attract). The functional monomer and template are mixed prior to synthesis to allow time for self-assembly in solution. This step promotes the formation of binding sites on the MIP product with size, shape, and affinity specifically tailored to the template. Another important component of the MIP is the crosslinker which connects functional monomers and holds the MIP together. The crosslinker typically comprises a large fraction of the MIP mass, making crosslinker selection an important aspect of final MIP morphology and physicochemical characteristics.[57, 179] Crosslinkers are often chosen to interact favorably with the synthesis solvent (e.g., N,N'-methylene bisacrylamide is often chosen for synthesis in water).[53, 57, 179] Recently, MIPs have been investigated as PFAS adsorbents because of their high selectivity. These studies have often immobilized the MIP onto a substrate such as biochar,[116] carbon microspheres,[53] or titanium dioxide nanotubes[137] to overcome challenges associated with MIP morphology and size which make them difficult to implement in water treatment without additional modification. Biochar in particular is an ideal substrate for MIP functionalization due to its high surface area[1, 20, 67, 126] and the abundance of easily modifiable surface functional groups present on most biochar.[93, 180] To date, studies have focused on single template imprinting with longer chain, anionic PFAS compounds.[53, 56, 61, 116, 137, 181] The MIP products have high imprinting factors (a measure of templating success) due to the high affinity of long chain PFAS for a variety of hydrophobic and cationic functional monomers; however, adsorption of short-chain PFAS remains low.[56, 116] For example, competitive sorption of three PFAS was evaluated with our previously synthesized PFOS-imprinted polymer-biochar (BC@MIP) in ultrapure water with initial concentrations of 1476 ± 207 μg/L PFOS, 1166 ± 153 μg/L PFBS, and 1453 ± 582 μg/L PFOA and an adsorbent

dose of 100 mg/L.[116] Preferential PFOS adsorption was observed with 10 times higher loading of PFOS than the short-chain analogue (PFBS). Thus, additional strategies are needed to improve short chain PFAS removal by MIP adsorbents.

Multi-template MIPs have been leveraged in previous studies to achieve effective removal of a number of compounds in the same class or otherwise having similar structure.[58, 60, 130, 182-185] For example, Gao et al. prepared a silica-based multi-template MIP on a magnetic, ferrous oxide nanoparticle substrate for selective removal of endocrine disrupting compounds (EDCs) from water.[130] Three EDCs were chosen as templates–17β-estradiol, estriol, and diethylstilbestrol–and the resulting material demonstrated high imprinting factors ($IF = Q_{MIP}/Q_{non\text{-}imprinted\ polymer}$) of 1.80 to 6.38 for the three template molecules and four analog EDCs.[130] This approach is advantageous because compounds within a class often co-occur and have similar toxicological endpoints. For example, over 240 individual PFAS analytes comprising 57 sub-classes have been identified in aqueous film forming foam (AFFF) or in groundwater from impacted sites,[10] including precursors and polyfluorinated compounds which will transform in the environment.[186] When choosing templates for a multi-template MIP synthesis, it is important to select templates with similar affinity for the functional monomer to achieve similar imprinting factors [equation (4.7)] in the final material. Prior studies have also explored the use of a molecular crowding agent to improve the imprinting factor.[187-190] In this approach, large, inert macromolecules (e.g., polystyrene) are included in the pre-polymerization mixing step to increase interactions between the functional monomer and template; however, this technique is more common in syntheses that utilize organic solvents since most of the viable macromolecules are hydrophobic and have little to no solubility in water.[191] This multi-template MIP approach has not, to our knowledge, been previously explored for PFAS removal in water treatment. Therefore, the objectives of this study were

threefold: First, to synthesize a multi-template MIP-biochar composite using three PFAS templates of varying head group [PFBS, perfluoropentanoate (PFPeA)], and extent of fluorination [6:2-fluorotelomer sulfonate (6:2-FTS)]. The 6:2-FTS template was chosen both because of its similarity to the previously used PFOS template[116] and because it is one of the more common aerobic biotransformation products from fluorotelomer thioether amido sulfonate, one of the key components of AFFF.[192] Second, this study aims to compare the physicochemical properties and PFAS removal capabilities of this multi-template MIP to analogous single-template and non-imprinted MIPs and the unmodified biochar. Third, this study aims to evaluate adsorption and regeneration capabilities of the multi-template MIP through batch tests at PFAS concentrations relevant to (waste)water treatment and a column filtration study using spiked, real wastewater effluent. The viability of the macromolecular crowding approach in aqueous MIP synthesis was also explored and is detailed further in ***Appendix C*** (***section C1***)**.**

4.2 MATERIALS AND METHODS

4.2.1 Adsorbent Materials and Chemicals

Spent coffee grounds for biochar production were donated by Bay Laurel Catering Services at the University of Washington (Seattle, WA) from Starbucks® Pike Place® grounds, medium roast, arabica coffee sourced from Latin America after use in an industrial drip coffee maker. For column testing, the commercially available activated carbon Filtrasorb® 400 (F400) was obtained from Calgon Carbon (Pittsburg, PA). F400 was chosen because it is a commonly used adsorbent for PFAS treatment owing to its high point of zero charge (pzc) which allows it to have a slightly positive surface charge at neutral pH, increasing PFAS adsorption through electrostatic attraction with negatively charged PFAS.[193, 194] Prior to use, it was ground, sieved to obtain the #30 – 50 mesh fraction (595 – 297 μm), and washed with deionized water to remove fine particulates. Sand was obtained from The Home Depot (Atlanta, GA) to be used as an inert column packing. Coarse

gravel was obtained from The Home Depot and was used to pack the ends of the columns to distribute flow and prevent washout of column packing. Prior to use, sand and gravel were washed with 1 M and 0.5 mM nitric acid, respectively (ACS grade nitric acid obtained from Macron Fine Chemicals^{TM} was diluted with ultrapure water), and then washed with deionized water until the rinse reached a pH of approximately 7.0.

All chemicals used for this study were ACS reagent grade or equivalent unless otherwise noted. Potassium hydroxide pellets and high purity nitrogen gas (99.998%) for biochar production were purchased from Thermo Fisher Scientific (Waltham, MA) and Praxair (Danbury, CT), respectively. Molecularly imprinted polymers were synthesized using PFBS and PFPeA purchased from Sigma Aldrich (St Louis, MO), and 6:2-FTS from AA Blocks (San Diego, CA) as templates; vinylbenzyl trimethylammonium chloride (VBTAC, 96.0%) purchased from Acros Organics as the functional monomer; N,N'-methylenebisacrylamide (MBA, 96.0%) purchased from Thermo Fisher Scientific as the crosslinker; and 2,2'-azobis(2-methylpropionitrile) (AIBN, 98%) purchased from Sigma Aldrich as the initiator. Methanol and potassium hydroxide purchased from Thermo Fisher Scientific and sodium chloride (NaCl) purchased from VWR Chemical were used for template washing and regeneration of spent adsorbent.

Optima^{TM} LC/MS grade methanol purchased from Thermo Fisher Scientific was used for preparation of stock solutions and LC-MS/MS samples for all batch tests. Perfluorooctanesulfonate potassium salt (PFOS) from Matrix Scientific; perfluorohexanesulfonate potassium salt (PFHxS), perfluorobutanesulfonic acid (PFBS), perfluorooctanoic acid (PFOA), perfluoropentanoic acid (PFPeA), perfluorohexanoic acid (PFHxA), perfluorobutanoic acid (PFBA), trifluoroacetic acid (TFA) from Sigma Aldrich (St Louis, MO); and 6:2-fluorotelemere sulfonate (6:2-FTS) from AA Blocks (San Diego, CA) were used as adsorbates. Batch test and

wastewater samples were processed using 0.22 μm cellulose acetate (CA) syringe filters from Sigma Aldrich.

Puriss p.a. grade potassium hydrogen phthalate monobasic for preparation of DOC calibration standards from Sigma Aldrich, 1.6 micron glass fiber (GF/A) 42.5 mm filter paper from Whatman (United Kingdom), sodium chloride from VWR, sodium nitrate from VWR, sodium sulfite from Fisher Chemical, sodium sulfate from VWR, trace metals grade nitric acid from Thermo Fisher Scientific, and ICP standards from Inorganic Ventures (Christiansburg, PA) were used for initial characterization of wastewater treatment plant effluent samples. Fipronil from Chem Impex International (Wood Dale, IL), ultrapure acetaminophen (99.0%) from Spectrum Chemical Manufacturing Corporation (New Brunswick, NJ), and HPLC grade benzotriazole and HPLC grade sulfamethoxazole from TCI Chemicals (Tokyo, Japan) were used for spiking co-occurring organics into the column test influent solution along with the nine PFAS used in batch testing.

4.2.2 Synthesis of Multi-Template MIP Immobilized on Spent Coffee Grounds Biochar

Several types of single- and multi-template molecularly imprinted polymer (MIP)-biochar composites were synthesized via thermally activated radical initiated polymerization as described in our prior study.[116] The names, surface area, and templates of these materials are outlined in **table 4.1**. Briefly, spent coffee grounds biochar (BC) was produced via a two-step process of pyrolysis at 400°C followed by activation with a 1:1 weight ratio of potassium hydroxide at 800°C, as described previously,[1] and then sieved to obtain the #30 – 50 mesh fraction (595 – 297 μm). MIP was immobilized directly on the surface of the BC via a three-step process. First 0.1820 g functional monomer (VBTAC) and PFAS template(s) were pre-mixed at a by stirring for 10 h at 150 rpm in 170 mL of deaerated ultrapure water to allow time for alignment in solution. For all MIP composites, a 4:1 molar ratio of total template to functional monomer was maintained. In

situations where more than one template was used, equimolar quantities of each template were added to achieve this ratio. Second, 1.3240 g crosslinker (MBA) and 0.5 g pre-wetted BC were added and allowed to mix for 30 min before adding 0.1642 g of initiator (AIBN) and starting the polymerization reaction by heating the solution to 60°C in an oil bath while maintaining stirring at 150 rpm. Polymerization was allowed to proceed for 15 h (which was assumed to be sufficient time to allow natural termination of the polymerization) before removing the solution from the oil bath and separating the BC@MIP composite material via vacuum filtration. Finally, the PFAS template was removed from the BC@MIP by adding 100 mL of a template wash solution (70% methanol, 1% sodium chloride, and 2.8 mM sodium hydroxide in water) and placing it on a shaker at 200 rpm and 33°C for a minimum of 24 h before decanting to separate. This wash was repeated for a total of five times with template wash solution followed by one ultrapure water wash. Template extraction was considered successful if PFAS concentrations in the fifth wash solution were at or below 200 μg/L (around three orders of magnitude lower than the concentration in the

Table 4.1 MIP composite composition, BET specific surface area, pore size, and cumulative pore surface area.

	templates			BET analysis		
adsorbent name	PFBS (B) 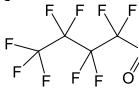	PFPeA (P) 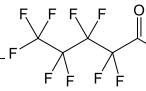	6:2-FTS (F) 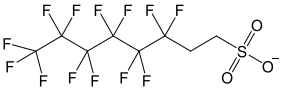	BET surface area (m^2/g)	pore size (nm)	pore surface area (m^2/g)
BC	-	-	-	1319	3.3	60
BC@NP	-	-	-	580	3.0	39
BC@MIP(F)	-	-	Y	904	7.4	50
BC@MIP(B)	Y	-	-	1056	6.5	63
BC@MIP(P)	-	Y	-	881	9.8	52
BC@mMIP	Y	Y	Y	995	4.7	54
F400	-	-	-	917	5.6	123

polymerization solution). Following washing, BC@MIP materials were dried at 60°C for 24 h, sieved to obtain the #50 – 30 mesh (297 – 595 micron) fraction, and then stored in glass vials in a desiccator for further analysis. A non-imprinted polymer composite (BC@NP) was synthesized via the same process without the use of a template PFAS analyte, and the final washing was limited to a 24 h ultrapure water wash to remove excess monomers and polymer.

4.2.3 Characterization of Biochar-Molecularly Imprinted Polymer Composite

Specific surface area (SSA) was measured for the unmodified and polymer-modified BC adsorbents via nitrogen adsorption at 77K with a Micromeritics 3Flex Version 5.00 (Norcross, GA). Degassing was conducted *in situ* at 300°C for 12 h prior to analysis followed by a two min leak test with a pressure fluctuation limit of 0.0025 mmHg/min to confirm successful degassing. Free space analysis was conducted with helium gas after adsorption to eliminate the effects of trapped helium gas in the micropores on nitrogen adsorption. Adsorption data was evaluated using the Brunauer-Emmett-Teller (BET) model to obtain the SSA, and the Barrett-Joyner-Halenda (BJH) model to obtain average pore diameter and cumulative pore surface area.

The multi-template BC@mMIP material was imaged using transmission electron microscopy (TEM) to better visualize the thickness and uniformity of the MIP layer. First, a small amount of sample was embedded into resin (see ***section C2*** for recipe), dried at 60 °C for 24 h, and sliced into 80 nm sections using a Leica Ultracut 6 microtome and hard diamond knife. Finally, the sample was imaged using a Tecnai G2 F20 SuperTwin TEM (FEI, Hillsboro, OR).

4.2.4 Batch Adsorption Testing

4.2.4.1 PFAS Selectivity in Ultrapure Water

An adsorption competition test was conducted in ultrapure water to evaluate the impact of the multi-template approach on adsorption capabilities for a range of PFAS. All six adsorbent

materials listed in **table 4.1** were included in this test. Adsorbates included short- and long-chain sulfonic and carboxylic PFAA and one polyfluoroalkyl acid (i.e., PFOS, PFHxS, PFBS, PFOA, PFHxA, PFPeA, PFBA, TFA, and 6:2-FTS). Briefly, 5.0 mg of adsorbent was added to a 50 mL polypropylene tube, with triplicate samples of each adsorbent prepared. At the same time, the PFAS solution was prepared in ultrapure water in a 1 L Erlenmeyer flask with concentrated methanolic stocks to achieve an initial concentration of 50 μg/L of each PFAS while maintaining a methanol concentration of no more than 0.02 % v/v. This solution was allowed to mix for 10 min and then the pH was measured and adjusted if needed with dilute sodium hydroxide or hydrochloric acid solutions to achieve a pH of 7.00. This method of pH control was chosen over buffering to eliminate potential effects of the buffer compound on PFAS adsorption. A 50 mL aliquot of the initial PFAS solution was added to each sample, and tubes were placed on a Fisherbrand™ Multi-Purpose Tube Rotator (Fisher Scientific, Waltham, MA) and rotated at 40 rpm for 4 days.

Following the 4-day equilibration period, tubes were removed from the rotator and filtered through 0.22 μm cellulose acetate syringe filters. To minimize PFAS losses on the filter, approximately 25 mL of sample was collected for filtration and the first 20 mL were wasted before collecting around 1.5 mL for subsequent analysis. Samples were prepared and analyzed via liquid chromatography tandem mass spectrometry (LC-MS/MS) as detailed in the supplemental information (***section C11***). Final sample pH was measured following removal of the LC-MS/MS sample and ranged from 6.21 – 7.33.

Percent removal, normalized equilibrium adsorption capacity ($q_{e,SSA}$), solid-liquid distribution coefficient (K_d), and selectivity coefficients were calculated from adsorption data using equations

(4.1) – (4.6) below. Selectivity calculations were performed using template compound(s) as the reference adsorbate and the unmodified BC as the reference adsorbent.[131, 151]

$$Percent\ removal = \frac{(C_0 - C_e)}{C_0} * 100\% \quad \text{Eqn. (4.1)}$$

$$q_e = (C_0 - C_e) * \frac{V}{m_{ads}} \quad \text{Eqn. (4.2)}$$

$$K_d = \frac{C_0 - C_e}{C_e} * \frac{V}{m_{ads}} \quad \text{Eqn. (4.3)}$$

$$K_{imprinted} = \frac{q_{e,BC@MIP,template}}{q_{e,BC@MIP,adsorbate}} \quad \text{Eqn. (4.4)}$$

$$K_{comparison} = \frac{q_{e,BC@NP,template}}{q_{e,BC@NP,adsorbate}} \quad \text{Eqn. (4.5)}$$

$$K_{selectivity} = \frac{K_{imprinted}}{K_{comparision}} \quad \text{Eqn. (4.6)}$$

$$IF = \frac{q_{e,BC@MIP,template}}{q_{e,BC@NP,template}} \quad \text{Eqn. (4.7)}$$

Where C_0 and C_e are the initial and equilibrium adsorbent concentrations (mg/L), V is the sample volume (L), and m_{ads} is the mass of adsorbate on the adsorbent (g).

4.2.4.2 Adsorption Isotherms with Molecular Imprinting Template PFAS

Adsorption isotherms were conducted with each template PFAS individually using the BC@mMIP to gain a more complete understanding of the adsorption mechanisms and capabilities of the material for removal of different types of PFAS. Similar to ***section 4.2.4.1***, all samples were run in triplicate in a 50 mL polypropylene tube containing 50 mL of PFAS solution in ultrapure water and 100 mg/L adsorbent. Initial concentrations ranged from 5 - 5000 μg/L of PFBS, PFPeA, and 6:2-FTS for each single adsorbate sample. Multiple methanolic stock solutions were used to prepare these samples such that the methanol concentration remained below 0.2% v/v and pipetted

volumes of methanol were no smaller than 10 µL. The initial pH of the two highest concentration PFPeA replicate sets was adjusted with dilute hydrochloric acid to 6.7 ± 0.7 to match the pH of the rest of the isotherm samples. This step was necessary for these samples only because the methanolic stock solutions for the perfluorocarboxylic acids (PFCAs) contain four mole equivalents of sodium hydroxide to prevent methylation of PFCAs during long term storage.[195] Once prepared, sample tubes were placed on a tube rotator at 40 rpm and allowed to equilibrate for 4 d before filtering as described in ***section 4.2.4.1*** and preparing LC-MS/MS samples for PFAS quantification as described in ***section C11***. Adsorption results were fit to the Langmuir and Freundlich isotherm models described in equations (4.8) and (4.9) to gain a better understanding of adsorption behavior:

$$q_e = \frac{q_{max} K_L C_e}{1 + K_L C_e} \qquad \text{Eqn. (4.8)}$$

$$q_e = K_F C_e^{1/n} \qquad \text{Eqn. (4.9)}$$

Where q_e and q_{max} are the equilibrium and maximum adsorption densities, C_e is the equilibrium adsorbate concentration, K_L and K_F are the Langmuir and Freundlich adsorption rate constants, respectively, and *1/n* is the Freundlich coefficient of non-linearity.

4.2.4.3 Adsorption and Regeneration at Environmentally Relevant Concentrations

Simultaneous adsorption of approximately 100 ng/L each of nine PFAS (i.e., PFOS, PFHxS, PFBS, 6:2-FTS, PFOA, PFHxA, PFPeA, PFBA, and TFA) onto BC@mMIP in ultrapure water was observed to better understand the capabilities of this materials for PFAS removal at concentrations relevant to (waste)water treatment. Prior to the start of the experiment, all glassware was washed three times with methanol and once with ultrapure water. First, 3.3 L of ultrapure water were added to a 4 L Erlenmeyer flask and spiked with methanolic stocks of each PFAS to achieve the desired starting concentration of 100 ng/L. The solution was stirred for 10 min to fully

mix the reagents, and then the initial pH was adjusted to 7.0 with dilute sodium hydroxide. The PFAS solution was then measured into six 500 mL high density polyethylene (HDPE) bottles (i.e., three BC@mMIP replicates and three PFAS control replicates) and three 50 mL polypropylene tubes (i.e., PFAS initial concentration replicates). Three additional 500 mL HDPE bottles were filled with ultrapure water for blank control replicates. BC@mMIP was added to the samples where relevant to achieve an adsorbent concentration of 100 mg/L and then all HDPE sample bottles were placed on a shaker table at 180 rpm and allowed to equilibrate for 4 d. The initial concentration controls were concentrated via solid phase extraction (SPE; see ***section C12***) and stored in the refrigerator for no more than two weeks prior to analysis via LC-MS/MS (***section C11***). After 4 d, the solid and liquid phases of the BC@mMIP samples were separated, and all nine liquid samples were concentrated via SPE and PFAS concentrations were quantified via LC-MS/MS.

PFAS loaded on spent BC@mMIP adsorbents were recovered using the template wash solution described in ***section 4.2.2*** for 7 d to better understand PFAS recovery and material lifetimes. Briefly, spent adsorbent from each BC@mMIP sample bottle was placed in individual 50 mL tubes and suspended in 50 mL of template wash solution. Tubes were wrapped in parafilm and placed on a tube rotator at 40 rpm. A 0.05 mL sample aliquot was collected at 1 d and 3 d timepoints to evaluate regeneration kinetics, and an equal volume of fresh template wash solution was added to maintain a total volume of 50 mL throughout the regeneration test. After 7 d, the regeneration samples were removed from the rotator and a sample was collected from each. PFAS concentrations in all samples were quantified via LC-MS/MS (***section C11***).

4.2.5 Column Testing

Column tests were performed using wastewater treatment plant effluent spiked with nine PFAS and four organics to better evaluate adsorption capabilities under wastewater treatment-relevant conditions and to evaluate material lifetimes. In this test, the BC@mMIP material was compared to the BC@NP, commercial activated carbon (F400) and sand control columns.

4.2.5.1 Column Set Up

4.2.5.1.1 Column Assembly and Packing

Triplicate columns were run for each of four packing types [sand (control), F400 (commercial AC), BC@NP, and BC@mMIP] for twelve columns in total. Columns were constructed from PVC pipes and fittings with HDPE tubing and tubing fittings. Columns were run in an up-flow configuration. Influent solution was stored in a covered 55 L linear low-density polyethylene (LLDPE) tank at room temperature with constant stirring. An Ismatec IP High Precision Multichannel peristaltic pump was used to convey water to the columns, and PharMed® BPT tubing was used within the pump housing. Sample ports were located at the top of the columns and effluent was subsequently collected in a PVC pipe and collected for disposal. A photo of the assembled columns is provided in **figure C3**. Adsorbents (BC@mMIP, BC@NP and F400) were packed at 1 weight percent (wt. %) with pre-washed sand (approximately 56 g sand and 0.56 g adsorbent media per column). Columns were weighed pre- and post-packing, and both wet and dry to quantify the pore volume in each column (**table C6**).

4.2.5.1.2 Tracer Testing

Following column assembly, a tracer test was performed using sodium borate to confirm the column pore volumes calculated in ***section 4.2.5.1.1***. Tracer stock solutions of 2.5 mM and 50 mM Br^- as NaBr were prepared in ultrapure water. The lower concentration stock was used for the sand,

BC@NP, and BC@mMIP columns while the high concentration stock was used for the F400 columns to account for the moderate levels of bromide adsorption by that material. A flow of 1 mL/min of deionized (DI) water was started through the first column replicate of each adsorbent type (for a total of four columns). The columns were allowed to equilibrate for 60 min, and then a 1 minute duration sample was collected from each column and weighed to confirm the flow rate.

Once the columns were equilibrated at the correct flow rate, influent lines were removed from the DI water, placed in the appropriate NaBr stock for 8 seconds, and then placed back in the DI water. Small air bubbles were allowed to form in the tubing lines on either side of the NaBr stock to track the location of the tracer. The movement of the tracer aliquot through the influent lines to the start of the column was timed and recorded for future reference. Tracer test sampling was started once the tracer stock reached the column with 1 minute (1 mL) samples collected every two minutes from each column.

4.2.5.2 Wastewater Effluent Characterization and Preparation for Column Influent

Wastewater treatment plant (WWTP) effluent was obtained from the West Point Treatment Plant located in Seattle, WA and operated by the King County Wastewater Treatment Division. Samples were collected weekly in 5-gal buckets and stored at room temperature until use. Aliquots of each weekly sample were characterized as follows to gain a better understanding of the chemical composition of the WWTP effluent and results from all analyses are tabulated in **table 4.3**.

4.2.5.2.1 Quantification of Organic Matter and pH

Dissolved organic carbon (DOC) was quantified as described by Standard Method 5310[196] using a Shimadzu TOC-L analyzer (Kyoto, Japan) using the non-purgeable organic carbon analysis mode. A 20 mL sample of wastewater effluent was filtered with a 0.22 μm cellulose acetate syringe

filter by first wasting approximately 10 mL of sample through the filter prior to collecting a 9 mL aliquot for DOC analysis.

Total dissolved solids (TDS) and total suspended solids (TSS) were quantified as described by Standard Methods 5240C and 2540D, respectively.[196] Briefly, a Whatman glass fiber filter was pre-washed with 60 mL of ultrapure water, dried at 100 °C overnight, weighed, and washed with an additional 30 mL of ultrapure water. A 250 mL glass beaker was also washed with ultrapure water, dried at 180 °C overnight and weighed. A 250 mL aliquot of WWTP effluent sample was passed through this filter using high vacuum, and the filtrate was collected in the 250 mL beaker. Filtrate was evaporated to dryness at 100 °C, then heated at 180 °C for 1 h and weighed once cool. The difference in mass compared to the washed beaker was attributed to TDS. Organics retained on the filter were dried at 100 °C overnight and weighed, and the change in mass compared to the washed filter was attributed to TSS.

Sample pH was measured with an Orion Star A111 pH meter equipped with an Orion Ross Ultrap pH/ATC Triode probe.

4.2.5.2.2 Quantification of Ions and Trace Organic Contaminants

Ions from common salts were measured via ion chromatography (for anions: chloride, nitrate, and sulfate) and inductively coupled plasma optical emission spectroscopy [ICP-OES; for cations: sodium, calcium(II), magnesium(II), lead(II), aluminum(III), and total iron]. Instrument and methodology details for both analyses are given in the supplemental information (***section C13***). For both analyses, samples were filtered with a 0.22 μm syringe filter by first wasting approximately 10 mL of sample through the filter prior to collecting the aliquot for analysis. ICP-OES samples were also acidified with nitric acid to obtain a final acid concentration of 1% v/v.

Initial concentrations of adsorbates of interest (i.e., PFOS, PFHxS, PFBS, 6:2-FTS, PFOA, PFHxA, PFPeA, PFBA, TFA, acetaminophen, fipronil, sulfamethoxazole, and benzotriazole) were quantified via liquid chromatography tandem mass spectrometry (LC-MS/MS) and high performance liquid chromatography followed by ultra-violet spectroscopy (HPLC-UV) as described in ***sections C11*** *and* ***C13***. No quantifiable amounts of PFAS, fipronil, or sulfamethoxazole were found in the wastewater effluent samples; benzotriazole was quantified in the wastewater effluent at 7.7 ± 1.9 μg/L and was factored into the initial concentration of the column test influent accordingly.

4.2.5.2.3 Preparation of Column Influent Stock Solution

Column influent stock comprised of WWTP effluent spiked with approximately 20 μg/L each of PFOS, PFHxS, PFBS, 6:2-FTS, PFOA, PFHxA, PFPeA, PFBA, TFA, acetaminophen, fipronil, sulfamethoxazole, and benzotriazole was prepared in batches of no more than 55 L. Briefly, a concentrated adsorbate stock was prepared in ultrapure water from individual methanolic stocks. The ultrapure water stock was stirred for 10 minutes to completely mix, and then a 1 mL aliquot was collected for adsorbate quantification. This stock was then added to the appropriate volume of WWTP effluent to obtain the desired goal concentration and stirred overnight to obtain a homogeneous mixture. Slow stirring was maintained for the duration of the column test and influent stock was refreshed every 3 – 4 days as needed. WWTP effluent samples were collected weekly.

4.2.5.3 Column Adsorption and Regeneration

PFAS adsorption and recovery capabilities in the columns were evaluated over four sequential cycles of adsorption and regeneration with each cycle consisting of a six day adsorption period followed by six hours of regeneration and then an 18 hour low flow DI wash. During the

adsorption phase, a constant flow of 1 mL/min of the column influent stock described in ***section 4.2.5.2.3*** was delivered to each column as described in ***section 4.2.5.1.1***. Samples were collected as one minute composites (1 mL sample volume) and stored at -20 °C prior to analyte quantification. After six days, flow to the columns was briefly stopped, and influent lines were washed with ultrapure water and placed in the regeneration solution (column wash). The column wash was 70% methanol, 1% sodium chloride and 2.8 mM sodium hydroxide in ultrapure water. During the regeneration phase, column wash was delivered at 0.5 mL/min for six hours. Samples were collected as two minute composites (1 mL sample volume) and stored at -20 °C prior to analyte quantification. Following regeneration, DI water was passed through the columns at 0.5 mL/min for 18 hours to wash out any residual methanol or sodium chloride in preparation for the next adsorption phase.

4.3 RESULTS AND DISCUSSION

4.3.1 High BC@MIP Specific Surface Area is Attributed to Biochar Morphology and Templated Binding Sites

BET surface area analysis and TEM imaging revealed a thin, variable polymer coating on the BC@mMIP composite with high SSA derived from both the microporous biochar morphology and templated binding sites in the polymer layer. Only a minor reduction in SSA was observed following immobilization of the single- and multi-template imprinted polymers to the biochar surface (**table 4.1**).

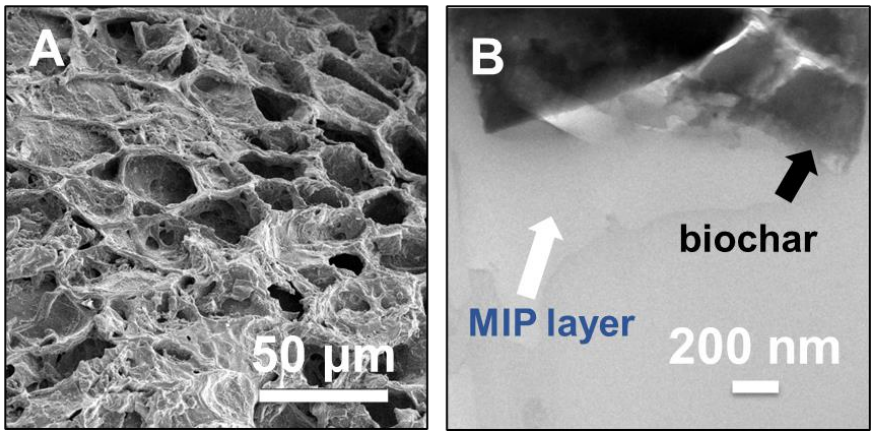

Figure 4.1 Scanning electron microscope image of BC substrate (A)[1] and transmission electron microscope image of multi-template MIP-BC composite (B) showing adsorbent morphology.

All four BC@MIP materials had a SSA of around 1000 m^2/g compared to 1319 m^2/g for the unmodified biochar. The average pore diameter increased slightly following MIP immobilization from 3.3 nm for the BC to 4.1 – 9.8 nm for the BC@MIP materials. This increase in pore size can be primarily attributed to the formation of templated binding sites since the non-imprinted polymer (BC@NP) did not experience a similar increase in pore size. Polymer thickness for the BC@mMIP material can be estimated in the range of 10 – 500 nm from the TEM image shown in **figure 4.1**. It should be noted that significant spatial variability in polymer thickness appears to be present, likely a result of the irregular morphology of the biochar surface as well as irregularity inherent in the radical initiated polymerization process. This high surface area is expected to contribute to high PFAS adsorption capacities, as discussed further in ***section 4.3.3***.

4.3.2 Batch Adsorption Behavior

4.3.2.1 Inclusion of multiple templates improves adsorption of short- and long-chain PFAS

Inclusion of multiple PFAS templates in the BC@MIP synthesis rather than a single template compound appears to result in a synergistic effect (i.e., improved self-assembly of template and functional monomer) which is revealed through an examination of the imprinting factors (IFs). For all three template compounds, IFs are significantly higher for the BC@mMIP than for the corresponding single-template BC@MIP [**figure 4.2 (B – D) text**]. The improved imprinting approach using multiple PFAS templates resulted in a subsequent improvement in adsorption of both short- and long-chain PFSAs and PFCAs, as demonstrated by the results of the PFAS competition test described in ***section 4.2.4.1*** and shown in **figure 4.2 (A – D)**. Single template BC@MIP materials do show improved adsorption of the template over other PFAS compounds when compared to the non-imprinted BC@NP. This is demonstrated by the selectivity coefficients [graphed in **figure 4.2 (B – D)** and tabulated in **table C5**] which are generally greater than or equal

to one. A $K_{selectivity}$ value of greater than one indicates the templating process improved selectivity for the template compared to the other adsorbate of interest while a $K_{selectivity}$ value of less than one indicates templating improved selectivity for the other adsorbate of interest compared to the template. One notable exception is the low $K_{selectivity}$ values for PFPeA and PFBA adsorption onto BC@MIP(F) which supports a hypothesis from our prior work[116] that MIPs templated solely by long-chain PFAS perform poorly for short chain PFAS removal, likely due to competition between short- and long-chain PFAS for adsorption sites. By contrast, the BC@mMIP material had lower template selectivity but higher percent removals, making it a more ideal adsorbent for treatment of a suite of PFAS compounds. This is demonstrated through a closer look at the $K_{selectivity}$ values for BC@mMIP. For 6:2-FTS and PFBS, which are removed relatively well by all adsorbents of interest, $K_{selectivity}$ values were around 1.0 or lower, indicating little to no improvement in selectivity for the template over other PFAS. For PFPeA, which was removed poorly by other polymer modified adsorbents, $K_{selectivity}$ values were high for the PFSAs and long-chain PFCAs and very low for PFBA. This reflects the significant improvement in short-chain PFCA adsorption achieved through the multi-template approach, which can also be seen in **figure 4.2 (A)**. This ability to remove long- and short-chain PFSAs and PFCAs makes BC@mMIP a better candidate for treatment of PFAS in waters containing a complex mixture of PFAS.

Compared to the non-imprinted polymer, the BC@mMIP showed similar adsorption of long chain PFAS (i.e., PFOS, PFHxS, 6:2-FTS, and PFOA) but significantly improved adsorption of shorter-chain PFAS. This indicates binding to templated sites is likely an important adsorption mechanism for short-chain PFAS removal while long-chain PFAS likely participate in both template site and non-specific adsorption. This may be due to competition between short- and long-chain PFAS at non-specific binding sites which is avoided due to size exclusion of larger

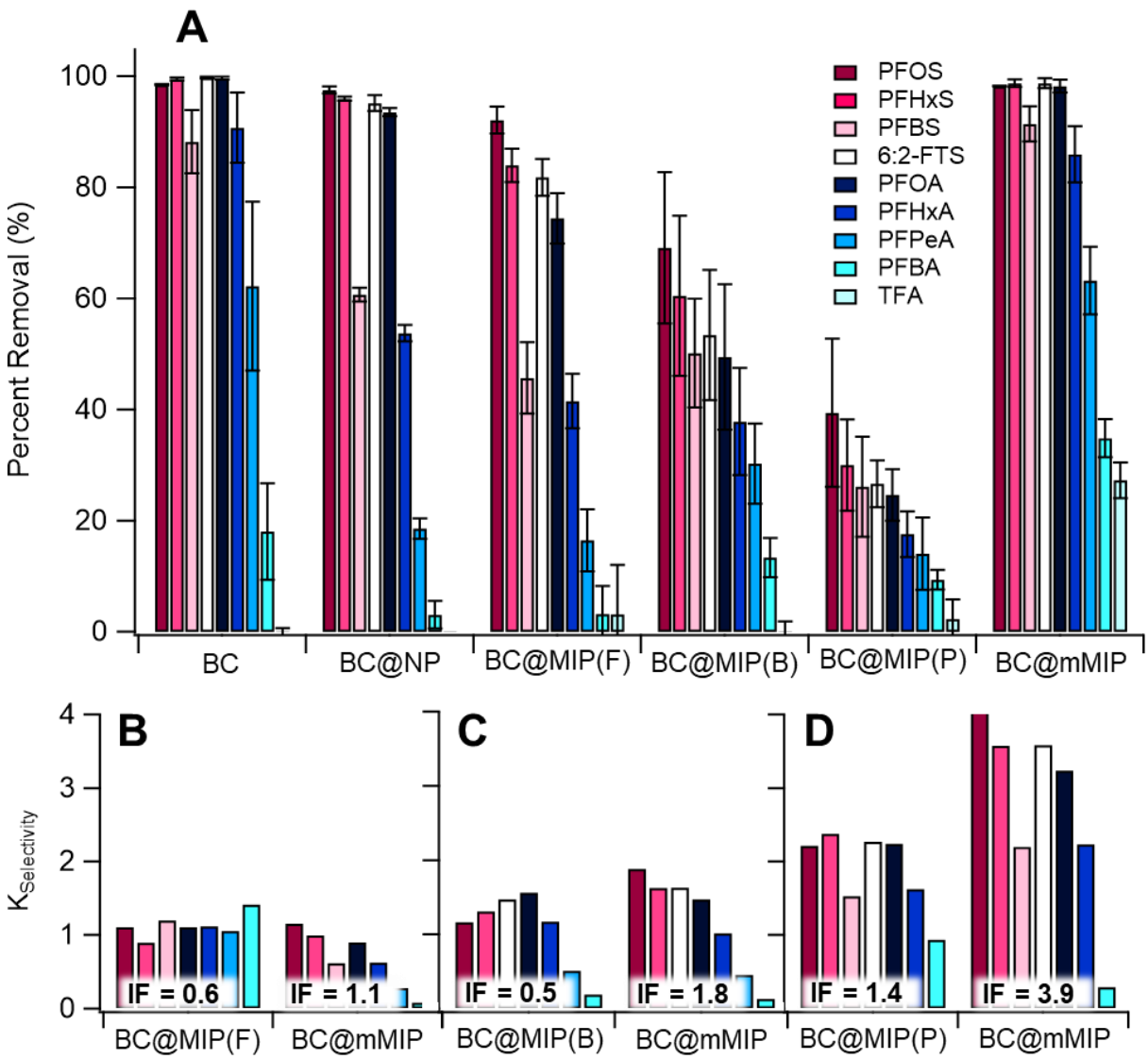

Figure 4.2 (A) Adsorption of nine PFAS by 100 mg/L of unmodified and polymer modified biochar materials over a 4-day equilibration time. Error bars represent standard deviation from triplicate samples. Initial concentrations were 58 ± 3.7 µg/L PFOS, 50 ± 5.5 µg/L PFHxS, 49 ± 5.1 µg/L PFBS, 48 ± 3.2 µg/L 6:2-FTS, 50 ± 4.9 µg/L PFOA, 58 ± 4.8 µg/L PFHxA, 52 ± 5.4 µg/L PFPeA, 53 ± 5.5 µg/L PFBA, and 41 ± 7.8 µg/L TFA. Figures (B) through (D) show a comparison of selectivity coefficients for single- and multi-template BC@MIP materials calculated from adsorption of nine PFAS shown in (A) with 6:2-FTS, PFBS, and PFPeA used as templates in calculations for (B), (C), and (D), respectively. Non-imprinted polymer (BC@NP) was used as a reference material for these calculations.

PFAS at templated binding sites that were imprinted by short-chain PFAS (i.e., PFBS or PFPeA).

Despite the improvement in short-chain PFAS adsorption observed for the BC@mMIP, a hierarchy of PFAS removals was still observed with removal of PFSAs > PFCAs and long-chain

PFAS > short-chain PFAS. The reason for this is threefold. First, PFSAs generally have a higher electronegativity than their PFCA counterparts (owing to the sulfonic head group),[115] increasing electrostatic attraction to the quaternary nitrogen moiety on the functional monomer. Second, as discussed above, long-chain PFAS are able to participate in adsorption to both non-specific and templated binding sites while short-chain PFAS appear more likely to adsorb to templated binding sites only. Finally, a significant decrease in adsorption is observed between PFHxA and PFPeA as well as between PFPeA and PFBA. This corresponds to significant increases in water solubility from 27.1 mg/L for PFHxA to 197 mg/L for PFPeA and to 1370 mg/L for PFBA (as shown in **table C3**) which decreases the adsorptive driving forces for these shorter-chain PFAS, making them prefer to remain in the aqueous phase rather than adsorb to the more hydrophobic organic carbon of the BC@mMIP. This hierarchy of adsorption capabilities is not surprising when considering the physicochemical properties of these PFAS but should be considered when evaluating the adsorption capabilities of the BC@mMIP.

4.3.2.2 PFAS head group and chain length have a significant impact on adsorption capacity and mechanism

Isotherm adsorption tests revealed PFBS adsorption onto BC@mMIP was described best by the Freundlich model (R^2 = 0.996), indicating the presence of heterogeneous binding sites with variable affinity for the templates, as shown in **figure 4.3**. This is attributed to multiple modes of adsorption: (i) binding to template-specific sites, (ii) binding to sites templated by other PFAS, and (iii) non-specific adsorption to the composite surface. Firstly, preferential adsorption at templated sites is expected to occur due to a combination of electrostatic attraction between the negatively charged sulfonate head group and the positively charged quaternary nitrogen moiety on the VBTAC template[46, 53, 116, 146] as well as hydrophobic attraction between the fluorocarbon tail

of the PFBS and the aromatic ring on the VBTAC.[53, 56, 61, 116] Adsorption to PFBS-templated sites should be preferred over 6:2-FTS-templated or PFPeA-templated sites due to the size and shape selectivity inherent in the templating process. Finally, non-specific adsorption to untemplated sites on the MIP surface is expected to occur primarily as a lower affinity mechanism, primarily via hydrophobic attraction.[53, 137] Additional adsorption at high PFAS concentrations is likely to occur from PFAS-PFAS hydrophobic interaction resulting in the formation of micelles or hemimicelles on the adsorbent surface, a phenomenon that has been reported at equilibrium concentrations several orders of magnitude below the critical micelle concentration[61, 197] (i.e., approximately 6600 mg/L at 32 °C for PFBS).[198] The 1/n value for the PFBS Freundlich model was less than 0.7 (see **figure 4.3 table**), which is characteristic of highly curved isotherms and indicative of saturation of available binding sites near the high concentration end of the isotherm. This supports the conclusion that at PFBS concentrations near or above the high end of this isotherm data (i.e., greater than or equal to around 3000 μg/L) additional PFBS adsorption would be minimal and primarily the result of PFAS-PFAS interactions and some non-specific binding.

Adsorption of PFPeA was described well by the Langmuir model (R^2 = 0.989), indicating adsorption mainly occurred to binding sites with homogeneous affinity as shown in **figure 4.3**. This may be the result of PFPeA primarily binding at templated sites via electrostatic attraction with little to no non-specific binding occurring due to hydrophobic attraction to non-templated areas of the MIP surface. Another important consideration from these results is the low equilibrium adsorption capacities for PFPeA compared to the other templates. This is consistent with the results from the PFAS competition test (the q_e for PFPeA adsorption onto BC@mMIP in that test was 0.38 mg/g). However, this indicates PFHxA or another longer chain PFAS may be a better choice

for a PFCA template compound in future synthesis efforts while PFBS or other short-chain PFSAs are good choices for short-chain PFAS templates.

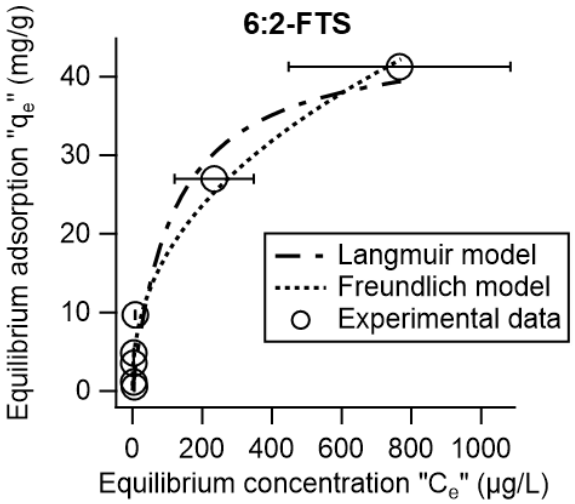

	6:2-FTS	PFBS	PFPeA
$q_{max,L}$	45.4	64.9	7.69
K_L	0.009	0.003	0.003
R^2	0.980	0.980	0.989
$q_{max,exp}$	41.3	50.8	6.80
K_F	2.40	0.933	0.272
1/n	0.432	0.529	0.402
R^2	0.984	0.996	0.973

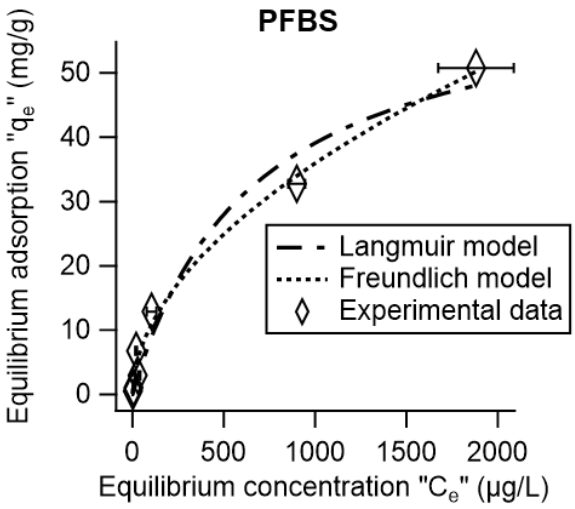

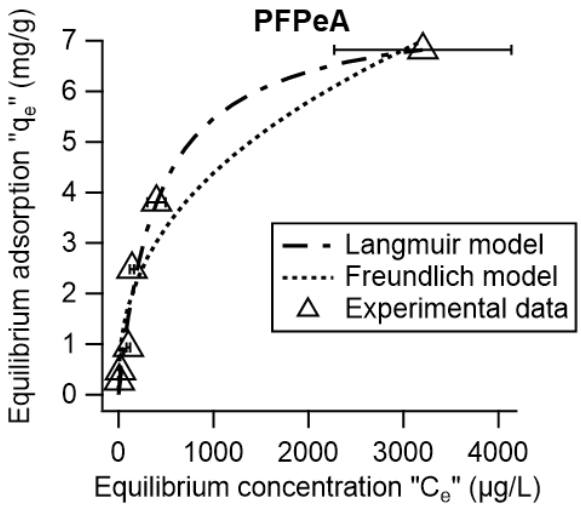

Figure 4.3 Adsorption of approximately 5 – 5000 µg/L of individual templates (6:2-FTS, PFBS, PFPeA) onto BC@mMIP. Error bars represent standard deviation of triplicate samples. Data is modeled with the Langmuir and Freundlich isotherms. Calculated model parameters are shown in the **Figure 4.3 table**.

The adsorption of 6:2-FTS onto BC@mMIP by contrast, was described well by both the Langmuir (R^2 = 0.980) and Freundlich (R^2 = 0.984) models. The 6:2-FTS adsorption results indicate a much smaller difference in adsorption affinity between templated and non-specific binding sites for 6:2-FTS than for either PFBS or PFPeA. These isotherm results also reflect the

high $\log K_{oc}$ and low water solubility of 6:2-FTS (see **table C3**) which make adsorption of this compound easier onto a range of adsorbents, as demonstrated in the prior section. Thus, 6:2-FTS is likely to adsorb to both templated and non-specific binding sites across the range of concentrations investigated.

4.3.2.3 BC@mMIP removes PFOA to below the proposed EPA MCL at (waste)water-relevant concentrations

The BC@mMIP demonstrated high removals of PFAS at (waste)water treatment relevant concentrations, as demonstrated in **figure 4.4**, indicating this material may be a promising alternative for selective adsorption of PFAS. Over 90% removal was observed for four PFSAs (92.5% of PFOS, 99.4% of PFHxS, 91.7% of PFBS, and 97.7% of 6:2-FTS) and two long-chain PFCAs (99.4% of PFOA and 97.7% of PFHxA). Of particular note is the low equilibrium PFOA concentration (0.5 ng/L) which is well below the proposed EPA MCL of 4 ng/L. Two additional contaminants included in the proposed MCL, PFBS (9.1 ng/L at equilibrium) and PFHxS (0.6 ng/L at equilibrium), were similarly treated to well below their referenced Health Based Water Concentrations of 2000 ng/L and 10 ng/L, respectively. The equilibrium PFOS concentration (16.4 ng/L) was notably higher than the proposed MCL of 4 ng/L. This is attributed in part to the higher than expected initial PFOS concentration (217 ± 93 ng/L) and in part to PFOS contamination observed during the SPE concentration step. However, despite these challenges, it is clear that high PFOS removal is possible. Over 50% removal of three short-chain PFCAs was also observed (57.8% of PFPeA, 54.0% of PFBA, and 88.5% of TFA). This drop in percent removal of PFCAs from the C6 to C5 and C4 compounds can be primarily attributed to the increased water solubility, as discussed in ***section 4.3.3.1*** and is commonly observed during adsorption of complex PFAS mixtures by AC and ion exchange (IX) resin.[20, 199] Of particular note is the TFA removal, which

was higher than expected considering the results presented in ***section 4.3.3.1***. Additional investigation is needed to further elucidate the mechanism for this high removal. These results indicate the BC@mMIP adsorbent is capable of PFAS removal sufficient to meet regulatory requirements, making it a promising alternative to less selective adsorbent materials like AC and BC.

High PFAS recovery from spent adsorbent (shown in **figure 4.4)** indicates long material lifetimes may be possible, an essential characteristic given the higher expected production cost compared to commercial AC adsorbents. Interestingly, PFAS recovery did not appear to follow a specific trend with respect to PFAS chain length, although recovery of PFSAs generally appeared higher than that of PFCAs. For example, 84.3% of PFHxS was recovered compared to only 56.4% of PFOA and 73.3% of PFHxA. These results are somewhat in contrast to prior studies which have generally demonstrated increasing recovery with increasing chain length and higher recovery for PFSAs than PFCAs.[116] Recovery of the three PFAS template compounds (i.e., PFBS, 6:2-FTS, and PFPeA) was significantly higher than 100%. This is attributed to the incomplete recovery of the templates remaining within the BC@mMIP following the washing step described in ***section 4.2.2***. It is important to note that this unrecovered template mass was relatively low (0.28 μg PFBS, 0.86 μg 6:2-FTS, and 0.15 μg PFPeA) and did not appear to leach during the adsorption phase. Thus, unrecovered template remaining in the MIP layer is not expected to significantly impact adsorption performance of this material. Another key finding was that PFAS recovery did not increase significantly with time after the first day, as demonstrated in **figure C2**. For example, PFHxS recovery was 35% on day one and 42% on day seven. These desorption kinetics results indicate PFAS desorption kinetics from the BC@mMIP are relatively fast, which is beneficial for use in water treatment scenarios. It should be noted that the total mass of PFAS sorbed to the

BC@mMIP in this test was fairly low. Therefore, it would be beneficial to repeat this test either with higher PFAS concentrations or in a column test set up to confirm the validity of this conclusion about the desorption kinetics.

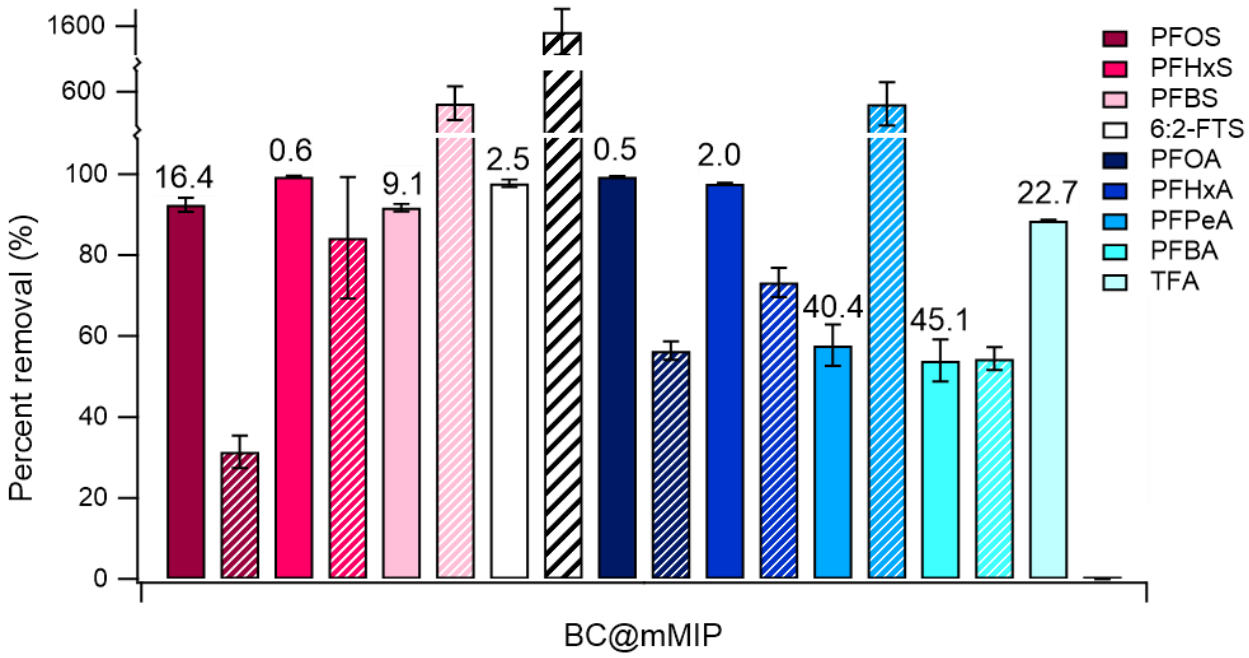

Figure 4.4 Adsorption of nine PFAS by 100 mg/L of BC@mMIP over four in ultrapure water with an initial pH of 7.0 are shown as solid bars. Subsequent PFAS recovery over 7 days in a 70% methanol, 1% sodium chloride, and 2.8 mM sodium hydroxide solution at a solids concentration of 1 g/L are shown as hashed bars. Error bars represent standard deviation of triplicate samples. Data labels give equilibrium solution concentration in ng/L following the adsorption phase. Initial PFAS concentrations were: 217 ± 93 ng/L PFOS, 114 ± 28 ng/L PFHxS, 109 ± 29 ng/L PFBS, 112 ± 10 ng/L 6:2-FTS, 93 ± 10 ng/L PFOA, 87 ± 19 ng/L PFHxA, 96 ± 19 ng/L PFPeA, 98 ± 6 ng/L PFBA, and 197 ± 50 ng/L TFA.

4.3.3 Column Test Results

4.3.3.1 PFAS Adsorption to BC@mMIP was Hindered by the Presence of Effluent Organic Matter and Total Dissolved Solids

The high total dissolved solids (TDS) load in the wastewater effluent, particularly from sulfate salts, contributed to low PFAS removal by the polymer modified biochar the during column filtration studies (TDS = 286 mg/L and sulfate = 16.3 mg/L in round one, see **table 4.2)**. This result

can be observed in the concentration time series plots for each analyte from the first adsorption cycle (**figure 4.5** and **C5**) where PFAS removal by BC@mMIP was lower than removal by F400 and lower than expected given the batch test results described in ***section 4.3.2***. For example, complete breakthrough of the long-chain PFOS and PFOA occurred around 125 pore volumes for the BC@mMIP compared to a much slower breakthrough on F400 which did not experience complete breakthrough by the end of round one (261 pore volumes). A similar comparison can be made for the short-chain PFBS and PFBA which show the same trend but with BC@mMIP breakthroughs around 50 pore volumes. In a high TDS matrix, competition for adsorption sites between PFAS and ionic species (particularly sulfur-containing salts) has been observed in previous studies of PFAS adsorption by MIP materials or IX resins containing quaternary nitrogen-containing moieties.[38, 46, 178] In mixed matrices containing PFAS and sulfate salts, electrostatic attraction between the sulfate ions and quaternary nitrogen moieties within templated binding sites is expected to block PFAS adsorption at these sites, thereby decreasing the PFAS removal capabilities of the MIP adsorbent and making it behave more like the non-imprinted BC@NP. The performance of the F400 was less impacted by matrix effects, as demonstrated by the later breakthrough times observed for almost all compounds (**figure 4.5** and **C5**). This can be attributed to the primary adsorption mechanism for PFAS onto F400 (hydrophobic attraction to non-specific binding sites) which will not be impacted by competition with ionic species. The PFAS adsorption during column testing followed a similar trend to that observed in the batch tests with greater removal of long-chain PFAS compared to short-chain PFAS. Interestingly, very little difference was observed in adsorption of similar chain-length PFSAs and PFCAs. This result can also be attributed to adsorption of sulfate ions which will exert a larger repellant force on the more electronegative PFSAs. The impaired PFAS adsorption results by the BC@mMIP composite

indicate pretreatment of wastewater effluent and other matrices with high sulfate concentrations (e.g., with IX) is needed to realize the full PFAS removal potential of the BC@mMIP.

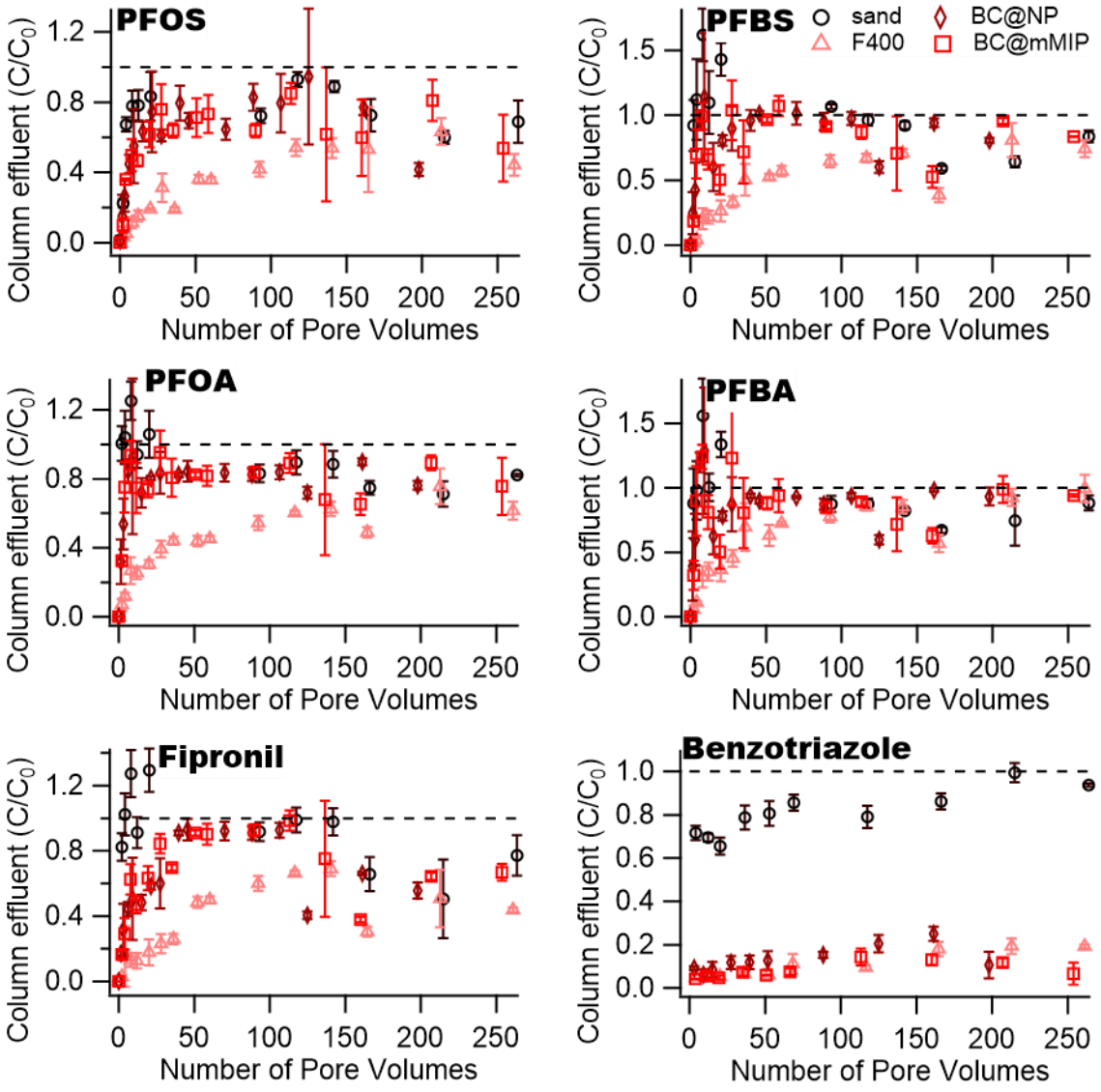

Figure 4.5 Time series normalized column effluent concentrations for representative PFAS and organic compounds with initial concentration of approximately 20 µg/L each in a wastewater effluent matrix delivered at 1 mL/min to columns containing 1 wt% of adsorbent in sand. Error bars represent standard deviation from triplicate columns for each media type.

Table 4.2 Chemical characteristics of weekly wastewater treatment plant effluent samples.

Collection Date	4/3/2023	4/10/2023	4/17/2023	4/24/2023
DOC (mg/L)	9.4 ± 0.3	6.7 ± 0.2	9.3 ± 0.2	10.2 ± 0.5
TSS (mg/L)	3.6	2.0	2.4	4.8
TDS (mg/L)	286	255	130	442
pH (S.U.)	7.12	7.20	7.15	7.38
Chloride (mg/L)	113	64.4	71.4	192
Nitrate (mg/L)	5.49	0.94	0.79	1.49
Sulfate (mg/L)	16.3	11.5	14.2	22.3
Sodium (mg/L)	41.7 ± 2.4	36.2 ± 2.5	24.1 ± 2.1	53.5 ± 4.2
Calcium(II) (mg/L)	17.5 ± 0.1	16.1 ± 0.1	17.1 ± 0.3	20.9 ± 0.4
Magnesium(II) (mg/L)	9.8 ± 0.0	9.3 ± 0.1	8.7 ± 0.2	14.5 ± 0.3
Lead(II) (mg/L)	ND	ND	ND	ND
Aluminum(III) (mg/L)	0.01 ± 0.0	0.01 ± 0.0	0.01 ± 0.0	0.01 ± 0.0
Total iron (mg/L)	0.5 ± 0.0	0.1 ± 0.0	0.1 ± 0.0	0.1 ± 0.0

ND: below limit of detection

The presence of effluent organic matter (EfOM) and TDS did not appear to affect co-occurring organics adsorption to as great of an extent since removal of organics was generally higher than PFAS (**figure 4.5**). Adsorption of acetaminophen, benzotriazole, and sulfamethoxazole in particular were significantly higher than any PFAS compound, with greater than 80%, 70%, and 50% removal, respectively, observed for the duration of round one. This can be attributed to the relatively high organic carbon distribution coefficients ($logD_{oc}$; **table C3**) of these compounds at pH 7.0 which range from 1.09 to 1.65 compared to the $logD_{oc}$ values of the PFAS compounds which range from -1.65 (6:2-FTS) to -9.75 (PFBS). The higher $logD_{oc}$ values of the co-occurring organics are due in large part to their higher pK_a values and are responsible for increased adsorption both to the adsorbent media and to the suspended organics that may be physically removed by any of the four types of media. Fipronil is the exception to this trend with a high $logD_{oc}$

of 3.77 similar to the other organics but exhibiting lower adsorption and faster breakthrough similar to that of the PFAS compounds (**figure 4.5**). This may be due in part to the large molecular size of fipronil which would hinder adsorption at templated binding sites, limiting its adsorption potential on the BC@mMIP. It is also important to note that according to the Organization for Economic Cooperation and Development's (OECD) definition of a PFAS (i.e., compounds containing at least one fully fluorinated carbon) fipronil is categorized as a PFAS, which may also contribute to similarities in their adsorption behavior.[200]

PFAS and organic analyte removal by the sand only control columns was higher than expected for several compounds including PFOS (**figure 4.5**), acetaminophen, and sulfamethoxazole (**figure C5**). This removal is attributed to adsorption of analytes onto suspended effluent organic matter which was physically removed by the media in the sand columns.

4.3.3.2 BC@mMIP Maintains Consistent PFAS Removal Over Multiple Cycles

The PFAS removal capabilities of BC@mMIP were maintained over four cycles of adsorption and regeneration with a 70% methanol, 1% sodium chloride, and 2.8 mM sodium hydroxide solution in water. This consistent removal is demonstrated by the mass adsorbed and recovered (shown in **figures 4.6 and C6**) and which is steady or increasing across adsorption cycles for all nine PFAS. Notably, PFAS removal increased from the second to third adsorption rounds, particularly for the short-chain PFBS and PFBA (**figure 4.6**) and PFPeA (**figure C6)**. This increase can be attributed to the relatively lower influent TDS in round three (130 mg/L compared to 255 mg/L in round 2) as shown in **table 4.2** which is expected to have reduced competition for templated adsorption sites on the BC@mMIP between PFAS and sulfate species. The improved PFAS adsorption during round three also supports the earlier hypothesis that high TDS levels severely impacted PFAS sorption by the BC@mMIP. In contrast to the trend observed for

BC@mMIP, the F400 PFAS adsorption performance decreased over the four cycles of adsorption and regeneration for most of the PFAS compounds (except PFOS and 6:2-FTS) and fipronil. The drop in adsorption by F400 indicates adsorption sites on F400 are not able to be regenerated to the extent that those on the polymer modified biochar adsorbents are. The relatively consistent removal of PFOS, 6:2-FTS, acetaminophen, benzotriazole, and sulfamethoxazole by F400 reflects the higher adsorption affinities of the F400 for these compounds, as discussed previously. It is expected that over additional adsorption and regeneration cycles the removal of these compounds by F400 would begin to decrease as well. The consistent PFAS removal capabilities of the MIP modified biochar material indicate this adsorbent is likely to experience longer material lifetimes than traditional activated carbon, potentially offsetting the higher production cost and making it a promising alternative.

Interestingly, the calculated mass of PFAS recovered from the BC@mMIP was significantly lower than the mass adsorbed for all nine PFAS compounds (**figures 4.6** and **C6**). This result was surprising given the relatively consistent PFAS removal across all four cycles which would seem to indicate good regeneration of adsorption sites between each adsorption cycle. This discrepancy is likely due to one or both of the following factors. First, the regeneration step may have facilitated high recovery of sulfate ions and other salts adsorbed to quaternary nitrogen moieties in templated binding sites. This regeneration of sites blocked by ions may have been sufficient to allow for good PFAS removal in subsequent adsorption cycles despite low PFAS recovery during the regeneration step. Second, the mass of PFAS recovered may have been underestimated due to a lack of granularity in the data collected from the regeneration step (only three samples were collected over the six hour regeneration time). If PFAS recovery primarily occurred in the first hour or two, the

midpoint integration method used to calculate the mass recovered may be a significant underestimate.

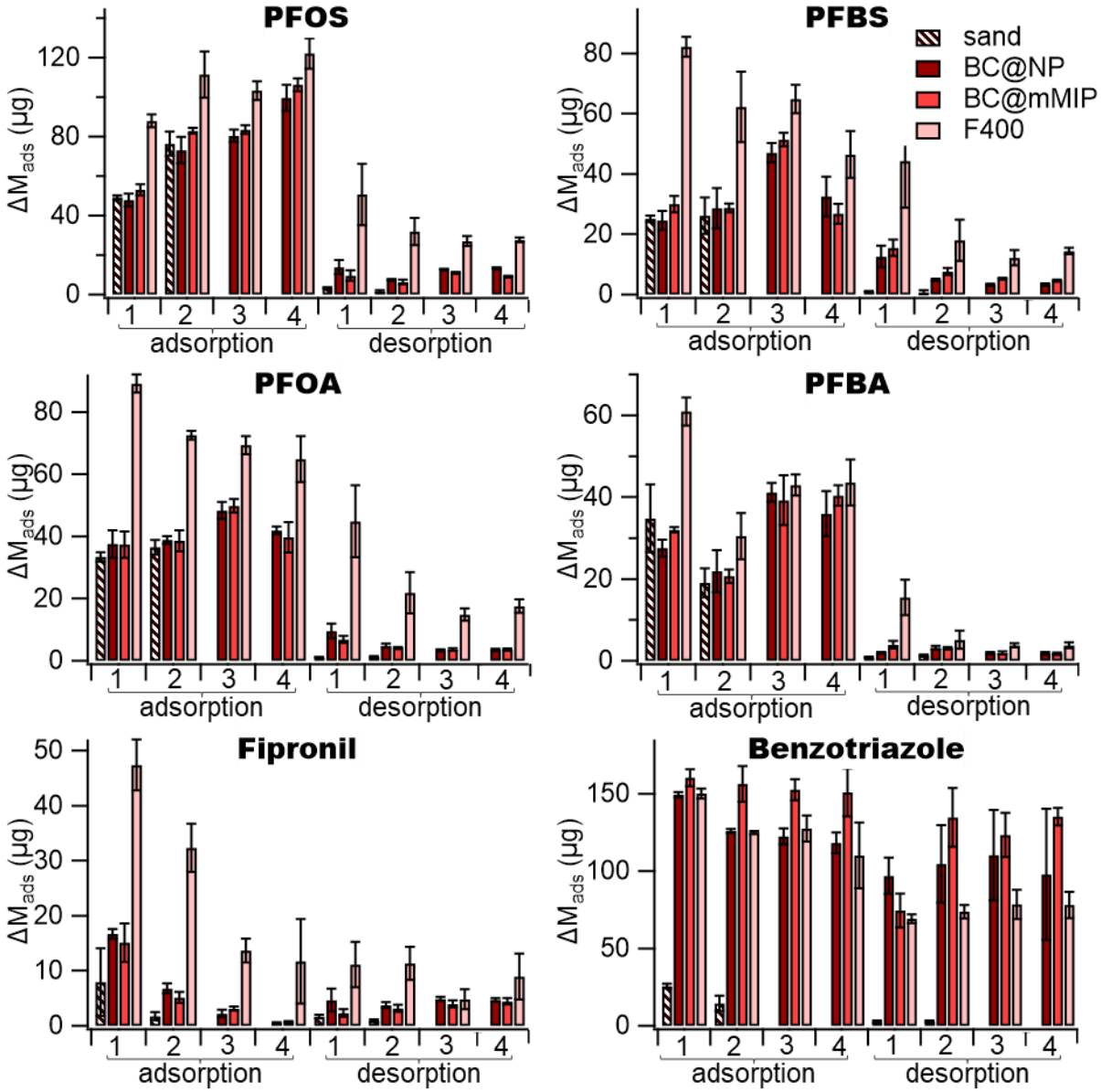

Figure 4.6 Mass adsorbed and desorbed over from column media over four sequential cycles for representative PFAS and organic compounds. Initial concentrations for each compound during adsorption was approximately 20 μg/L in a wastewater effluent matrix delivered at 1 mL/min to columns containing 1 wt% of adsorbent media in sand. Desorption was achieved by flushing with the column wash solution at 0.5 mL/min. Error bars represent standard deviation from triplicate columns for each media type.

4.4 CONCLUSIONS

Selective PFAS adsorbents are needed to address the issue of PFAS contamination in a range of water sources, including wastewater. In particular, there is a need for adsorbent materials capable of high short-chain PFAS removal to address the increasing occurrence of short-chain PFAS. The multi-template BC@MIP adsorbent described herein has the potential to fulfill both of these needs. Our BC@mMIP material was able to remove PFOA, PFHxS, and PFBS to below their respective proposed MCLs in a batch adsorption test with (waste)water-relevant initial concentrations of nine PFAS. Column adsorption testing with higher concentrations of the same nine PFAS spiked into real wastewater effluent showed lower removal than expected which was attributed to interference from competing organics and ions, particularly sulfate species. Additional adsorption testing in wastewater effluent with lower initial PFAS concentrations, and IX pre-treatment should be considered to further evaluate the capabilities and limitations of this adsorbent. Given the results presented herein, the BC@mMIP material is expected to be an excellent option for treatment of long- and short-chain PFAS in lower TDS/TOC containing waters like typical drinking water treatment and some water reuse scenarios.

This work also demonstrated some of the benefits of the multi-template imprinting approach compared to the traditional, single-template MIP, particularly for removal of a complex suite of compounds like PFAS. For PFAS removal, the high selectivity for a single template compound that is characteristic of traditional MIP materials is not necessarily desirable since removal of a number PFAS is often desired. The multi-templating approach significantly improved adsorption, particularly of short-chain and carboxylic PFAS when compared to the non-imprinted and single-template MIPs. We hypothesize that there is a synergistic interaction between multiple types of templates and the functional monomer that was unable to occur in the single-template scenarios. The complex interactions between the different templates and the BC@mMIP were reflected in

the adsorption isotherm results. Electrostatic attraction was expected to be most dominant in interactions between PFBS and the VBTAC monomer owing to the high electronegativity of the sulfonate head group and the relatively short chain length of the four carbon PFBS tail which promote preferential adsorption at templated binding sites. Hydrophobic interaction was expected to dominate interactions between PFPeA and VBTAC, although the short chain length and high water solubility of PFPeA resulted in a much lower adsorption capacity for PFPeA. The sulfonic head group and long chain length of 6:2-FTS allowed for both hydrophobic and electrostatic attraction to the VBTAC and resulted in good adsorption both to templated and non-specific binding sites. The success and versatility of the multi-template approach make it an ideal option for synthesis of PFAS adsorbents and adsorbents for other complex contaminant mixtures.

Chapter 5: Implications and Conclusion

Innovative treatment technologies are needed for the removal of emerging contaminants in water and wastewater treatment to reduce human and environmental exposures to these potentially harmful compounds. One such class of emerging compounds that has received significant recent attention are PFAS—a surfactant-like chemical widely used in the manufacture of a range of products. PFAAs are a subclass of PFAS which have been found to have high environmental prevalence, persistence, and toxicity, making them the target of recent regulatory efforts. The novel spent coffee grounds biochar described in this research presents an exciting alternative to commercially available activated carbon materials for removal of PFAAs in water treatment applications. The widely available food waste feedstock source and relatively low chemical and energy in put requirements for production make this material viable even for low-resource communities. This adsorbent is expected to be particularly effective for removal of PFAA compounds in systems where organic components are low (e.g., drinking water treatment) and has been shown to perform comparably to a commercially available activated carbon, Calgon F300.

Wastewater effluent is increasingly being recognized as an important source of PFAAs and precursor compounds to environmental systems and, in some cases, to drinking water sources. The spent coffee grounds biochar coated with a PFOS molecularly imprinted polymer described herein present a prototype for a more cost-effective option for PFAA removal in water treatment applications. The increased selectivity of the material for PFAA compounds compared to non-MIP coated biochar in complex matrices will reduce the need for pretreatment of PFAA-containing waters. Preliminary results for composite regeneration showed promise for long adsorbent lifetimes with multiple reuse cycles possible. However, this PFOS-template MIP lacks high

removal rates for the short-chain PFAAs (i.e., PFBS) for which treatment is becoming increasingly important due to greater use of short-chain PFAAs and improved understanding of their toxicity.

A multi-PFAA templated MIP immobilized on the spent coffee grounds was explored to improve adsorption of both short- and long-chain PFAAs as well as precursor compounds. Multi-template MIP adsorbents have been successfully employed in prior studies to achieve high removal of several compounds within a class of organic contaminants (e.g., PAHs or alkaline pharmaceuticals) from aqueous systems. Results showed a synergistic effect between multiple PFAS templates and the VBTAC functional monomer which resulted in a higher imprinting factor and improved adsorption of both long- and short-chain PFAS by the BC@mMIP compared to the single-template BC@MIP counterparts. In an ultrapure water matrix, the BC@mMIP demonstrated treatment capabilities sufficient to meet the proposed EPA MCL for several PFAS. A column test in wastewater effluent revealed interference by competing organics and salts. Thus, this adsorbent is recommended for use in lower TDS/TOC matrices like drinking water or water reuse, or in series with other treatment technologies like AC or IX which could reduce concentrations of competing ions and improve PFAS removal by the BC@mMIP. Further testing of the BC@mMIP is needed (1) in various real water matrices, (2) in concert with pretreatment technologies like AC or IX, and (3) for removal of a wider range of PFAS compounds and concentrations relevant to (waste)water treatment, including short- and ultrashort-chain PFAS, to better understand the capabilities and limitations of this novel adsorbent.

The nitrogen modification and polymer coating methods detailed in ***Chapters 3 and 4*** of this study are expected to be easily adapted to any highly aromatic carbon substrate and a range of PFAS templates for synthesis of highly selective adsorbent materials able to be tailored to a variety of treatment needs. Other substrate options (e.g., activated carbon) which are already commercially

available could be substituted into the synthesis process, allowing the carbon substrate@MIP composite adsorbent to be more easily produced at a commercial scale. Ideally, this technology could be paired with a destructive PFAS treatment method capable of mineralizing PFAS in the concentrated regeneration solution or otherwise breaking the PFAS down into less toxic end products. A comprehensive adsorption-destruction treatment process like this would reduce the likelihood of reintroduction of PFAS to the water system later in its lifecycle (e.g., through leachate from landfills holding spent AC containing PFAS). Additional work is needed to determine whether this BC@MIP could help facilitate PFAS treatment through sequential adsorption and destruction and what modifications may be needed to optimize this treatment. For example, current destruction technologies often do not work well with methanolic solutions (like the adsorbent wash solution employed in this study) so alternative regeneration techniques or PFAS destruction technologies may need to be explored to make this type of treatment possible. This multi-template BC@MIP composite adsorbent presents a promising alterative to activated carbon for selective adsorption of both short- and long-chain PFAS, particularly in drinking water and water reuse applications, which merits further study to explore and optimize its treatment capabilities.

Appendix A: Supplemental Information for Chapter 2

A1. PFOS Losses from Sample Filtration

Several filtration options were evaluated for batch adsorption samples to identify a method that would minimize PFOS losses. Two types of filter materials previously shown to result in low PFAS losses were tested: cellulose acetate (CA) and glass fiber (GF).[201] Both types of filters were 0.2 µm syringe filters, 25 mm in diameter. PFOS loss filtration tests were conducted using 50 mL of ultrapure water in a 50-mL polypropylene tube with initial PFOS concentrations of approximately 5, 50, and 500 µg/L obtained through spiking with concentrated PFOS stock in methanol while maintaining a volumetric methanol concentration in water of no greater than 0.2%. Triplicate samples of each PFOS concentration were rotated at 40 rpm for 5 to 10 minutes after PFOS addition to ensure adequate mixing, and a 500 µL aliquot was then removed to be used as a non-filtered control. Filters were pre-wet with 5 mL of ultrapure water and then approximately 20 mL of sample was wasted through each filter prior to collection of 2 to 3 mL of sample to be used for analysis. The same filter was used for replicates of each concentration, and filters were washed with 20 mL of each new sample before collection of aliquots for analysis. PFOS quantification was done with LC-MS/MS as described in ***section A2***.

PFOS loss was calculated as the percent difference between the filtered and non-filtered samples, and results are shown in **table A1**. Although the GF filter performed well at high concentrations (i.e., negligible PFOS loss across the filter), performance decreased at lower concentrations (14.5% loss at 31.69 µg/L) leading to issues with recovery of sufficient PFOS for sample analysis around 5 µg/L. The CA filter, by contrast, showed more consistent PFOS loss

(around 13%) at higher concentrations with decreased loss at low concentrations (1.4% loss at 3.11 µg/L).

Sample purification via centrifugation was also attempted using a method detailed by Zhi and Liu[110] and results were compared to the CA and GF filtration results. Briefly, 5 mg of MCG biochar was added to triplicate samples of 50 mL of ultrapure water in a 50-mL polypropylene tube and spiked with 50 µg/L of PFOS from a concentrated methanol stock. MCG char was chosen for this test because it had significantly more fines observed during sieving and washing than either the F300 or the SCGKOH and thus seemed most likely to exhibit challenges with removal of small particles from solution during centrifugation. A set of control samples without MCG were prepared in the same manner. Samples were rotated at 40 rpm for 24 h to equilibrate and then a 500 µL aliquot was removed from the control samples for a non-centrifuged control. Samples were then centrifuged for 10 minutes at 2300 rpm to remove the large biochar particulates and a 1000 µL aliquot was removed from the center of the supernatant (to avoid floating char particles) and added to a 15-mL polypropylene tube. The aliquot was then diluted with 900 µL of methanol and centrifuged at 4000 rpm for 10 minutes. The supernatant was then divided into a 950 µL volume placed in an LC-MS vial for future analysis and a 950 µL volume placed in a capped and parafilm-sealed test tube in the refrigerator for SEM imaging to evaluate the char removal capabilities of this method. Briefly, a 1 × 0.5 inch silicon wafer was washed with ethanol and allowed to dry in a dust free area. A 5 µL drop of each MCG sample was placed on the mirrored side of the wafer and allowed to dry in a dust free area for SEM analysis.

Results from the PFOS analysis of the centrifuged and non-centrifuged ultrapure water sample showed negligible PFOS loss from centrifugation (**table A1**). However, SEM imaging indicated the presence of a significant amount of both fine MCG particulates and those greater than 0.2 µm

in diameter, making this a non-viable option for char removal from PFOS adsorption testing with char material adsorbents. Therefore, the CA filtration method, including pre-wetting of the filter material and wasting of 20 mL of sample prior to collection of an aliquot for analysis, was selected and used for the kinetics, isotherm, and effluent organic matter and divalent cation effects tests.

Table A1 PFOS losses during sample purification via centrifugation and filtration with glass fiber or cellulose acetate membranes.

purification method	concentration (ppb)	% loss
glass fiber	31.69	14.2%
	422.09	-0.5%
cellulose acetate	4.11	1.4%
	31.79	13.9%
	369.77	12.0%
Centrifugation	37.64	-3.7%

A2. Liquid Chromatography Mass Spectrometry Methodology

PFOS ($C_8F_{17}SO_3$; **figure A1, A)** was analyzed with a Waters (Milford, MA) Quattro Micro API triple quadrupole tandem mass spectrometer (MS/MS) preceded by liquid chromatography (LC) using an Agilent (Santa Clara, CA) Zorbax Rapid Resolution Eclipse XBD-18C column (2.1 x 50 mm, 1.8 µm). An Agilent, XDB-C18 guard cartridge (80Å, 4.6 x 12.5 mm, 5 µm) was placed before the LC column to pre-filter the sample. The MS/MS operation mode was set to negative electrospray ionization with multiple reaction monitoring (MRM) transitions (**table A2**). The LC was operated with a stationary phase of HPLC grade water with 10 mM ammonium acetate (A) and a mobile phase of HPLC grade methanol with 10 mM ammonium acetate (B). Details of the gradient program are given in **table A3**. Mass labeled PFOS (mPFOS) was used as an internal standard. Calibration standards and samples were prepared with 50:50 volumetric ratio of methanol and water to minimize PFOS losses to the tube walls.

Caffeine ($C_8H_{10}N_4O_2$; **figure A1, B)** was analyzed with a Waters Corporation (Milford, MA) Quattro Micro quadrupole tandem mass spectrometer (MS/MS) preceded by a Phenomenex

(Torrence, CA) Gemini 3 μm NX-C18 110A (3 x 50 mm) liquid chromatography column. The MS operation mode was set to positive electrospray ionization with MRM transitions (**table A2**). The LC was operated with a stationary phase of acetonitrile and methanol at a 50:50 volumetric ratio (A) and a mobile phase of 10 mM ammonium acetate in HPLC grade water (B). Details of the gradient program are given in **table A4**. Diuron-d6 was used an internal standard. All liquid chemicals used in LC-MS/MS analysis of PFOS and caffeine were Optima® LCMS Grade and the Ammonium Acetate was certified ACS Grade (98.1% purity), all purchased from Fisher Chemical (Hampton, NH).

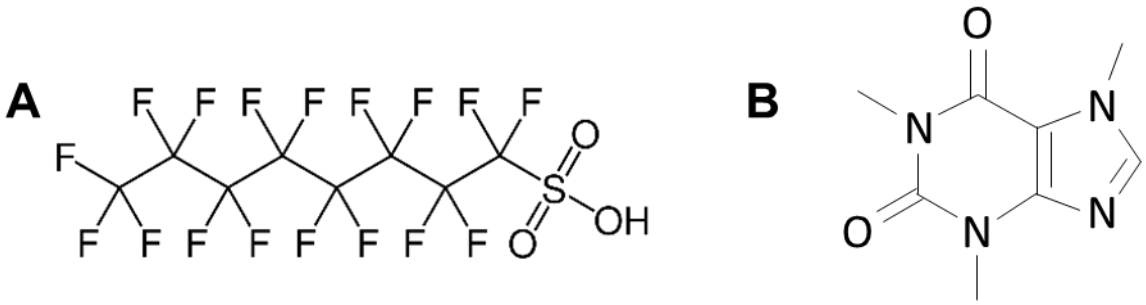

Figure A1 Chemical structures of PFOS (A) and caffeine (B).

Table A2 LC-MS/MS parameters used for quantification of PFOS and caffeine.

	ionization mode	parent (m/z)	product ion (m/z)	cone energy (V)	collision energy (V)	RT (min)
PFOS	-	498.95	79.40	53	40	9.808
PFOS	-	498.95	98.50	53	35	9.840
mPFOS	-	503.10	79.40	53	40	9.800
Caffeine	+	195.15	138.15	32	23	3.17
Caffeine	+	195.15	110.15	32	20	3.17
Diuron-d6	+	239.15	52.05	27	15	5.33
Diuron-d6	+	239.15	52.05	27	18	5.33

Table A3 LC gradient program for elution of PFOS using 10 mM ammonium acetate in water and methanol as the stationary and mobile phases.

time (min)	%A (10 mM ammonium acetate)	%B (10 mM ammonium acetate in methanol)	flow rate (mL/min)
0.0	80	20	0.4
8.0	5	95	0.4
10.0	5	95	0.4
10.5	80	20	0.4
16.0	80	20	0.4

Table A4 LC gradient program for elution of caffeine using acetonitrile and methanol (50:50 v/v ratio) as the stationary phase, and 10 mM ammonium acetate in water as the stationary phase.

time (min)	%A (acetonitrile and methanol 50:50 v/v)	%B (10 mM ammonium acetate)	flow rate (mL/min)
0.0	90	10	0.2
1.5	45	55	0.2
4.0	36	64	0.2
5.0	1	99	0.2
7.0	1	99	0.2
7.5	90	90	0.3
10.0	90	90	0.2

A3. Batch Test Model Calculations

A3.1. Kinetics Model Calculations

Three models were employed to evaluate the kinetic PFOS adsorption data for the SCGKOH, F300, and MCG. The first two were linear fits of the pseudo first order (PFO) and pseudo second order (PSO) kinetic models, commonly used to describe adsorption kinetics for a range of adsorbent materials and contaminants.[20, 202, 203] Pseudo-alpha-order reactions are those that in actuality depend on the concentrations of multiple reactants but in practice are assumed to depend on the concentration of only one reactant (i.e., PFOS) because the others are present in excess.[204] The equations for these models are as follows:

$$\frac{dq_t}{dt} = k_1(q_e - q_t) \qquad \text{Eqn. (A.1)}$$

$$\ln(q_e - q_t) = \ln(q_e) - k_1 t \qquad \text{Eqn. (A.2)}$$

$$\frac{dq_t}{dt} = k_2(q_e - q_t)^2 \qquad \text{Eqn. (A.3)}$$

$$\frac{t}{q_t} = \frac{1}{k_2 q_e^2} + \frac{t}{q_e} \qquad \text{Eqn. (A.4)}$$

where q_t and q_e are the PFOS adsorption density at time t and at equilibrium in mg PFOS/g char material; t is time in hours; and k_1 and k_2 are the PFO and PSO kinetic rate constants.

For the linear PFO model, a graph of the natural log of ($q_e - q_t$) was plotted as a function of time, and the equilibrium adsorption capacity (q_e) was evaluated as the adsorption capacity at five

days to calculate the y-variables. The rate constant (k_1) and equilibrium adsorption capacity (q_e) were then determined using equation (A.2) and the slope and intercept of this graph. For the linear PSO model, a graph of t/q_t versus time was plotted, and the rate constant (k_2) and equilibrium adsorption capacity (q_e) were then solved using equation (A.4) and the slope and intercept of this graph.

A modified non-linear PFO model derived from the Langmuir kinetic adsorption model [equation (A.5)] by Liu and Shen was the third model used to fit the PFOS adsorption data for all three char materials.[109] The relevant equations for this model are as follows:

$$\frac{d\theta_t}{dt} = k_a C_t(1-\theta_t) - k_d\theta_t = k_1(\theta_e - \theta_t) + k_2(\theta_e - \theta_t)^2 \qquad \text{Eqn. (A.5)}$$

$$\frac{k_1}{k_2} = \frac{\sqrt{K_L^2(C_0 - q_{max}X)^2 + 2K_L(C_0 + q_{max}X) + 1}}{K_L q_{max} X} \qquad \text{Eqn. (A.6)}$$

$$\theta_e = \frac{K_L(q_{max}X + C_0) + 1 - \sqrt{K_L^2(C_0 - q_{max}X)^2 + 2K_L(C_0 + q_{max}X) + 1}}{2K_L q_{max} X} \qquad \text{Eqn. (A.7)}$$

$$\theta_t = \theta_e(1 - e^{-k_1 t}) \qquad \text{Eqn. (A.8)}$$

$$\theta_t = \frac{(C_e - C_t) * M_{ads}}{q_{max}} = \frac{q_t}{q_{max}} \qquad \text{Eqn. (A.9)}$$

where θ_t and θ_e are the fraction of PFOS adsorption sites occupied at time t and at equilibrium; t is time in hours; k_a, k_d, k_1, and k_2 are the adsorption and desorption, and first and second order kinetic rate constants, respectively; K_L is the Langmuir adsorption constant; q_{max} is the maximum adsorption capacity determined by the Langmuir adsorption isotherm; X is the concentration of adsorbent (g/L); C_0, C_e, and C_t are the PFOS concentration at time zero, equilibrium, and time t, respectively; and M_{ads} is the mass (g) of adsorbent. Liu and Shen determined that if the ratio of k_1/k_2 is greater than or equal to θ_e, the Langmuir kinetic model reduces to the PFO model; if the ratio of k_1/k_2 is instead much smaller than θ_e, the Langmuir model reduces to the PSO model; and

for all other conditions, the full Langmuir kinetic model applies. This relationship was evaluated for the kinetic adsorption data from the SCGKOH, F300, and MCG adsorbents using equations (A.6) and (A.7), and the PFO derivation of the Langmuir kinetic model [equation (A.8)] was found to be accurate for all three materials at PFOS concentrations below 3200, 3100, and 5200 µg/L for SCGKOH, F300, and MCG, respectively. The non-linear PFO derivation of the Langmuir kinetic model was applied for all three char materials using equation (A.8). Briefly, the value for θ_e can be solved from the Langmuir adsorption isotherm parameters as shown in equation (A.7) while experimental values for θ_t can be solved from experimentally determined PFOS solution concentrations using equation (A.9). The rate constant (k_1) was solved using the Microsoft Excel® solver function to minimize the square error between experimental and theoretical values of θ_t. The goodness of fit of the linear PFO and PSO and the non-linear PFO kinetic models were compared using the square error as shown in **figure A2**.

A3.2. Adsorption Isotherm Model Calculations

Adsorption isotherm data for the three char materials were fit to both the Langmuir and Freundlich adsorption isotherm models whose original and linear forms are given below as equation (A.10) through (A.13).[112]

$$q_e = \frac{q_{max} K_L C_e}{1 + K_L C_e} \qquad \text{Eqn. (A.10)}$$

$$\frac{C_e}{q_e} = \frac{1}{q_{max}} C_e + \frac{1}{K_L q_{max}} \qquad \text{Eqn. (A.11)}$$

$$q_e = K_F C_e^{1/n} \qquad \text{Eqn. (A.12)}$$

$$\log(q_e) = \frac{1}{n} \log(C_e) + \log(K_F) \qquad \text{Eqn. (A.13)}$$

where q_e and q_{max} were the equilibrium and maximum adsorption densities, C_e is the equilibrium adsorbate concentration, K_L and K_F are the Langmuir and Freundlich adsorption rate constants, respectively, and *1/n* is the Freundlich coefficient of non-linearity.

For both models, experimental data was transformed to the appropriate linear variables shown in equations (A.11) and (A.13) and plotted to obtain linear isotherm values for the model parameters (q_{max} and K_L for the Langmuir model and K_F and *1/n* for the Freundlich model) from the slope and intercept of the plotted data. Non-linear isotherm values for the model parameters were also obtained through minimization of the square error between experimentally and theoretically derived equilibrium adsorption densities (q_e) using the Microsoft Excel® solver function. Theoretical values for q_e were obtained using equations (A.10) and (A.12) with the linearly derived isotherm values as starting points. In all cases the non-linear model parameters provided a better fit for the data and were used for all further analysis and discussion.

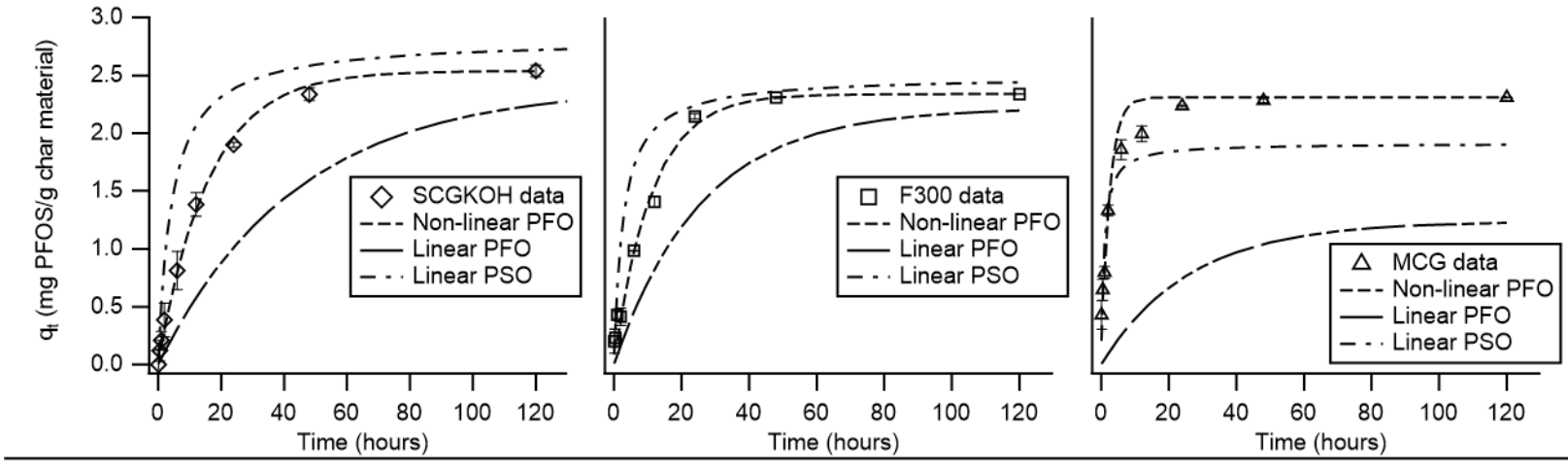

		non-linear pseudo first order		linear pseudo first order			linear pseudo second order			
	$q_{e,exp}$ (mg/g)	k_1 (h^{-1})	σ^2	$q_{e,calc}$ (mg/g)	k_1 (h)	σ^2	$q_{e,calc}$ (mg/g)	v_0 (mg/g*h)	log ($K_{d,eq}$) (L/kg)	σ^2
SCGKOH	2.538	0.069	0.003	2.480	0.065	0.025	2.818	0.230	5.359	0.232
F300	2.337	0.090	0.016	2.343	0.148	0.023	2.495	0.368	6.212	0.183
MCG	2.309	0.414	0.040	2.169	0.483	1.137	2.337	1.680	6.762	0.083

Figure A2 Kinetics modeling of PFOS adsorption rates onto (a) SCGKOH, (b) F300, and (c) MCG with the Langmuir-derived non-linear pseudo first order, linear pseudo first order, and linear pseudo second order models.

Appendix B: Supplemental Information for Chapter 3

B1. Production of Nitrogen Modified Biochar via Alternative Methods

Two alternative methods for nitrogen modification of biochar were used. The first was similar to the melamine modification method adapted from Kasera et al. (Kasera et al., 2021) and described in the main text, ***section 3.2.2***. The first alternative method was similar to the melamine modification method adapted from Kasera et al. (Kasera et al., 2021). Briefly, 0.2051 g melamine was mixed with 0.244 g SCGKOH and 2.5 mL water and placed in a quartz boat (rather than the ceramic crucible used previously). The quartz boat was placed in a Hogentogler Protégé Split Tube Furnace (Hogentogler, Colombia, MD) with 500 mL/min nitrogen gas flow for 20 minutes to purge all oxygen from the atmosphere. Next, the furnace was heated to 400 °C at a ramp rate of 10 °C/min and held there for 1 hour to catalyze the reaction with melamine. After the process was completed, the final material was rinsed with ultrapure water and the final product was designated BC-M1-2.

The second alternative method was adapted from Liu et al. (Liu et al., 2018), which also used melamine as the nitrogen source. First, melamine was mixed with Milli-Q water at a 1 g melamine to 100 mL water ratio and stirred for 20 - 30 minutes until the melamine was well mixed (the solubility of melamine in water at 20 °C is 3240 mg/L, therefore the melamine did not completely dissolve). The melamine and water mixture was then added to a Teflon lined, stainless steel hydrothermal autoclave along with 1g of biochar placed in a muffle furnace at 160 °C for 24 hours. At the end of the reaction time, the autoclave was taken out of the muffle furnace and allowed to cool to room temperature before removing the modified biochar. The biochar was placed in a 50 mL polypropylene tube with 50 mL Milli-Q water and rotated at 40 rpm for at least 30 minutes to

remove excess melamine. This wash step was repeated until the pH was circumneutral. Washed biochar was placed in and oven and dried overnight at 90 °C. The final biochar product was stored in an air-tight container until further use and was designated BC-M2.

B2. Additional Physicochemical Characterization of Nitrogen Modified Biochar

Characterization of nitrogen-modified biochar composition via thermogravimetric analysis (TGA, **figure B1**) and elemental analysis (**table B1**) were conducted as a first pass evaluation of the success of nitrogen modification for all modification methods employed and to rule out modification methods with poor attachment of nitrogen functional groups. In particular, biochars modified with the same nitrogen source (e.g., nitration or melamine addition) were compared against each other to select the optimal method for each nitrogen source. Comparison of TGA spectra from the BC-N and BC-N2 materials revealed the BC-N nitrogen modification resulted in a much greater mass of added nitrogen-containing surface functional groups on the BC-N. These results indicated the BC-N2 was unlikely to perform well for molecularly imprinted polymer (MIP) functionalization, and excluded from future analyses. PFAA adsorption on the BC-N2 and BC-N2@MIP were performed to validate the exclusion of more comprehensive BC-N2 evaluation (see ***section B4*** and ***section B5***). The BC-M1-2 material was also excluded from future evaluation because the percent nitrogen from elemental analysis was low compared to the BC-M substrate. Similarly, the BC-M2 method was excluded for two reasons. First, although the percent nitrogen from elemental analysis was comparable to that of BC-M, TGA results indicated the melamine was poorly attached to biochar matrix compared the BC-M attachment as evidenced by the much larger weight loss difference. Secondly, the production process for the BC-M2 was more energy and time intensive than for BC-M, making this a less desirable modification method.

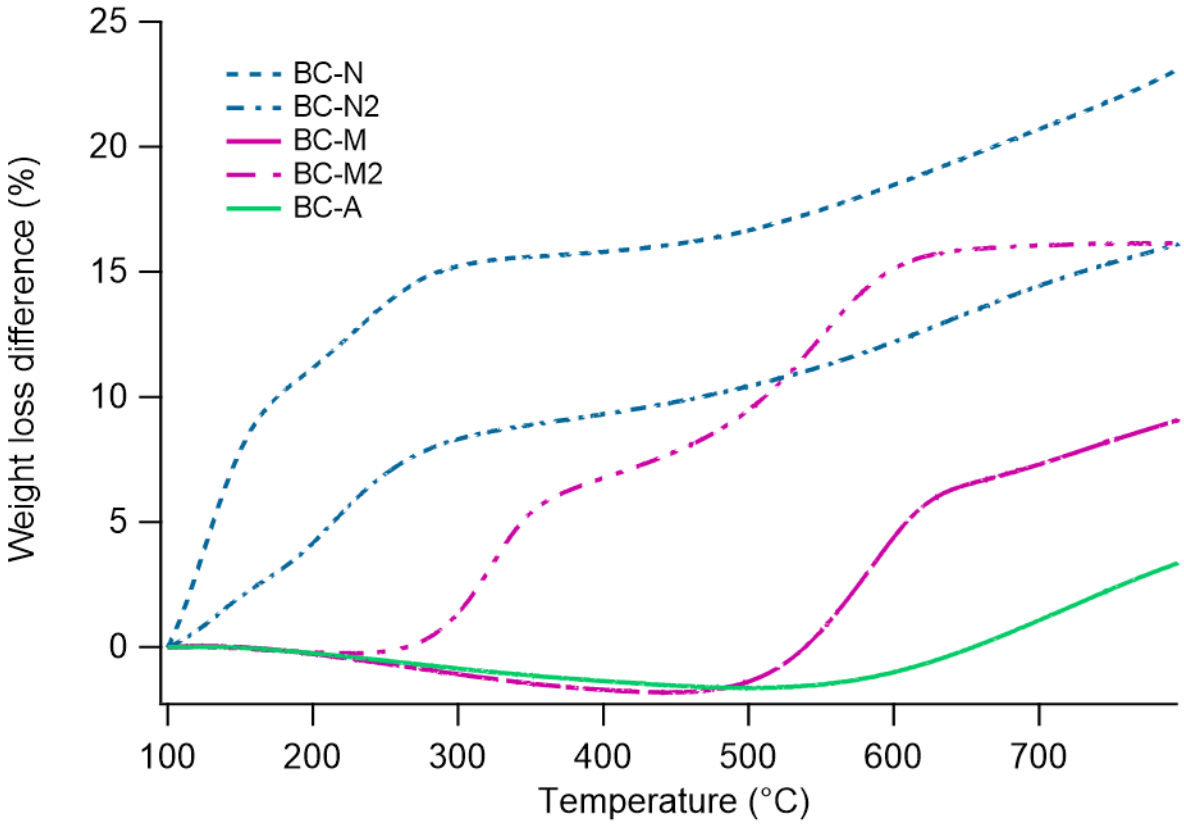

Figure B1 Thermogravimetric analysis of nitrogen modified biochar materials.

Table B1 Elemental composition of nitrogen modified biochar materials from elemental analysis and proximate carbon analysis.

	Elemental Analysis					
Sample ID	**C %**	**H %**	**N %**	**O %***	**Ash%**	**%N increase**
SCGKOH	81.4 ± 2.3	0.76 ± 0.0	2.17 ± 0.1	12.2	3.85 ± 0.2	-
BC-N	69.4 ± 0.2	2.19 ± 0.0	1.8 ± 0.1	23.7	2.9 ± 0.5	-0.3
BC-M	64.6 ± 3.5	1.1 ± 0.0	13.0 ± 0.6	19.5	1.8 ± 0.2	10.8
BC-M1-2	73.7 ± 1.6	1.3 ± 0.0	5.8 ± 0.2	ND	ND	3.6
BC-M2	68.5 ± 3.3	1.6 ± 0.1	14.4 ± 0.6	13.9	1.5 ± 0.1	12.3
BC-A	65.0 ± 1.5	1.0 ± 0.1	3.0 ± 0.1	29.4	1.6 ± 0.1	0.9

ND: not detected

DRIFTS spectra were collected for the remaining nitrogen modified biochar materials to provide additional information about the surface functional groups (**figure B2**). The BC-M and BC-A DRIFTS spectra show clear peaks at 1600 cm^{-1} and 1250 cm^{-1} that correspond to N–H bending and C–N stretching from aromatic amines.[205] These peaks are notably absent in the SCGKOH base material spectra. The BC-N also displayed the 1600 cm^{-1} and 1250 cm^{-1} peaks, although they are harder to distinguish due to their smaller size and the masking effect of the broad band (from around 1100 – 1700 cm^{-1}) seen on all four spectra which corresponds to aromatic and aliphatic hydrocarbon peaks typical of activated carbons and biochar. [106] The smaller 1600 cm^{-1} nitrogen peak size in the BC-N spectra also indicates a lower nitrogen density for this material.

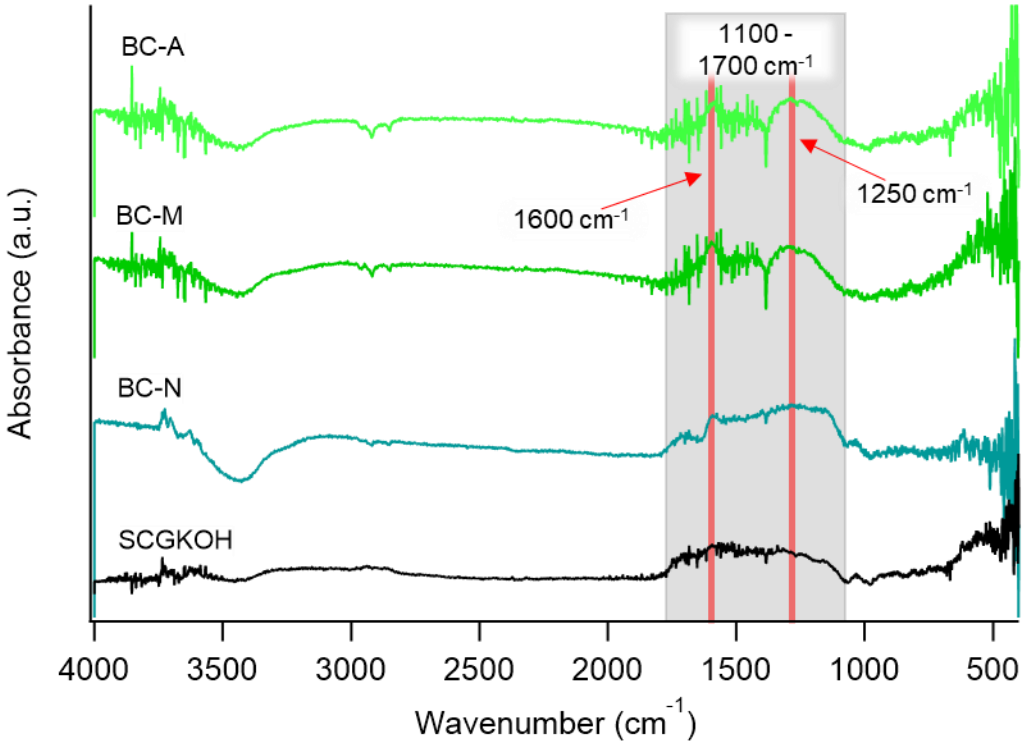

Figure B2 DRIFTS spectra of nitrogen modified and unmodified spent coffee grounds biochar.

B3. XPS Peak Fitting Details, and Supplemental Carbon (C1s) and Oxygen (O1s) High Resolution Spectra

XPS data were collected from biochar samples using the #30 – 50 mesh size fraction via three scan types. A survey scan combined with a detailed nitrogen scan was used to determine the atomic percentages of each element on the material surface. A high resolution scan for nitrogen (N1s), carbon (C1s), and oxygen (O1s) were used to obtain more detailed information about the binding energy and types of functional groups present. XPS data was fitted with the Casa XPS software, version 2.3.25 using a Shirley background and a Gaussian-Lorentzian peak shape (70% Gaussian, 30% Lorentzian). Peak shape was further constrained such that the full width at half max (FWHM) was approximately 0.7 – 1.9 eV and was consistent between peaks from a single scan. Peak separation was limited to no less than 0.5 eV, and all peaks were referenced to an adventitious carbon peak at 285.0 eV. The high resolution carbon and oxygen spectra are shown in **figure B3A - D** and **figure B4A - D**.

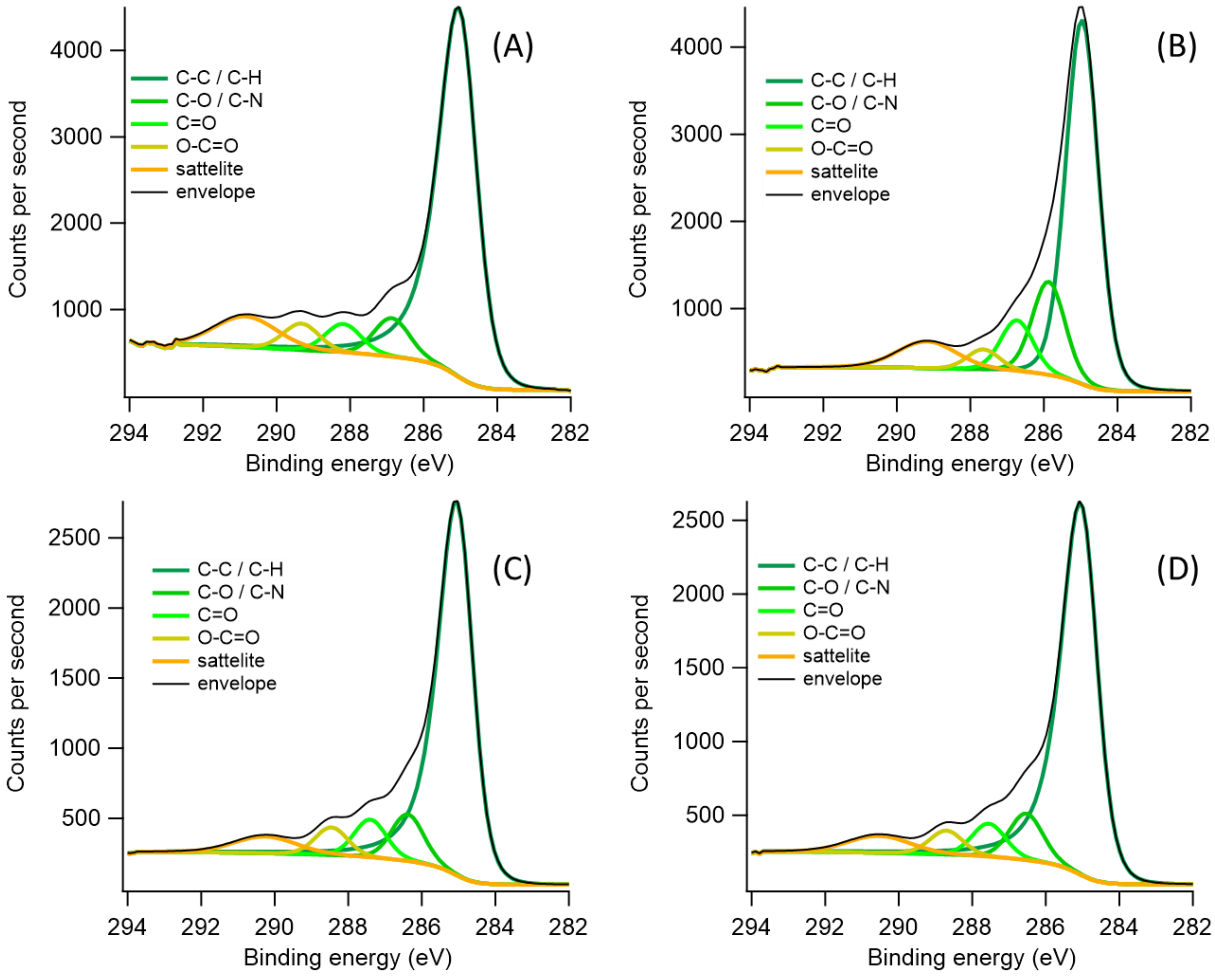

Figure B3 Carbon (C1s) XPS data for SCGKOH (A), BC-N (B), BC-M (C), and BC-A (D).

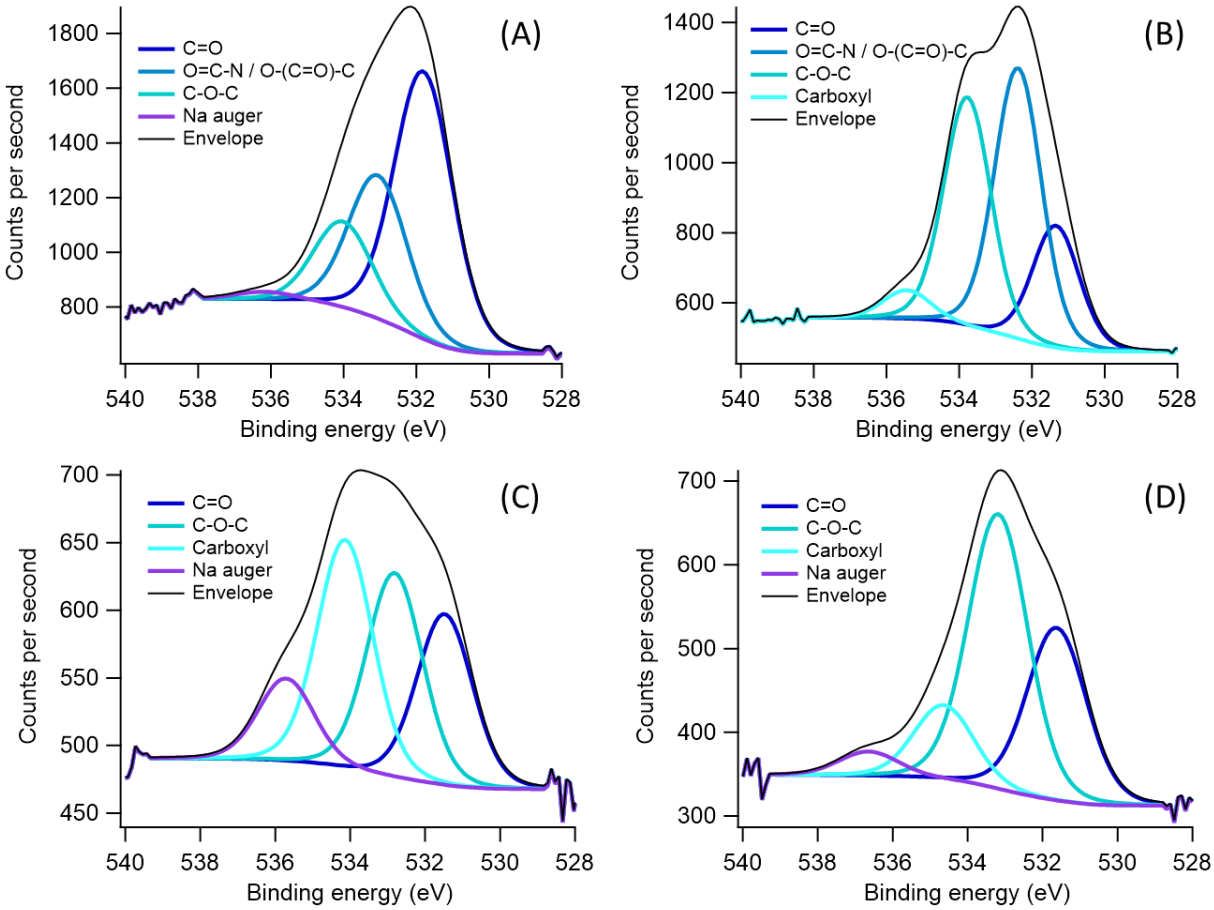

Figure B4 Oxygen (O1s) XPS data for SCGKOH (A), BC-N (B), BC-M (C), and BC-A (D).

B4. Effect of Nitrogen Modification on PFAA Adsorption Capabilities

PFOS adsorption by nitrogen modified biochar materials was compared to that on the base material (SCGKOH) to evaluate any change in adsorption capabilities from the modification process. Briefly, 5 mg biochar and 50 mL ultrapure water were placed in a 50 mL polypropylene centrifuge tube and PFOS was added from concentrated methanol stock to achieve an initial concentration of 4490 ± 478 µg/L PFOS with a methanol concentration of not more than 0.2%.[1] Samples were prepared in triplicate and allowed to rotate at 40 rpm on a Fisherbrand™ Multi-Purpose Tube Rotator (Fisher Scientific, Waltham, MA) for 4 days to achieve equilibrium. At the end of the equilibration time, samples were filtered with a 0.2 micron cellulose acetate (CA) syringe filter (VWR, Radnor, PA) and prepared for analysis as described in ***section B8***. Results

from this test are shown in **figure B5** and indicate decreased adsorption capability after nitrogen modification with only slight variation observed between the different modification methods.

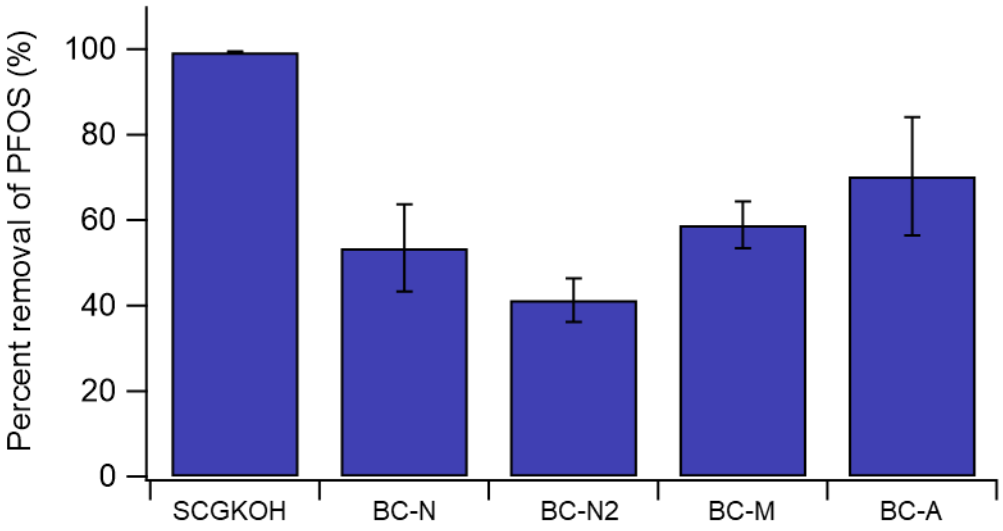

Figure B5 Percent removal of 4490 ± 478 μg/L PFOS by 100 mg/L of nitrogen modified and unmodified SCGKOH biochar in an ultrapure water matrix following a 4-day equilibration period. Error bars represent standard deviation from triplicate samples.

B5. Effects of Alternative Nitrogen Modification Methods and Functional Monomer Selection on PFAA Removal by Molecularly Imprinted Polymer (MIP) Functionalized Biochar

Several biochar MIP composite adsorbents were synthesized in addition to those discussed in detail in ***section 3.2.4*** of the main text to evaluate the effect of nitrogen modification method and functional monomer selection on the final BC@MIP composite performance. The composition of these adsorbents is given in **table B2**. Preliminary screening of MIP performance was conducted via two batch adsorption tests, both performed in ultrapure water using the methods and parameters (i.e., solution volume, adsorbent concentration, test time, and sample preparation methods) described in ***section 3.2.6***. The first batch test evaluated adsorption of 4174 ± 302 μg/L of the PFOS template. The second batch test evaluated competitive adsorption of three PFAAs: 1478 ± 185 μg/L PFOS, 1152 ± 135 μg/L PFBS, and 1380 ± 515 μg/L PFOA. Regeneration of spent

adsorbent was not evaluated since the purpose of these preliminary tests was merely to screen adsorbent performance in order to inform further testing.

Table B2 Molecularly imprinted polymer (MIP) naming convention by nitrogen modification method and functional monomer selection.

		functional monomers		
adsorbent name	**biochar substrate**	**VBTAC** 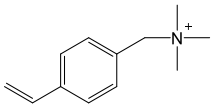	**DMC** 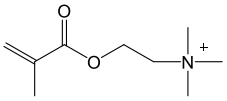	**TFMA** 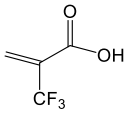
BC-N@MIP-V	BC-N	Y	-	-
BC-N@MIP-VF	BC-N	Y	-	Y
BC-N@MIP-DF	BC-N	-	Y	Y
BC-N2@MIP-VF	BC-N2	Y	-	Y
BC-N2@MIP-DF	BC-N2	-	Y	Y
BC-A@MIP-VF	BC-A	Y	-	Y
BC-M@MIP-VF	BC-M	Y	-	Y
BC-M@MIP-V	BC-M	Y	-	-

Preliminary adsorption test results (**figure B6** and **figure B7**) revealed poor performance of biochar MIP composite materials synthesized with the DMC functional monomer and with the BC-N2 substrate. It is hypothesized that the oxygen containing moieties on the DMC may have repelled the anionic PFAAs, decreasing overall adsorption efficiency. The poor performance of adsorbents produced with the BC-N2 substrate agrees with the conclusions drawn in ***section B2***. Thus, both the DMC and BC-N2 were excluded from future use and no additional testing was performed with the adsorbent materials made using these components. The BC-M@MIP-V material also experienced low percent removal of PFAAs in both tests; however, this was attributed to the low specific surface area (SSA) of the material (as discussed in ***section 3.3.1***) rather than the functional monomer selection or nitrogen modification method. Low SSA was not expected to

be a factor in the low percent removal by the BC-N@MIP-DF, BC-N2@MIP-VF, or BC-N2@MIP-DF for two reasons. First, the biochar substrates had relatively low –NH moiety density compared to the BC-M. Second, all three materials contained the TFMA monomer. Both of these factors appear to preclude the possibility of low SSA as demonstrated in ***section 3.3.1***.

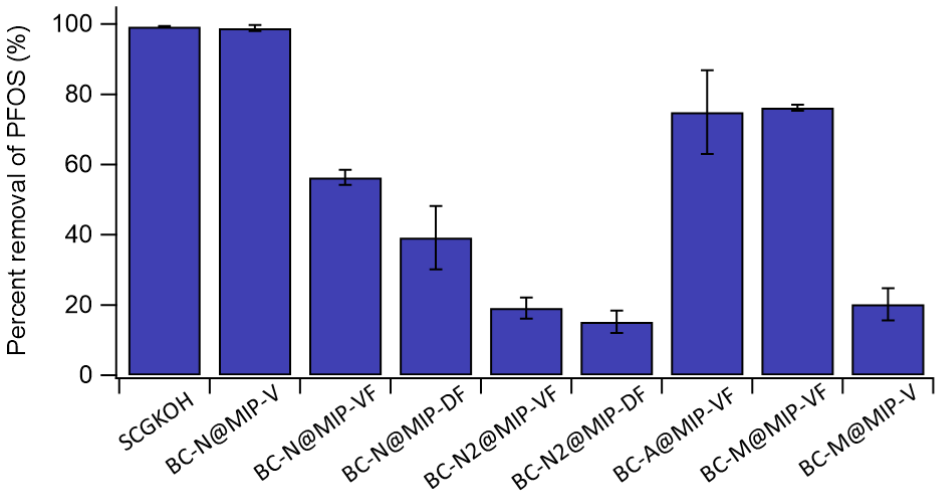

Figure B6 Percent removal of 4174 ± 302 µg/L PFOS by 100 mg/L of MIP coated and unmodified SCGKOH biochar in an ultrapure water matrix following a 4-day equilibration period. Error bars represent standard deviation from triplicate samples.

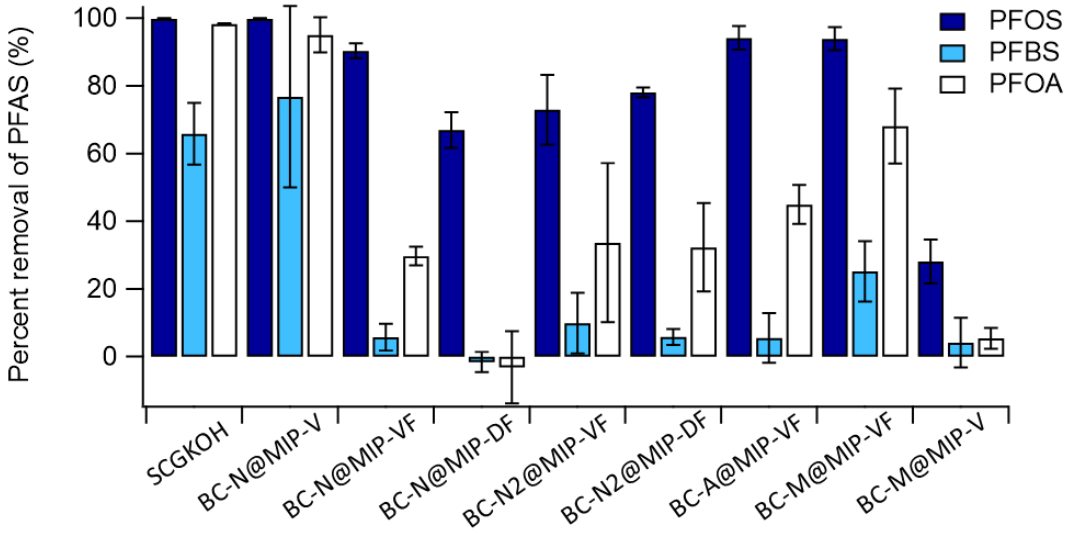

Figure B7 Percent removal of 1478 ± 185 µg/L PFOS, 1152 ± 135 µg/L PFBS, and 1380 ± 515 µg/L PFOA by 100 mg/L of MIP coated and unmodified SCGKOH biochar in an ultrapure water matrix following a 4-day equilibration period. Error bars represent standard deviation from triplicate samples.

B6. Synthetic Wastewater Composition and Adsorption of PFAAs and Co-Occurring Organics onto Synthetic Effluent Organic Matter

A synthetic wastewater matrix was produced as described by Steigerwald and Ray, 2021[1] to evaluate the performance of selected biochar MIP composite adsorbents under conditions more representative of those expected for real treatment applications. The composition of this synthetic wastewater is detailed in **table B3**. Synthetic effluent organic matter (sEfOM) stock solutions were prepared at 1000 mg/L and stirred at 150 rpm overnight. Total organic carbon (TOC) content was then evaluated using a Sievers 900 Portable TOC analyzer (GE Instruments, Boulder, CO). Stock solution volumes needed to achieve the final sample concentration listed in **table B3** were calculated using the results of this TOC analysis.

Table B3 Composition of synthetic wastewater matrix.

compound	concentration
Bovine serum albumin (protein)	2.5 mg C/L
Sodium alginate (carbohydrate)	2.0 mg C/L
Humic acid	5.0 mg C/L
Octanoic acid (fat)	0.5 mg C/L
Calcium (Ca^{2+})	26.0 mg/L
Magnesium (Mg^{2+})	12.6 mg/L
Chloride (Cl^{-})	82.8 mg/L

Adsorption of PFAAs and co-occurring organic compounds onto the sEfOM in particular was evaluated during the synthetic wastewater batch test described in ***section 3.2.6*** with the addition of a control sample containing all components of the synthetic wastewater listed in **table B3** but no adsorbent. Percent removal of each adsorbate of interest onto the sEfOM as well as the four biochar and biochar MIP composite adsorbents is shown in **figure B8**. Results indicate low removal of PFAAs, caffeine, and PCP with slightly higher removal of fipronil. The percent removal of PFOS is notably higher than other PFAAs, however it is important to note the high

standard deviation of this data point, indicating low precision of this result. Thus, adsorption to sEfOM was not expected to be a significant contributor to PFAA removal.

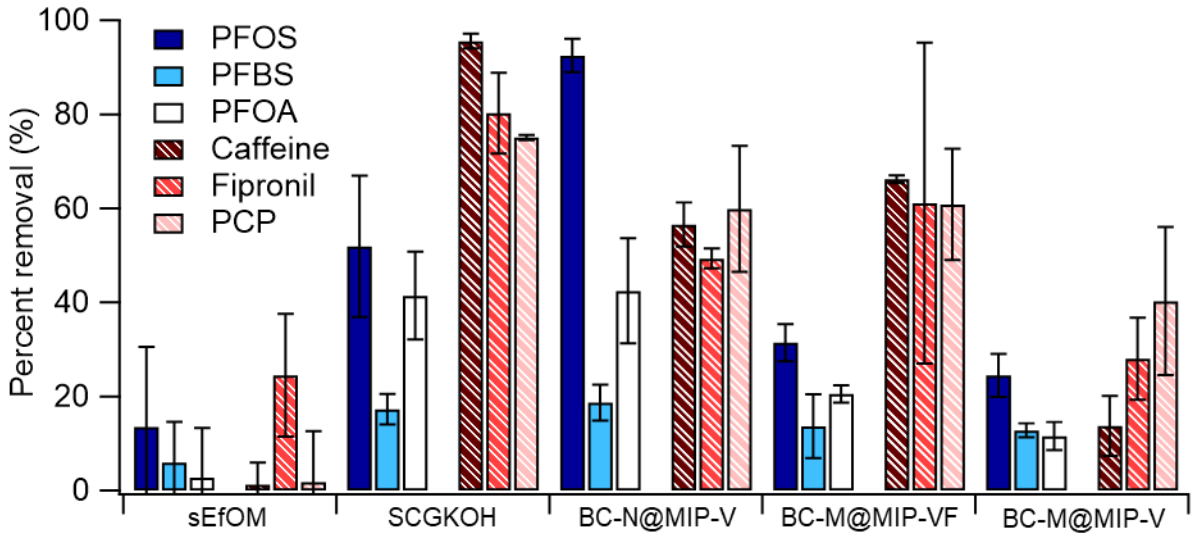

Figure B8 Percent removal of 1659 ± 99 µg/L PFOS, 1400 ± 11 µg/L PFBS, 2313 ± 71 µg/L PFOA, 1916 ± 76 µg/L caffeine, 1520 ± 63 µg/L fipronil, and 3385 ± 217 µg/L pentachlorophenol by sEfOM, biochar, and biochar MIP composite materials in a synthetic wastewater matrix with pH controlled to 7.0 ± 0.2 using a 5 mM HEPES buffer following a 4-day equilibration period. Error bars represent standard deviation from triplicate samples.

B7. Normalized Equilibrium Adsorption Figures and Selectivity Coefficient Calculations

Normalized equilibrium adsorption ($q_{e,SSA}$) results are presented in **figures B9**, **B10**, and **B11**, the full size counter parts to **figure 3.3** and **3.4 insets** in the main text. Results from the selectivity coefficient ($K_{selectivity}$) calculations for the synthetic wastewater batch test and PFAS competition test in ultrapure water (equations described in ***section 3.2.6***) are given in **table B4**.

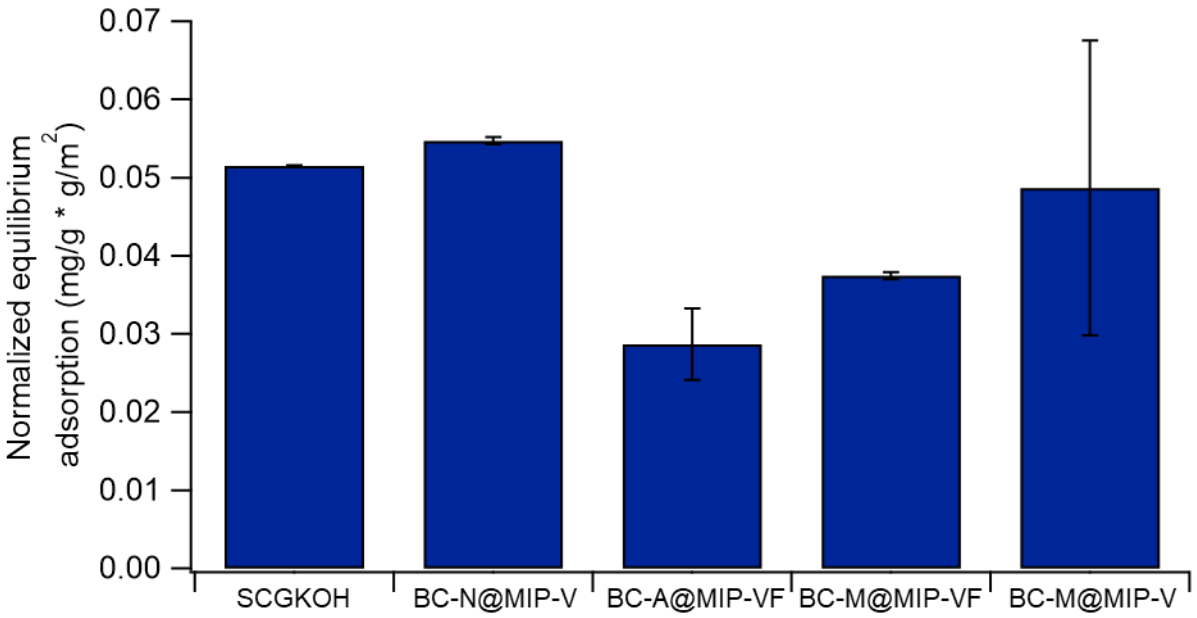

Figure B9 Equilibrium adsorption of 4275 ± 342 µg/L PFOS by 100 mg/L MIP modified and unmodified biochar materials in an ultrapure water only matrix following a 4-day equilibration period. Error bars represent the standard deviation from triplicate samples.

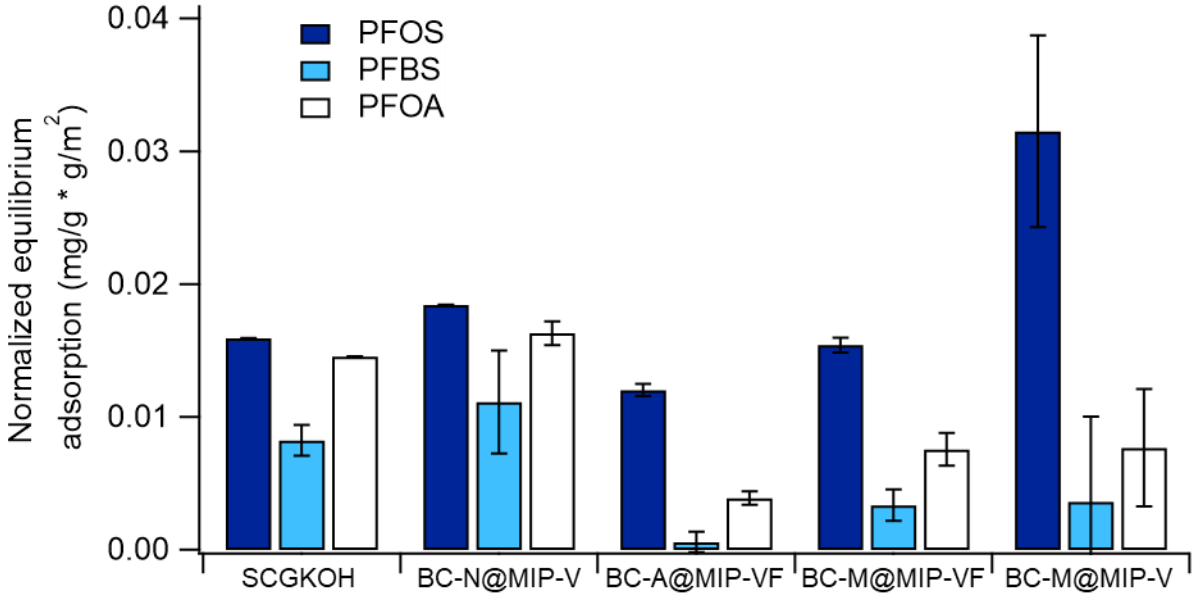

Figure B10 Equilibrium adsorption of 1476 ± 207 µg/L PFOS, 1166 ± 153 µg/L PFBS, and 1453 ± 582 µg/L PFOA by 100 mg/L MIP modified and unmodified biochar materials in an ultrapure water only matrix following a 4-day equilibration period. Error bars represent the standard deviation from triplicate samples.

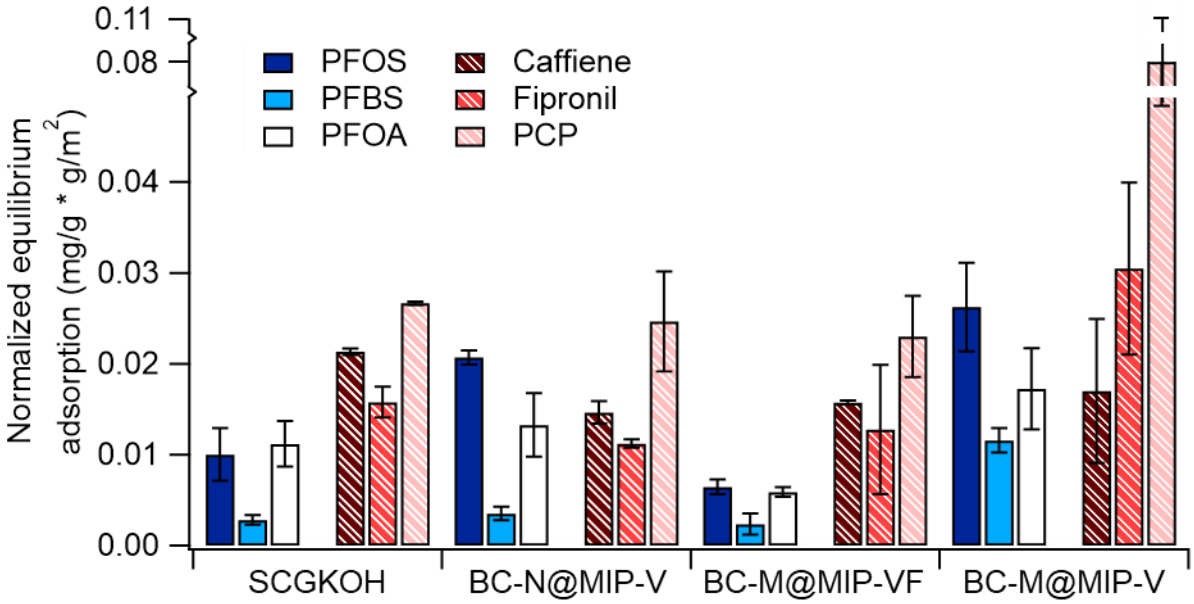

Figure B11 Equilibrium adsorption of 1659 ± 99 µg/L PFOS, 1400 ± 11 µg/L PFBS, 2313 ± 71 µg/L PFOA, 1916 ± 76 µg/L caffeine, 1520 ± 63 µg/L fipronil, and 3385 ± 217 µg/L pentachlorophenol by 100 mg/L MIP modified and unmodified biochar materials in synthetic wastewater following a 4-day equilibration period. Error bars represent the standard deviation from triplicate samples.

Table B4 Selectivity coefficients comparing adsorption of PFOS template to other contaminants of interest (COI; i.e., PFBS, PFOA, and co-occurring organics) on MIP-modified and unmodified biochar.

		Ultrapure water matrix			Synthetic wastewater matrix		
Adsorbent	**COI**	$K_{imprinted}$	$K_{comparison}$	$K_{selectivity}$	$K_{imprinted}$	$K_{comparison}$	$K_{selectivity}$
SCGKOH	PFBS		1.93			3.56	
BC-N@MIP-V	PFBS	1.66		0.86	5.86		1.65
BC-A@MIP-VF	PFBS	20.90		10.82	ND		
BC-M@MIP-VF	PFBS	4.59		2.37	2.72		0.76
BC-M@MIP-V	PFBS	8.73		4.52	2.27		0.64
SCGKOH	PFOA		1.09			0.90	
BC-N@MIP-V	PFOA	1.13		1.03	1.56		1.74
BC-A@MIP-VF	PFOA	3.10		2.83	ND		
BC-M@MIP-VF	PFOA	2.04		1.87	1.10		1.22
BC-M@MIP-V	PFOA	4.11		3.76	1.52		1.69
SCGKOH	Caffeine					0.47	
BC-N@MIP-V	Caffeine				1.42		3.01
BC-A@MIP-VF	Caffeine				ND		
BC-M@MIP-VF	Caffeine				0.41		0.87
BC-M@MIP-V	Caffeine				1.54		3.28
SCGKOH	Fipronil					0.64	
BC-N@MIP-V	Fipronil				1.85		2.90
BC-A@MIP-VF	Fipronil				ND		
BC-M@MIP-VF	Fipronil				0.51		0.80
BC-M@MIP-V	Fipronil				0.86		1.35
SCGKOH	PCP					0.38	
BC-N@MIP-V	PCP				0.84		2.23
BC-A@MIP-VF	PCP				ND		
BC-M@MIP-VF	PCP				0.28		0.75
BC-M@MIP-V	PCP				0.33		0.88

B8. LC-MS/MS Analysis of PFAAs and Co-Occurring Organic Compounds

Concentrations of all PFAAs and co-occurring organic contaminants (i.e., caffeine, fipronil, PCP) were quantified by mass spectroscopy using a Waters Corporation (Milford, MA) triple quadrupole mass spectrometer (MS/MS) preceded by liquid chromatography (LC). Prior to analysis, samples were filtered to remove biochar fines and (where applicable) organic compounds that would negatively impact instrument performance. Briefly, samples were filtered with a cellulose acetate (CA) syringe filter by first filtering 5 mL of Milli-Q water followed by filtering 20 mL of sample into waste and then collecting 1 mL of filtered sample. Cellulose acetate was

chosen as a filter media for its low PFAA loss, as detailed in prior publications.[1, 201] All liquid chemicals used in LC-MS/MS analysis of PFAAs and caffeine were Optima® LCMS Grade and the Ammonium Acetate was certified ACS Grade (98.1% purity), all purchased from Fisher Chemical (Hampton, NH).

PFOS ($C_8F_{17}SO_3$; **figure B12A**), PFBS ($C_4F_9SO_3$; **figure B12B**), and PFOA ($C_8HF_{15}O_2$; **figure B12C**) were analyzed via LC-MS/MS using an Agilent (Santa Clara, CA) Zorbax Rapid Resolution Eclipse XBD-18C column (2.1 x 50 mm, 1.8 μm). An Agilent, XDB-C18 guard cartridge (80Å, 4.6 x 12.5 mm, 5 μm) was placed before the LC column to pre-filter the sample. The MS/MS operation mode was set to negative electrospray ionization with multiple reaction monitoring (MRM) transitions (**table B5**). The LC was operated with a stationary phase of HPLC grade water with 10 mM ammonium acetate (A) and a mobile phase of HPLC grade methanol with 10 mM ammonium acetate (B). Details of the gradient program are given in **table B6**. Mass labeled PFOS (mPFOS), PFBA (mPFBA), and PFOA (mPFOA) were used as internal standards for PFOS, PFBS, and PFOA, respectively. Calibration standards were prepared with 60:40 volumetric ratio of methanol and water while samples were prepared with a 50:50 volumetric ratio of methanol and water to minimize PFOS losses to the walls of the borosilicate glass LCMS vials.

Caffeine ($C_8H_{10}N_4O_2$; **figure B12D**), fipronil ($C_{12}H_4Cl_2F_6N_4OS$; **figure B12E**), and PCP (C_6HCl_5O; **figure B12F**) were analyzed via LC-MS/MS using a Phenomenex (Torrence, CA) Gemini 3 μm NX-C18 110A (3 x 50 mm) liquid chromatography column. Mass labeled diuron (diuron-d_6) and PCP (PCP-^{13}C) were used as internal standards. For caffeine and diuron-d_6 quantification, the MS operation mode was set to positive electrospray ionization with MRM transitions (**table B5**). For fipronil, PCP, and PCP-^{13}C quantification, the MS operation mode was set to negative electrospray ionization with MRM transitions (**table B5**). The LC was operated

with acetonitrile and acetic acid (5% each) in water as the stationary phase (A) acetonitrile and methanol (50:50 v/v ratio) as the mobile phase (B). Details of the gradient program are given in **table B7**. Diuron-d6 was used an internal standard.

Table B5 LC-MS/MS parameters used for quantification of PFAAs and organic co-contaminants.

	ionization mode	parent (m/z)	product ion (m/z)	cone energy (V)	collision energy (V)	RT (min)
PFBS	-	299.00	79.40	14	35	7.46
PFBS	-	299.00	98.50	52	35	5.88
mPFBA	-	217.00	172.00	11	13	5.88
PFOS	-	498.95	79.40	53	40	9.81
PFOS	-	498.95	98.50	53	35	9.84
mPFOS	-	503.10	79.40	53	40	9.80
PFOA	-	413.10	169.00	18	19	9.32
PFOA	-	413.10	369.00	18	10	9.32
mPFOA	-	417.10	372.00	18	10	9.32
Caffeine	+	195.15	138.15	32	23	3.06
Caffeine	+	195.15	110.15	32	20	3.06
Diuron-d6	+	239.15	52.05	27	15	5.06
Diuron-d6	+	239.15	78.05	27	18	5.06
Fipronil	-	434.90	330.2	32	16	5.65
Fipronil	-	436.90	330.2	32	16	5.65
Pentachlorophenol	-	262.85	263.10	38	7	4.70
Pentachlorophenol	-	264.85	265.10	38	7	4.70
Pentachlorophenol-^{13}C	-	270.95	271.15	38	7	4.70
Pentachlorophenol-^{13}C	-	272.95	273.15	38	7	4.70

Table B6 LC gradient program for elution of PFAA compounds using 10 mM ammonium acetate in water and methanol as the stationary and mobile phases.

time (min)	%A (10 mM ammonium acetate)	%B (10 mM ammonium acetate in methanol)	flow rate (mL/min)
0.0	80	20	0.4
8.0	5	95	0.4
10.0	5	95	0.4
10.5	80	20	0.4
16.0	80	20	0.4

Table B7 LC gradient program for elution of organic co-contaminants using acetonitrile and acetic acid (5% each) in water as the stationary phase acetonitrile and methanol (50:50 v/v ratio) as the mobile phase.

time (min)	%A (5% acetonitrile and 5% acetic acid in water)	%B (acetonitrile and methanol 50:50 v/v)	flow rate (mL/min)
0.0	90	10	0.2
1.5	45	55	0.2
3.5	40	60	0.2
4.0	1	99	0.2
6.0	1	99	0.2
6.5	90	90	0.3
9.0	90	90	0.2

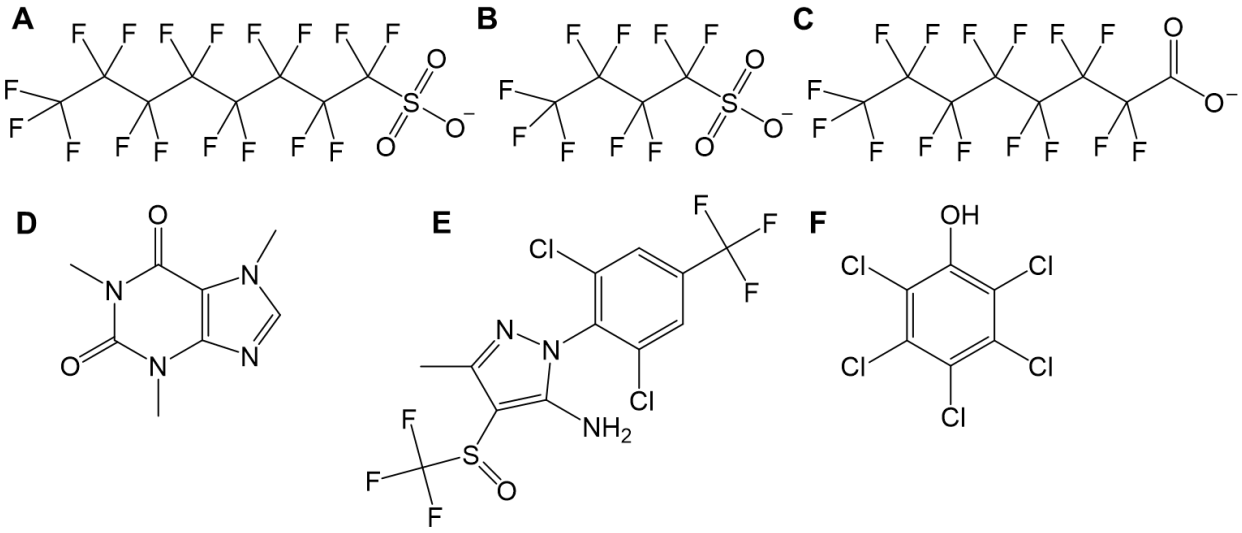

Figure B12 Chemical structures of PFOS (A), PFBS (B), PFOA (C), caffeine (D), fipronil (E), and pentachlorophenol (F).

Appendix C: Supplemental Information for Chapter 4

C1. Viability of the Macromolecular Crowding Approach to BC@mMIP Synthesis

A modified synthesis approach for the multi-template BC@mMIP was attempted using polystyrene sulfonate as macromolecular crowding agent to increase interactions between the template and functional monomer and thus improve the imprinting factor of the MIP product. Polystyrene sulfonate was chosen for its high water solubility and similarity in structure to the commonly used macromolecular crowding agent polystyrene.[187-190] Results shown in **figure C1** showed poor PFAS removal by the resulting adsorbent (BC@mMIP-mc), thus this approach was not employed for further adsorbent synthesis.

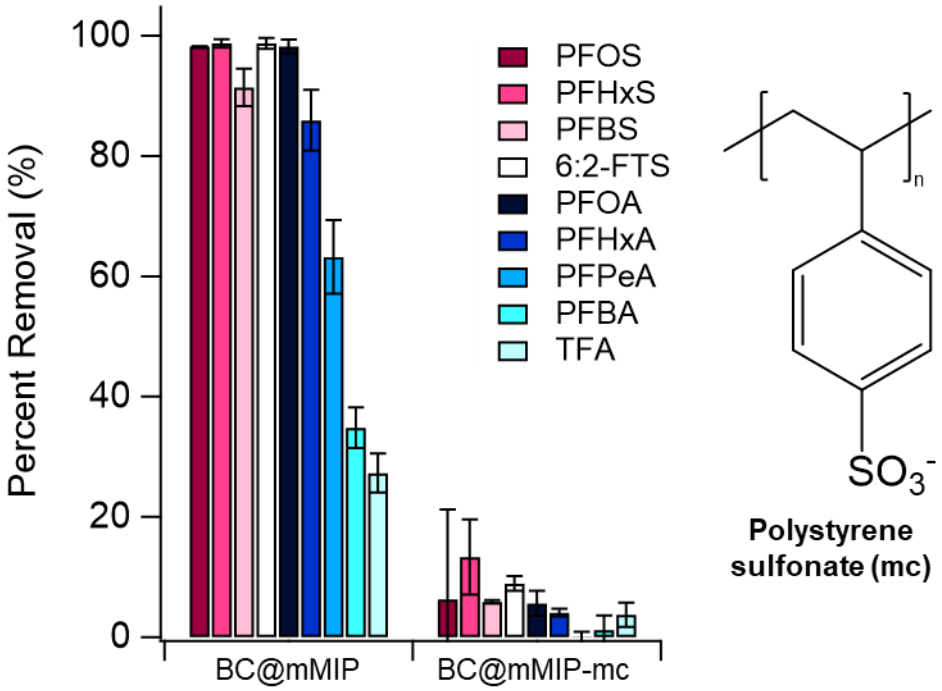

Figure C1 PFAS adsorption 100 mg/L of BC@mMIP synthesized with and without the macromolecular crowding approach. Equilibrium adsorption was evaluated after 4 days. Error bars represent standard deviation from triplicate samples. Initial concentrations were 58 ± 3.7 µg/L PFOS, 50 ± 5.5 µg/L PFHxS, 49 ± 5.1 µg/L PFBS, 48 ± 3.2 µg/L 6:2-FTS, 50 ± 4.9 µg/L PFOA, 58 ± 4.8 µg/L PFHxA, 52 ± 5.4 µg/L PFPeA, 53 ± 5.5 µg/L PFBA, and 41 ± 7.8 µg/L TFA.

C2. TEM Embedding Resin Recipe

Transmission electron microscopy (TEM) samples were embedded in a resin prepared as shown in **table C1**. Approximately 5 mg of sample was placed in a plastic conical tube mold approximately 1 x 2 cm and allowed to harden overnight at 60 °C.

Table C1 TEM Embedding Resin Recipe.

component	quantity
epoxy resin (Poly/Bed 812)	24 g
dodecenyl succinic anhydride (DDSA)	16 g
nadic methyl anhydride (NMA)	10 g
2,4,6-tris(dimethylaminomethyl)phenol (DMP-30) Or benzyldimethylamine (BDMA)	1.5% – 2%

C3. Effect of Swelling on BET Surface Area of Multi-template and Non-imprinted Polymers

The effect of polymer swelling on BC@MIP/NP morphology was evaluated via a 4-day equilibration in ultrapure water followed by drying at 60 °C. Subsequently, the surface area, pore size, and pore surface area were evaluated via nitrogen adsorption as described in ***section 4.2.3***. Swelling appeared to have minimal impact on surface area, but significantly increased the pore size and surface area (**table C2**). These changes could impact adsorption kinetics over multiple cycles of adsorption and regeneration with these materials, particularly if the adsorbent is allowed to dry out during this process.

Table C2 Changes in BET surface area (SA), pore size, and pore SA following polymer layer swelling and redrying.

adsorbent name	BET SA (m^2/g)	pore size (nm)	pore SA (m^2/g)
BC@NP	580	3.0	39
BC@NP post-swelling	562	66.9	230
BC@mMIP	625	9.0	54
BC@mMIP post-swelling	653	20.3	36

C4. Chemical Properties of PFAS and Organics

Table C3 Chemical properties of nine PFAS adsorbates and four co-occurring organics.

name	structure	pKa[a]	solubility[b] (mg/L)	$logK_{oc}$[b]	$logD_{oc}$[c] (at pH 7)
PFOS	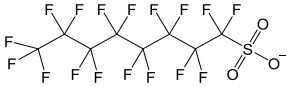	-6 to -2.6	0.104	4.86	-4.74
PFHxS	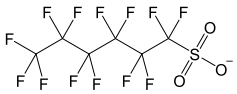	-6 to -5.0	6.17	3.55	-8.45
PFBS	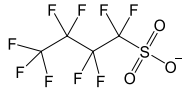	-6 to -5.0	344	2.25	-9.75
6:2-FTS	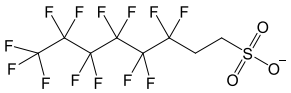	1.31	11.0	4.05	-1.64
PFOA	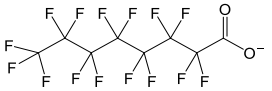	-0.16 to 3.8	0.481	4.42	-2.74
PFHxA	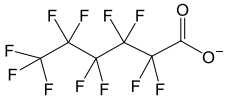	-0.13	27.1	3.12	-4.01
PFPeA	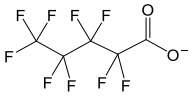	-0.06	197	2.46	-4.60
PFBA	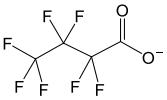	-0.2 to 0.7	1370	1.81	-4.49
TFA	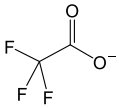	0.23	97,500	0.51	-6.26
fipronil	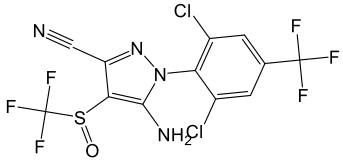	no dissociation	1.90	3.77	3.77
acetaminophen	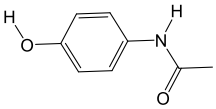	9.38	30,400	1.65	1.65
benzotriazole	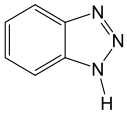	8.37	19,800	1.72	1.70
sulfamethoxazole	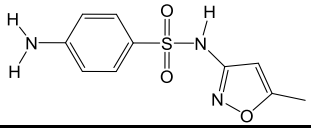	pK_{a1}: 1.6 pK_{a2}: 5.7	3,940	2.41	1.09

a. PFAS source: SGS. "Physical and Chemical Properties of PFAS Compounds." (accessed 10/4/2022).[206] Fipronil source: Bonmatin et al. 2015.[207] Other compounds source: PubChem.[208]

b. US EPA. 2020. Estimation Programs Interface Suite™ for Microsoft® Windows, v 4.1. United States Environmental Protection Agency, Washington, DC, USA.[209]

c. Calculated from pKa and $logK_{oc}$

C5. Limits of Detection and Quantification

Method limits of detection (LoD) and quantification (LoQ) were calculated for LC-MS/MS and HPLC-UV samples run in either (A) 50% v/v ultrapure water and Optima Grade methanol, and (B) 50% v/v Optima Grade methanol and 25% v/v each of ultrapure water and wastewater final effluent (**table C4**) using equations (C.1) through (C.4) below. LoD and LoQ represent analytical method limits only and do not account for concentration factors resulting from solid phase extraction (see ***section C12***). Values presented are the average of LoD and LoQ values calculated for each analysis run (+/-) the standard deviation.

$$s^2 = \frac{\sum_{i=1}^{n}(y_i - f_i)^2}{n-2} \qquad \text{Eqn. (C.1)}$$

$$s_{intercept} = \sqrt{\frac{s^2 \times \sum_{i=1}^{n} x_i^2}{n \times \sum_{i=1}^{n} x_i^2 - (\sum_{i=1}^{n} x_i)^2}} \qquad \text{Eqn. (C.2)}$$

$$LoD = {3.3 \times s_{intercept}}\Big/{slope} \qquad \text{Eqn. (C.3)}$$

$$LoQ = {10 \times s_{intercept}}\Big/{slope} \qquad \text{Eqn. (C.4)}$$

Where s^2 is the sum of the squared differences between the calibration curve data and a linear regression fit, y_i is the measured dependent variable from the calibration curve (i.e., the signal), f_i is the predicted dependent variable (i.e., the signal calculated using the slope and intercept from a linear regression of the calibration curve data), n is the number of data points in the calibration curve, $s_{intercept}$ is the standard deviation of the intercept, x_i is the known dependent variable from the calibration curve (i.e., the concentration), *LoD* is the limit of detection, *slope* is the slope value of a linear regression of the calibration curve, and *LoQ* is the limit of quantification. A similar calculation was performed to determine the *LoD* and *LoQ* from the standard deviation of the slope; however, these values were consistently lower than the *LoD* and *LoQ* presented here and thus have been excluded from this discussion.

Table C4 Limit of detection and limit of quantification for nine PFAS and four organic contaminants in (A) 50% v/v ultrapure water and Optima Grade methanol, and (B) 50% v/v Optima Grade methanol and 25% v/v each of ultrapure water and wastewater final effluent.

	(A)		(B)	
Analyte	**LoD**	**LoQ**	**LoD**	**LoQ**
PFOS	0.15 ± 0.09	0.47 ± 0.26	0.43 ± 0.31	1.29 ± 0.93
PFHxS	0.33 ± 0.15	1.00 ± 0.46	0.52 ± 0.23	1.57 ± 0.70
PFBS	0.23 ± 0.11	0.71 ± 0.34	0.38 ± 0.21	1.15 ± 0.64
6:2-FTS	0.32 ± 0.21	0.97 ± 0.64	0.77 ± 0.39	2.34 ± 1.18
PFOA	0.15 ± 0.09	0.44 ± 0.26	0.22 ± 0.11	0.66 ± 0.32
PFHxA	0.28 ± 0.09	0.84 ± 0.26	0.38 ± 0.15	1.17 ± 0.45
PFPeA	0.27 ± 0.08	0.82 ± 0.24	0.35 ± 0.19	1.05 ± 0.59
PFBA	0.19 ± 0.11	0.59 ± 0.34	0.40 ± 0.16	1.21 ± 0.48
TFA	0.32 ± 0.19	0.98 ± 0.59	0.73 ± 0.36	2.21 ± 1.08
Fipronil			0.68 ± 0.52	1.51 ± 0.69
Acetaminophen			0.74 ± 0.29	2.26 ± 0.88
Benzotriazole			1.00 ± 0.28	3.04 ± 0.86
Sulfamethoxazole			0.94 ± 0.34	2.86 ± 1.02

C6. Selectivity Coefficient Calculations

Selectivity coefficients were calculated from the results of the PFAS competition test as discussed in ***section 4.2.4.1***.

Table C5 Selectivity coefficients comparing adsorption of 6:2-FTS, PFBS, and PFPeA templates to other contaminants of interest (COI; e.g., PFOS) on single and multi-template BC@MIP adsorbents to adsorption on the non-imprinted BC@NP.

		6:2-FTS template			PFBS template			PFPeA template		
adsorbent	**COI**	$K_{imprinted}$	$K_{comparison}$	$K_{selectivity}$	$K_{imprinted}$	$K_{comparison}$	$K_{selectivity}$	$K_{imprinted}$	$K_{comparison}$	$K_{selectivity}$
BC@NP			0.74			0.46			0.16	
BC@MIP	PFOS	0.82		1.11	0.54		1.17	0.35		2.22
BC@mMIP		0.86		1.16	0.87		1.88	0.65		4.14
BC@NP			0.97			0.60			0.21	
BC@MIP	PFHxS	0.87		0.90	0.79		1.31	0.49		2.38
BC@mMIP		0.97		1.00	0.98		1.62	0.73		3.57
BC@NP			1.60						0.34	
BC@MIP	PFBS	1.92		1.20				0.52		1.53
BC@mMIP		0.99		0.61				0.75		2.20
BC@NP						0.62			0.21	
BC@MIP	6:2-FTS				0.92		1.47	0.48		2.27
BC@mMIP					1.01		1.63	0.76		3.58
BC@NP			1.00			0.62			0.21	
BC@MIP	PFOA	1.11		1.11	0.97		1.56	0.47		2.24
BC@mMIP		0.90		0.90	0.91		1.47	0.69		3.24
BC@NP			1.45			0.91			0.31	
BC@MIP	PFHxA	1.63		1.12	1.06		1.17	0.50		1.63
BC@mMIP		0.91		0.62	0.92		1.02	0.69		2.24
BC@NP			4.71			2.94				
BC@MIP	PFPeA	4.98		1.06	1.49		0.51			
BC@mMIP		1.32		0.28	1.33		0.45			
BC@NP			28.75			17.92			6.10	
BC@MIP	PFBA	40.70		1.42	3.37		0.19	5.72		0.94
BC@mMIP		2.33		0.08	2.36		0.13	1.77		0.29

C7. Desorption Kinetics Following Adsorption of (Waste)water Relevant Concentrations of Nine PFAS on BC@mMIP

Desorption kinetics from the batch sorption and desorption test described in ***section 4.2.4.3*** are presented in **figure C2** below and indicate fast desorption of all nine PFAS from the BC@mMIP adsorbent material.

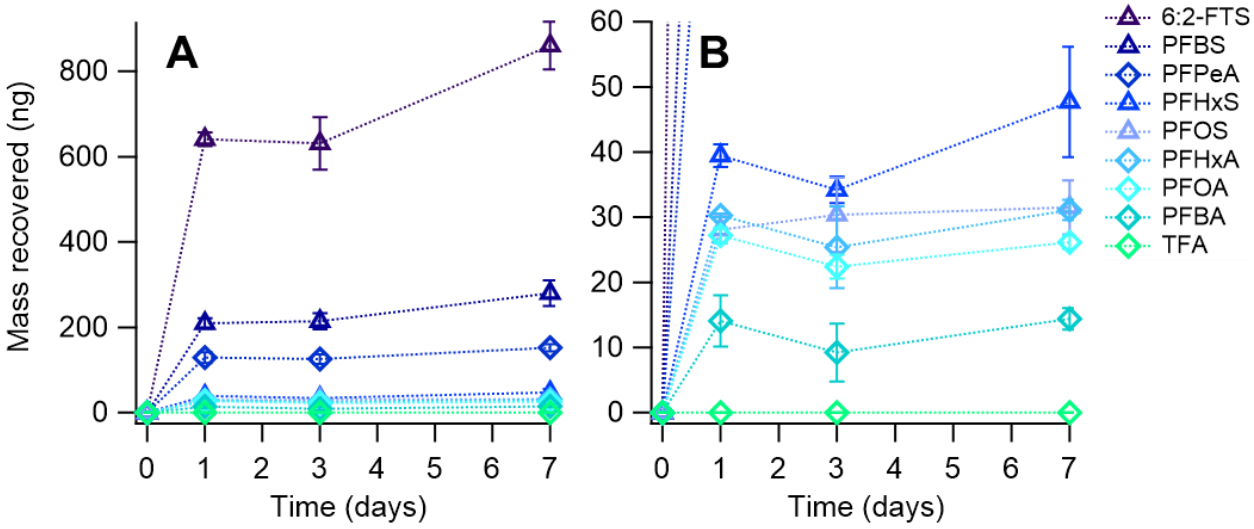

Figure C2 PFAS desorption kinetics from BC@mMIP following a 4-day adsorption of (waste)water relevant concentrations in ultrapure water. PFAS recovery was achieved in a 70% methanol, 1% sodium chloride, 2.8 mM sodium hydroxide solution with a solids concentration of 1 g/L. Graph (A) displays the full dataset while (B) displays a closer look at the PFAS with recovered mass from 0 – 60 ng.

C8. Column Set-Up

Triplicate columns were run for each of four packing types [sand (control), F400 (commercial AC), BC@NP, and BC@mMIP] for twelve columns in total, as shown in **figure C3** below.

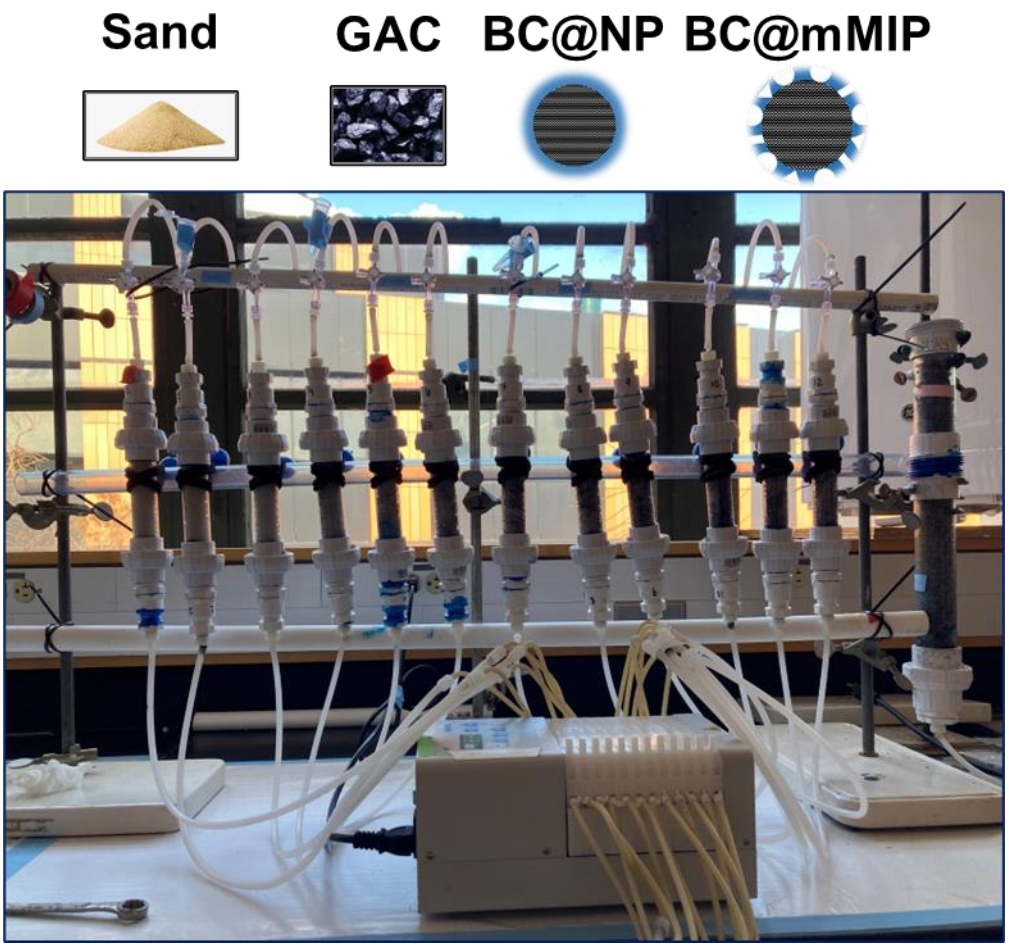

Figure C3 Column test set-up. Test columns contain 1 wt.% of adsorbate in sand.

C9. Column Pore Volumes

Table C6 presents average adsorbent media masses for triplicate columns assembled following the description in ***section 4.2.5.1.***1, and column pore volumes calculated from both the mass change in wet versus dry column weights and from tracer test results described in ***section 4.2.5.1.2*** and **figure C4** (graphical tracer test results).

Table C6 Column packing characteristics and calculated pore volumes.

Media type	Sand	F400 (1 wt%)	BC@NP (1 wt%)	BC@mMIP (1 wt%)
mass active media (g)	---	0.52	0.54	0.54
$PV_{mass\ calculation}$ (mL)	11.1	12.5	9.7	11.0
$PV_{tracer\ test}$ (mL)	27.1	27.4	37.2	27.9

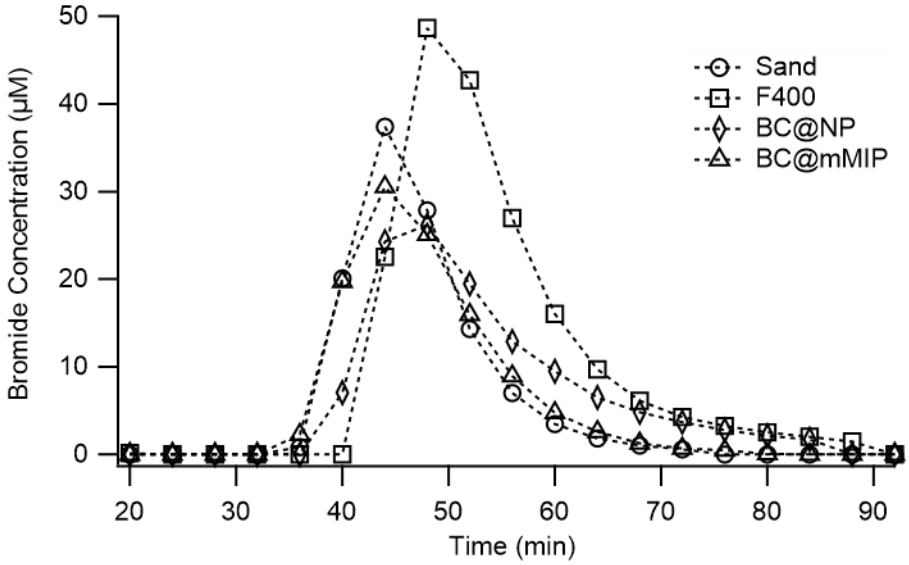

Figure C4 Column tracer test graphical results.

C10. Additional Column Test Plots of Time Series Adsorption and Mass Change

Time series and mass change plots of column test results for analytes not included in **figures 4.5** and **4.6** are presented in **figures C5** and **C6** below. A discussion of these results is included in ***sections 4.3.3.1*** and ***4.3.3.2***.

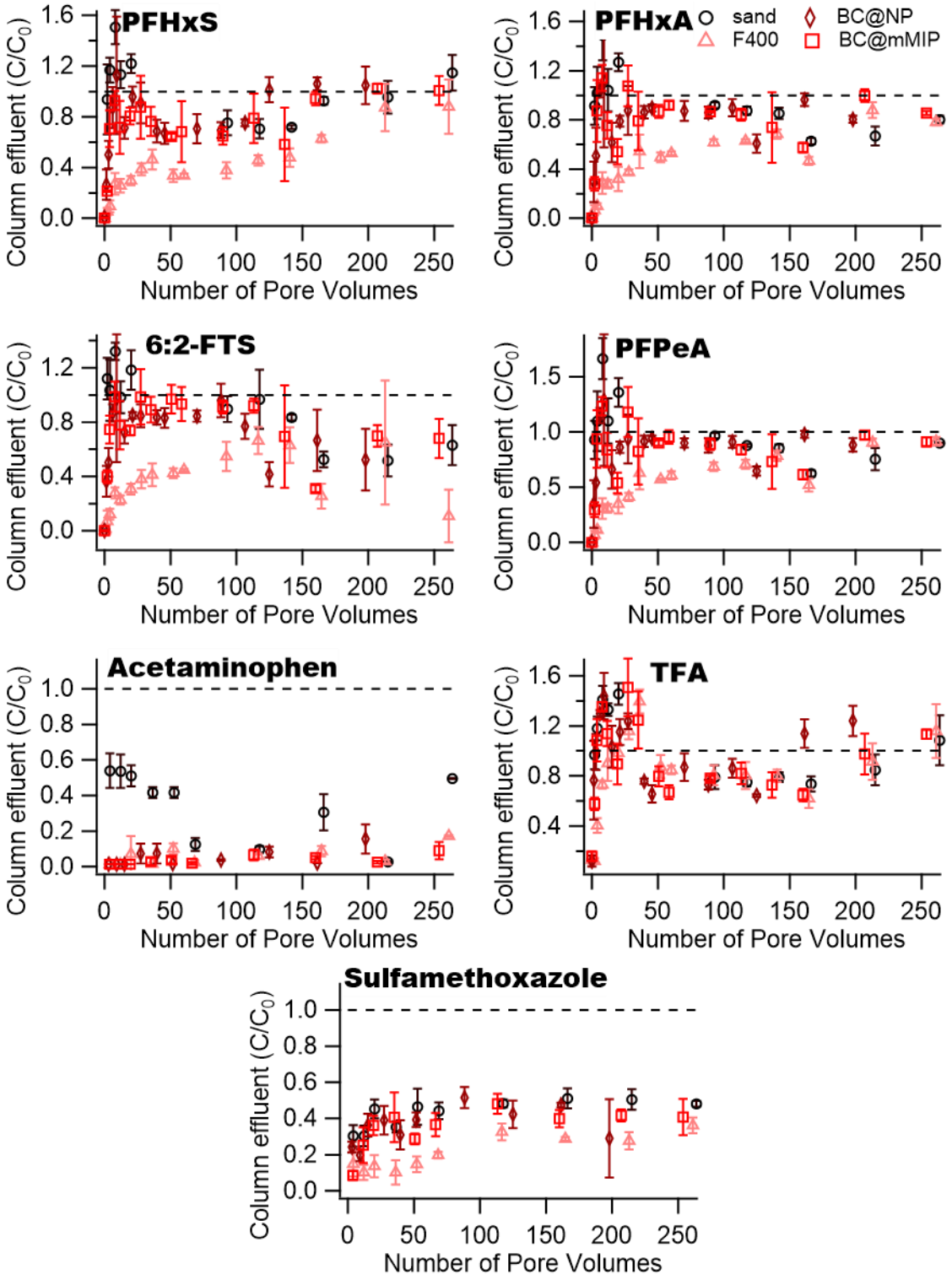

Figure C5 Time series adsorption of for PFAS and organic compounds not shown in **Figure 4.5**. Initial concentrations for each compound during adsorption was approximately 20 µg/L in a wastewater effluent matrix delivered at 1 mL/min. Error bars represent standard deviation from triplicate columns for each media type.

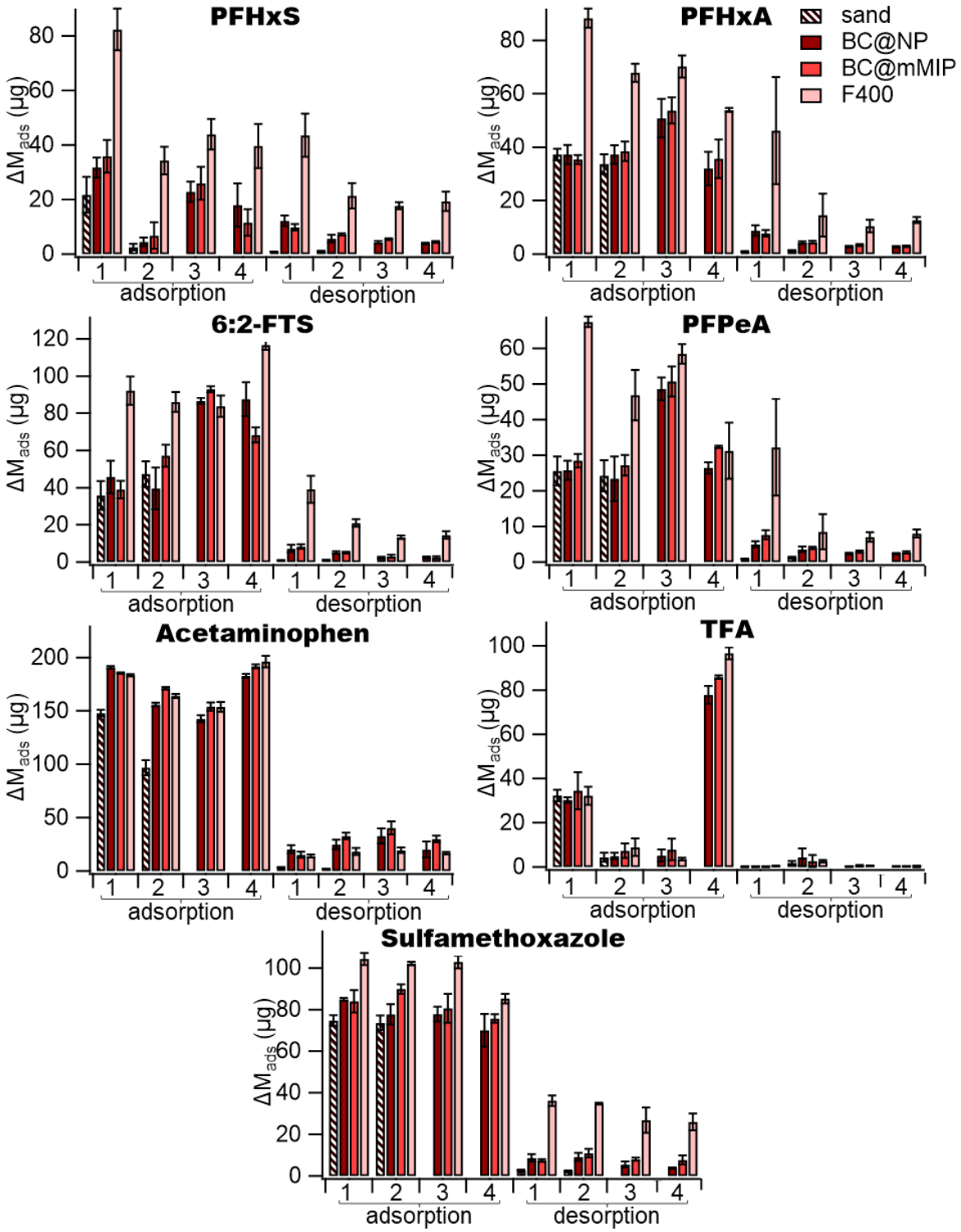

Figure C6 Mass adsorbed and desorbed from column media over four sequential cycles for PFAS and organic compounds not shown in **Figure 4.6**. Initial concentrations for each compound during adsorption was approximately 20 µg/L in a wastewater effluent matrix delivered at 1 mL/min. Desorption was achieved by flushing with 70% methanol and 1% sodium chloride at 0.5 mL/min. Error bars represent standard deviation from triplicate columns for each media type.

C11. LC-MS/MS Analysis for Quantification of PFAS and Fipronil

Concentrations of all PFAS were quantified by mass spectroscopy using a Waters Corporation (Milford, MA) triple quadrupole mass spectrometer (MS/MS) preceded by liquid chromatography (LC). Prior to analysis, samples were filtered to remove biochar fines and (where applicable) organic compounds that would negatively impact instrument performance. Briefly, samples were filtered with a cellulose acetate (CA) syringe filter by first filtering 20 mL of sample into waste and then collecting 1.5 mL of filtered sample. Cellulose acetate was chosen as a filter media for its low PFAS loss, as detailed in prior publications.[1, 201] All liquid chemicals used in LC-MS/MS analysis of PFAS were Optima® LCMS Grade and the Ammonium Acetate was certified ACS Grade (98.1% purity), all purchased from Fisher Chemical (Hampton, NH). All PFAS calibration and internal standards were purchased from Wellington Laboratories (Ontario, CA) unless otherwise noted.

PFOS ($C_8F_{17}SO_3$; **figure C7A**), PFHxS ($C_6F_{13}SO_3$; **figure C7B**), PFBS ($C_4F_9SO_3$; **figure C7C**), 6:2-FTS ($C_8F_{13}H_4SO_3$; **figure C7D**), PFOA ($C_8HF_{15}O_2$; **figure C7E**), PFHxA ($C_6HF_{11}O_2$; **figure C12F**), PFPeA ($C_5HF_9O_2$; **figure C7**), PFBA ($C_4HF_7O_2$; **figure C7H**), TFA ($C_2HF_3O_2$; **figure C7I**), and fipronil ($C_{12}H_4Cl_2F_6N_4OS$; **figure C7J**) were analyzed via LC-MS/MS using an Agilent (Santa Clara, CA) Zorbax Rapid Resolution Eclipse XBD-18C column (2.1 x 50 mm, 1.8 µm). An Agilent, XDB-C18 guard cartridge (80Å, 4.6 x 12.5 mm, 5 µm) was placed before the LC column to pre-filter the sample. For samples run without concentration, mass labeled PFOS ($^{13}C_4$-PFOS), PFOS ($^{18}O_2$-PFHxS), PFOA ($^{13}C_4$-PFOA), PFHxA ($^{13}C_2$-PFHxA), and PFBA ($^{13}C_4$-PFBA) were used as performance internal standards as shown in **table C7**. For samples requiring concentration, solid phase extraction was performed as described in ***section C12***; mass labeled PFOS ($^{13}C_4$-PFOS), PFOS ($^{18}O_2$-PFHxS), 6:2-FTS ($^{13}C_2$-6:2-FTS), PFOA ($^{13}C_4$-PFOA), PFHxA ($^{13}C_2$-PFHxA), and PFBA ($^{13}C_4$-PFBA) were used as extraction internal standards while mass

labeled PFNA ($^{13}C_9$-PFNA) purchased from Cambridge Isotope Laboratories (Tewksbury, MA) was used as a performance internal standard, as shown in **table C8**.

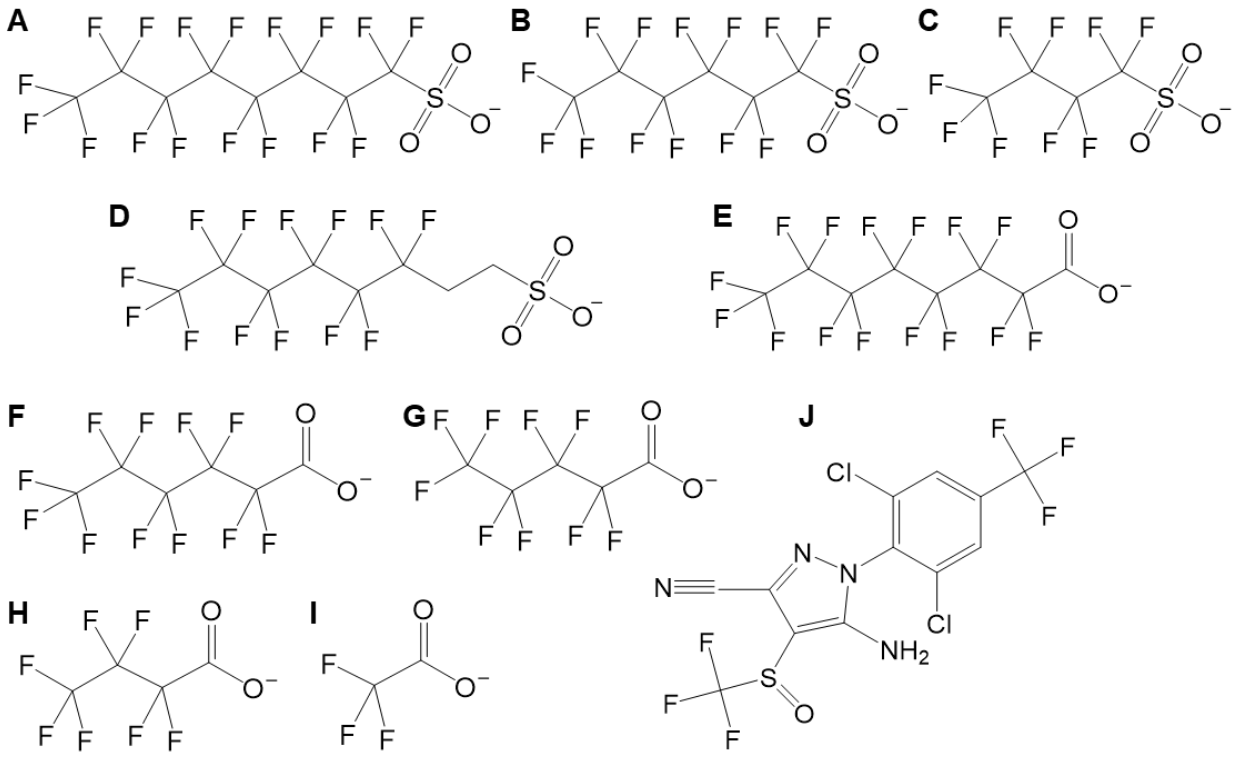

Figure C7 Chemical structures of PFOS (A), PFHxS (B), PFBS (C), 6:2-FTS (D), PFOA (E), PFHxA (F), PFPeA (G), PFBA (H), TFA (I), and Fipronil (J).

The MS/MS operation mode was set to negative electrospray ionization with multiple reaction monitoring (MRM) transitions (**table C9**). The LC was operated with a stationary phase of HPLC grade water with 10 mM ammonium acetate (A) and a mobile phase of HPLC grade methanol with 10 mM ammonium acetate (B). Details of the gradient program are given in **table C10**. Batch test calibration standards and samples were prepared with a 50:50 volumetric ratio of methanol and ultrapure water (or sample in ultrapure water) to minimize PFOS losses to the walls of the polypropylene LCMS vials. Column test samples and the corresponding calibration standards were prepared in a 50:25:25 volumetric ratio of methanol, ultrapure water, and filtered effluent wastewater (or sample in wastewater matrix). This matrix matching of column test samples

allowed for normalization of the impact of high wastewater TDS on analyte retention on/recovery from the chromatography column, particularly for low molecular weight PFAS (i.e., TFA and PFBA).

Table C7 Performance internal standards for unconcentrated PFAS samples.

PFAS compound	performance standard
PFBS	$^{13}C_2$-PFHxA
PFHxS	$^{18}O_2$-PFHxS
PFOS	$^{13}C_4$-PFOS
6:2-FTS	$^{13}C_4$-PFOA
TFA	$^{13}C_4$-PFBA
PFBA	$^{13}C_4$-PFBA
PFPeA	$^{13}C_2$-PFHxA
PFHxA	$^{13}C_2$-PFHxA
PFOA	$^{13}C_4$-PFOA
fipronil	$^{13}C_4$-PFOA

Table C8 Extraction and performance internal standards for analysis of PFAS samples including solid phase extraction (SPE).

PFAS compound	extraction standard	performance standard
PFBS	$^{13}C_2$-PFHxA	$^{13}C_9$-PFNA
PFHxS	$^{18}O_2$-PFHxS	$^{13}C_9$-PFNA
PFOS	$^{13}C_4$-PFOS	$^{13}C_9$-PFNA
6:2-FTS	$^{13}C_4$-6:2-FTS	$^{13}C_9$-PFNA
TFA	$^{13}C_4$-PFBA	$^{13}C_9$-PFNA
PFBA	$^{13}C_4$-PFBA	$^{13}C_9$-PFNA
PFPeA	$^{13}C_2$-PFHxA	$^{13}C_9$-PFNA
PFHxA	$^{13}C_2$-PFHxA	$^{13}C_9$-PFNA
PFOA	$^{13}C_4$-PFOA	$^{13}C_9$-PFNA

Table C9 LC-MS/MS parameters used for quantification of PFAS.

	ionization mode	parent (m/z)	product ion (m/z)	cone energy (V)	collision energy (V)	RT (min)
TFA	-	112.70	68.40	19.0	10.0	1.5
PFBA	-	213.00	169.00	11.0	13.0	5.6
$^{13}C_4$-PFBA	-	217.00	172.00	11.0	13.0	5.6
PFPeA	-	263.00	219.00	17.0	8.0	7.2
PFBS	-	299.00	79.40	20.0	35.0	7.3
PFBS	-	299.00	98.50	25.0	35.0	7.3
PFHxA	-	313.10	118.60	18.0	22.0	8.0
PFHxA	-	313.10	269.10	18.0	9.0	8.0
$^{13}C_2$-PFHxA	-	315.00	270.00	18.0	9.0	8.0
PFHxS	-	399.00	79.40	54.0	35.0	8.6
PFHxS	-	399.00	98.50	54.0	35.0	8.6
$^{18}O_2$-PFHxS	-	403.00	83.50	65.0	35.0	8.6
6:2-FTS	-	427.00	79.40	47.0	35.0	9.2
6:2-FTS	-	427.00	407.00	47.0	19.0	9.2
$^{13}C_4$-6:2-FTS	-	429.00	409.00	47.0	19.0	9.2
PFOA	-	413.10	169.00	18.0	19.0	9.2
PFOA	-	413.10	369.00	18.0	10.0	9.2
$^{13}C_4$-PFOA	-	417.10	372.00	18.0	10.0	9.2
PFOS	-	498.95	79.40	53.0	40.0	9.6
PFOS	-	498.95	98.50	53.0	35.0	9.6
$^{13}C_4$-PFOS	-	503.10	79.40	53.0	40.0	9.6
$^{13}C_9$-PFNA	-	463.00	219.00	18.0	11.0	9.6
fipronil	-	436.90	330.20	32	16	9.9

Table C10 LC gradient program for elution of PFAS compounds using 10 mM ammonium acetate in water and methanol as the stationary and mobile phases.

time (min)	%A (10 mM ammonium acetate)	%B (10 mM ammonium acetate in methanol)	flow rate (mL/min)
0.0	80	20	0.4
8.0	5	95	0.4
10.0	5	95	0.4
10.5	80	20	0.4
16.0	80	20	0.4

C12. Concentration of PFAS Samples via Solid Phase Extraction

Low concentration PFAS samples from the batch test described in ***section 4.3.3.3*** were processed via solid phase extraction (SPE) prior to LC-MS/MS analysis to concentrate the sample using a modified version of the EPA Draft Method 1633.[210] Solvents used were Optima™ LC-MS/MS grade unless otherwise noted. Briefly, 2.5 μg of each extraction internal standard ($^{13}C_4$-PFOS, $^{18}O_2$-PFHxS, $^{13}C_2$-6:2-FTS, $^{13}C_4$-PFOA, $^{13}C_2$-PFHxA, and $^{13}C_4$-PFBA) were added to each sample as methanolic stocks, and the samples were inverted approximately 20 times to mix. Phenomenex Strata X-AW SPE cartridges were preconditioned with 1% ammonium hydroxide (ACS grade) in methanol and 0.3 M formic acid (ACS grade) in ultrapure water as described in Draft Method 1633 and then the sample was passed through under low vacuum at 5 mL/min. Sample bottles and cartridges were washed with two 5 mL aliquots of ultrapure water followed by 5 mL of 1:1 methanol and 0.1 M formic acid in ultrapure water and then dried by applying low vacuum for 10 min followed by high vacuum for 30 s. The sample was eluted by passing through approximately 7 mL of 1% v/v ammonium hydroxide in methanol under low vacuum at a flow rate of 1 mL/min and collected in a 15 mL polypropylene tube. Samples were evaporated to dryness in a nitrogen evaporator with the water bath at 50 °C and a nitrogen flow of 30 SCFH. Samples were reconstituted in the polypropylene tube with 500 μL of ultrapure water and 490 μL of methanol, vortexed for 30 s, allowed to sit at 4 °C overnight, and then vortexed for 30 s before transferring to a polypropylene LC-MS/MS vial. A 10 μL aliquot of a 600 μg/L methanolic stock of the performance internal standard ($^{13}C_9$-PFNA) was added to each LC-MS/MS vial for a total volume of 1 mL. Samples were stored at 4 °C before LC-MS/MS analysis was performed as described in ***section C11***.

C13. Ion Chromatography and ICP-OES Analysis for Quantification of Ionic Salts in Wastewater Treatment Plant Effluent

Selected anions (chloride, nitrate, sulfate) were quantified in the wastewater final effluent samples obtained from King County West Point Treatment Plant via ion chromatography (IC). IC analysis was performed on a Thermo Scientific™ Dionex™ ICS 3000 instrument equipped with a Thermo Scientific™ Dionex™ IonPac™ AS-9 high capacity analytical column preceded by an AG-9 guard column and a ERS 500 carbonate suppressor. The instrument was operated using the gradient described in **table C11**. Prior to analysis, samples were filtered with a 0.22 μm cellulose acetate syringe filter by first wasting 10 mL of sample through the filter before collecting approximately 1.5 mL for analysis. Differentiation between sulfate and sulfite peaks was not possible with this method; however, the presence of sulfite species in aerobic waters (e.g., wastewater effluent) is unlikely, thus the entire peak area was attributed to sulfate.

Table C11 Ion Chromatography Gradient for Determination of Selected Anions in Wastewater.

time (min)	%A (deaerated ultrapure water)	%B (9 mM sodium carbonate in water)	flow rate (mL/min)
0.0	67	33	0.25
10.0	85	15	0.25
16.0	0	100	0.25
18.0	67	33	0.25
25.0	67	33	0.25

Selected cations (calcium, magnesium, iron, lead, aluminum, and sodium) were quantified by ion coupled plasma optical emission spectroscopy (ICP-OES) on a Perkin Elmer Optima 8300 instrument using a modified version of Standard Method 3010.[196] Briefly, prior to analysis samples were filtered with a 0.45 μm nylon syringe filter by first wasting 10 mL of sample through the filter before collecting approximately 10 mL for analysis. Nitric acid was added to filtered samples to achieve a concentration of 1% v/v and acidified samples were stored at 4 °C until analysis.

C14. HPLC-UV Analysis for Quantification of Acetaminophen, Benzotriazole, and Sulfamethoxazole

Acetaminophen, benzotriazole, and sulfamethoxazole in column test samples were quantified via high performance liquid chromatography coupled with UV spectrophotometry. Analysis was performed on a Thermo Scientific™ Dionex™ UltiMate™ 3000 instrument equipped with a Millipore Sigma™ Supelco™ Ascentis™ C18 analytical column (3 µm particle size, 15 cm x 2.1 mm) preceded by a Supelco™ Ascentis™ C18 Supelguard™ guard column (3 µm particle size). An isometric mobile phase of (A) 81% v/v of HPLC grade water containing 0.1% v/v HPLC grade formic acid and (B) 19% v/v of HPLC grade methanol was delivered at 0.2 mL/min for the duration of the run. Analyte retention times, detection wavelengths, and chemical structure are given in **table C12** below. All samples were run without dilution to account for the relatively high limits of quantification (**table C4**) compared to the expected concentrations. Matrix matching of calibration standards was performed to account for any impact of wastewater salts and organics on HPLC performance.

Table C12 HPLC Analysis Conditions and Molecular Structures of Select Organic Compounds.

analyte	RT (min)	wavelength (nm)	structure
acetaminophen	6.1	244	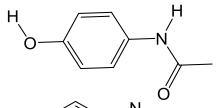
benzotriazole	19.0	270	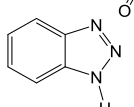
sulfamethoxazole	23.0	272	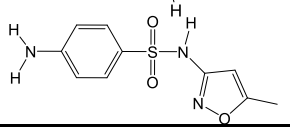

REFERENCES

(1) Steigerwald, J. M.; Ray, J. R. Adsorption behavior of perfluorooctanesulfonate (PFOS) onto activated spent coffee grounds biochar in synthetic wastewater effluent. *JHM Letters* **2021**, *2*, 100025. DOI: https://doi.org/10.1016/j.hazl.2021.100025.

(2) Foley, J. A.; Ramankutty, N.; Brauman, K. A.; Cassidy, E. S.; Gerber, J. S.; Johnston, M.; Mueller, N. D.; O'Connell, C.; Ray, D. K.; West, P. C. Solutions for a cultivated planet. *Nature* **2011**, *478* (7369), 337-342.

(3) Molden, D.; Frenken, K.; Barker, R.; De Fraiture, C.; Mati, B.; Svendsen, M.; Sadoff, C. W.; Finlayson, M.; Atapattu, S.; Giordano, M. *Trends in water and agricultural development*; International Water Management Institute, 2007.

(4) Lu, J.; Vecchi, G. A.; Reichler, T. Expansion of the Hadley cell under global warming. *Geophysical Research Letters* **2007**, *34* (6).

(5) USEPA, U., CDM Smith. 2012 Guidelines for Water Reuse. Office of Wastewater Management, O. o. W., Ed.; U.S. EPA,: Washington, D.C., 2012.

(6) Scruggs, C. E.; Thomson, B. M. Opportunities and challenges for direct potable water reuse in arid inland communities. *Journal of Water Resources Planning and Management* **2017**, *143* (10), 04017064.

(7) Inyang, M.; Dickenson, E. The potential role of biochar in the removal of organic and microbial contaminants from potable and reuse water: a review. *Chemosphere* **2015**, *134*, 232-240. DOI: https://doi.org/10.1016/j.chemosphere.2015.03.072.

(8) Inyang, M.; Dickenson, E. R. V. The use of carbon adsorbents for the removal of perfluoroalkyl acids from potable reuse systems. *Chemosphere* **2017**, *184*, 168-175. DOI: https://doi.org/10.1016/j.chemosphere.2017.05.161.

(9) Bolong, N.; Ismail, A.; Salim, M. R.; Matsuura, T. A review of the effects of emerging contaminants in wastewater and options for their removal. *Desalination* **2009**, *239* (1-3), 229-246.

(10) Barzen-Hanson, K. A.; Roberts, S. C.; Choyke, S.; Oetjen, K.; McAlees, A.; Riddell, N.; McCrindle, R.; Ferguson, P. L.; Higgins, C. P.; Field, J. A. Discovery of 40 classes of per- and polyfluoroalkyl substances in historical aqueous film-forming foams (AFFFs) and AFFF-impacted groundwater. *Environ. Sci. Technol.* **2017**, *51* (4), 2047-2057. DOI: 10.1021/acs.est.6b05843.

(11) Hu, X. C.; Andrews, D. Q.; Lindstrom, A. B.; Bruton, T. A.; Schaider, L. A.; Grandjean, P.; Lohmann, R.; Carignan, C. C.; Blum, A.; Balan, S. A.; et al. Detection of poly- and perfluoroalkyl substances (PFASs) in U.S. drinking water linked to industrial sites, military fire training areas, and wastewater treatment plants. *Environ. Sci. Technol. Lett.* **2016**, *3* (10), 344-350. DOI: 10.1021/acs.estlett.6b00260.

(12) Li, F.; Duan, J.; Tian, S.; Ji, H.; Zhu, Y.; Wei, Z.; Zhao, D. Short-chain per-and polyfluoroalkyl substances in aquatic systems: Occurrence, impacts and treatment. *Chem. Eng. J.* **2020**, *380*, 122506.

(13) Houtz, E. F.; Higgins, C. P.; Field, J. A.; Sedlak, D. L. Persistence of perfluoroalkyl acid precursors in AFFF-impacted groundwater and soil. *Environ. Sci. Technol.* **2013**, *47* (15), 8187-8195. DOI: 10.1021/es4018877.

(14) Fenton, S. E.; Ducatman, A.; Boobis, A.; DeWitt, J. C.; Lau, C.; Ng, C.; Smith, J. S.; Roberts, S. M. Per-and polyfluoroalkyl substance toxicity and human health review: Current state of

knowledge and strategies for informing future research. *Environ. Toxicol. Chem.* **2021**, *40* (3), 606-630.

(15) IRIS Toxicological Review of Perfluorobutanoic Acid (PFBA) and Related Compound Ammonium Perfluorobutanoic Acid (Public Comment and External Review Draft, 2021). U.S. Environmental Protection Agency: Washington, DC, 2021.

(16) Tsuda, S. Differential toxicity between perfluorooctane sulfonate (PFOS) and perfluorooctanoic acid (PFOA). *J. Toxicol. Sci.* **2016**, *41* (Special), SP27-SP36. DOI: 10.2131/jts.41.sp27.

(17) Mueller, R.; Yingling, V. History and use of per-and polyfluoroalkyl substances (PFAS). *Interstate Technology & Regulatory Council* **2017**.

(18) Buck, R. C.; Franklin, J.; Berger, U.; Conder, J. M.; Cousins, I. T.; De Voogt, P.; Jensen, A. A.; Kannan, K.; Mabury, S. A.; van Leeuwen, S. P. Perfluoroalkyl and polyfluoroalkyl substances in the environment: terminology, classification, and origins. *Integr. Environ. Assess. Manag.* **2011**, *7* (4), 513-541.

(19) USEPA. Interim Guidance on the Destruction and Disposal of Perfluoroalkyl and Polyfluoroalkyl Substances and Materials Containing Perfluoroalkyl and Polyfluoroalkyl Substances. U.S. Environmental Protection Agency,: Washington D.C., 2020.

(20) Xiao, X.; Ulrich, B. A.; Chen, B.; Higgins, C. P. Sorption of poly- and perfluoroalkyl substances (PFASs) relevant to aqueous film-forming foam (AFFF)-impacted groundwater by biochars and activated carbon. *Environ. Sci. Technol.* **2017**, *51* (11), 6342-6351. DOI: 10.1021/acs.est.7b00970.

(21) Washington State Department of Ecology. Per-and Polyfluoroalkyl Substances Chemical Action Plan. Hazardous Waste and Toxics Reduction Program, Ed.; Washington State Department of Ecology,: Olympia, Washington, 2021.

(22) Moody, C. A.; Field, J. A. Perfluorinated surfactants and the environmental implications of their use in fire-fighting foams. *Environ. Sci. Technol.* **2000**, *34* (18), 3864-3870. DOI: 10.1021/es991359u.

(23) Cadore, A.; Chou, C.-H.; Jones, D. G.; Llados, F.; Pohl, H. R. Draft Toxicological Profile for Perfluoroalkyls. U.S. Agency for Toxic Substances and Disease Registry: Atlanta, GA, 2009.

(24) ATSDR. Toxicological Profile for Perfluoroalkyls. Agency for Toxic Substances and Disease Registry,: 2021.

(25) CDC. *Fourth national report on human exposure to environmental chemicals*; US Department of Health and Human Services,, Centers for Disease Control and Prevention, Atlanta, GA, 2009. https://www.cdc.gov/exposurereport/ (accessed 1/7/2020).

(26) Post, G. B.; Cohn, P. D.; Cooper, K. R. Perfluorooctanoic acid (PFOA), an emerging drinking water contaminant: a critical review of recent literature. *Environmental research* **2012**, *116*, 93-117.

(27) IARC monographs on the evaluation of the carcinogenic risk of chemicals to man. **1972**.

(28) van Raalte, D. H.; Li, M.; Pritchard, P. H.; Wasan, K. M. Peroxisome proliferator-activated receptor (PPAR)-α: a pharmacological target with a promising future. *Pharmaceutical research* **2004**, *21* (9), 1531-1538.

(29) USEPA. Drinking water health advisories for PFOA and PFOS. U.S. Environmental Protection Agency, Ed.; 2016.

(30) Drinking Water Health Advisories for PFAS: Fact Sheet for Public Water Systems. U.S. Environmental Protection Agency: Washington D.C., 2022.

(31) Thompson, K. A.; Mortazavian, S.; Gonzalez, D. J.; Bott, C.; Hooper, J.; Schaefer, C. E.; Dickenson, E. R. V. Poly- and Perfluoroalkyl Substances in Municipal Wastewater Treatment Plants in the United States: Seasonal Patterns and Meta-Analysis of Long-Term Trends and Average Concentrations. *ACS ES&T Water* **2022**. DOI: 10.1021/acsestwater.1c00377.

(32) Phong Vo, H. N.; Ngo, H. H.; Guo, W.; Hong Nguyen, T. M.; Li, J.; Liang, H.; Deng, L.; Chen, Z.; Hang Nguyen, T. A. Poly-and perfluoroalkyl substances in water and wastewater: A comprehensive review from sources to remediation. *J. Water Process. Eng.* **2020**, *36*, 101393. DOI: 10.1016/j.jwpe.2020.101393.

(33) Furl, C. V.; Meredith, C. A.; Strynar, M. J.; Nakayama, S. F. Relative importance of wastewater treatment plants and non-point sources of perfluorinated compounds to Washington State rivers. *Sci. Total Environ.* **2011**, *409* (15), 2902-2907. DOI: https://doi.org/10.1016/j.scitotenv.2011.04.035.

(34) Arvaniti, O. S.; Stasinakis, A. S. Review on the occurrence, fate and removal of perfluorinated compounds during wastewater treatment. *Sci. Total Environ.* **2015**, *524-525*, 81-92. DOI: https://doi.org/10.1016/j.scitotenv.2015.04.023.

(35) Loganathan, B. G.; Sajwan, K. S.; Sinclair, E.; Senthil Kumar, K.; Kannan, K. Perfluoroalkyl sulfonates and perfluorocarboxylates in two wastewater treatment facilities in Kentucky and Georgia. *Water Res.* **2007**, *41* (20), 4611-4620. DOI: https://doi.org/10.1016/j.watres.2007.06.045.

(36) Sinclair, E.; Kannan, K. Mass loading and fate of perfluoroalkyl surfactants in wastewater treatment plants. *Environ. Sci. Technol.* **2006**, *40* (5), 1408-1414. DOI: 10.1021/es051798v.

(37) USEPA. Memorandum Regarding Per- and Polyfluoroalkyl Substances. U.S. Environmental Protection Agency: Washington, D.C., 2021.

(38) Boyer, T. H.; Fang, Y.; Ellis, A.; Dietz, R.; Choi, Y. J.; Schaefer, C. E.; Higgins, C. P.; Strathmann, T. J. Anion exchange resin removal of per- and polyfluoroalkyl substances (PFAS) from impacted water: A critical review. *Water Res.* **2021**, *200*, 117244. DOI: https://doi.org/10.1016/j.watres.2021.117244.

(39) Ulrich, B. A.; Im, E. A.; Werner, D.; Higgins, C. P. Biochar and activated carbon for enhanced trace organic contaminant retention in stormwater infiltration systems. *Environ. Sci. Technol.* **2015**, *49* (10), 6222-6230. DOI: 10.1021/acs.est.5b00376.

(40) Yu, J.; Lv, L.; Lan, P.; Zhang, S.; Pan, B.; Zhang, W. Effect of effluent organic matter on the adsorption of perfluorinated compounds onto activated carbon. *J. Hazard. Mater.* **2012**, *225-226*, 99-106. DOI: https://doi.org/10.1016/j.jhazmat.2012.04.073.

(41) Gagliano, E.; Sgroi, M.; Falciglia, P. P.; Vagliasindi, F. G. A.; Roccaro, P. Removal of poly- and perfluoroalkyl substances (PFAS) from water by adsorption: Role of PFAS chain length, effect of organic matter and challenges in adsorbent regeneration. *Water Res.* **2020**, *171*, 115381. DOI: https://doi.org/10.1016/j.watres.2019.115381.

(42) Bunani, S.; Yörükoğlu, E.; Yüksel, Ü.; Kabay, N.; Yüksel, M.; Sert, G.; Pek, T. Ö. Application of nanofiltration for reuse of wastewater. *International Journal of Global Warming* **2014**, *6* (2-3), 325-338.

(43) Ross, I.; McDonough, J.; Miles, J.; Storch, P.; Thelakkat Kochunarayanan, P.; Kalve, E.; Hurst, J.; S. Dasgupta, S.; Burdick, J. A review of emerging technologies for remediation of PFASs. *Remediation Journal* **2018**, *28* (2), 101-126.

(44) Kumarasamy, E.; Manning, I. M.; Collins, L. B.; Coronell, O.; Leibfarth, F. A. Ionic Fluorogels for Remediation of Per- and Polyfluorinated Alkyl Substances from Water. *ACS Cent. Sci.* **2020**, *6* (4), 487-492. DOI: 10.1021/acscentsci.9b01224.

(45) Quan, Q.; Wen, H.; Han, S.; Wang, Z.; Shao, Z.; Chen, M. Fluorous-Core Nanoparticle-Embedded Hydrogel Synthesized via Tandem Photo-Controlled Radical Polymerization: Facilitating the Separation of Perfluorinated Alkyl Substances from Water. *ACS Appl. Mater. Interfaces* **2020**, *12* (21), 24319-24327. DOI: 10.1021/acsami.0c04646.

(46) Ateia, M.; Arifuzzaman, M.; Pellizzeri, S.; Attia, M. F.; Tharayil, N.; Anker, J. N.; Karanfil, T. Cationic polymer for selective removal of GenX and short-chain PFAS from surface waters and wastewaters at ng/L levels. *Water Res.* **2019**, *163*, 114874. DOI: https://doi.org/10.1016/j.watres.2019.114874.

(47) Saad, A.; Mills, R.; Wan, H.; Mottaleb, M. A.; Ormsbee, L.; Bhattacharyya, D. Thermo-responsive adsorption-desorption of perfluoroorganics from water using PNIPAm hydrogels and pore functionalized membranes. *Journal of membrane science* **2020**, *599*, 117821.

(48) Huang, P.-J.; Hwangbo, M.; Chen, Z.; Liu, Y.; Kameoka, J.; Chu, K.-H. Reusable functionalized hydrogel sorbents for removing long-and short-chain perfluoroalkyl acids (PFAAs) and GenX from aqueous solution. *ACS omega* **2018**, *3* (12), 17447-17455.

(49) Long, L.; Hu, X.; Yan, J.; Zeng, Y.; Zhang, J.; Xue, Y. Novel chitosan–ethylene glycol hydrogel for the removal of aqueous perfluorooctanoic acid. *Journal of Environmental Sciences* **2019**, *84*, 21-28.

(50) Cheng, Y. H.; Barpaga, D.; Soltis, J. A.; Shutthanandan, V.; Kargupta, R.; Han, K. S.; McGrail, B. P.; Motkuri, R. K.; Basuray, S.; Chatterjee, S. Metal–organic framework-based microfluidic impedance sensor platform for ultrasensitive detection of perfluorooctanesulfonate. *ACS applied materials & interfaces* **2020**, *12* (9), 10503-10514.

(51) Li, R.; Alomari, S.; Stanton, R.; Wasson, M. C.; Islamoglu, T.; Farha, O. K.; Holsen, T. M.; Thagard, S. M.; Trivedi, D. J.; Wriedt, M. Efficient removal of per-and polyfluoroalkyl substances from water with zirconium-based metal–organic frameworks. *Chemistry of Materials* **2021**, *33* (9), 3276-3285.

(52) Li, R.; Alomari, S.; Islamoglu, T.; Farha, O. K.; Fernando, S.; Thagard, S. M.; Holsen, T. M.; Wriedt, M. Systematic study on the removal of per-and polyfluoroalkyl substances from contaminated groundwater using metal–organic frameworks. *Environ. Sci. Technol.* **2021**, *55* (22), 15162-15171.

(53) Guo, H.; Liu, Y.; Ma, W.; Yan, L.; Li, K.; Lin, S. Surface molecular imprinting on carbon microspheres for fast and selective adsorption of perfluorooctane sulfonate. *J. Hazard. Mater.* **2018**, *348*, 29-38. DOI: https://doi.org/10.1016/j.jhazmat.2018.01.018.

(54) Glasscott, M. W.; Vannoy, K. J.; Kazemi, R.; Verber, M. D.; Dick, J. E. μ-MIP: Molecularly Imprinted Polymer-Modified Microelectrodes for the Ultrasensitive Quantification of GenX (HFPO-DA) in River Water. *Environ. Sci. Technol. Lett.* **2020**, *7* (7), 489-495. DOI: 10.1021/acs.estlett.0c00341.

(55) Takayose, M.; Nishimoto, K.; Matsui, J. A fluorous synthetic receptor that recognizes perfluorooctanoic acid (PFOA) via fluorous interaction obtained by molecular imprinting. *Analyst* **2012**, *137* (12), 2762-2765, 10.1039/C2AN15936H. DOI: 10.1039/C2AN15936H.

(56) Cao, F.; Wang, L.; Yao, Y.; Wu, F.; Sun, H.; Lu, S. Synthesis and application of a highly selective molecularly imprinted adsorbent based on multi-walled carbon nanotubes for selective

removal of perfluorooctanoic acid. *Environ. Sci. Water Res. Technol.* **2018**, *4* (5), 689-700, 10.1039/C7EW00443E. DOI: 10.1039/C7EW00443E.

(57) Ye, L. Synthetic Strategies in Molecular Imprinting. *Adv Biochem Eng Biotechnol* **2015**, *150*, 1-24. DOI: 10.1007/10_2015_313 From NLM.

(58) Dai, C.-M.; Zhang, J.; Zhang, Y.-L.; Zhou, X.-F.; Duan, Y.-P.; Liu, S.-G. Selective removal of acidic pharmaceuticals from contaminated lake water using multi-templates molecularly imprinted polymer. *Chem. Eng. J.* **2012**, *211-212*, 302-309. DOI: https://doi.org/10.1016/j.cej.2012.09.090.

(59) BelBruno, J. J. Molecularly Imprinted Polymers. *Chemical Reviews* **2019**, *119* (1), 94-119. DOI: 10.1021/acs.chemrev.8b00171.

(60) Xie, X.; Ma, X.; Guo, L.; Fan, Y.; Zeng, G.; Zhang, M.; Li, J. Novel magnetic multi-templates molecularly imprinted polymer for selective and rapid removal and detection of alkylphenols in water. *Chem. Eng. J.* **2019**, *357*, 56-65. DOI: https://doi.org/10.1016/j.cej.2018.09.080.

(61) Deng, S.; Shuai, D.; Yu, Q.; Huang, J.; Yu, G. Selective sorption of perfluorooctane sulfonate on molecularly imprinted polymer adsorbents. *Front Environ Sci Eng China* **2009**, *3* (2), 171-177.

(62) Shields, F. E.; Reed, T. B. All Biochars are Not Created Equal, and How to Tell Them Apart.

(63) Linares-Solano, Á.; Lillo-Ródenas, M. A.; Lozar, J. P. M.; Kunowsky, M.; Anaya, A. J. R. NaOH and KOH for preparing activated carbons used in energy and environmental applications. *International Journal of Energy, Environment and Economics* **2012**, *2* (4), 59 - 91.

(64) Mark R. Fuchs, M. G.-P., P. Small and G. Flora. Campfire Lessons - breaking down the combustion process to understand biochar production. *The Biochar Journal* **2014**. (acccessed 07/18/2022).

(65) Sajjadi, B.; Chen, W.-Y.; Mattern, D. L.; Hammer, N.; Dorris, A. Low-temperature acoustic-based activation of biochar for enhanced removal of heavy metals. *J. Water Process. Eng.* **2020**, *34*, 101166.

(66) Rajapaksha, A. U.; Chen, S. S.; Tsang, D. C. W.; Zhang, M.; Vithanage, M.; Mandal, S.; Gao, B.; Bolan, N. S.; Ok, Y. S. Engineered/designer biochar for contaminant removal/immobilization from soil and water: potential and implication of biochar modification. *Chemosphere* **2016**, *148*, 276-291. DOI: https://doi.org/10.1016/j.chemosphere.2016.01.043.

(67) Evans, M.; Halliop, E.; MacDonald, J. The production of chemically-activated carbon. *Carbon* **1999**, *37* (2), 269-274.

(68) Fornes, F.; Belda, R. M. Use of raw and acidified biochars as constituents of growth media for forest seedling production. *New Forests* **2019**, *50* (6), 1063-1086.

(69) Kasera, N.; Hall, S.; Kolar, P. Characterization data of N-doped biochars using different external nitrogen precursors. *J. Environ. Chem. Eng.* **2021**, *35*, 106870-106870. DOI: 10.1016/j.dib.2021.106870 PubMed.

(70) Liu, S.-H.; Huang, Y.-Y. Valorization of coffee grounds to biochar-derived adsorbents for CO2 adsorption. *J. Clean. Prod.* **2018**, *175*, 354-360. DOI: https://doi.org/10.1016/j.jclepro.2017.12.076.

(71) Nguyen, V.-T.; Nguyen, T.-B.; Chen, C.-W.; Hung, C.-M.; Vo, T.-D.-H.; Chang, J.-H.; Dong, C.-D. Influence of pyrolysis temperature on polycyclic aromatic hydrocarbons production and tetracycline adsorption behavior of biochar derived from spent coffee ground. *Bioresour. Technol.* **2019**, *284*, 197-203. DOI: https://doi.org/10.1016/j.biortech.2019.03.096.

(72) Yang, G.-X.; Jiang, H. Amino modification of biochar for enhanced adsorption of copper ions from synthetic wastewater. *Water Res.* **2014**, *48*, 396-405. DOI: https://doi.org/10.1016/j.watres.2013.09.050.

(73) USEPA. EPA PFAS action plan: program update. U.S. Environmental Protection Agency, Ed.; Washington D.C., 2020.

(74) USEPA. Human health toxicity values for hexafluoropropylene oxide (HFPO) dimer acid and its ammonium salt (CASRN 13252-13-6 and CASRN 62037-80-3) also known as "GenX chemicals". U.S. Environmental Protection Agency, Ed.; Washington D.C., 2018.

(75) Song, X.; Vestergren, R.; Shi, Y.; Huang, J.; Cai, Y. Emissions, transport, and fate of emerging per- and polyfluoroalkyl substances from one of the major fluoropolymer manufacturing facilities in China. *Environ. Sci. Technol.* **2018**, *52* (17), 9694-9703. DOI: 10.1021/acs.est.7b06657.

(76) DuPont. DuPont GenX processing aid for making fluoropolymer resins: setting a new industrial standard for sustainable replacement technology. www.genx.dupont.com.

(77) McNamara, J. D.; Franco, R.; Mimna, R.; Zappa, L. Comparison of activated carbons for removal of perfluorinated compounds from drinking water. *J. Am. Water Work. Assoc.* **2018**, *110* (1), E2-E14. DOI: 10.5942/jawwa.2018.110.0003.

(78) Becker, A. M.; Gerstmann, S.; Frank, H. Perfluorooctanoic acid and perfluorooctane sulfonate in the sediment of the roter main river, Bayreuth, Germany. *Environ. Pollut.* **2008**, *156* (3), 818-820. DOI: https://doi.org/10.1016/j.envpol.2008.05.024.

(79) Arvaniti, O. S.; Hwang, Y.; Andersen, H. R.; Stasinakis, A. S.; Thomaidis, N. S.; Aloupi, M. Reductive degradation of perfluorinated compounds in water using Mg-aminoclay coated nanoscale zero valent iron. *Chem. Eng. J.* **2015**, *262*, 133-139. DOI: https://doi.org/10.1016/j.cej.2014.09.079.

(80) Plumlee, M. H.; Larabee, J.; Reinhard, M. Perfluorochemicals in water reuse. *Chemosphere* **2008**, *72* (10), 1541-1547. DOI: https://doi.org/10.1016/j.chemosphere.2008.04.057.

(81) Washington Department of Health. *Draft recommended state action levels for per- and polyfluoroalkyl substances (PFAS) in drinking water: approach, methods and supporting information*; Chapter 246-290 WAC; Washington Department of Health, Office of Environmental Public Health Sciences, 2019. https://www.doh.wa.gov/Portals/1/Documents/4200/PFASToxicologicalAssessment.pdf (accessed 5/6/2020).

(82) New York State Department of Health. Drinking water quality council recommends nation's most protective maximum contaminant levels for three unregulated contaminants in drinking water. New York State Department of Health,: Albany, NY, 2018.

(83) New Jersey Department of Health. Per- and Polyfluoroalkyl Substances (PFAS) in Drinking Water. Environmental and occupational health surveillance program, New Jersey Department of Health, Ed.; 2020.

(84) Kearns, J. P.; Wellborn, L. S.; Summers, R. S.; Knappe, D. R. U. 2,4-D adsorption to biochars: effect of preparation conditions on equilibrium adsorption capacity and comparison with commercial activated carbon literature data. *Water Res.* **2014**, *62*, 20-28. DOI: https://doi.org/10.1016/j.watres.2014.05.023.

(85) Deng, S.; Nie, Y.; Du, Z.; Huang, Q.; Meng, P.; Wang, B.; Huang, J.; Yu, G. Enhanced adsorption of perfluorooctane sulfonate and perfluorooctanoate by bamboo-derived granular

activated carbon. *J. Hazard. Mater.* **2015**, *282*, 150-157. DOI: https://doi.org/10.1016/j.jhazmat.2014.03.045.

(86) Laksaci, H.; Khelifi, A.; Trari, M.; Addoun, A. Synthesis and characterization of microporous activated carbon from coffee grounds using potassium hydroxides. *J. Clean. Prod.* **2017**, *147*, 254-262. DOI: https://doi.org/10.1016/j.jclepro.2017.01.102.

(87) Alcaraz, L.; Escudero, M. E.; Alguacil, F. J.; Llorente, I.; Urbieta, A.; Fernández, P.; López, F. A. Dysprosium removal from water using active carbons obtained from spent coffee ground. *Nanomaterials-Basel* **2019**, *9* (10). DOI: 10.3390/nano9101372 From NLM.

(88) Kim, M.-S.; Min, H.-G.; Koo, N.; Park, J.; Lee, S.-H.; Bak, G.-I.; Kim, J.-G. The effectiveness of spent coffee grounds and its biochar on the amelioration of heavy metals-contaminated water and soil using chemical and biological assessments. *J. Environ. Manage.* **2014**, *146*, 124-130. DOI: https://doi.org/10.1016/j.jenvman.2014.07.001.

(89) Ray, J. R.; Shabtai, I. A.; Teixidó, M.; Mishael, Y. G.; Sedlak, D. L. Polymer-clay composite geomedia for sorptive removal of trace organic compounds and metals in urban stormwater. *Water Res.* **2019**, *157*, 454-462. DOI: https://doi.org/10.1016/j.watres.2019.03.097.

(90) ASTM International. *ASTM D1762-84, standard test method for chemical analysis of wood charcoal*; ASTM International, West Conshohocken, PA, 2007. www.astm.org (accessed 6/19/2020).

(91) Mukherjee, A.; Zimmerman, A. R.; Harris, W. Surface chemistry variations among a series of laboratory-produced biochars. *Geoderma* **2011**, *163* (3), 247-255. DOI: https://doi.org/10.1016/j.geoderma.2011.04.021.

(92) Belay, A.; Ture, K.; Redi, M.; Asfaw, A. Measurement of caffeine in coffee beans with UV/vis spectrometer. *Food Chem.* **2008**, *108* (1), 310-315. DOI: https://doi.org/10.1016/j.foodchem.2007.10.024.

(93) Vega, E.; Valdés, H. New evidence of the effect of the chemical structure of activated carbon on the activity to promote radical generation in an advanced oxidation process using hydrogen peroxide. *Micropor. Mesopor. Mat.* **2018**, *259*, 1-8. DOI: https://doi.org/10.1016/j.micromeso.2017.09.018.

(94) Lee, S.; Uliana, A.; Taylor, M. K.; Chakarawet, K.; Bandaru, S. R. S.; Gul, S.; Xu, J.; Ackerman, Cheri M.; Chatterjee, R.; Furukawa, H.; et al. Iron detection and remediation with a functionalized porous polymer applied to environmental water samples. *Chemical Science* **2019**, *10* (27), 6651-6660, 10.1039/C9SC01441A. DOI: 10.1039/C9SC01441A.

(95) Hafeznezami, S.; Zimmer-Faust, A. G.; Jun, D.; Rugh, M. B.; Haro, H. L.; Park, A.; Suh, J.; Najm, T.; Reynolds, M. D.; Davis, J. A.; et al. Remediation of groundwater contaminated with arsenic through enhanced natural attenuation: Batch and column studies. *Water Res* **2017**, *122*, 545-556. DOI: 10.1016/j.watres.2017.06.029 From NLM.

(96) Miera, R. E. Investigation of Acetaminophen and Caffeine Removal Using Manganese Oxides and Granular Activated Carbon in Column Experiments. University of New Mexico, Albuquerque, NM, 2018. https://digitalrepository.unm.edu/ce_etds/220.

(97) Motsa, M. M.; Mamba, B. B.; Verliefde, A. R. D. Forward osmosis membrane performance during simulated wastewater reclamation: fouling mechanisms and fouling layer properties. *J. Water Process. Eng.* **2018**, *23*, 109-118. DOI: https://doi.org/10.1016/j.jwpe.2018.03.007.

(98) Miranda-García, N.; Suárez, S.; Sánchez, B.; Coronado, J. M.; Malato, S.; Maldonado, M. I. Photocatalytic degradation of emerging contaminants in municipal wastewater treatment plant

effluents using immobilized TiO2 in a solar pilot plant. *Appl. Catal. B.* **2011**, *103* (3), 294-301. DOI: https://doi.org/10.1016/j.apcatb.2011.01.030.

(99) Tang, L.; Li, L.; Chen, R.; Wang, C.; Ma, W.; Ma, X. Adsorption of acetone and isopropanol on organic acid modified activated carbons. *J. Environ. Chem. Eng.* **2016**, *4* (2), 2045-2051. DOI: https://doi.org/10.1016/j.jece.2016.03.031.

(100) Dittmar, S.; Zietzschmann, F.; Mai, M.; Worch, E.; Jekel, M.; Ruhl, A. S. Simulating effluent organic matter competition in micropollutant adsorption onto activated carbon using a surrogate competitor. *Environ. Sci. Technol.* **2018**, *52* (14), 7859-7866. DOI: 10.1021/acs.est.8b01503.

(101) Lei, Y.; Remmers, J. C.; Saakes, M.; van der Weijden, R. D.; Buisman, C. J. N. Is there a precipitation sequence in municipal wastewater induced by electrolysis? *Environ. Sci. Technol.* **2018**, *52* (15), 8399-8407. DOI: 10.1021/acs.est.8b02869 From NLM.

(102) USEPA. NPDES Writers Manual, Chapter 5: Technology Based Effluent Limitations. U.S. Environmental Protection Agency, Ed.; 2010.

(103) *Visual MINTEQ*; released 2014. (accessed.

(104) Gromov, A.; Dittmer, S.; Svensson, J.; Nerushev, O. A.; Perez-García, S. A.; Licea-Jiménez, L.; Rychwalski, R.; Campbell, E. E. B. Covalent amino-functionalisation of single-wall carbon nanotubes. *J. Mater. Chem.* **2005**, *15* (32), 3334-3339, 10.1039/B504282H. DOI: 10.1039/B504282H.

(105) Zhuang, Q. L.; Kyotani, T.; Tomita, A. DRIFT and TK/TPD analyses of surface oxygen complexes formed during carbon gasification. *Energy Fuels* **1994**, *8* (3), 714-718. DOI: 10.1021/ef00045a028.

(106) Keiluweit, M.; Nico, P. S.; Johnson, M. G.; Kleber, M. Dynamic molecular structure of plant biomass-derived black carbon (biochar). *Environ. Sci. Technol.* **2010**, *44* (4), 1247-1253. DOI: 10.1021/es9031419.

(107) Du, Z.; Deng, S.; Bei, Y.; Huang, Q.; Wang, B.; Huang, J.; Yu, G. Adsorption behavior and mechanism of perfluorinated compounds on various adsorbents—a review. *J. Hazard. Mater.* **2014**, *274*, 443-454. DOI: https://doi.org/10.1016/j.jhazmat.2014.04.038.

(108) Moussout, H.; Ahlafi, H.; Aazza, M.; Maghat, H. Critical of linear and nonlinear equations of pseudo-first order and pseudo-second order kinetic models. *Karbala International Journal of Modern Science* **2018**, *4* (2), 244-254. DOI: https://doi.org/10.1016/j.kijoms.2018.04.001.

(109) Liu, Y.; Shen, L. From langmuir kinetics to first- and second-order rate equations for adsorption. *Langmuir* **2008**, *24* (20), 11625-11630. DOI: 10.1021/la801839b.

(110) Zhi, Y.; Liu, J. Adsorption of perfluoroalkyl acids by carbonaceous adsorbents: effect of carbon surface chemistry. *Environ. Pollut.* **2015**, *202*, 168-176. DOI: https://doi.org/10.1016/j.envpol.2015.03.019.

(111) Simonin, J.-P. On the comparison of pseudo-first order and pseudo-second order rate laws in the modeling of adsorption kinetics. *Chem. Eng. J.* **2016**, *300*, 254-263. DOI: https://doi.org/10.1016/j.cej.2016.04.079.

(112) Crittenden, J. C.; Howe, K. J.; Hand, D. W.; Tchobanoglous, G.; Trussell, R. R. *Principles of water treatment*; Hoboken, New Jersey : John Wiley & Sons, Inc., 2012.

(113) Yu, Q.; Zhang, R.; Deng, S.; Huang, J.; Yu, G. Sorption of perfluorooctane sulfonate and perfluorooctanoate on activated carbons and resin: kinetic and isotherm study. *Water Res.* **2009**, *43* (4), 1150-1158. DOI: https://doi.org/10.1016/j.watres.2008.12.001.

(114) Johnson, R. L.; Anschutz, A. J.; Smolen, J. M.; Simcik, M. F.; Penn, R. L. The adsorption of perfluorooctane sulfonate onto sand, clay, and iron oxide surfaces. *J. Chem. Eng. Data* **2007**, *52* (4), 1165-1170. DOI: 10.1021/je060285g.

(115) Higgins, C. P.; Luthy, R. G. Sorption of perfluorinated surfactants on sediments. *Environ. Sci. Technol.* **2006**, *40* (23), 7251-7256. DOI: 10.1021/es061000n.

(116) Steigerwald, J. M.; Peng, S.; Ray, J. R. Novel Perfluorooctanesulfonate-Imprinted Polymer Immobilized on Spent Coffee Grounds Biochar for Selective Removal of Perfluoroalkyl Acids in Synthetic Wastewater. *ACS ES&T Engineering* **2023**. DOI: 10.1021/acsestengg.2c00336.

(117) PFAS Strategic Roadmap: EPA's commitments to Action 2021 - 2024. U.S. Environmental Protection Agency: Washington D.C., 2021.

(118) Rahman, M. F.; Peldszus, S.; Anderson, W. B. Behaviour and fate of perfluoroalkyl and polyfluoroalkyl substances (PFASs) in drinking water treatment: A review. *Water Res.* **2014**, *50*, 318-340. DOI: https://doi.org/10.1016/j.watres.2013.10.045.

(119) Appleman, T. D.; Higgins, C. P.; Quiñones, O.; Vanderford, B. J.; Kolstad, C.; Zeigler-Holady, J. C.; Dickenson, E. R. V. Treatment of poly- and perfluoroalkyl substances in U.S. full-scale water treatment systems. *Water Res.* **2014**, *51*, 246-255. DOI: 10.1016/j.watres.2013.10.067.

(120) Houtz, E. F.; Sutton, R.; Park, J.-S.; Sedlak, M. Poly- and perfluoroalkyl substances in wastewater: Significance of unknown precursors, manufacturing shifts, and likely AFFF impacts. *Water Res.* **2016**, *95*, 142-149. DOI: https://doi.org/10.1016/j.watres.2016.02.055.

(121) Lenka, S. P.; Kah, M.; Padhye, L. P. A review of the occurrence, transformation, and removal of poly- and perfluoroalkyl substances (PFAS) in wastewater treatment plants. *Water Res.* **2021**, *199*, 117187. DOI: https://doi.org/10.1016/j.watres.2021.117187.

(122) Ahrens, L.; Bundschuh, M. Fate and effects of poly- and perfluoroalkyl substances in the aquatic environment: A review. *Environ. Toxicol. Chem.* **2014**, *33* (9), 1921-1929. DOI: https://doi.org/10.1002/etc.2663.

(123) Vestergren, R.; Cousins, I. T. Tracking the pathways of human exposure to perfluorocarboxylates. *Environ. Sci. Technol.* **2009**, *43* (15), 5565-5575.

(124) Lang, J. R.; Allred, B. M.; Field, J. A.; Levis, J. W.; Barlaz, M. A. National estimate of per-and polyfluoroalkyl substance (PFAS) release to US municipal landfill leachate. *Environ. Sci. Technol.* **2017**, *51* (4), 2197-2205.

(125) Masoner, J. R.; Kolpin, D. W.; Cozzarelli, I. M.; Smalling, K. L.; Bolyard, S. C.; Field, J. A.; Furlong, E. T.; Gray, J. L.; Lozinski, D.; Reinhart, D. Landfill leachate contributes per-/poly-fluoroalkyl substances (PFAS) and pharmaceuticals to municipal wastewater. *Environ. Sci. Water Res. Technol.* **2020**, *6* (5), 1300-1311.

(126) Chen, W.; Zhang, X.; Mamadiev, M.; Wang, Z. Sorption of perfluorooctane sulfonate and perfluorooctanoate on polyacrylonitrile fiber-derived activated carbon fibers: in comparison with activated carbon. *RSC Adv.* **2017**, *7* (2), 927-938, 10.1039/C6RA25230C. DOI: 10.1039/C6RA25230C.

(127) Davis, M. L. Chapter 12: General Wastewater Collection and Treatment Decision Considerations. In *Water and Wastewater Engineering: Design Principles and Practice*, McGraw Hill, 2011.

(128) Benotti, M. J.; Trenholm, R. A.; Vanderford, B. J.; Holady, J. C.; Stanford, B. D.; Snyder, S. A. Pharmaceuticals and Endocrine Disrupting Compounds in U.S. Drinking Water. *Environ. Sci. Technol.* **2009**, *43* (3), 597-603. DOI: 10.1021/es801845a.

(129) Horst, J.; McDonough, J.; Ross, I.; Houtz, E. Understanding and Managing the potential by-products of PFAS destruction. *Ground Water Monit. Remediat.* **2020**, *40* (2), 17-27.

(130) Gao, R.; Hao, Y.; Zhao, S.; Zhang, L.; Cui, X.; Liu, D.; Tang, Y.; Zheng, Y. Novel magnetic multi-template molecularly imprinted polymers for specific separation and determination of three endocrine disrupting compounds simultaneously in environmental water samples. *RSC Adv.* **2014**, *4* (100), 56798-56808, 10.1039/C4RA09825K. DOI: 10.1039/C4RA09825K.

(131) Fan, Y.; Zeng, G.; Ma, X. Effects of prepolymerization on surface molecularly imprinted polymer for rapid separation and analysis of sulfonamides in water. *Journal of Colloid and Interface Science* **2020**, *571*, 21-29.

(132) Krupadam, R. J.; Khan, M. S.; Wate, S. R. Removal of probable human carcinogenic polycyclic aromatic hydrocarbons from contaminated water using molecularly imprinted polymer. *Water Res.* **2010**, *44* (3), 681-688. DOI: https://doi.org/10.1016/j.watres.2009.09.044.

(133) Kazemi, R.; Potts, E. I.; Dick, J. E. Quantifying Interferent Effects on Molecularly Imprinted Polymer Sensors for Per- and Polyfluoroalkyl Substances (PFAS). *Anal. Chem.* **2020**, *92* (15), 10597-10605. DOI: 10.1021/acs.analchem.0c01565.

(134) Chi, T.-Y.; Chen, Z.; Kameoka, J. Perfluorooctanesulfonic Acid Detection Using Molecularly Imprinted Polyaniline on a Paper Substrate. *Sensors* **2020**, *20* (24), 7301. DOI: 10.3390/s20247301.

(135) Gauczinski, J.; Liu, Z.; Zhang, X.; Schönhoff, M. Surface Molecular Imprinting in Layer-by-Layer films on Silica Particles. *Langmuir* **2012**, *28* (9), 4267-4273. DOI: 10.1021/la205027j.

(136) Tran.T, T.; Li, J.; Feng, H.; Cai, J.; Yuan, L.; Wang, N.; Cai, Q. Molecularly imprinted polymer modified TiO2 nanotube arrays for photoelectrochemical determination of perfluorooctane sulfonate (PFOS). *Sens. Actuators B Chem.* **2014**, *190*, 745-751. DOI: https://doi.org/10.1016/j.snb.2013.09.048.

(137) Wu, Y.; Li, Y.; Tian, A.; Mao, K.; Liu, J. Selective Removal of Perfluorooctanoic Acid Using Molecularly Imprinted Polymer-Modified TiO2 Nanotube Arrays. *Int. J. Photoenergy* **2016**, *2016*, 7368795. DOI: 10.1155/2016/7368795.

(138) León, M.; Silva, J.; Carrasco, S.; Barrientos, N. Design, Cost Estimation and Sensitivity Analysis for a Production Process of Activated Carbon from Waste Nutshells by Physical Activation. *Processes* **2020**, *8* (8), 945.

(139) Wong, S.; Ngadi, N.; Inuwa, I. M.; Hassan, O. Recent advances in applications of activated carbon from biowaste for wastewater treatment: A short review. *J. Clean. Prod.* **2018**, *175*, 361-375. DOI: https://doi.org/10.1016/j.jclepro.2017.12.059.

(140) Zhang, D.; Zhang, W.; Liang, Y. Adsorption of perfluoroalkyl and polyfluoroalkyl substances (PFASs) from aqueous solution-A review. *Sci. Total Environ.* **2019**, *694*, 133606.

(141) Chen, Z.; Li, C.; Gao, J.; Dong, H.; Chen, Y.; Wu, B.; Gu, C. Efficient Reductive Destruction of Perfluoroalkyl Substances under Self-Assembled Micelle Confinement. *Environ. Sci. Technol.* **2020**, *54* (8), 5178-5185. DOI: 10.1021/acs.est.9b06599 From NLM.

(142) Li, Y.-F.; Chien, W.-Y.; Liu, Y.-J.; Lee, Y.-C.; Lo, S.-L.; Hu, C.-Y. Perfluorooctanoic acid (PFOA) removal by flotation with cationic surfactants. *Chemosphere* **2021**, *266*, 128949. DOI: 10.1016/j.chemosphere.2020.128949.

(143) Feng, H.; Wang, N.; Tran.T, T.; Yuan, L.; Li, J.; Cai, Q. Surface molecular imprinting on dye–(NH2)–SiO2 NPs for specific recognition and direct fluorescent quantification of

perfluorooctane sulfonate. *Sensors and Actuators B: Chemical* **2014**, *195*, 266-273. DOI: https://doi.org/10.1016/j.snb.2014.01.036.

(144) Karoyo, A. H.; Wilson, L. D. Nano-Sized Cyclodextrin-Based Molecularly Imprinted Polymer Adsorbents for Perfluorinated Compounds-A Mini-Review. *Nanomaterials-Basel* **2015**, *5* (2), 981-1003. DOI: 10.3390/nano5020981 From NLM.

(145) Maddi, C.; Bourquard, F.; Barnier, V.; Avila, J.; Asensio, M.-C.; Tite, T.; Donnet, C.; Garrelie, F. Nano-Architecture of nitrogen-doped graphene films synthesized from a solid CN source. *Scientific Reports* **2018**, *8* (1), 3247. DOI: 10.1038/s41598-018-21639-9.

(146) Deng, S.; Zheng, Y. Q.; Xu, F. J.; Wang, B.; Huang, J.; Yu, G. Highly efficient sorption of perfluorooctane sulfonate and perfluorooctanoate on a quaternized cotton prepared by atom transfer radical polymerization. *Chem. Eng. J.* **2012**, *193-194*, 154-160. DOI: https://doi.org/10.1016/j.cej.2012.04.005.

(147) Gong, J.; Fang, T.; Peng, D.; Li, A.; Zhang, L. A highly sensitive photoelectrochemical detection of perfluorooctanic acid with molecularly imprined polymer-functionalized nanoarchitectured hybrid of AgI–BiOI composite. *Biosensors and Bioelectronics* **2015**, *73*, 256-263. DOI: https://doi.org/10.1016/j.bios.2015.06.008.

(148) Teerlink, J.; Hernandez, J.; Budd, R. Fipronil washoff to municipal wastewater from dogs treated with spot-on products. *Sci. Total Environ.* **2017**, *599-600*, 960-966. DOI: https://doi.org/10.1016/j.scitotenv.2017.04.219.

(149) Lopez, J.; Monsalvo, V. M.; Puyol, D.; Mohedano, A. F.; Rodriguez, J. J. Low-temperature anaerobic treatment of low-strength pentachlorophenol-bearing wastewater. *Bioresour. Technol.* **2013**, *140*, 349-356. DOI: https://doi.org/10.1016/j.biortech.2013.04.049.

(150) Rigueto, C. V. T.; Nazari, M. T.; De Souza, C. F.; Cadore, J. S.; Brião, V. B.; Piccin, J. S. Alternative techniques for caffeine removal from wastewater: An overview of opportunities and challenges. *J. Water Process. Eng.* **2020**, *35*, 101231. DOI: https://doi.org/10.1016/j.jwpe.2020.101231.

(151) de Escobar, C. C.; Moreno Ruiz, Y. P.; dos Santos, J. H. Z.; Ye, L. Molecularly imprinted TiO2 photocatalysts for degradation of diclofenac in water. *Colloids and Surfaces A: Physicochemical and Engineering Aspects* **2018**, *538*, 729-738. DOI: https://doi.org/10.1016/j.colsurfa.2017.11.044.

(152) Sun, Y.; Kunc, F.; Balhara, V.; Coleman, B.; Kodra, O.; Raza, M.; Chen, M.; Brinkmann, A.; Lopinski, G. P.; Johnston, L. J. Quantification of amine functional groups on silica nanoparticles: a multi-method approach. *Nanoscale Adv.* **2019**, *1* (4), 1598-1607, 10.1039/C9NA00016J. DOI: 10.1039/C9NA00016J.

(153) Li, L.; Yao, X.; Li, H.; Liu, Z.; Ma, W.; Liang, X. Thermal Stability of Oxygen-Containing Functional Groups on Activated Carbon Surfaces in a Thermal Oxidative Environment. *J. Chem. Eng. Japan* **2014**, *47* (1), 21-27. DOI: 10.1252/jcej.13we193.

(154) *Ammonium chloride*; SDS No. 017-014-00-8 [Online]; Sigma Aldrich, St. Louis, MO, 2021.

(155) Campos Pereira, H.; Ullberg, M.; Kleja, D. B.; Gustafsson, J. P.; Ahrens, L. Sorption of perfluoroalkyl substances (PFASs) to an organic soil horizon – Effect of cation composition and pH. *Chemosphere* **2018**, *207*, 183-191. DOI: https://doi.org/10.1016/j.chemosphere.2018.05.012.

(156) Turner, N. W.; Piletska, E. V.; Karim, K.; Whitcombe, M.; Malecha, M.; Magan, N.; Baggiani, C.; Piletsky, S. A. Effect of the solvent on recognition properties of molecularly imprinted polymer specific for ochratoxin A. *Biosens. Bioelectron.* **2004**, *20* (6), 1060-1067.

(157) Tang, C. Y.; Shiang Fu, Q.; Gao, D.; Criddle, C. S.; Leckie, J. O. Effect of solution chemistry on the adsorption of perfluorooctane sulfonate onto mineral surfaces. *Water Res.* **2010**, *44* (8), 2654-2662. DOI: https://doi.org/10.1016/j.watres.2010.01.038.

(158) Wang, F.; Shih, K. Adsorption of perfluorooctanesulfonate (PFOS) and perfluorooctanoate (PFOA) on alumina: Influence of solution pH and cations. *Water Res.* **2011**, *45* (9), 2925-2930.

(159) Radjabian, M.; Abetz, V. Advanced porous polymer membranes from self-assembling block copolymers. *Progress in Polymer Science* **2020**, *102*, 101219. DOI: https://doi.org/10.1016/j.progpolymsci.2020.101219.

(160) Appleman, T. D.; Higgins, C. P.; Quiñones, O.; Vanderford, B. J.; Kolstad, C.; Zeigler-Holady, J. C.; Dickenson, E. R. Treatment of poly-and perfluoroalkyl substances in US full-scale water treatment systems. *Water Res.* **2014**, *51*, 246-255.

(161) Hopkins, Z.; Sun, M.; DeWitt, J.; Knappe, D. Recently Detected Drinking Water Contaminants: GenX and Other Per- and Polyfluoroalkyl Ether Acids. *J. Am. Water Work. Assoc.* **2018**, *110*. DOI: 10.1002/awwa.1073.

(162) Arvaniti, O. S.; Ventouri, E. I.; Stasinakis, A. S.; Thomaidis, N. S. Occurrence of different classes of perfluorinated compounds in Greek wastewater treatment plants and determination of their solid–water distribution coefficients. *J. Hazard. Mater.* **2012**, *239-240*, 24-31. DOI: https://doi.org/10.1016/j.jhazmat.2012.02.015.

(163) Schaefer, C. E.; Hooper, J. L.; Strom, L. E.; Abusallout, I.; Dickenson, E. R. V.; Thompson, K. A.; Mohan, G. R.; Drennan, D.; Wu, K.; Guelfo, J. L. Occurrence of Quantifiable and Semi-Quantifiable Poly- and Perfluoroalkyl Substances in United States Wastewater Treatment Plants. *Water Res.* **2023**, 119724. DOI: https://doi.org/10.1016/j.watres.2023.119724.

(164) Poothong, S.; Thomsen, C.; Padilla-Sanchez, J. A.; Papadopoulou, E.; Haug, L. S. Distribution of novel and well-known poly-and perfluoroalkyl substances (PFASs) in human serum, plasma, and whole blood. *Environ. Sci. Technol.* **2017**, *51* (22), 13388-13396.

(165) Jian, J.-M.; Chen, D.; Han, F.-J.; Guo, Y.; Zeng, L.; Lu, X.; Wang, F. A short review on human exposure to and tissue distribution of per-and polyfluoroalkyl substances (PFASs). *Sci. Total Environ.* **2018**, *636*, 1058-1069.

(166) Olsen, G. W.; Mair, D. C.; Lange, C. C.; Harrington, L. M.; Church, T. R.; Goldberg, C. L.; Herron, R. M.; Hanna, H.; Nobiletti, J. B.; Rios, J. A. Per-and polyfluoroalkyl substances (PFAS) in American Red Cross adult blood donors, 2000–2015. *Environmental research* **2017**, *157*, 87-95.

(167) Jha, G.; Kankarla, V.; McLennon, E.; Pal, S.; Sihi, D.; Dari, B.; Diaz, D.; Nocco, M. Per-and Polyfluoroalkyl Substances (PFAS) in Integrated Crop–Livestock Systems: Environmental Exposure and Human Health Risks. *International Journal of Environmental Research and Public Health* **2021**, *18* (23), 12550.

(168) Death, C.; Bell, C.; Champness, D.; Milne, C.; Reichman, S.; Hagen, T. Per-and polyfluoroalkyl substances (PFAS) in livestock and game species: A review. *Sci. Total Environ.* **2021**, *774*, 144795.

(169) Drew, R.; Hagen, T. G.; Champness, D. Accumulation of PFAS by livestock–determination of transfer factors from water to serum for cattle and sheep in Australia. *Food Additives & Contaminants: Part A* **2021**, *38* (11), 1897-1913.

(170) Barbo, N.; Stoiber, T.; Naidenko, O. V.; Andrews, D. Q. Locally caught freshwater fish across the United States are likely a significant source of exposure to PFOS and other perfluorinated

compounds. *Environmental Research* **2023**, *220*, 115165. DOI: https://doi.org/10.1016/j.envres.2022.115165.

(171) Kaboré, H. A.; Goeury, K.; Desrosiers, M.; Duy, S. V.; Liu, J.; Cabana, G.; Munoz, G.; Sauvé, S. Novel and legacy per-and polyfluoroalkyl substances (PFAS) in freshwater sporting fish from background and firefighting foam impacted ecosystems in Eastern Canada. *Sci. Total Environ.* **2022**, *816*, 151563.

(172) Rüdel, H.; Radermacher, G.; Fliedner, A.; Lohmann, N.; Koschorreck, J.; Duffek, A. Tissue concentrations of per-and polyfluoroalkyl substances (PFAS) in German freshwater fish: Derivation of fillet-to-whole fish conversion factors and assessment of potential risks. *Chemosphere* **2022**, *292*, 133483.

(173) Brennan, N. M.; Evans, A. T.; Fritz, M. K.; Peak, S. A.; von Holst, H. E. Trends in the regulation of per-and polyfluoroalkyl substances (PFAS): a scoping review. *International journal of environmental research and public health* **2021**, *18* (20), 10900.

(174) USEPA. PFAS National Primary Drinking Water Regulation Rulemaking: Proposed Rule. 2023.

(175) USEPA. Draft Aquatic Life Ambient Water Quality Criteria for Perfluorooctane Sulfonate (PFOS). Office of Water, O. o. S. a. T., Health and Ecological Criteria Division,, Ed.; Washington, D.C., 2022.

(176) USEPA. Draft Aquatic Life Ambient Water Quality Criteria for Perfluorooctanoic Acid (PFOA). Office of Water, O. o. S. a. T., Health and Ecological Criteria Division,, Ed.; Washington, D.C., 2022.

(177) Li, F.; Duan, J.; Tian, S.; Ji, H.; Zhu, Y.; Wei, Z.; Zhao, D. Short-chain per- and polyfluoroalkyl substances in aquatic systems: Occurrence, impacts and treatment. *Chem. Eng. J.* **2020**, *380*, 122506. DOI: https://doi.org/10.1016/j.cej.2019.122506.

(178) Maimaiti, A.; Deng, S.; Meng, P.; Wang, W.; Wang, B.; Huang, J.; Wang, Y.; Yu, G. Competitive adsorption of perfluoroalkyl substances on anion exchange resins in simulated AFFF-impacted groundwater. *Chem. Eng. J.* **2018**, *348*, 494-502.

(179) Cormack, P. A.; Elorza, A. Z. Molecularly imprinted polymers: synthesis and characterisation. *Journal of chromatography B* **2004**, *804* (1), 173-182.

(180) Fidel, R. B.; Laird, D. A.; Thompson, M. L. Evaluation of modified Boehm titration methods for use with biochars. *Journal of environmental quality* **2013**, *42* (6), 1771-1778.

(181) Yu, Q.; Deng, S.; Yu, G. Selective removal of perfluorooctane sulfonate from aqueous solution using chitosan-based molecularly imprinted polymer adsorbents. *Water Res.* **2008**, *42* (12), 3089-3097. DOI: https://doi.org/10.1016/j.watres.2008.02.024.

(182) Deng, D.; He, Y.; Li, M.; Huang, L.; Zhang, J. Preparation of multi-walled carbon nanotubes based magnetic multi-template molecularly imprinted polymer for the adsorption of phthalate esters in water samples. *Environmental Science and Pollution Research* **2021**, *28* (5), 5966-5977. DOI: 10.1007/s11356-020-10970-2.

(183) Fan, Y.; Zeng, G.; Ma, X. Multi-templates surface molecularly imprinted polymer for rapid separation and analysis of quinolones in water. *Environmental Science and Pollution Research* **2020**, *27* (7), 7177-7187. DOI: 10.1007/s11356-019-07437-4.

(184) Lu, W.; Wang, X.; Wu, X.; Liu, D.; Li, J.; Chen, L.; Zhang, X. Multi-template imprinted polymers for simultaneous selective solid-phase extraction of six phenolic compounds in water

samples followed by determination using capillary electrophoresis. *Journal of Chromatography A* **2017**, *1483*, 30-39. DOI: https://doi.org/10.1016/j.chroma.2016.12.069.

(185) Chen, L.; Wang, X.; Lu, W.; Wu, X.; Li, J. Molecular imprinting: perspectives and applications. *Chemical society reviews* **2016**, *45* (8), 2137-2211.

(186) Bruton, T. A.; Sedlak, D. L. Treatment of Aqueous Film-Forming Foam by Heat-Activated Persulfate Under Conditions Representative of In Situ Chemical Oxidation. *Environ. Sci. Technol.* **2017**, *51* (23), 13878-13885. DOI: 10.1021/acs.est.7b03969.

(187) Chen, W.-J.; Shang, P.-P.; Fang, S.-B.; Huang, Y.-P.; Liu, Z.-S. Origin of macromolecular crowding: Analysis of recognition mechanism of dual-template molecularly imprinted polymers by in silico prediction. *Journal of Chromatography A* **2022**, *1662*, 462695. DOI: https://doi.org/10.1016/j.chroma.2021.462695.

(188) Jia, M.; Yang, J.; Zhao, Y.-X.; Liu, Z.-S.; Aisa, H. A. A strategy of improving the imprinting effect of molecularly imprinted polymer: Effect of heterogeneous macromolecule crowding. *Talanta* **2017**, *175*, 488-494. DOI: https://doi.org/10.1016/j.talanta.2017.07.075.

(189) Matsui, J.; Goji, S.; Murashima, T.; Miyoshi, D.; Komai, S.; Shigeyasu, A.; Kushida, T.; Miyazawa, T.; Yamada, T.; Tamaki, K.; et al. Molecular Imprinting under Molecular Crowding Conditions: An Aid to the Synthesis of a High-Capacity Polymeric Sorbent for Triazine Herbicides. *Analytical Chemistry* **2007**, *79* (4), 1749-1757. DOI: 10.1021/ac060441m.

(190) Sun, G. Y.; Zhong, D. D.; Li, X. J.; Luo, Y. Q.; Ba, H.; Liu, Z. S.; Aisa, H. A. Effect of minimizing amount of template by addition of macromolecular crowding agent on preparation of molecularly imprinted monolith. *Anal Bioanal Chem* **2015**, *407* (24), 7401-7412. DOI: 10.1007/s00216-015-8902-0 From NLM.

(191) Tang, L.; Zhao, C.-Y.; Wang, X.-H.; Li, R.-S.; Yang, J.-R.; Huang, Y.-P.; Liu, Z.-S. Macromolecular crowding of molecular imprinting: A facile pathway to produce drug delivery devices for zero-order sustained release. *International Journal of Pharmaceutics* **2015**, *496* (2), 822-833. DOI: https://doi.org/10.1016/j.ijpharm.2015.10.031.

(192) Harding-Marjanovic, K. C.; Houtz, E. F.; Yi, S.; Field, J. A.; Sedlak, D. L.; Alvarez-Cohen, L. Aerobic biotransformation of fluorotelomer thioether amido sulfonate (Lodyne) in AFFF-amended microcosms. *Environ. Sci. Technol.* **2015**, *49* (13), 7666-7674.

(193) Park, M.; Wu, S.; Lopez, I. J.; Chang, J. Y.; Karanfil, T.; Snyder, S. A. Adsorption of perfluoroalkyl substances (PFAS) in groundwater by granular activated carbons: Roles of hydrophobicity of PFAS and carbon characteristics. *Water Res.* **2020**, *170*, 115364.

(194) Zhang, Y.; Thomas, A.; Apul, O.; Venkatesan, A. K. Coexisting ions and long-chain per-and polyfluoroalkyl substances (PFAS) inhibit the adsorption of short-chain PFAS by granular activated carbon. *J. Hazard. Mater.* **2023**, *460*, 132378.

(195) Hanari, N.; Itoh, N.; Ishikawa, K.; Yarita, T.; Numata, M. Variation in concentration of perfluorooctanoic acid in methanol solutions during storage. *Chemosphere* **2014**, *94*, 116-120.

(196) Pawlowski, L. Standard methods for the examination of water and wastewater. *Sci. Total Environ.* **1994**, *142* (3), 227-228.

(197) Schwarzenbach, R. P.; Gschwend, P. M.; Imboden, D. M. *Environmental organic chemistry*; John Wiley & Sons, 2016.

(198) Sørli, J. B.; Låg, M.; Ekeren, L.; Perez-Gil, J.; Haug, L. S.; Da Silva, E.; Matrod, M. N.; Gützkow, K. B.; Lindeman, B. Per- and polyfluoroalkyl substances (PFASs) modify lung

surfactant function and pro-inflammatory responses in human bronchial epithelial cells. *Toxicology in Vitro* **2020**, *62*, 104656. DOI: https://doi.org/10.1016/j.tiv.2019.104656.

(199) Riegel, M.; Haist-Gulde, B.; Sacher, F. Sorptive removal of short-chain perfluoroalkyl substances (PFAS) during drinking water treatment using activated carbon and anion exchanger. *Environmental Sciences Europe* **2023**, *35* (1), 1-12.

(200) Wang, Z.; Buser, A. M.; Cousins, I. T.; Demattio, S.; Drost, W.; Johansson, O.; Ohno, K.; Patlewicz, G.; Richard, A. M.; Walker, G. W.; et al. A New OECD Definition for Per- and Polyfluoroalkyl Substances. *Environ. Sci. Technol.* **2021**, *55* (23), 15575-15578. DOI: 10.1021/acs.est.1c06896.

(201) Lath, S.; Knight, E. R.; Navarro, D. A.; Kookana, R. S.; McLaughlin, M. J. Sorption of PFOA onto different laboratory materials: Filter membranes and centrifuge tubes. *Chemosphere* **2019**, *222*, 671-678.

(202) Wang, W.; Maimaiti, A.; Shi, H.; Wu, R.; Wang, R.; Li, Z.; Qi, D.; Yu, G.; Deng, S. Adsorption behavior and mechanism of emerging perfluoro-2-propoxypropanoic acid (GenX) on activated carbons and resins. *Chem. Eng. J.* **2019**, *364*, 132-138. DOI: https://doi.org/10.1016/j.cej.2019.01.153.

(203) Ray, J. R.; Wan, W.; Gilbert, B.; Jun, Y.-S. Effects of formation conditions on the physicochemical properties, aggregation, and phase transformation of iron oxide nanoparticles. *Langmuir* **2013**, *29* (4), 1069-1076. DOI: 10.1021/la3034319.

(204) Lawler, D. F.; Benjamin, M. M. *Water quality engineering : physical/chemical treatment processes*; Hoboken, New Jersey : John Wiley & Sons, 2013.

(205) Millipore Sigma. *IR Spectrum Table and Chart*. Merck KGaA, 2022. https://www.sigmaaldrich.com/US/en/technical-documents/technical-article/analytical-chemistry/photometry-and-reflectometry/ir-spectrum-table (accessed 3/31/2022).

(206) SGS. Physical and Chemical Properties of PFAS Compunds.

(207) Bonmatin, J. M.; Giorio, C.; Girolami, V.; Goulson, D.; Kreutzweiser, D. P.; Krupke, C.; Liess, M.; Long, E.; Marzaro, M.; Mitchell, E. A. D.; et al. Environmental fate and exposure; neonicotinoids and fipronil. *Environmental Science and Pollution Research* **2015**, *22* (1), 35-67. DOI: 10.1007/s11356-014-3332-7.

(208) National Institutes of Health. *PubChem*. https://pubchem.ncbi.nlm.nih.gov/ (accessed 2023.

(209) Estimation Programs Interface Suite™ for Microsoft® Windows, v 4.1. (accessed 2023).

(210) USEPA. Draft Method 1633: Analysis of Per- and Polyfluoroalkyl Substances (PFAS) in Aqueous, Solid, Biosolids, and Tissue Samples by LC-MS/MS. Office of Water, O. o. S. a. T., Engineering and Analysis Division, Ed.; Washington, D.C., 2021.